Investigating the specialized metabolism of the novel plant pathogen *Streptomyces* sp. 11-1-2

By

Gustavo Adolfo Díaz Cruz

A thesis submitted to the School of Graduate Studies in partial fulfillment of the requirements for the degree of

Doctor of Philosophy

Department of Biology

Memorial University of Newfoundland

September 2023

St. John's, Newfoundland and Labrador

ABSTRACT

Streptomyces is a genus of Gram-positive bacteria that are found in a wide range of environments and are capable of producing numerous specialized metabolites with diverse bioactivities. A small group of *Streptomyces* species is capable of causing plant diseases on a variety of crops. Notably, *Streptomyces scabiei* is one of the main causal agents of common scab disease, which affects multiple plants but is most relevant in potato production, as it significantly diminishes profits due to unmarketable tubers. To cause the disease, *S. scabiei* and most CS-causing pathogens use a specialized metabolite called thaxtomin A as the main pathogenicity factor.

Recently, several reports have shown the isolation of plant-pathogenic *Streptomyces* strains that do not produce thaxtomin A, but instead produce other phytotoxic specialized metabolites. One example is *Streptomyces* sp. 11-1-2 a strain isolated in 2011 from a CS-symptomatic potato tuber in Newfoundland, Canada. This strain was shown to be highly pathogenic against differerent plant hosts, but it does not produce thaxtomin A or other reported phytotoxins. Notably, the phytotoxic activity of the strain was retained by extracts obtained with organic solvent, suggesting that the activity was associated with one or more specialized metabolites.

The main objective of this work was to investigate the metabolic potential of *Streptomyces* sp. 11-1-2 in order to gain insights into the mechanisms used by this strain to inflict tissue damage on living plant hosts. In Chapter 3, the aim was to identify the main specialized metabolite(s) associated with the observed phytotoxic activity of the 11-1-2 strain using a combined genomics and metabolomics approach. Among the metabolites produced by the strain, nigericin and geldanamycin, which have previously been reported to exhibit

phytotoxic activity, were identified. Bioassays with the pure compounds showed pitting and necrosis of potato tissue, while nigericin also impacted the development of radish seedlings. In Chapter 4, the aim was to further explore the specialized metabolites that are produced by the 11-1-2 strain and their associated bioactivities. The "One Strain, Many Compounds" (OSMAC) approach was used together with untargeted metabolomics and genomics to evaluate the production of predicted and novel specialized metabolites. It was determined that the 11-1-2 strain can produce elaiophylins, echosides, and niphimycins, and elaiophylin was found to exhibit some phytotoxic activity against potato tuber tissue. In Chapter 5, the aim was to construct mutants of 11-1-2 that were deficient in the synthesis of nigericin and geldanamycin in order to assess the contribution of these metabolites to the pathogenic phenotype of 11-1-2. Different plasmids targeting specific genes in the geldanamycin and nigericin biosynthetic gene clusters (BGC) were designed and constructed. The introduction of DNA into 11-1-2 via intergeneric conjugation was achieved using the integrative plasmid pSET152, but no DNA introduction was accomplished when using the plasmids targeting the nigericin and geldanamycin BGCs. Overall, this study represents an in-depth characterization of the novel plant pathogen *Streptomyces* sp. 11-1-2, which may utilize a different plant pathogenicity mechanism compared to other *Streptomyces* species.

ACKNOWLEDGEMENTS

This Ph.D. journey would not have been a great experience without the support, guidance, and love of many people.

First, thanks to my supervisor Dr. Dawn Bignell for her patience, guidance, and continuous support. Entering the *Streptomyces* world was a big challenge for me, and I will be forever thankful for teaching me so much about it and sharing so much about research and life.

To my committee members, Dr. Kapil Tahlan and Dr. Martin Mulligan, for all their contributions, advice, and overall interest in my project. Your experience and knowledge significantly improved my research.

To the Bignell lab members over the years: thanks to Dr. Lancy Cheng, Dr. Jingyu Liu, and Dr. Phoebe Li for their endless mentorship, advice, and friendship. Your help made the transition into the lab and the *Streptomyces* world much easier. To Hannah Perry, for being a great labmate, Pokémon GO trading friend, and being supportive during our time in the lab. To Corrie Vincent, thanks for the entertaining stories, rides to Costco, and help in the last stretch of my program. To my undergrads Leah Walters, Matthew Drodge, Shelby MacNeil, and Joshua Butt, for all their hard work and contributions to my project.

To the Tahlan lab members: special thanks to Arshad Shaikh for sharing this journey with me, side by side, for his friendship and constant help in every aspect, and for making LB agar that one time. To Alex Byrne and Menus Garg, for all their help with many things, especially the bioinformatics stuff. Also to Jody-Ann Clarke, Dr. Nader AbuSara, Brandon Piercey, Madelyn Swackhammer, and Kajal Gupta for all their contributions and shared time.

Thanks to Andrea-Darby King and Heather Fifield for their diligence whenever I needed access to special equipment in the Biology and Biochemistry departments. To all the Biology lab instructors from whom I learned so much in the many courses I TA'd. And to the Biology faculty members and staff who always had a few minutes to chat with me about research and life.

Thanks to Dr. Stefana Egli and Dr. Ibrahim M. Abu-Reidah at C-CART for their expertise and guidance during my time using the LC-MS to detect and quantify my metabolites.

To my friends who never stopped rooting for me from afar and had encouragement words whenever I needed them: Alisha Poole, María Inés Chaves, and Stefany Redondo Romero. Despite our physical distance, I always felt you right by my side.

To the Sehn and Quintero-Ordóñez families: thanks for always caring about my well-being, and the many snacks and meals that you provided for me over the years.

To Dr. Dennis Sánchez Mora and Andrés Beita Jiménez, for helping me adapt to the life in St. John's and the Ph.D. life at MUN.

A mi familia: Alex, Ana Iris, María Fernanda, Esteban y David, muchas gracias por siempre estar ahí, por todo el amor y apoyo en este largo proceso. Todo lo que he logrado ha sido porque ustedes me enseñaron a superarme constantemente.

And thanks to Mariana. When the world was reaching a dark time, you were and continue to be the brightest light to shine over my path.

CO-AUTHORSHIP STATEMENT

Chapter 3 is a version of an article published in Microbiology Spectrum: Díaz-Cruz, G.A., Liu, J., Tahlan, K., Bignell, D.R.D. 2022. Nigericin and Geldanamycin Are Phytotoxic Specialized Metabolites Produced by the Plant Pathogen *Streptomyces* sp. 11-1-2. 10(2). https://doi.org/10.1128/spectrum.02314-21. The study concept was designed by D.R.D. Bignell, G.A. Díaz-Cruz and K. Tahlan. The work was performed by G.A. Díaz-Cruz except for the BiG-SCAPE genomics analysis, which was conducted by J. Liu. Equipment and materials were provided by D.R.D. Bignell and K. Tahlan. The LC-MS^2 analysis was facilitated by K. Tahlan. The manuscript was drafted and prepared by G.A. Díaz-Cruz and D.R.D. Bignell, with input from the co-authors.

Chapter 4 is a version of a manuscript in preparation for submission to Scientific Reports. The study concept and methodology was designed by D.R.D. Bignell and G.A. Díaz-Cruz. The experimental work was performed by G.A. Díaz-Cruz except for the LC-MS^2 analysis, which was performed by the BioZone Mass Spectrometry Facility at the University of Toronto. The manuscript was drafted and prepared by G.A. Díaz-Cruz, with editorial input from D.R.D. Bignell.

Chapter 5 is a version of a manuscript in preparation for future submission. The study concept and methodology was designed by D.R.D. Bignell and G.A. Díaz-Cruz. The experimental work was performed by G.A. Díaz-Cruz, and the manuscript was drafted and prepared by G.A. Díaz-Cruz with editorial input from D.R.D. Bignell.

TABLE OF CONTENTS

LIST OF FIGURES

LIST OF TABLES

LIST OF SYMBOLS, ABBREVIATIONS AND NOMENCLATURE

ACP: acyl carrier protein

ACT: actinorhodin

ANI: average nucleotide identity

ANOVA: analysis of variance

antiSMASH: antibiotics and secondary metabolite analysis shell

$Apra^R$: apramycin resistance

ARR: atypical response regulator

AS: acid scab

AT: acyltransferase

ATP: Adenosine triphosphate

BGC: Biosynthetic gene cluster

BiG-SCAPE: Biosynthetic Gene Similarity Clustering and Prospecting Engine

bp: base pair

CAGECAT: Comparative Gene Cluster Analysis Toolbox

CCR: carbon catabolite repression

c-di-GMP: cyclic diguanylate

CFA: coronafacic acid

CFA-Ile: *N*-coronafacoyl-L-isoleucine

CFU: colony-forming units

CMA: coronamic acid

CoA: coenzyme-A

COR: coronatine

CS: common scab

CSR: cluster-situated regulator

DMSO: dimethyl sulfoxide

DNA: deoxyribonucleic acid

dNTPs: Deoxynucleoside triphosphates

ECF: extracytoplasmic function

EFE: ethylene-forming enzyme

EMP: Embden Meyerhof-Parnas

FBMN: Feature-based molecular networking

GBL: gamma-butyrolactones

GCF: gene cluster family

GNPS: Global Natural Products Social Molecular Networking

GSY: Gause's No. 1 synthetic with yeast extract medium

HPLC: High performance liquid chromatography

Hyg^R: hygromycin resistance

IAA: indole-3-acetic acid

IIMN: Ion identity molecular networking

ISP-4: International Streptomyces project medium 4

JA: jasmonic acid

JA-L-Ile: jasmonic acid-isoleucine

Kan^R: kanamycin resistance

KS: ketosynthase

LB: lysogeny broth

LC-MS: liquid chromatography mass spectrometry

$LC\text{-}MS^2$: liquid chromatography-tandem mass spectrometry

m/z: mass-to-charge ratio

Mb: megabases

MIBiG: Minimum information about a biosynthetic gene cluster

MMM: minimal medium with mannitol

mMYM: modified Maltose-Yeast Extract-Malt Extract agar

NA: nutrient agar

NADPH: Nicotinamide adenine dinucleotide phosphate

NAG: *N*-Acetylglucosamine

NAP: Network annotation propagation

NCBI: National Center for Biotechnology Information

NRP: Non-ribosomal peptide

NRPS: Non-ribosomal peptide synthase

OBA: oat bran agar

OSMAC: one-strain, many compounds

P buffer: Protoplast buffer

PAI: pathogenicity island

PCD: programmed cell death

PCP: peptidyl carrier protein

PCR: Polymerase chain reaction

PEG: polyethylene glycol

PI: pimaricin-inducer factor

PK: polyketide

PKS: polyketide synthase

PMA: potato mash agar

PPP: Pentose phosphate pathway

REBASE: Restriction Enzyme Database

RED: undecylprodigiosin

RM: Restriction-methylation

RNA: ribonucleic acid

RP-HPLC: reverse-phase high performance liquid chromatography

SA: starch asparagine agar

SARP: *Streptomyces* antibiotic regulatory proteins

SFM: soy flour mannitol agar

SLB: sucrose lysogeny broth

SM: specialized metabolites

SOB: super optimal broth

SOC: super optimal broth with catabolite repression

T1PKS: Type I Polyketide synthase

T2PKS: Type II Polyketide synthase

T3PKS: Type III Polyketide synthase

TB buffer: tris-borate buffer

TBE buffer: Tris base-boric acid-EDTA buffer

TCS: two-component system

TE buffer: Tris-EDTA buffer

TE: thioesterase

TMA: trimethylamine

tRNA: transfer RNA

TSA: tryptic soy agar

TSB: tryptic soy broth

TSB-S: tryptic soy broth with starch

v/v: volume/volume

w/v: weight/volume

wHTH: winged-Helix-turn-helix

YEME: Yeast extract-malt extract

YMS: yeast extract-malt extract broth-soluble starch agar

YPD: yeast extract-peptone-dextrose

YT: yeast extract-tryptone

CHAPTER 1

INTRODUCTION

1.1 The *Streptomyces*: General characteristics

Streptomyces is a genus within the phylum Actinobacteria, which is comprised of Gram-positive bacteria found in a wide range of environments, including many different types of soil (Zhao et al. 2020a; Besaury et al. 2021; Duangupama et al. 2021), plants (Viaene et al. 2016; Rey and Dumas 2017), insects (Chevrette et al. 2019), marine sediments and organisms (Seipke et al. 2012), among others. In soils, it is estimated that *Streptomyces* species can be found at concentrations of 10^5-10^7 colony-forming units per gram (CFU/g), and this can vary due to environmental and management conditions (Schlatter et al. 2009; Bakker et al. 2010; Kinkel et al. 2012; Andam et al. 2016; Hamid et al. 2020). Many species have been isolated and widely studied due to the production of metabolites utilized in plant, animal, and human health, including many with antimicrobial or antitumor activity (Donald et al. 2022). To date, more than 600 validated species of *Streptomyces* have been included in the "List of Prokaryotic names with Standing in Nomenclature" database (https://lpsn.dsmz.de) (Parte et al. 2020). However, numerous strains are frequently isolated and analyzed for new bioactive chemical compounds (Donald et al. 2022).

Streptomyces species usually contain a single linear chromosome ranging from 5-12 Mb, with one to four plasmids that can be linear or circular and, in some cases, very large (Caicedo-Montoya et al. 2021). Furthermore, *Streptomyces* genomes are characterized by a G+C content of ~60-70%, which is much higher than that of other prokaryotes (Zhou et al. 2012; Tian et al. 2016; Becher et al. 2020). A large-scale analysis of more than 700 *Streptomyces* genomes has shown the presence of a core of proteins (or core genome) in the

central region of the chromosome, while the arms of the chromosome contain variable regions characterized by presence of biosynthetic gene clusters (BGC), carbohydrate-active enzymes, and genes with TTA codons, suggesting that the arms are more likely to evolve rapidly and provide diversity within the genus (Nikolaidis et al. 2023).

Streptomyces species are also characterized by their ability to produce spores (Manteca and Sanchez 2009; Bobek et al. 2017), which allows for a greater dispersal of these non-motile organisms through different methods (Becher et al. 2020; Muok et al. 2021).

1.2 The life cycle of *Streptomyces*

Streptomyces are established in different environments by growing as a mycelium, a feature that distinguishes them from most other bacteria but is shared with filamentous fungi (Fig. 1.1). After finding favourable environmental conditions, a *Streptomyces* spore will germinate and its metabolism will be activated. It has been hypothesized that spores contain some metabolites and enzymes like trehalose and hydrolases that are readily available for germination (Bobek et al. 2017); however, there is also evidence of many different classes of proteins being synthesized within just a few hours after dormancy disruption, with a predominance of energy metabolism-associated proteins (Strakova et al. 2013). Furthermore, in *Streptomyces coelicolor,* spore germination activates biosynthetic gene clusters, providing metabolites with antimicrobial activity and potential chemical signals for interaction with other microorganisms (Čihák et al. 2017).

The active spores develop a germ tube that displays apical growth due to a complex system of proteins named the polarisome (Flärdh et al. 2012). In this system, the protein DivIVA accumulates at the tip and guides the development of the vegetative hyphae, where

compounds such as peptidoglycan and teichoic acids are synthesized and assembled (Flärdh 2003; Flärdh and Buttner 2009). Internal and external factors can regulate this process, and in both cases, the phosphorylation of DivIVA by a Serine/Threonine protein kinase called AfsK is proposed as the primary regulatory mechanism. Interestingly, the effect of AfsK can be reverted by the phosphoprotein phosphatase SppA (Passot et al. 2022).

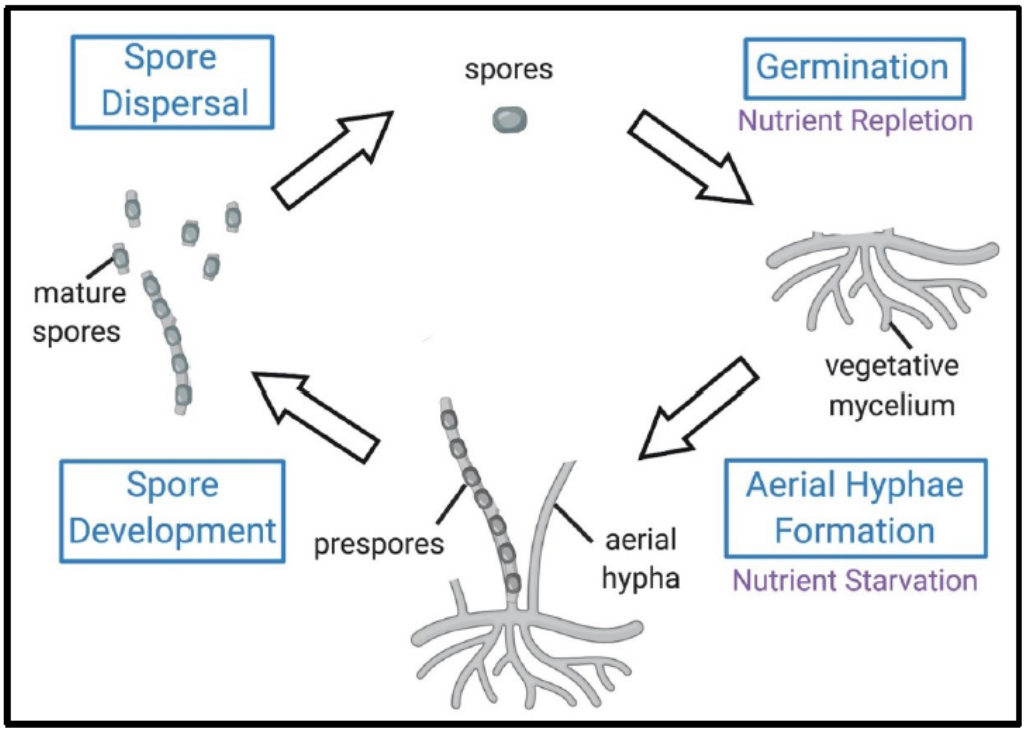

Figure 1.1. The life cycle of *Streptomyces*. Figure provided by Yuting (Phoebe) Li.

Similarly, hyphal branching occurs through the action of the polarisome. Here, sections of the polarisome are split and remain latent until the apical tip is far enough away to initiate new growth (Hempel et al. 2008, 2012). Eventually, the vegetative hyphae develop septa that do not fully separate the cells, but they provide a level of compartmentalization that differs from the cell segregation that occurs during spore formation (Jakimowicz and Van Wezel 2012). The compartmentalization and apical growth depend on the protein FtsZ,

which forms a Z-ring that guides the synthesis of peptidoglycan and creates new cell walls (Yang et al. 2017; Bisson-Filho et al. 2020). Other proteins also complement the activity of FtsZ during cell division (collectively named the divisome); however, at the hyphal level, the actinobacterial-specific protein SepX interacts with FtsZ and is critical for the integrity of the Z-ring and, subsequently, of the hyphae (Bush et al. 2022).

Upon nutrient depletion, the growth of the vegetative hyphae ceases, and aerial hyphae formation is initiated. This process requires the activity of the *bld* (bald) genes (named for the smooth, shiny appearance of the colonies in their absence), which function as global regulators of both morphological development and specialized metabolism in some cases (Hackl and Bechthold 2015). The aerial hyphae grow upright and impart a fuzzy appearance to the colony surface, partly due to the production of SapB, a lantibiotic-like peptide that acts as a biological surfactant (Tillotson et al. 1998). Immature SapB is produced in the cell and is post-translationally modified to allow its exportation from the cell to cover the hyphal surface, thus enabling the hyphae to break surface tension and grow upwards (Willey et al. 2006). Moreover, the presence of proteins called chaplins and rodlins is also necessary to provide structural support and hydrophobicity to the aerial hyphae (Flärdh and Buttner 2009).

The formation of aerial hyphae is followed by the production of spores, which occurs through two parallel processes. First, the tip of the hyphae becomes a sporogenic cell by transitioning from an elongation into a cell division state. This transition occurs due to the expression of the *whi* (white) genes (named for the lack of the spore-associated pigment in their absence) (Willemse et al. 2012) and the action of FtsZ, which creates helices that turn into rings, thus establishing a septum that physically separates each compartment (Flärdh and

Buttner 2009). Then, the protein MreB finalizes the ring formation when a thick cell wall is created around the spore (Mazza et al. 2006). At the same time, multiple copies of the chromosome are produced in the sporogenic cell, and a single copy is correctly segregated into each spore compartment due to the function of several proteins including FtsK, ParA, ParB, and SMC (Wang et al. 2007; Dedrick et al. 2009). Finally, the spore cell wall is completed by adding peptidoglycan, rodlins, chaplins, and hydrolases targeting the hyphal cell wall to facilitate the dispersal of the spores (Claessen et al. 2004; Dedrick et al. 2009). The *Streptomyces* spores are mainly composed of sugars and proteins that confer basic protection against osmotic changes and other stress sources (Bobek et al. 2017).

Recently, it was determined that ~10% of *Streptomyces* species could undergo an exploratory behaviour instead of the typical sporulation life cycle. This behaviour is prompted by glucose depletion, pH changes, and volatile compounds like trimethylamine (TMA) that signal the necessity of exploring the substrate for better resources to engage in sporulation (Jones et al. 2017). Furthermore, *Streptomyces venezuelae* in exploratory mode produces alternative siderophores to take up iron from the environment, thus limiting the element's availability to other microorganisms (Shepherdson and Elliot 2022).

1.3 Metabolism of *Streptomyces*

1.3.1 Carbon metabolism

The life cycle of *Streptomyces* requires the activation of different metabolic pathways to process the resources needed to obtain full development. Primary metabolism in *Streptomyces* refers to the processes of anabolic and catabolic reactions to obtain energy, polysaccharides, nucleic acids, proteins, lipids, and biomass (Hodgson 2000).

Carbon is a significant nutritional resource present in multiple environments. To take advantage of this element, *Streptomyces* have evolved different pathways that convert carbohydrates into glucose, which is then metabolized into energy using the Embden-Meyerhof-Parnas (EMP) pathway and the pentose phosphate pathway (PPP) (Hodgson 2000). The EMP or glycolysis pathway converts glucose from the environment into pyruvate and results in an energy gain in the form of ATP, whereas the pentose phosphate pathway provides pentoses for nucleotides and produces NADPH, which provides energy in multiple reactions (Cohen 2011). Both processes require a concerted effort of multiple enzymes working sequentially; more importantly, these pathways interconnect at different steps.

1.3.2 Complex carbohydrates and disaccharides

In natural settings, glucose and simple carbohydrates are limited. Instead, the presence of complex carbohydrates of different origins (i.e., arthropods, fungi, plant litter) is more prominent, but *Streptomyces* cannot immediately use them. Instead, they have evolved to employ enzymes that can catabolize complex polysaccharides into monomers (Hodgson 2000; Chater et al. 2010).

Streptomyces genomes encode a diverse array of extracellular and intracellular enzymes. For example, there are α-amylases present across *Streptomyces* species that target the glycosidic linkage between glucose units in starch, a plant carbohydrate, resulting in the production of disaccharides that can be more easily imported into the cells (Lakshmi et al. 2020; Visvanathan et al. 2020). Species like *Streptomyces gulbargensis* (Syed et al. 2009), *Streptomyces* sp. D-1 (Chakraborty et al. 2009) and *S. avermitilis* (Hwang et al. 2013), among

others, have been reported as α-amylase producers with good activity over starch from pure and mixed sources.

Streptomyces also use cellulases, which catabolize cellulose, a structural component of plant tissues. The enzymatic activity is carried out by cleaving the β-1,4 linkages, resulting in glucose units (Hodgson 2000). However, cellulose also occurs as more complex matrices like hemicellulose, xylan, and lignin, which require separate enzymes that target other specific sugar linkages (Houfani et al. 2020). The enzymatic activity of cellulases can yield different products, such as glucose or cellobiose, which induce more cellulolytic activity upon accumulation (Hodgson 2000). *Streptomyces* species with cellulolytic capabilities are often associated with plants or herbivorous organisms. For example, *Streptomyces* sp. DpondAA-B6 and *Streptomyces* sp. SirexAA-E were isolated from herbivorous insects, and both showed high cellulolytic activity in proteomic and transcriptomic analyses (Book et al. 2014). Similarly, soil-isolated *Streptomyces* sp. F1 and F7 show good catabolic activity against different complex polysaccharides, including cellulose (de Melo et al. 2018).

Streptomyces can also produce chitin-degrading enzymes. Chitin is mainly found in fungi and the exoskeleton of arthropods, and it is sequentially broken down into *N*-acetylglucosamine (NAG) units that act as carbon and nitrogen sources (Chater et al. 2010; Lacombe-Harvey et al. 2018). Furthermore, NAG is highly relevant as it is a structural component of the bacterial cell wall, and it functions as a regulator of specialized metabolism in bacteria, particularly in *Streptomyces* (see Section 1.3.3.4) (van der Aart et al. 2018).

Many of the complex carbohydrates are not immediately degraded into monomers. Instead, some stable disaccharides remain at the end of the enzymatic activity. For example, maltose follows the degradation of starch (Hwang et al. 2013), or cellobiose remains after

cellulose catabolism (Book et al. 2014). Therefore, other enzymes are needed to further facilitate the degradation of compounds into monomers that can be absorbed by bacterial cells. For example, *Streptomyces hygroscopicus* 9628 shows good cellulolytic activity parallel to intracellular β-glucosidase activity, which degrades cellobiose into glucose (Spear et al. 1993).

1.3.3 Specialized metabolism

The products of primary metabolism, like nucleic acids, lipids, amino acids, etc., act as building blocks utilized by different organisms to produce a plethora of chemical compounds named specialized metabolites (Romero-Rodríguez et al. 2018). For some time, these metabolites were known as "secondary metabolites" based on the notion that they had a less significant role in the success of the organism. However, there is a better understanding regarding their biosynthesis and role in nature, and although this term is no longer used, older literature retains the term instead of specialized metabolites (Davies 2013; Fernández-Martínez and Hoskisson 2019).

The specialized metabolites include peptides, polyketides, terpenoids, and alkaloids (O'Connor 2015), many of which are produced by *Streptomyces* species and are used in medicine and agriculture to treat different types of human, animal, and plant diseases (Donald et al. 2022). However, from an ecological point of view, these compounds are part of intricate interactions between microbes, plants and animals, with great value for the ecosystem (O'Brien and Wright 2011).

Streptomyces specialized metabolites are proposed to have roles as mediators of mutualistic interactions or as part of predatory/competitive interactions (O'Brien and Wright 2011). Within those main categories, more specific roles have been postulated according to the ecological niches from which the bacteria are isolated and the confirmed biological activity of their specialized metabolites (Tyc et al. 2017).

Mutualistic interactions between *Streptomyces* and eukaryotes have been widely studied. *Streptomyces* can colonize and live within plant tissue (endophytes) or be part of the root microbial communities (Viaene et al. 2016; Rey and Dumas 2017). For example, the strain *S. hygroscopicus* OsiSh-2 confers protection against the rice fungal pathogen *Magnaporthe oryzae* by boosting the plant immunity systems and helping in carbon and nitrogen fixation while also producing antimicrobial compounds (Gao et al. 2021). There are also mutualistic interactions with animals. *Streptomyces* sp. SPB74, a southern pine beetle (*Dendroctonus frontalis*) symbiont, produces the polyene peroxide mycangimycin, which protects the beetle from an antagonist fungus, *Ophiostoma minus* (Scott et al. 2008; Oh et al. 2009). Another strain, *Streptomyces globisporus* SP6C4, isolated from strawberry pollen and flowers, is dispersed by pollinator bees. Interestingly, *S. globisporus* SP6C4 protects the plants against the causal agent of gray mold, *Botrytis cinerea*, and the bees against the entomopathogenic bacteria *Paenibacillus larvae* and *Serratia marcescens* (Kim et al. 2019).

On the other hand, antimicrobial and phytotoxic compounds represent the competition and predatory roles of specialized metabolites, respectively. It has been proposed that bacteria perform exploitative competition, in which there is indirect competition for nutritional resources, and interference competition, in which one organism harms another directly (Traxler and Kolter 2015). The role of antimicrobial compounds may be more

suitable for exploitative competition since the natural settings usually harbour many different microbial species attempting to access the same resources (Cornforth and Foster 2013; Traxler and Kolter 2015). Moreover, antimicrobials at low concentrations act as signaling molecules for inter- and intra-species communication; the outcome of these communications is diverse and dependent on the strains involved, as some *Streptomyces* seem to increase the production of antimicrobials to inhibit competitors, while others remain unaffected (Vaz Jauri and Kinkel 2014).

Some specialized metabolites are detrimental to plants due to their phytotoxic activity. A vast number of them are produced by *Streptomyces* strains, as previously reviewed (Shi et al. 2020). For example, *Streptomyces scabiei* and other closely related species produce thaxtomin A, a highly phytotoxic compound that causes necrosis and damage to different plant tissues (Li et al. 2019c). The herbicide bialaphos, produced by *Streptomyces hygroscopicus*, inhibits the glutamine synthetase enzyme, leading to the accumulation of ammonia and cell death (Tachibana and Kaneko 1986). Another strain, *Streptomyces* sp. KRA18-249, produces the compound 249-Y1, also known as rubiginone D2, which showed high herbicidal activity and reduced chlorophyll content in different plants (Umurzokov et al. 2022).

1.3.3.1 Pathways for specialized metabolism

Most specialized metabolites are small molecules assembled from a few precursors. In order to obtain more elaborate structures, it is necessary to utilize multiple genes encoding proteins with specific functions. A group of genes working together towards a particular end product is called a biosynthetic gene cluster (BGC) (Osbourn 2010). BGCs are not limited to bacteria, as they can also be found in fungi and plants. However, given the vast array of

specialized metabolites for human applications that are derived from bacteria, especially *Streptomyces* and other closely related Actinobacteria, there has been great interest in understanding how BGCs are composed and regulated in this group for potential industrial use (Donald et al. 2022).

In *Streptomyces*, there are usually more than thirty BGCs responsible for producing different specialized metabolites in each strain (Nett et al. 2009; Lee et al. 2020a). The BGCs can be categorized based on the core biosynthetic enzymes and the resulting metabolite. Thus, there are macrolide polyketides, aromatic polyketides, non-ribosomal peptides, hybrid peptide-polyketides, terpenoids, etc. (Nett et al. 2009; Hwang et al. 2014). For this work, I will focus on polyketides (PKs) and non-ribosomal peptides (NRPs), given their significance for the *Streptomyces* genus.

1.3.3.2 Polyketide biosynthesis

The PK metabolites are built from precursors such as acetyl-coenzyme A (CoA) or malonyl-CoA. The presence of multifunctional enzymes called polyketide synthases (PKSs) is required for the biosynthesis of PKs. However, the architecture of the PKSs can vary and occurs in three types, namely, type I, II, and III, which can all be found in *Streptomyces* (Hwang et al. 2014).

The type I PKS (T1PKS) is characterized by large modules containing multiple enzyme domains that work like an assembly line (Nivina et al. 2019). The first module is the loading module, and it contains two main domains, an acyltransferase (AT) and an acyl carrier protein (ACP). A starter unit is selected by the AT which transfers the acyl group and attaches it to the ACP domain via a thioester linkage. Then, the extension or elongation modules, comprised of a ketosynthase (KS), AT, ACP, and other accessory domains,

assemble the compound backbone by adding extension units such as methylmalonyl-CoA or ethylmalonyl-CoA. Finally, a termination module consisting of a thioesterase domain (TE) performs hydrolysis for linear compounds or cyclization for macrocyclic compounds (Hwang et al. 2014, 2020; Nivina et al. 2019; Risdian et al. 2019).

The type II PKS (T2PKS) assembles the metabolites using discrete polypeptides with a specific function, as opposed to the modular system used in T1PKSs (Wang et al. 2020). Moreover, iterative reactions are required for compound elongation with T2PKSs. The first step, or priming, involves two ketosynthases, KS_{α} and KS_{β}, which process the precursor unit and determine the chain length, respectively. Next, an ACP starts the chain's elongation, and other enzymatic reactions result in the extended compound. The product is finished by a cyclization or aromatization of the elongated chain, followed by post-PKS tailoring modifications (Hwang et al. 2014, 2020; Risdian et al. 2019; Wang et al. 2020).

The type III PKS (T3PKS) uses homodimeric ketosynthases that catalyze the condensation of a starter unit, an acyl-CoA, within their active sites. Then, the ketosynthases work iteratively to perform the extension using more acyl-CoA units. The final cyclization step is then carried out by different condensation enzymes (Katsuyama and Ohnishi 2012; Palmer and Alper 2019).

1.3.3.3 Non-ribosomal peptide biosynthesis

The biosynthesis of NRPs is performed by three multidomain modules: initiation, elongation, and termination. The initiation module contains an adenylation (A) domain, which selects the starter unit and loads it onto a thiolation (T) or peptidyl carrier protein (PCP) domain. The starter units for NRPs are proteinogenic and non-proteinogenic amino acids obtained from the primary metabolism (Süssmuth and Mainz 2017).

Then, the amino acid is transported to the elongation module, where condensation (C) and other secondary domains are present. The elongation module also contains an A and T/PCP domain, which allows for extension of the new peptide. Finally, a thioesterase (T) domain comprises the termination module, where hydrolysis or macrocyclization is performed, and the newly synthesized compound is released (Süssmuth and Mainz 2017; Hwang et al. 2020; Duban et al. 2022).

The non-ribosomal peptide synthetases (NRPS) can be further divided into types based on the arrangement of the modules. In a linear NRPS, each module works once, while in a non-linear NRPS, at least one domain is used multiple times during biosynthesis. There are also iterative NRPSs, in which the modules are utilized multiple times in a cycle-like way until the end product is obtained. Lastly, stand-alone NRPSs are multidomain modules or single domains that supply other biosynthetic processes with specific compounds required to finish a metabolite biosynthesis (Süssmuth and Mainz 2017).

1.3.3.4 Regulation of specialized metabolism: Global regulators

When resources are depleted by either competition or the transition from vegetative to developmental stages, there are significant changes in spore development and the production of specialized metabolites in *Streptomyces*. These processes must be tightly coordinated across the organism. *Streptomyces* have genes encoding regulatory mechanisms that intervene with morphological differentiation and specialized metabolite production simultaneously (Fig. 1.2). These are commonly referred to as global regulators (Hoskisson and Fernández-Martínez 2018).

In *Streptomyces*, several of the *bld* genes encode global regulators. The best-studied *bld* gene, *bldA*, encodes the only tRNA recognizing the leucine-specific TTA codon, which

is rare in *Streptomyces* genomes (Lawlor et al. 1987; Leskiw et al. 1991). Many genes contain TTA codons, especially regulatory genes within BGCs, but they are absent from essential genes; thus, it is likely that *bldA* plays a regulatory role at a global level in *Streptomyces* (Chandra and Chater 2008). Mutant strains of *bldA* generally display reduced production of specialized metabolites and no aerial hyphae development (Koshla et al. 2017; Hou et al. 2018), although a *Streptomyces clavuligerus bldA*-mutant strain still expressed proteins with TTA codons, suggesting that an alternative mechanism for translation is in place (Ferguson et al. 2016).

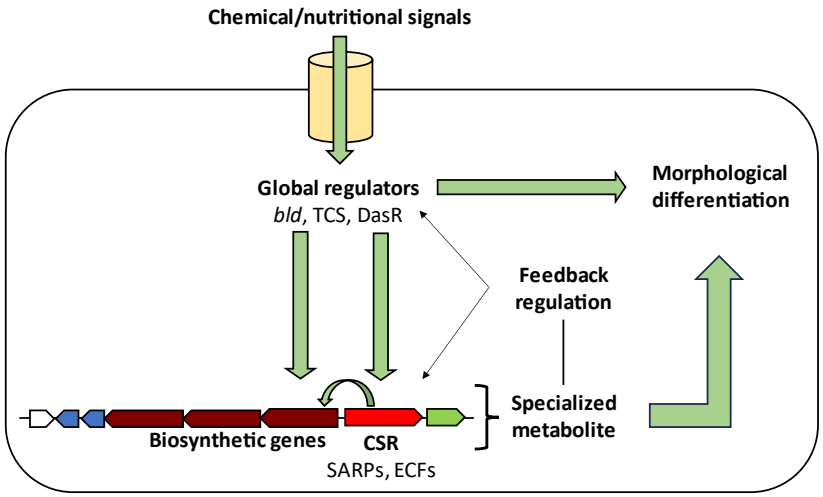

Figure 1.2. Schematic of specialized metabolite regulation in *Streptomyces*.

Another well-studied *bld* gene considered a global regulator is *bldD*. This gene is involved in aerial hyphae formation and differentiation into spores, and it also regulates the transcription of multiple genes associated with antibiotic production in different *Streptomyces* species (Elliot et al. 2001; Schumacher et al. 2017; Li et al. 2019a; Yan et al. 2020). The BldD protein binds to the messenger molecule cyclic diguanylate (c-di-GMP),

resulting in a complex called BldD2-(c-di-GMP)$_4$, which is required for binding to DNA and acts as a regulator of expression (Schumacher et al. 2017).

Global regulation also occurs due to the activity of two-component systems (TCS), such as the MtrAB system. MtrA is a response regulator protein associated with the sensor kinase MtrB. The deletion of *mtrA* in *S. coelicolor* results in a bald phenotype, upregulation of actinorhodin, streptorubin B, undecylprodigiosin, and downregulation of desferrioxamines and germicidin A production (Zhang et al. 2017; Som et al. 2017). Moreover, *bldD* is a target of MtrA, representing another level of regulation in *Streptomyces* (Zhang et al. 2017). Other TCSs in *Streptomyces* have been previously reviewed (Rodríguez et al. 2013; Hoskisson and Fernández-Martínez 2018).

The transition from the vegetative to sporulation stage in *Streptomyces* involves the programmed cell death (PCD) of mycelial cells. The peptidoglycan from the cell wall is broken down into monomers due to proteolytic activity, making NAG available for the organism (Manteca et al. 2006). NAG acts as a carbon and nitrogen source and a signal recognized by active cells. A phosphotransferase system imports NAG into the cell and modifies it to NAG-6-phosphate, and this is followed by deacetylation performed by NagA. The resulting glucosamine-6-phosphate binds to the protein DasR, a GntR-like global transcriptional regulator, thus impeding it from binding to specific elements called *dasR*-responsive elements (*dre*), which are located throughout the *Streptomyces* genome and associated with a variety of genes, including transcriptional activators in antibiotic gene clusters (Colson et al. 2006; Rigali et al. 2006, 2008). However, the addition of NAG and subsequent DasR regulation is dependent on the nutritional conditions in which *Streptomyces* is growing. In *S. coelicolor* grown under "feast" conditions (i.e., nutrient-rich media), NAG

blocks morphological development and production of undecylprodigiosin and actinorhodin, whereas when *S. coelicolor* is grown under "famine" conditions (i.e., minimal media), the addition of NAG resulted in increased antibiotic production (Rigali et al. 2008). This has been proposed as evidence that *Streptomyces* cells can differentiate between NAG originating from external sources (chitin degradation) and the NAG obtained from the PCD process (cell wall lysis), which represent nutrient-rich and nutrient-poor conditions, respectively (Rigali et al. 2008). In *Streptomyces cinnamonensis*, DasR acts as an activator by binding to the promoter region of a CSR and three biosynthetic genes in the ionophore monensin BGC, resulting in upregulation of the metabolite biosynthesis under nutrient rich conditions (Zhang et al. 2016c). The addition of NAG to culture media suppressed the production of monensin, likely due to NAG binding to DasR, thus limiting its activity in the transcription of the genes (Zhang et al. 2016c).

1.3.3.5 Regulation of specialized metabolism: Cluster-situated regulators

As opposed to global regulators, BGCs usually contain one or more genes encoding cluster-situated regulators (CSRs), which modulate the production of the corresponding metabolite rather than controlling the production of multiple metabolites. The CSR-encoding genes are often regulated by global regulators or environmental conditions (Fig. 1.2) (Van Wezel and McDowall 2011; Hoskisson and Fernández-Martínez 2018).

CSRs can belong to several different protein families. For example, the production of actinorhodin (ACT) in *S. coelicolor* is controlled by the CSR ActII-ORF4 (Arias et al. 1999), which is a member of the *Streptomyces* antibiotic regulatory proteins (SARP) family (Wietzorrek and Bibb 1997). The SARP family is characterized by a winged-Helix-Turn-Helix (wHTH) architecture with the presence of an N-terminal motif that binds to DNA and

a C-terminal β-strand hairpin unit that conforms the "wing" (Aravind et al. 2005; Bibb 2005; Romero-Rodríguez et al. 2015). The SARP family is widely distributed among *Streptomyces* species as regulators of different metabolites, as previously reviewed (Romero-Rodríguez et al. 2015).

Recently, the extracytoplasmic function (ECF) sigma factors have been described as regulators in *Streptomyces*. Sigma factors are part of the RNA polymerase complex, providing promoter recognition and specificity during transcription (Romero-Rodríguez et al. 2015). Based on their function, sigma factors have been categorized into four groups, as previously reviewed (Heimann 2002; Sun et al. 2017). In this work, I will only focus on ECFs, which belong to group 4.

ECFs are a subgroup of sigma factors that contain only two of the four domains present in primary sigma factors, namely, domains σ^2 and σ^4. ECF domains bind at the -10 and -35 positions within the promoter, thus acting as transcription activators (Sineva et al. 2017; Hoskisson and Fernández-Martínez 2018). ECFs are usually associated with an anti-sigma factor that negatively regulates their activity. The ECF interacts with an anti-sigma factor, which prevents the ECF from being recruited by the RNA polymerase, thus blocking gene expression. Upon induction of a triggering signal, the anti-sigma factor bound to the ECF is released, and the RNA polymerase can recruit it, allowing for the recognition of the promoter sequence and its activation (Hoskisson and Fernández-Martínez 2018).

In *Streptomyces*, ECFs are typically associated with morphological development and stress signaling (López-García et al. 2018). However, one ECF has been identified as a CSR in this genus. In *Streptomyces albus*, the gene *antA*, located in the antimycin BGC, encodes the ECF sigma factor σ^{AntA}, which regulates the expression of *antG* and *antH,* two genes that

are located in separate operons within the same cluster (Seipke et al. 2014). Interestingly, σ^{AntA} is an orphan ECF, as no anti-sigma is associated with it (Seipke et al. 2014). Instead, the ECF is controlled by the ClpXP protease, which also represents a novel mechanism of ECF regulation (Bilyk et al. 2020).

1.3.3.6 Regulation by chemical and nutritional signals

The presence of small molecules also regulates specialized metabolite biosynthesis in *Streptomyces*. The chitin monomer NAG is known for acting as a regulator of specialized metabolites thanks to its interaction with the DNA-binding protein DasR (see Section 1.3.3.4). Hormone-like signaling molecules can alter specialized metabolite production by interacting with proteins that regulate gene expression. The first small molecule identified as a regulator was the autoregulatory factor, or A-factor, a γ-butyrolactone (GBL) that is required for streptomycin production in *S. griseus* (Takano 2006). Since then, other GBLs and other small molecules (e.g., furans, γ-butenolides) have been characterized as regulators of specialized metabolism that are distributed across various *Streptomyces* species (Takano 2006; Niu et al. 2016). In addition, species-specific autoregulatory factors have been described, including the PI factor in *Streptomyces natalensis* and *N*-methylphenylalanyl-dehydrobutyrine diketopiperazine in *Streptomyces globisporus* (Niu et al. 2016).

Metabolite biosynthesis can also be autoregulated via feedback mechanisms. For example, in *S. venezuelae*, the metabolite jadomycin B (JadB) is detected by the atypical response regulator (ARR) JadR1. In the presence of low concentrations of JadB and the intermediate JadA, JadR1 binds to a region upstream of *jadJ*, the first gene in the BGC, thus increasing the BGC expression. When concentrations of JadB or JadA are high, they act as ligands to JadR1, causing the dissociation of the protein from the promoter regions of *jadR1*

and *jadJ*, and the BGC is inactivated (Wang et al. 2009). The same study reported similar results with undecylprodigiosin (RED) and the NarL-type ARR RedZ in *S. coelicolor* (Wang et al. 2009). Specialized metabolites auricin (Kutas et al. 2013), sansanmycin (Li et al. 2013), and simocyclinone (Horbal et al. 2012) also show autoregulation by a feedback mechanism of intermediates and/or end products (Fig. 1.2).

In natural and artificial settings, *Streptomyces* may be presented with multiple carbon sources simultaneously, either by the action of their extracellular enzymes or by other organisms in the same space. The order of carbon source utilization is determined by the enzymatic machinery of the cell, which favours some carbon sources over others by regulating or repressing specific pathways. In *S. coelicolor*, it was demonstrated that glucose uptake inhibits the utilization of other carbon sources like galactose and fructose (Hodgson 1982). This process, called carbon catabolite repression (CCR), affects morphological development in different *Streptomyces* (Hodgson 2000; Romero-Rodríguez et al. 2017).

In *Streptomyces noursei*, the yield of nystatin and biomass was differentially affected by the carbon source utilized during fermentation (Jonsbu et al. 2002). Furthermore, glucose negatively affects the biosynthesis of ACT by repressing the transcription of the regulator *afsR2* in *S. lividans*. When supplied with glycerol as the carbon source, *afsR2* is activated, and ACT is produced (Kim et al. 2001). Multiple examples of similar mechanisms have been previously reviewed (Romero-Rodríguez et al. 2017).

1.3.3.7 Methods to study specialized metabolism in *Streptomyces*

The metabolite diversity of *Streptomyces* has generated tremendous interest in these organisms as sources of novel metabolites for different applications. One strategy that is routinely used for exploring the metabolic diversity of *Streptomyces* is the One Strain-Many

Compounds (OSMAC) approach, which involves changing the culture conditions of the organism in order to promote or enhance the production of different or novel compounds (Bode et al. 2002; Romano et al. 2018).

The access to specialized databases and the development of data analysis tools have accelerated and expanded the goal of the OSMAC approach (Romano et al. 2018). The increasing accessibility to high-quality genome sequencing has provided vast information that otherwise would be difficult to elucidate (Palazzotto and Weber 2018). Furthermore, the organization of genomes into BGCs and the modular architecture of most BGCs have facilitated the development of tools like the Minimum Information about a Biosynthetic Gene cluster (MIBiG) database and antiSMASH. The MiBiG database is a collaborative effort that established the guidelines for curated BGCs associated with metabolite biosynthesis (Terlouw et al. 2022). The database serves as a reference for genomic analyses using tools like antiSMASH (Blin et al. 2021), which performs genome mining to compare and predict the presence of BGCs in microbial genomes.

However, the presence of BGCs determined bioinformatically is insufficient evidence of metabolite production. The use of untargeted liquid chromatography-tandem mass spectrometry (LC-MS^2) has proven especially useful in characterizing the metabolic profile of *Streptomyces* strains and other microbes subject to the OSMAC approach (Wu et al. 2015; van Bergeijk et al. 2020; Bayona et al. 2022). The use of LC-MS^2 allows for the detection of low molecular weight (<2000 Da) metabolites in biological samples based on physical separation in a column, while the identification is made by the ionization of the compounds and the resulting fragmentation pattern and mass-to-charge ratio or *m/z* (Kind et al. 2018).

There have been significant advances in the methods, instruments, and data analysis capabilities used to perform untargeted metabolomics studies. The establishment of specialized databases has facilitated and improved the compound annotation following untargeted metabolomics (Chaleckis et al. 2019). In particular, the development of the Global Natural Products Social Molecular Networking (GNPS) platform has gained significant value in recent years. This platform compares and correlates compound spectra, which are then visualized as a network of related metabolites (e.g., intermediates or analogues), even if the compounds do not match known compounds (Wang et al. 2016). Further updates to the platform have made available tools to enhance the identification of compounds, like Network Annotation Propagation (NAP) (da Silva et al. 2018), MolNetEnhancer (Ernst et al. 2019b), Feature-Based Molecular Networking (FBMN) (Nothias et al. 2020) and Ion Identity Molecular Networking (Schmid et al. 2021).

Similar to genomics and metabolomics, there have been significant advances in analyzing global gene expression. The use of polymerase chain reaction (PCR)-based methods was limited to some genes and required previous knowledge of the sequence to study. Hybridization-based microarrays permitted a more extensive study of gene expression, but it also required significant knowledge of the sequences to be analyzed (Wilhelm and Landry 2009; Kukurba and Montgomery 2015). The development of massive parallel sequencing has facilitated the implementation of RNA sequencing (RNA-Seq) studies. This method does not require previous knowledge of the sequences (*de novo* transcriptomics), although using the genome sequence as a reference is also used (reference-based transcriptomics) (McGettigan 2013). The use of transcriptomics for global gene expression in *Streptomyces* has been reviewed elsewhere (Palazzotto and Weber 2018; Lee et al. 2020b).

Overall, the OSMAC approach is now expanded through multi-omics technologies, which provide a more comprehensive analysis of microbial metabolism, providing a framework for the characterization of microorganisms of interest (Fig. 1.3).

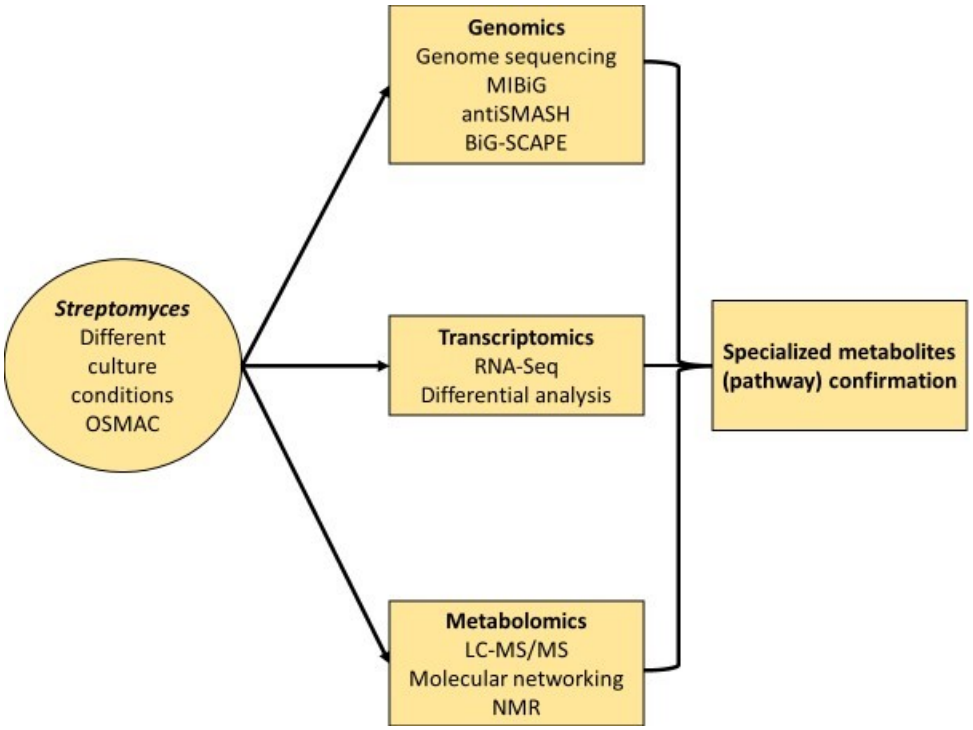

Figure 1.3. Schematic of omics technologies used for studying *Streptomyces* specialized metabolism.

1.4 Plant-pathogenic *Streptomyces*

1.4.1 Common scab disease

Streptomyces species are widely distributed across different ecological settings, and they closely interact with a great variety of organisms. In agricultural settings, *Streptomyces* are commonly considered beneficial bacteria thanks to the production of diverse antimicrobial compounds that exert control over plant pathogenic organisms (Kinkel et al.

2012). However, some *Streptomyces* are capable of parasitic interactions with plants, which results in these species acting as plant pathogens with the ability to cause plant disease.

Common scab (CS) is a plant disease caused by *Streptomyces* spp. and it affects several crops such as carrots (*Daucus carota*), beets (*Beta vulgaris*), radishes (*Raphanus raphanistrum* subsp. *sativus*), and potatoes (*Solanum tuberosum* L.) (Clarke et al. 2022). On potatoes, the disease is characterized by superficial, raised, and/or deep pitted scab-like lesions on the tuber surface (Fig. 1.4) (Dees and Wanner 2012). These lesions result from alterations of the tuber tissue that become more apparent as the tuber expands during development, and their size can vary from small lesions to ones covering most of the tuber surface (Loria et al. 2006). The variability in the severity of CS symptoms is thought to be dependent on multiple factors, including the environment, aggressiveness of the strain, and plant susceptibility (Lerat et al. 2009; Khatri et al. 2011; Thangavel et al. 2016; Braun et al. 2017). Moreover, CS can be so severe that the potato tubers are no longer marketable for fresh or industrial consumption, resulting in a loss of profits for farmers. Significant economic losses due to CS have been documented in Canada (Hill and Lazarovits 2005), although the disease has been reported to occur worldwide (Dees and Wanner 2012).

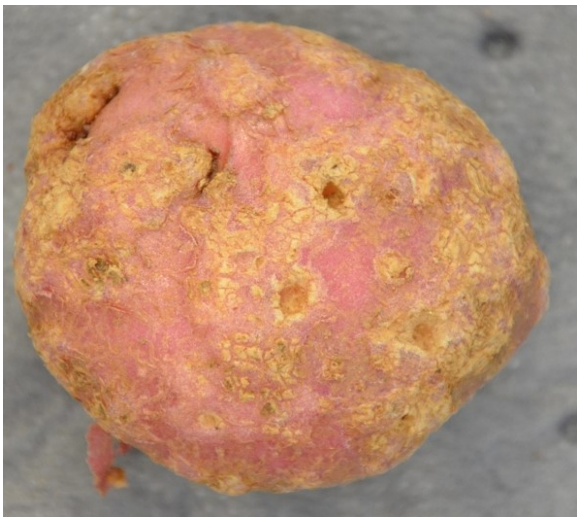

Figure 1.4. Potato showing symptoms of common scab. Image provided by Dawn Bignell.

Other related *Streptomyces*-associated plant diseases include acid scab (AS), which is caused by *Streptomyces acidiscabies* and has very similar disease symptomology as CS, except that it occurs in acidic soils where CS is suppressed (Loria et al. 1997; Tashiro et al. 2012). Netted scab is caused by *Streptomyces reticuliscabiei* and is characterized by brown superficial lesions with a netted pattern (Loria et al. 1997; Bouchek-Mechiche et al. 2000; Pasco et al. 2005). Recently, a disease called fissure scab was described, and it is associated with *Streptomyces solaniscabiei* and other species in South Africa (Cruywagen et al. 2021).

1.4.2 Causal agents of CS disease

Streptomyces scabiei (syn. *Streptomyces scabies*) was the first species to be described as a causal agent of the CS disease (Loria et al. 1997), and the genome of the strain 87-22 was the first to be sequenced and made available. Other *Streptomyces* species have been described as causal agents of CS besides *S. scabiei*, including *Streptomyces europaeiscabiei*, *Streptomyces bottropensis*, *Streptomyces caviscabies*, *Streptomyces turgidiscabies*, and *Streptomyces stelliscabiei*, among others (Jiang et al. 2012; Gong et al. 2017; Sarwar et al. 2017, 2018, 2019a; Lin et al. 2018; Chalupowicz et al. 2022).

1.4.3 Pathogenicity and virulence factors of CS pathogens

The pathogenicity is the capacity of an organism to damage a host, while the virulence is the relative capacity to cause damage to the host (Casadevall and Pirofski 1999). In order to cause disease, plant pathogens use different pathogenicity and virulence factors to facilitate

the colonization and infection of living plant tissues. Thus, a pathogenicity factor can be defined as an essential factor for the establishment of the disease, whereas a virulence factor is not essential but it enhances the severity of the symptoms. CS-causing *Streptomyces* species have the potential to produce different virulence factors that are known or suspected to contribute to the pathogenicity of these organisms, and these have been described in detail elsewhere (Li et al. 2019; Perry and Bignell 2022). In the following sections, I will discuss the specialized metabolites that are known or predicted to function as pathogenicity and virulence factors in plant pathogenic *Streptomyces* spp., and the mechanism of regulation of these factors.

1.4.3.1 Thaxtomin A

Early studies showed that *S. scabiei* can produce chemical compounds with phytotoxic activity (Lawrence et al. 1990). Further characterization determined that *S. scabiei* secretes two members of the thaxtomin family, which consists of cyclic dipeptides (2,5 diketopiperazines) derived from 4-nitro-L-tryptophan and L-phenylalanine (reviewed by King and Calhoun 2009). Thaxtomin production was shown to be highly correlated with the phytotoxicity of *S. scabiei* and the development of scab-like lesions on potato tubers (Lawrence et al. 1990). The main thaxtomin produced by *S. scabiei* is thaxtomin A (Fig. 1.5), and it is considered the main pathogenicity factor contributing to CS disease development by this species on potato tubers and other root crops (Clarke et al. 2022). Thaxtomin A is also produced by other *Streptomyces* species, including *S. turgidiscabies*, *S. acidiscabies* and *S. europaeiscabiei* (Li et al. 2019c).

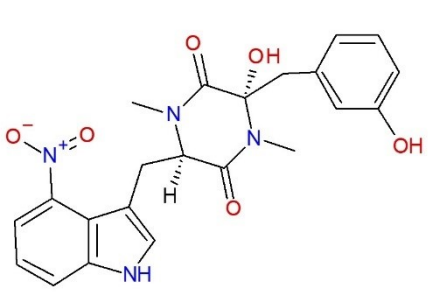

Thaxtomin A

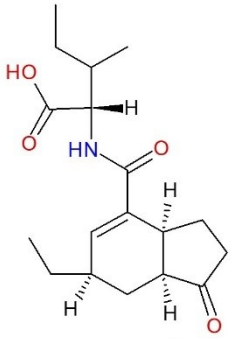

CFA-Ile

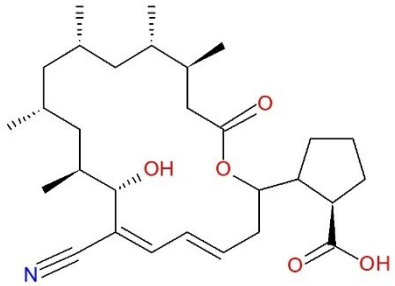

Borrelidin

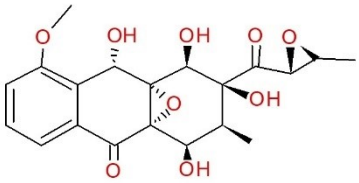

Desmethylmensacarcin

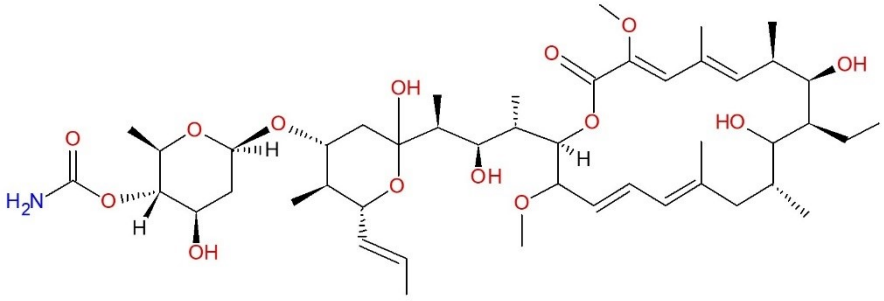

Concanamycin A

Figure 1.5. Phytotoxic specialized metabolites produced by plant-pathogenic *Streptomyces* spp.

To date, thaxtomin A is considered a cellulose biosynthesis inhibitor, although the target at the cellular level remains elusive. Treatment with a range of thaxtomin A concentrations reduces the total length of radish and onion seedlings, and increases cell hypertrophy and necrosis in a dose-dependent manner (Leiner et al. 1996; Fry and Loria 2002). Moreover, tobacco cell elongation and onion cell cycle were shown to be affected by thaxtomin A, suggesting that the cell wall is the target of the molecule (Fry and Loria 2002). Plant assays with thaxtomin A as a herbicide revealed similar effects as those seen by cellulose biosynthesis inhibitors like dichlobenil and isoxaben, thus suggesting it has the same mode of action (King et al. 2001). Furthermore, it was determined that increasing amounts of thaxtomin A disrupt the incorporation of ^{14}C-labeled glucose into the cellulosic cell wall fraction of *Arabidopsis thaliana* seedlings (Scheible et al. 2003). Also, thaxtomin A and isoxaben, separately, caused an atypical programmed cell death process in *A. thaliana* cells, in which no reactive oxygen species or hypersensitive response were detected (Duval et al. 2005). Thaxtomin A seems to interfere with the defence response and physical assembly of the cell wall, allowing the *Streptomyces* to infect the potato tissue. When the infection is recognized, the expanding tissue starts the formation of suberized cells to prevent the spread of the pathogen, thus leading to the formation of scab lesions (Thangavel et al. 2016).

The biosynthesis of thaxtomin A is controlled by a BGC that is located on a pathogenicity island (PAI) along with other known and virulence factors in *S. scabiei* and other scab-causing species (Kers et al. 2005; Zhang et al. 2016b). The BGC is comprised of seven genes that are highly conserved among scab-causing species. Six genes in the cluster

(*txtACBDEH*) are involved in molecular assembly (Healy et al. 2000, 2002; Johnson et al. 2009; Barry et al. 2012; Li et al. 2019b), while the remaining gene (*txtR*) encodes a CSR of thaxtomin biosynthesis (Joshi et al. 2007). TxtR activates the expression of the thaxtomin biosynthetic genes in the presence of the cellooligosaccharides cellobiose and cellotriose, which are subunits of cellulose (Johnson et al. 2007; Joshi et al. 2007). Further studies determined that this regulation occurs due to the interaction of cellooligosaccharides with CebR, a DNA-binding protein that is conserved across diverse *Streptomyces* species (Francis et al. 2015). The binding of cellooligosaccharides to CebR prevents the protein from binding to the cellobiose-binding sites (*cbs*) located both upstream of *txtR* and within *txtB*, thus allowing for expression of the BGC and the production of the phytotoxin (Johnson et al. 2007; Francis et al. 2015; Planckaert et al. 2018).

Thaxtomin A production in *S. scabiei* is also induced by suberin, a lipidic biopolymer that represents a major component of the potato periderm. The presence of suberin in culture media induces the production of cellulases and other enzymes for the degradation of complex carbohydrates while upregulating other proteins involved in the development and specialized metabolites (Padilla-Reynaud et al. 2015).

The biosynthesis of thaxtomin A is additionally controlled by several *bld* gene global regulators in *S. scabiei*. Deleting *bldA* leads to a complete loss of thaxtomin production, likely due to the loss of translation of the *txtR* gene, which contains a TTA codon (Bignell et al. 2014). Deletion of *bldC* also abolishes the accumulation of thaxtomin A, while deletion of *bldD, bldH* and *bldG* reduces but does not abolish thaxtomin production (Bignell et al. 2014).

1.4.3.2 Coronafacoyl phytotoxins

The genome of *S. scabiei* contains a BGC that is closely related to the BGC for the biosynthesis of coronatine (COR), a phytotoxin produced by different pathovars of the plant pathogen *Pseudomonas syringae* (Ichinose et al. 2013). COR consists of a bicyclic hydrindane ring-based polyketide named coronafacic acid (CFA), which is attached to coronamic acid (CMA), an ethylcyclopropyl amino acid derived from L-isoleucine (Bignell et al. 2018). COR induces chlorosis, reduces seedling length, and affects different phytohormone production in tomato leaves (Uppalapati et al. 2005). Furthermore, COR affects callose deposition, a well-established defence mechanism against pathogen infections in plants (Geng et al. 2012). Due to the structural similarity, COR is recognized by the same receptor in plants as jasmonoyl-L-isoleucine (JA-Ile), a signaling molecule derived from jasmonic acid (JA) and involved in the regulation of the plant defence response. Thus, the competition for the receptor is considered a key element in the pathogenicity of *P. syringae* (Katsir et al. 2008). Although *S. scabiei* does not produce COR, it does produce another member of the coronafacoyl family of phytotoxins, *N*-coronafacoyl-L-isoleucine (CFA-Ile; Fig. 1.5), as the main product along with other minor related compounds (Fyans et al. 2015). Pure CFA-Ile induces potato tuber tissue hypertrophy and stunting of radish seedlings in a similar manner as pure COR, though CFA-Ile is less toxic (Fyans et al. 2015). Moreover, potato tissue treated with pure CFA-Ile + thaxtomin A (100:1 ratio) did not show increased tissue damage; however, the overexpression of the CFA-Ile BGC in *S. scabiei* did cause an increase in tissue pitting and necrosis when the strain was inoculated directly over potato tissue (Cheng et al. 2019). These results suggest that a high concentration of CFA-Ile and potentially other intrinsic factors associated with the pathogen development are required for enhanced phytotoxicity. The production of CFA-Ile is regulated by two different CSRs encoded in the BGC. The first one is CfaR, a PAS-LuxR transcriptional activator that binds

upstream of *cfa1* to induce the expression of the metabolite biosynthetic genes (Cheng et al. 2015). CfaR is essential for CFA-Ile production, and expression of the *cfaR* gene is controlled by the products of *bldA*, *bldD,* and *bldG* (Bignell et al. 2014). The other CSR is ORF1, a ThiF-family protein of unknown function. The *orf1* gene is located downstream of and is co-transcribed with *cfaR* (Cheng et al. 2015), suggesting that the protein products work together to control metabolite biosynthesis. Notably, the overexpression of both CfaR and ORF1 greatly enhances the production of CFA-Ile compared to the overexpression of either CfaR or ORF1 alone, suggesting that ORF1 may function as a helper protein for CfaR, though the mechanism of how this occurs remains unknown (Cheng et al. 2019).

Other CS-causing pathogens do not produce CFA-Ile or other coronafacoyl phytotoxins; however, other plant pathogenic bacteria such as *Pseudomonas amygdali, Pectobacterium cacticidium*, and *Xanthomonas campestris* pv. *phomiicola* produce at least one coronafacoyl phytotoxin, and several more species have the genes that would enable the production of these phytotoxins (Bown et al. 2017; Bignell et al. 2018). Interestingly, a number of bacterial strains harbouring coronafacoyl phytotoxin biosynthetic genes are not known to be plant pathogenic. This suggests that coronafacoyl phytotoxins may have a role for the producing organism that extends beyond host-pathogen interactions (Bown et al. 2017; Bignell et al. 2018).

1.4.3.3 Concanamycins

Another potential virulence factor contributing to CS disease is a family of compounds called the concanamycins, which are 18-membered macrocyclic lactones with a β-hydroxyhemiacetal side chain (Kinashi et al. 1984; Haydock et al. 2005). These compounds are not exclusively produced by plant-pathogenic *Streptomyces* as they were first

described from *Streptomyces diastatochromogenes,* but later it was found that concanamycin A (Fig. 1.5) and B are also produced by *S. scabiei* (Kinashi et al. 1984; Natsume et al. 1996). The concanamycins are inhibitors of the eukaryotic vacuolar-type ATPase (V-ATPase) activity, and they have been shown to exhibit antifungal activity and also inhibition of root development in seedlings of different plants (Kinashi et al. 1984; Natsume et al. 2005). The presence of concanamycins has been associated with the development of deep-pitted scab lesions on potato tubers but not with raised lesions, suggesting that concanamycin production by *S. scabiei* may contribute to the type of scab lesion that forms on tubers during disease development (Natsume et al. 2017). The concanamycin BGC contains a CSR, *scab84101,* which encodes an SARP-family regulator, and deletion of these gene abolishes concanamycin production in *S. scabiei* (C. Vincent, personal communication). The *scab84101* coding sequence contains a TTA codon, suggesting that the expression of the cluster is also subject to regulation by the *bldA* tRNA (Haydock et al. 2005). Indeed, the deletion of several different *bld* genes*,* including *bldA,* reduced the expression of multiple genes in the concanamycin BGC, thus confirming the importance of the *bld* gene global regulators for expression of this cluster (Bignell et al. 2014).

1.4.3.4 Phytohormones

The genome of the CS pathogen *S. turgidiscabies* Car8, which was originally isolated from an erumpent scab lesion (Miyajima et al. 1998), contains a plant fasciation (*fas*) operon located on the PAI. The *S. turgidiscabies fas* operon is homologous to the *Rhodococcus fascians fas* operon, which induces leafy galls on plants due to cytokinin biosynthesis (Huguet-Tapia et al. 2011). *S. turgidiscabies* expresses the operon under conditions that

support thaxtomin A production, and it was capable of inducing leafy galls in tobacco and Arabidopsis (Joshi and Loria 2007). It has been proposed that cytokinin production directed by the *fas* operon in *S. turgidiscabies* Car8 is responsible for the development of erumpent lesions on infected tubers, in contrast to the pitted scab lesions caused by *S. scabiei*, which lacks the *fas* operon (Joshi and Loria 2007).

The auxin indole-3-acetic acid (IAA) is an auxin that promotes plant growth and acts as a signal in plant defence responses, but it has also been associated with enhancing virulence in different phytopathogenic bacteria (Kunkel and Harper 2018). In *S. scabiei*, the presence of two biosynthetic genes, *iaaH* and *iaaM* is responsible for the production of this plant hormone. When these genes were deleted from the chromosome, radish seedlings treated with spores from the mutant strains were less necrotic than those treated with the wild-type strain, suggesting that IAA is a virulence factor for *S. scabiei* (Hsu 2010). The production of IAA and thaxtomin A is differentially affected by the addition of L-tryptophan to culture media, as the production of thaxtomin A is reduced while IAA production increases; consequently, radish seedlings treated with *S. scabiei* inoculum from media with higher amounts of L-tryptophan were less affected than seedlings treated with inoculum from media with lower amounts of the amino acid (Legault et al. 2011). Thus, the role of IAA as a virulence factor remains unclear.

Another phytohormone of interest is ethylene. This compound acts as a signal for senescence, ripening and in reactions against biotic and abiotic stress, but it is also used by plant pathogens like *P. syringae* to establish infections (van Loon et al. 2006). The genome of *S. scabiei* contains a homologue of the microbial ethylene-forming enzyme (EFE),

however, it remains unclear how this compound would participate in the establishment of the CS disease (Li et al. 2019c).

1.4.3.5 Borrelidin and desmethylmensacarcin

A study published in 2012 (Cao et al. 2012) describes the isolation of a strain of *Streptomyces* (GK18) from deep pitted lesions on potatoes harvested in Iran. It was determined that GK18 does not produce thaxtomin A, but instead it produces the 18-membered macrolide borrelidin (Fig. 1.5). Plant bioassays showed that pure borrelidin induces necrosis of potato tuber tissue and causes root and shoot stunting of radish seedlings, though it is less phytotoxic than thaxtomin A (Cao et al. 2012). Borrelidin has been previously described as an antimicrobial compound that acts as a threonyl-tRNA synthetase inhibitor (Maglangit et al. 2021), though its target in plants remains uncharacterized. Overall, the results of this study suggest the possible involvement of borrelidin in plant disease development, though further work is required to confirm that this compound serves as a bona fide virulence factor during plant-pathogen interactions.

Several strains of *Streptomyces niveascabiei* isolated from CS-infected potatoes in Uruguay were recently shown to produce the metabolite desmethylmensacarcin (Fig. 1.5), which causes more severe damage than thaxtomin A in plant bioassays (Lapaz et al. 2018; Croce et al. 2021). The desmethylmensacarcin mode of action appears to be similar to that of the closely related molecules mensacarcin and cervicarcin, which target the mitochondria and energy production in the cell (Plitzko et al. 2017). Mutational studies on the desmethylmensacarcin-producing strains have not been described, and so it is currently unclear how the production of this metabolite contributes to the pathogenicity of the strains.

1.5 Characterization of a novel plant pathogenic *Streptomyces* sp. isolated from a symptomatic CS-potato in Newfoundland

A study published from the Bignell lab in 2016 (Fyans et al. 2016) describes the isolation and characterization of plant pathogenic *Streptomyces* strains from CS-infected potato tubers harvested on the island of Newfoundland, Canada. Most of the isolates were determined to be strains of *S. europaeiscabiei* and were shown to produce thaxtomin A. However, several strains appeared to be novel pathogenic species that do not produce thaxtomin A. One strain in particular, 11-1-2, was found to be highly pathogenic in bioassays using different plant hosts (potato, radish, *Nicotiana benthamiana*). This strain was not phylogenetically related to the known plant pathogenic *Streptomyces* species and was negative for the presence of genes *txtA*, *txtD*, *nec1* and *tomA,* which are associated with the *Streptomyces* PAI. The 11-1-2 strain was shown to produce one or more phytotoxic compounds that were soluble with organic solvent, but the extracts did not contain thaxtomin A, concanamycin A or borrelidin. To further investigate the potential phytotoxins produced by 11-1-2, the genome of the strain was sequenced and made available (Bown and Bignell 2017). An initial screening for specialized metabolite BGCs confirmed that the strain does not harbour the genes for biosynthesizing thaxtomin A, nor does it harbour genes for producing other known or suspected virulence factors such as CFA-Ile, concanamycin A or borrelidin (Bown and Bignell 2017). Thus, the compound(s) associated with the observed phytotoxicity remain to be determined.

1.6 Thesis objectives

Plant-pathogenic *Streptomyces* species have been described as the causal agents of CS, an economically significant disease that affects potatoes and other crops worldwide. *S. scabiei* and closely related species have been widely studied, and thaxtomin A has been shown to serve key pathogenicity factor for these strains (Loria et al. 2006; Bignell et al. 2010; Li et al. 2019c). Due to the strong correlation between thaxtomin A production and CS severity, the identification of plant pathogenic *Streptomyces* has primarily been conducted using PCR-based detection of the biosynthetic genes for thaxtomin A (eg *txtAB*) (Wanner 2004, 2009; Qu et al. 2008). However, in recent years there have been multiple reports of CS-inducing *Streptomyces* that do not produce thaxtomin A, but instead they produce other phytotoxic compounds that are suspected to contribute to disease symptom development.

Streptomyces sp. 11-1-2 represents a novel plant pathogenic strain that does not produce the known phytotoxins thaxtomin A, concanamycin A, CFA-Ile or borrelidin. Instead, there is evidence that the strain secretes one or more compounds that may represent novel virulence factors that mediate plant-pathogen interactions. The overall objective of this thesis, therefore, was to characterize the metabolic potential of *Streptomyces* sp. 11-1-2 in order to gain insights into the mechanisms used by this strain to inflict tissue damage on living plant hosts.

This thesis is organized into three research chapters. In Chapter 3, the potential phytotoxins responsible for the plant pathogenic phenotype of strain 11-1-2 were investigated. The genome sequence of the strain was analyzed using antiSMASH to predict the presence of BGCs encoding for potential phytotoxins. The specialized metabolite elicitor NAG was added to different culture media to determine whether it stimulates or supresses

the production of the phytotoxic compound(s). Radish seedling and potato tuber bioassays were conducted to identify the culture conditions that promote phytotoxin production, and bioactive culture extracts were subjected to targeted and untargeted metabolomics to identify the compound(s) associated with the phytotoxic activity. Two compounds, nigericin and geldanamycin, were shown to be present in the bioactive culture extracts, and the pure compounds were further tested in plant bioassays to confirm their ability to exhibit phytotoxic effects against radish seedlings and potato tuber tissue.

In Chapter 4, the metabolic profile of 11-1-2 was further explored to determine what other types of metabolites are produced by the strain and what bioactivities are associated with these metabolites. The strain was grown on different solid culture media, and culture extracts were prepared using two different organic solvents. The bioactivity of the extracts was assessed using antimicrobial and plant bioassays, and metabolic profile of each extract was determined using untargeted metabolomics. Differences were observed in the bioactivities and metabolic profiles of the extracts prepared from the different culture media and using either ethyl acetate or methanol as the organic solvent. In addition to nigericin and geldanamycin, other known compounds were detected in several of the extracts, including echoside C and elaiophylin. Pure samples of these metabolite were tested in plant bioassays to investigate their potential function as phytotoxins. Furthermore, the metabolomics analysis revealed the presence of many other compounds that do not match known compounds in the spectral libraries, suggesting that they may represent novel metabolites.

In Chapter 5, the creation of mutant strains of 11-1-2 that are deficient in production of nigericin and geldanamycin was attempted in order to elucidate the role of these metabolites as pathogenicity or virulence factors. The first polyketide synthase gene in the

nigericin and geldanamycin BGCs, and two putative regulatory genes in the nigericin BGC were targeted for gene replacement using an antibiotic resistance cassette. As genetic manipulation of the 11-1-2 strain had not been done before, a protocol for the introduction of DNA into the strain needed to first be developed. Several methods for DNA introduction– intergeneric conjugation with *Escherichia coli*, protoplast transformation, and electroporation – were tested using the *Streptomyces* integrative plasmid pSET152. Several factors for each method were manipulated in order to find the conditions that promoted efficient DNA transfer into the 11-1-2 strain, and ultimately conditions for successful introduction of pSET152 via intergeneric conjugation were identified. Attempts were also made to introduce the plasmids that would enable targeted gene replacement, but mutant strains could not be isolated within the timespan of the project.

CHAPTER 2

MATERIALS AND METHODS

2.1 Bacterial strains, culture conditions and general procedures

2.1.1 *Escherichia coli* strains, cultivation and maintenance

E. coli strains used in this study are listed in Table 2.1. Strains were routinely grown at 37°C with shaking (200 rpm) in Lysogeny Broth (LB) Miller medium (Fisher Scientific, Canada) or on LB agar plates for 16-20 hours (herein referred to as overnight culture). When required, the antibiotics apramycin (50 μg/mL final concentration; Goldbio, USA), kanamycin (50 μg/mL final concentration; Sigma-Aldrich, Canada), hygromycin B (100 μg/mL; Thermo Fisher Scientific, Canada) and/or chloramphenicol (25 μg/mL final concentration; Sigma-Aldrich, Canada) were included in the culture medium. For strains requiring hygromycin B for selection, a low sodium version of LB was used for culturing. Recipes for all culture media used are provided in Appendix 1.

Table 2.1. Microbial strains used in this study.

Strain	Description	Resistance	Reference or Source
***Escherichia coli* strains**			
NEB5α	DH5α derivative, high efficiency competent cells	None	New England Biolabs
DH5α	General cloning host	None	Gibco-BRL
BW25113/pIJ790	Host for Redirect PCR targeting system	Chloramphenicol	(Gust et al. 2003a)
ET12567/pUZ8002	Non-methylating strain (*dam*$^-$ *dcm*$^-$ hsdM), carrying helper plasmid pUZ8002 for intergeneric conjugation	Chloramphenicol Kanamycin Tetracycline	(MacNeil et al. 1992; Paget et al. 1999)
***Streptomyces* strains**			
Streptomyces sp. 11-1-2	Wild type strain	None	(Fyans et al. 2016)
Streptomyces scabiei 87-22	Wild type strain	None	(Loria et al. 1995)
Streptomyces acidiscabies 84-104	Wild type strain	None	(Lambert and Loria 1989)
Streptomyces turgidiscabies Car8	Wild type strain	None	(Miyajima et al. 1998)
Streptomyces coelicolor M145	*S. coelicolor* A3(2) derivative, SCP1$^-$ and SCP2$^-$	None	(Bentley et al. 2002)
Streptomyces clavuligerus ATCC 27064	Wild type strain	None	(Higgens and Kastner 1971)
Indicator strains			
Bacillus subtilis	Indicator strain for antimicrobial bioassays	None	K. Tahlan, Memorial University of Newfoundland
Staphylococcus epidermidis	Indicator strain for antimicrobial bioassays	None	Memorial University of Newfoundland Biology Department
Saccharomyces cerevisiae	Indicator strain for antimicrobial bioassays	None	K. Tahlan, Memorial University of Newfoundland
Pseudomonas syringae pv. *tomato* DC3000	Indicator strain for antimicrobial bioassays	Rifampicin	(Buell et al. 2003)

For short-term storage (less than one month), *E. coli* strains were maintained on LB agar at 4°C. For long-term storage, 20% v/v glycerol stocks were prepared by mixing 500 µL of an overnight culture with an equal volume of sterile 40% v/v glycerol, and the stocks were kept at -80°C.

2.1.2 Preparation of chemically competent cells

Competent cells of *E. coli* DH5α and ET12567/pUZ8002 were prepared using a protocol modified from a previously published method (Inoue et al. 1990). The *E. coli* cells were cultured overnight in 3 mL of LB broth with the proper antibiotics when required. Then, the entire culture was added into 50 mL of SOB^{++} broth (Appendix 1), and the cells were incubated with shaking at 37°C until the optical density at 600 nm was between 0.4 and 0.6. Next, the cells were chilled on ice for approximately 10 minutes, and were then pelleted at 2328 × *g* for 10 minutes at 4°C. The pellet was resuspended in 10 mL of freshly prepared ice-cold TB buffer (Appendix 1), and the suspension was placed on ice for 10 minutes. The cells were pelleted again at 2328 × *g* for 10 minutes at 4°C, and the pellet was resuspended in 1.25 mL of TB buffer containing 7% v/v DMSO. The suspension was placed on ice for 10 minutes. Finally, the cell mixture was aliquoted into 50 or 100 µL volumes in 1.5 mL microcentrifuge tubes, and the tubes were flash-frozen in a dry ice/ethanol bath and were stored at -80°C.

2.1.3 Transformation of chemically competent cells

The transformation protocol was adapted from the NEB website (**dx.doi.org/10.17504/protocols.io.bddti26n**). A tube of *E. coli* competent cells was removed from the -80°C freezer and thawed on ice for 10 minutes. Then, 1-5 µL of plasmid DNA or ligation mixture (see Section 2.2.6) was added to the suspension, followed by mixing

by gently tapping the tube five times. The mixture was placed on ice for 30 minutes, and then the cells were heat shocked at 42°C for 45 seconds. Following the heat shock, the cells were placed on ice for 5 minutes. Then, 950 µL of room temperature SOC medium (Appendix 1) was added to the mixture and incubated at 37°C with shaking for 60 minutes. Finally, the cells were plated onto LB agar with the appropriate antibiotics and were incubated overnight.

2.1.4 Preparation of electrocompetent *E. coli* cells

Electrocompetent cells of *E. coli* BW25113/pIJ790 were prepared following a modified version of a previously described protocol (Gust et al. 2004). LB broth (5 mL) with appropriate antibiotics was inoculated with *E. coli* cells, and the culture was incubated overnight at 30°C with shaking. Then, 500 µL of the overnight culture was subcultured into 50 mL of SOB broth containing 20 mM of $MgSO_4$ and the appropriate antibiotics. The culture was incubated with shaking at 30°C until an OD_{600} of 0.4 was reached. Next, the cells were pelleted by centrifugation at 2328 × *g* for 5 minutes at 4°C, and after decanting the supernatant, the cells were resuspended in 10 mL of ice-cold sterile 10% v/v glycerol. The cells were pelleted again and resuspended in 5 mL of ice-cold sterile 10% v/v glycerol. Finally, the cells were pelleted as above, and the pellet was resuspended in the remaining ~100 µL of 10% v/v glycerol. The cell suspension was then used immediately for electroporation.

2.1.5 Transformation of DNA into electrocompetent *E. coli*

The cell suspension (100 µL) of freshly prepared electrocompetent *E. coli* cells was mixed with 100 ng (1-2 µL) of DNA in a pre-chilled electroporation cuvette (1 mm gap, VWR International, Canada). The electroporation was carried out using a Gene Pulser Xcell (Bio-Rad, Canada) with the following settings: 200 Ω, 25 µF, and 1.8 kV. Afterward, 1 mL

of ice-cold SOC was added to the cells, which were then transferred to a new microcentrifuge tube and incubated with shaking at 30°C for one hour. The cell suspension was plated onto two LB agar plates containing the appropriate antibiotics, and the plates were incubated overnight at 28°C if the pIJ790 plasmid was still required for downstream manipulations, or at 37°C to induce the loss of the pIJ790 plasmid.

2.1.6 Purification of plasmid DNA from *E. coli*

Plasmid DNA was extracted and purified from overnight *E. coli* cultures using the Alkaline Lysis miniprep protocol (Russell and Sambrook 2001) for preliminary assessments. For cloning and sequencing, purified plasmid DNA was prepared using the Geneaid Presto™ Mini Plasmid Kit (Froggabio, Canada), following the manufacturer's protocol.

2.1.7 *Streptomyces* strains, cultivation and maintenance

Streptomyces strains used in this study are listed in Table 2.1. Strains were routinely cultured at 28°C with or without shaking (125-200 rpm) in liquid or on solid media, respectively. The recipes for the different culture media used are provided in Appendix 1.

For spore stock preparation, *Streptomyces* strains were cultured for 7-12 days on potato mash agar (PMA) (Fyans et al. 2016), International *Streptomyces* Project Medium 4 (ISP-4; BD Difco™, USA) or YMS agar (Ikeda et al. 1988) (Appendix 1). For extraction of genomic DNA, *Streptomyces* sp. 11-1-2 was cultured for 4-5 days in 10 mL of tryptic soy broth (TSB; BD Biosciences, Canada) in a 50 mL spring flask. For metabolomics analyses, strain 11-1-2 was cultured on plates of M4 (Zhu et al. 2014), MMM (Kieser et al. 2000), mMYM (Liu et al. 2021b), OBA (Johnson et al. 2007), PMA (Fyans et al. 2016), SA (Paradkar and Jensen 1995), SFM (Kieser et al. 2000) and YMS (Ikeda et al. 1988) solid media for 14 days. To evaluate the effect of NAG on phytotoxicity, strain 11-1-2 was cultured

on MMM, YMS, mMYM and OBA supplemented with 50 mM of NAG for 14 days (Rigali et al. 2008). To evaluate the effect of NAG on geldanamycin and nigericin production, strain 11-1-2 was cultured for 14 days on YMS and mMYM agar supplemented with 0, 10, 20, 50, and 100 mM of NAG. The plates were kept at 4°C for short term (< 2 weeks) storage.

2.1.8 Spore stock preparation

Spore stocks of *Streptomyces* strains were prepared as follows. Three millilitres of a sterile Tween-20 solution (0.01% v/v in water) were added to a 7-12 day *Streptomyces* plate culture, and the spores were gently scraped using a sterile loop. The resulting suspension was transferred to a sterile conical tube (15 mL), and then another 3 mL of the Tween-20 solution was used to rinse the plate surface and was combined with the previous suspension. Next, the spore suspension was placed into a sonication bath for 5 minutes, after which it was filtered through sterile cotton in a 10 mL syringe, forcing the liquid through if the filter became clogged. The filter was rinsed with sterile water until the filtrate was clear. The spores were pelleted by centrifugation at 2328 × *g* for 10 minutes at room temperature. The supernatant was decanted into a beaker, and 10 mL of sterile water was added to resuspend the spore pellet by vortexing. The suspension was centrifuged as above, and the supernatant was discarded. Finally, the spore pellet was resuspended in 1000 µL of 20% v/v sterile glycerol, aliquoted in 100 µL volumes and stored at -20°C (short term) or -80°C (long term). To quantify the stock, the spores were serially diluted in sterile water and plated onto nutrient agar (NA; Appendix 1) or YMS plates in duplicate. The plates were then incubated until colonies were visible (~96-120 hours after inoculation), after which the colonies were counted on plates containing 20-200 colonies, and the CFU/mL was determined from the averaged count.

To prepare non-quantified *Streptomyces* spore stocks, 1 mL of sterile 0.01% v/v Tween-20 solution (in water) was added to a well-sporulated plate culture, after which the spores were gently scraped and the suspension was transferred to a sterile 1.5 mL microcentrifuge tube. After vortexing the suspension vigorously, the suspension was divided into two new tubes, and an equal volume of sterile 40% v/v glycerol was added to each. The tubes were then stored at -20°C.

2.1.9 Antibiotic testing

To test the susceptibility of *Streptomyces* sp. 11-1-2 to different antibiotics, apramycin, kanamycin, nalidixic acid, hygromycin and thiostrepton were added at 0, 10, 25, 50, 100 and 200 µg/mL to PMA, YMS and ISP-4 plates. Then, the plates were inoculated with 30 µL of a diluted spore stock and were incubated for 7 days, after which the presence/absence of growth was recorded.

2.1.10 *Streptomyces* growth curves

To evaluate the growth of *Streptomyces* sp. 11-1-2 in liquid media, a modified methylene blue adsorption assay was performed (Fischer and Sawers 2013; Gutierrez et al. 2022). In 6-well plates, 5 mL of SLB, SM, TSB, and TSB-S (Appendix 1) were inoculated with 11-1-2 spores from a stock to a final concentration of ~1×10^8 spores/ml, in triplicate. The plates were sealed with parafilm and incubated with shaking (125 rpm) at 30°C for 5 days. The media were sampled every 12 hours by obtaining 100 µL of culture with a cut pipette tip and transferring into a sterile 1.5 mL tube. The culture was centrifuged at 16873 × *g* for 7 minutes in a bench centrifuge, the supernatant was removed, and an equal volume of filter-sterilized aqueous methylene blue solution (2.5 mM) was added to the cell material.

The mixture was vortexed, briefly centrifuged and incubated for 10 minutes at 80°C and at 850 rpm in a thermomixer (Eppendorf, Germany). The tubes were then rapidly cooled to 25°C using ice for 3 minutes, and after a brief centrifugation step (3.5 minutes at 16873 × *g*), the supernatant was transferred to a fresh tube for storage at 4°C until ready for quantification.

The samples were diluted by adding 1.5 µL of sample to 148.5 µL of sterile distilled water per well in a 96-well plate, to a final volume of 150 µL. A methylene blue solution blank was prepared to the same dilution and included in the plate. The absorbance was measured at 660 nm using a plate reader Synergy H1 Hybrid Reader (BIOTEK, Winooski, Vermont, USA). The assay was performed twice.

2.1.11 *Streptomyces* genomic DNA preparation

Streptomyces sp. 11-1-2 was cultured in 10 mL of tryptic soy broth (TSB; BD Biosciences, Canada) using a 50 mL flask with a spring for 4-5 days at 28°C. One millilitre of culture was added to a 3 mL screw cap bead-beater tube containing sterile silica beads (400 µm; OPS Diagnostics, USA) to cover the bottom of the tube. The tube was then centrifuged at 5510 × *g* for 10 minutes, after which the supernatant was discarded. This process was repeated until the mycelia from the entire 10 mL culture was collected. Then, 200 µL of buffer AL and 200 µL of buffer ATL from the QIAamp DNA Mini Kit (Qiagen Inc., Canada) were each added to the tube, and the tube was placed in a SpeedMill PLUS tissue homogenizer (Analytik Jena, USA) set to the "Bacteria" preset. Following lysis of the mycelia, the tube was centrifuged at 8609 × *g* for 5 minutes, and the supernatant was transferred to a clean 1.5 mL microcentrifuge tube containing 200 µL of 95% v/v ethanol.

The mixture was vortexed and then added to a spin column from the QIAamp DNA Mini Kit, and the DNA was purified as per the manufacturer's protocol.

2.1.12 Introduction of DNA into *Streptomyces* by intergeneric conjugation with *E. coli*

2.1.12.1 Intergeneric conjugations using *Streptomyces* spores

Intergeneric conjugations were performed using spores of *Streptomyces* sp. 11-1-2 as described previously (Kieser et al. 2000) with some modifications. Competent cells of *E. coli* ET12567/pUZ8002 (Table 2.1) were transformed with the plasmids to be conjugated into 11-1-2. A seed culture of the plasmid-containing *E. coli* ET12567/pUZ8002 strain was prepared by inoculating a single colony into 5 mL of LB broth containing chloramphenicol and the plasmid-specific antibiotic(s), after which the culture was incubated overnight with shaking. Then, 1 mL of the seed culture was sub-cultured into 50 mL of fresh LB broth plus antibiotics in a 250 mL flask, and the flask was incubated with shaking until the OD_{600} reached 0.4-0.6, as determined using an Implen P300 nanophotometer (Implen, Inc., USA). The cells were pelleted by centrifugation at 2328 × *g* for 10 minutes and were washed twice with 50 mL of fresh LB broth to remove the residual antibiotics. Finally, the *E. coli* cells were resuspended in 500 µL of LB broth.

Streptomyces 11-1-2 spores were collected from a 10-day PMA plate culture using 10 mL 2×YT broth (Appendix 1) and were transferred to a 50 mL sterile conical tube. The spores were pelleted by centrifugation at 2328 × *g* for 10 minutes and were washed twice with 5 mL of LB broth. The spores were then resuspended in 500 µL of LB broth and were mixed with an equal volume of the plasmid-containing *E. coli* ET12567/pUZ8002 cell suspension. The *E. coli*-*Streptomyces* mixture was centrifuged at 2328 × *g* for 10 minutes, and the supernatant was discarded. The pellet was resuspended in 1 mL of LB broth, and the

suspension (500 µL per plate) was spread-plated onto two SFM + 10 mM $MgCl_2$ plates (Appendix 1). The plates were incubated for 16-20 h, after which they were overlaid with 1 mL of sterile water containing nalidixic acid (final concentration in the medium 20 µg/mL) and the appropriate antibiotic to select for the incoming plasmid (final concentration in the medium 25-50 µg/mL).

A second version of the protocol included a modification to the spore suspension preparation. The spores from a 10-12 day-old PMA plate culture were collected using 10 mL of 2×YT broth and were pelleted by centrifugation at 2328 × *g* for 10 minutes. Then, the spores were resuspended in 500 µL of 2×YT broth, heat shocked at 50°C for 10 min, and were cooled to room temperature for 10-15 minutes. The remaining steps of the conjugation protocol were as described above, except that the *E. coli-Streptomyces* mixture was also plated onto YMS and AS-1 (Appendix 1) agar media supplemented with 10 mM $MgCl_2$ (Baltz 1999).

A third version of the protocol included further modifications to the spore suspension preparation. The spores from a 10-12 day old PMA plate cultured were collected using 5 mL of pregermination broth medium (Kieser et al. 2000) (Appendix 1) and were pelleted by centrifugation at 2328 × *g* for 10 minutes. Then, the spores were resuspended in 10 mL of pregermination medium and were incubated at 28-30°C with shaking for 4 hours to enable spore germination. Next, the germinated spores were pelleted by centrifugation at 2328 × *g* for 10 minutes, and the pellet was resuspended in 1 mL of LB broth. The remaining steps were as described above, except that the *E. coli-Streptomyces* mixture was plated onto GSY (Wang and Jin 2014) and AS-1 media (Appendix 1).

A fourth version of the protocol included modifications to the *E. coli* and spore suspension preparation. The spores from a 15-18 day old ISP-4 plate were collected using 5 mL of 2×YT broth and pelleted by centrifugation at 2328 × *g* for 10 minutes. Then, the spores were resuspended in 500 µL of 2×YT broth. The plasmid-containing *E. coli* ET12567/pUZ8002 strain was prepared from a seed culture as previously described but it was grown until the OD_{600} reached 0.6. The cells were pelleted by centrifugation at 2328 × *g* for 10 minutes and were washed twice with a total of 30 mL of fresh LB broth to remove the residual antibiotics. Finally, the *E. coli* cells were resuspended in 500 µL of LB broth. The spores and *E. coli* cells were mixed together by pipetting up and down until homogeneous, and the mixture was plated onto SFM containing 20 mM of $MgCl_2$.

When potential exconjugants were obtained, the colonies were transferred into a fresh ISP-4 containing nalidixic acid and the selection antibiotic, and the plates were incubated at 28-30ºC for 5-7 days.

2.1.12.2 Intergeneric conjugations using *Streptomyces* mycelia

The *E.coli-Streptomyces* sp. 11-1-2 intergeneric conjugations were also attempted using mycelia of 11-1-2 instead of spores, and the protocol used was adapted from a previously published method (Du et al. 2012). The 11-1-2 mycelia were prepared by inoculating 5 mL of SM liquid medium (Appendix 1) with 100 µL of a glycerol spore stock and incubating the culture for 2, 3, and four days at 28-30ºC with shaking in a 25 mL spring flask. The mycelia were collected by centrifugation at 2328 × *g* for 10 minutes and were washed once with an equal volume of sterile 10% v/v glycerol and twice with 2×YT broth, vortexing strongly each time. Finally, the mycelia were resuspended in 500 µL of 2×YT broth.

The *E. coli* ET12567/pUZ8002 strain cells were prepared as described in Section 2.1.11.1, except that 10 mM $MgCl_2$ was added to the LB broth at all steps.

The prepared *E. coli* cells were mixed with the 11-1-2 mycelia, and the mixture was centrifuged at 2328 × *g* for 10 minutes. Most of the supernatant (400–600 µL) was removed, and the cells and mycelia were resuspended in the remaining liquid. The suspension was spread-plated onto a single SFM + 20 mM $MgCl_2$ agar plate, and the plate was incubated at 28°C for 20-24 hours. Following incubation, the plate was overlaid with 1 mL of sterile water containing nalidixic acid (final concentration in medium was 20 µg/mL) and the appropriate antibiotic to select for the incoming plasmid (final concentration in medium 25-50 µg/mL).

A second version of the protocol included two modifications. First, the amount of *E. coli* used for the conjugation was adjusted based on the OD_{600} of the culture. Thus, the mycelia were mixed with 1×10^8 *E. coli* cells per plate (Du et al. 2012). The second modification involved using GSY + 60 mM $MgCl_2$ + 60 mM $CaCl_2$ agar medium for plating the *E. coli*-*Streptomyces* mixture. The remaining steps of the conjugation protocol remained unchanged.

2.1.13 Electroporation of DNA into *Streptomyces* sp. 11-1-2

Introduction of DNA into *Streptomyces* sp. 11-1-2 was attempted using mycelial electroporation. The protocol used was adapted from a previously published method (Hamano et al. 2006). The mycelia were prepared by inoculating 500 µL of a 1×10^{10} CFU/mL glycerol spore stock into 50 mL of SLB or SM medium (Appendix 1) and then incubating overnight with shaking. The mycelia were collected by centrifugation at 2328 × *g* for 10 minutes and washed twice with 10 mL of ice-cold sterile water, after which they were resuspended in 1 mL of ice-cold 10% v/v glycerol. Then, 100 µL of the suspension was mixed

with 1 µg of plasmid DNA obtained from *E. coli* ET12567-transformed cells, and the mixture was transferred to a cold electroporation cuvette (inter-electrode distance = 0.1 cm, Bio-Rad, USA). The mixture was subjected to a single voltage shock using a Gene Pulser Xcell (Bio-Rad, Canada) with the following settings: 100 Ω, 25 µF, and 1.8 kV. Immediately after the shock, 250 µL of SLB medium was added, and the suspension was transferred to a fresh 1.5 mL tube. The suspension was incubated at 30°C with shaking for 8 hours, and then it was plated onto a YMS plate with the appropriate antibiotic and was incubated for a week at 30°C.

2.1.14 Preparation and transformation of *Streptomyces* protoplasts

Streptomyces sp. 11-1-2 protoplasts were prepared and transformed following a previously published method (Kieser et al. 2000). The protoplasts were prepared by adding 0.1 mL of a spore suspension to a 125-mL spring flask containing 25 mL of YEME medium (Appendix 1) and incubating with shaking at 30ºC for three days. The culture was then transferred to a sterile 14-mL round bottom tube and the mycelia were pelleted by two rounds of centrifugation at 1000 × *g* for 10 minutes. The supernatant was discarded, and the pellet was resuspended in 14 mL of 10.3% w/v sucrose by tapping the tube on the side, followed by centrifugation as described above. The wash with 10.3% w/v sucrose was repeated once more, and then the mycelia were resuspended in 4 mL of lysozyme solution (1 mg/mL) prepared in P buffer (Appendix 1). The mixture was incubated at 30ºC for 1 hour, with gentle mixing every 15 minutes. After the incubation, the mycelia were drawn in and out three times using a sterile 5 mL pipette with a cotton plug, and the mixture was incubated for another 15 minutes. Then, 5 mL of P buffer were added, and the mycelia were drawn in and out three times as before and incubated further for 15 minutes. The protoplast solution was filtered

through a sterile syringe and cotton plug into a new sterile 14-mL round bottom tube. The protoplasts were sedimented by centrifugation at 1000 × *g* for 7 minutes, the supernatant was decanted, and the protoplasts were resuspended in the remaining drop of liquid by gently tapping on the side of the tube. Once the pellet was dispersed, 5-10 mL of P buffer was added, and the protoplasts were ready for storage. To store them, 1 mL of the suspension was transferred to sterile 1.5 mL tubes, and then the tubes were placed on ice in a beaker, and the beaker was placed at -80ºC overnight. The next day, the tubes were removed from the ice and kept at -80ºC.

To transform the protoplasts, ~1-2 µg of the plasmid DNA, previously extracted from *E. coli* ET12567, was added to TE buffer for a final volume of 10 µL. Then, 2 µL of 1M NaOH were added to the solution and incubated at 37ºC for 10 minutes. Finally, the DNA was placed on ice, and 2 µL of 1M HCl were added to the solution. Additionally, non-denatured plasmid DNA was used to attempt protoplast transformation. The DNA was added to a final volume of 10 µL in TE buffer in this case.

If required, the protoplast tubes were thawed quickly under running tap water until no ice was visible. The protoplasts were then pelleted by centrifugation at 700 × *g* for 7 minutes at room temperature. At the same time, 3 mL of P buffer were added to 1.2 g of sterile PEG 1000 in a screw-cap tube. After centrifugation, the supernatant was removed, and the protoplasts were resuspended in the remaining drop of liquid by tapping on the side of the tube. The DNA was added to the protoplast tube, and then 0.5 mL of the PEG 1000/P Buffer solution was immediately added, and the contents were mixed by pipetting up and down once. Less than 3 minutes later, 5 mL of P buffer were added to the tube, and the protoplasts were pelleted by centrifugation as described above. The supernatant was

discarded, and the pellet was resuspended in the remaining drop of liquid. Finally, 400 µL of P buffer was added to the protoplast suspension, and 100 µL of this was spread-plated per R2YE plate (Appendix 1). The plates were incubated for 16-20 hours at 28ºC. Then, the plates were overlaid with 1 mL of an antibiotic solution to select for the incoming plasmid, and the plates were further incubated for 2 weeks until *Streptomyces* colonies were visible.

2.2 DNA Procedures

2.2.1 Plasmids

Plasmids used in this study are listed in Table 2.2.

Table 2.2. Plasmids used in this study.

Plasmid	Description*	Resistance	Reference or Source
pCR™-Blunt II-TOPO®	Cloning vector for PCR products	Kanamycin	Invitrogen
pIJ773	Template for amplification of the [Apra^R+*oriT*] cassette	Apramycin	(Gust et al. 2003a)
pIJ10700	Template for amplification of the [Hyg^R+*oriT*] cassette	Hygromycin, Ampicillin	(Gust et al. 2003a)
pGEM-neo 5	Template for amplification of the Kan^R cassette	Kanamycin	(Cheng 2018)
pSET152	Integrative *Streptomyces* cloning vector	Apramycin	(Bierman et al. 1992)
pGDC1	pCR™-Blunt II-TOPO® containing the 11-1-2 *gdmAI* flanking regions + [Apra^R+*oriT*] cassette	Kanamycin, Apramycin	This study
pGDC2	pCR™-Blunt II-TOPO® containing the 11-1-2 *nigAI* flanking regions + [Hyg^R+*oriT*] cassette	Kanamycin, Hygromycin	This study
pGDC3	pCR™-Blunt II-TOPO® containing the 11-1-2 *sigJ* flanking regions + [Hyg^R+*oriT*] cassette	Kanamycin, Hygromycin	This study
pGDC4	pCR™-Blunt II-TOPO® in which the Kan^R was replaced by [Apra^R+*oriT*] and also contains the 11-1-2 *nigAI* flanking regions + Kan^R cassette	Apramycin, Kanamycin	This study

pGDC5	pCR™-Blunt II-TOPO® containing the 11-1-2 *sigJ* flanking regions + [Apra^R+*oriT*] cassette	Kanamycin, Apramycin	This study
pGDC6	pCR™-Blunt II-TOPO® containing the 11-1-2 *nigR* flanking regions + [Apra^R+*oriT*] cassette	Kanamycin, Apramycin	This study
* Apra^R = Apramycin resistance; Hyg^R = Hygromycin resistance; Kan^R = Kanamycin resistance			

2.2.2 Primers

The primers used for this study are listed in Table 2.3. Primers were purchased from Integrated DNA Technologies (IDT; USA) and were purified by standard desalting. The annealing temperatures were estimated using the NEB Tm calculator (https://tmcalculator.neb.com/).

Table 2.3. Primers used in this study.

Primer code	**Sequence (5' → 3')***	**Use**	**Orientation and restriction site***	**Annealing temperature (°C)**
ApraR For	TCGATGGGCAGGTACTTCTC	Detection of the apramycin resistance gene	Forward	64
ApraR Rev	ACCGACTGGACCTTCCTTCT	Detection of the apramycin resistance gene	Reverse	
GDC23	GCGC**AATATT**ATTCCGGGGATCCGTCGACC	Amplification of [Apra^R+*oriT*] and [Hyg^R+*oriT*] cassettes from pIJ773 and pIJ10700, respectively	Forward with SspI	69

GDC24	GCGC**AATATT**TGTAGGCTGGAGCTGCTTC	Amplification of [Apra^R+*oriT*] and [Hyg^R+*oriT*] cassettes from pIJ773 and pIJ10700, respectively	Reverse with SspI	
GDC25	CTCTAGGGCGTCCACATCG	Amplification of the 11-1-2 *nigAI* downstream flanking region	Forward	58
GDC26	ATAT**AATATT**CCTCATGGCGAACGAAGAGA	Amplification of the 11-1-2 *nigAI* downstream flanking region	Reverse with SspI	
GDC27	ATAT**AATATT**GCTCCGGATTGATGATCGGT	Amplification of the 11-1-2 *nigAI* upstream flanking region	Forward with SspI	62
GDC28	TGGTGATTCAGGGCTTGTGG	Amplification of the 11-1-2 *nigAI* upstream flanking region	Reverse	
GDC29	GCTGATGCCGAAGAACGC	Sequencing of *nigAI* downstream flanking region and screening in *E. coli* colony PCR	Forward	60
GDC30	CGTTCGATCAGCAGATCCGT	Sequencing of *nigAI* upstream flanking region and screening in *E. coli* colony PCR	Reverse	
GDC33	CGATGTTGGACTTGATGGAG	Amplification of the 11-1-2 *gdmAI* downstream flanking region and *E. coli* colony PCR	Forward	62
GDC34	ATAT**AATATT**AGATGGCGAATGACGAAAAG	Amplification of the 11-1-2 *gdmAI* downstream flanking region	Reverse with SspI	

GDC35	ATAT**AATATT**CGGG AGAGAAAGCTCGAA	Amplification of the 11-1-2 *gdmAI* upstream flanking region	Forward with SspI	62
GDC36	GCGGAATTCCCAGTC GTAAG	Amplification of the 11-1-2 *gdmAI* upstream flanking region	Reverse	
GDC38	GGCCGAAGACCCCTT GTT	Sequencing of *gdmAI* upstream flanking region and *E. coli* colony PCR	Reverse	62
GDC41	GAGGTTCTCCAGGTT CCAGC	Sequencing of *gdmAI* downstream flanking region and *E. coli* colony PCR	Forward	62
GDC42	ATGTCCTGGGCATCA CGATC	Amplification of the 11-1-2 *nigR* upstream flanking region	Forward	65
GDC43	ATAT**AATATT**GAAGT GCCCGTGGTGTTTTC	Amplification of the 11-1-2 *nigR* upstream flanking region	Reverse with SspI	
GDC44	ATAT**AATATT**TGTTC CCGCATGAGGAAGA C	Amplification of the 11-1-2 *nigR* downstream flanking region	Forward with SspI	63
GDC45	GTCGTCAGATAGGA GGCGAA	Amplification of the 11-1-2 *nigR* downstream flanking region	Reverse	
GDC46	CGTCCGATCTTGTCC GTTCT	Sequencing of *nigR* upstream flanking region	Forward	62
GDC47	GTGAGCATACGGAC CTCCTG	Sequencing of *nigR* downstream flanking region	Reverse	62
GDC51	CCTGTGTGGGAGAGC AGATC	Amplification of the 11-1-2 *sigJ* upstream flanking region	Forward	65

GDC52	ATAT**GCTAGC**CAGCTCTGCCATGTCCTGAT	Amplification of the 11-1-2 *sigJ* upstream flanking region	Reverse with NheI	
GDC53	ATAT**GCTAGC**ATCACCGTCACATCTGGAGC	Amplification of the 11-1-2 *sigJ* downstream flanking region	Forward with NheI	65
GDC54	AGCATGCTGACCGTGGAG	Amplification of the 11-1-2 *sigJ* downstream flanking region	Reverse	
GDC55	AGACCAGGGCCAGAGTGATC	Sequencing of *sigJ* upstream flanking region	Forward	63
GDC56	AGCCTCTTGTGCAGTTCAGC	Sequencing of *sigJ* downstream flanking region	Reverse	63
GDC59	ATAT**GCTAGC**ATTCCGGGGATCCGTCGACC	Amplification of [Apra^R+*oriT*] and [Hyg^R+*oriT*] cassettes from pIJ773 and pIJ10700, respectively	Forward with NheI	69
GDC60	ATAT**GCTAGC**TGTAGGCTGGAGCTGCTTC	Amplification of [Apra^R+*oriT*] and [Hyg^R+*oriT*] cassettes from pIJ773 and pIJ10700, respectively	Reverse with NheI	
GDC61	GCTGGAACCTGGAGAACCTC	Sequencing of *gdmAI* downstream flanking region	Reverse	62
GDC62	AACAAGGGGTCTTCGGCC	Sequencing into *gdmAI* upstream flanking region	Forward	62
GDC63	GCGTTCTTCGGCATCAGC	Sequencing of *nigAI* downstream flanking region	Reverse	61
GDC64	ACGGATCTGCTGATCGAACG	Sequencing of *nigAI* upstream flanking region	Forward	62

GDC65	AGAACGGACAAGAT CGGACG	Sequencing of *nigR* upstream flanking region	Reverse	62
GDC66	CAGGAGGTCCGTATG CTCAC	Sequencing of *nigR* downstream flanking region	Forward	62
GDC67	GATCACTCTGGCCCT GGTCT	Sequencing of *sigJ* upstream flanking region	Reverse	63
GDC68	GCTGAACTGCACAA GAGGCT	Sequencing of *sigJ* downstream flanking region	Forward	63
GDC69	CACCACACCCAGATG AGACA	Amplification of the 11-1-2 *nigAI* downstream flanking region	Forward	64
GDC71	ATAT**AATATT**GTCGA GTACCTCAAGCGTGT	Amplification of the 11-1-2 *nigAI* downstream flanking region	Reverse with SspI	
GDC72	CGATGTGGACGCCCT AGAG	Sequencing of *nigAI* downstream flanking region	Reverse	61
GDC75	GTGCGATATGAGATC ATGGGACCTCTCCGG GTGGTAGAAATTCCG GGGATCCGTCGACC	Amplification of the [Hyg^R+*oriT*] cassette for replacement of the 11-1-2 *nigR* gene via REDIRECT PCR targeting	Forward	55
GDC76	TCATGCGGGAACATG CAGTTCCAGCCGGTC ATCCGAGGTTGTAGG CTGGAGCTGCTTC	Amplification of the [Hyg^R+*oriT*] cassette for replacement of the 11-1-2 *nigR* gene via REDIRECT PCR targeting	Reverse	

GDC92	ATGATTGAACAAGATGGATTGCACGCAGGTTCTCCGGCCATTCCGGGGATCCGTCGACC	Amplification of the [Apra^R+*oriT*] cassette for replacement of the *kanR* gene in pCR™-Blunt II-TOPO® via REDIRECT PCR targeting	Forward	55
GDC93	TCAGAAGAACTCGTCAAGAAGGCGATAGAAGGCGATGCGTGTAGGCTGGAGCTGCTTC	Amplification of the [Apra^R+*oriT*] cassette for replacement of the *kanR* gene in pCR™-Blunt II-TOPO® via REDIRECT PCR targeting	Reverse	
GDC94	GCGC**AATATT**CCGCCTCGGCCTCTGAGCTA	Amplification of the KanR gene from pGEM-neo 5	Forward with SspI	69
GDC95	GCGC**AATATT**ATCCCCGCGCTGGAGGATCA	Amplification of the Kan^R gene from pGEM-neo 5	Reverse with SspI	
*Restriction sites are in bold and non-homologous sequences are underlined				

2.2.3 Polymerase Chain Reaction (PCR)

PCR was routinely performed using a C1000^{TM} Thermal Cycler (Bio-Rad, Canada). Tables 2.4 and 2.5 provide the reaction conditions used with Phusion® High-Fidelity DNA Polymerase and Standard Taq DNA Polymerase (New England Biolabs, Canada), respectively. The cycling conditions were performed as per manufacturer's protocol.

Table 2.4. PCR protocol for cloning products and colony PCR using Phusion DNA polymerase.

Component	50 µl Reaction	Final Concentration
5× Phusion GC Buffer	10	1×
10 mM dNTPs	1	200 µM
10 µM Forward Primer	2.5	0.5 µM
10 µM Reverse Primer	2.5	0.5 µM
Template DNA	50-100 ng	50-100 ng
DMSO (100% v/v)	2.5	5%
Phusion DNA Polymerase	0.5	1.0 units/50 µL PCR
Nuclease-free water	To 50 µL	

Thermal cycling conditions:
Initial denaturation step: 98°C, 30 s (3 min for genomic DNA)
Then 30-35 cycles of:
Denaturation: 98°C, 10 s
Annealing: 60-68°C, 30 s
Extension: 72°C, X s (30 s/kb)
Final extension: 72°C, 5 min
Hold: 4°C

Table 2.5. PCR protocol for REDIRECT and colony PCR using Taq DNA polymerase.

Component	50 µl Reaction	Final Concentration
10× Standard Taq Buffer	5	1×
10 mM dNTPs	1	200 µM
10 µM Forward Primer	1	0.2 µM
10 µM Reverse Primer	1	0.2 µM
Template DNA	50-100 ng	50-100 ng
DMSO (100% v/v)	1	2%
Taq DNA Polymerase	0.25	1.25 units/50 µL PCR
Nuclease-free water	To 50 µL	

Thermal cycling conditions:
Initial denaturation step: 95°C, 30 s (3 min for genomic DNA)
Then 30-35 cycles of:
Denaturation: 95°C, 30 s
Annealing: 55°C, 30 s
Extension: 68°C, X s (1 min/kb)
Final extension: 68°C, 5 min
Hold: 4°C

Colony PCR was performed to confirm the presence of newly ligated genes in plasmids that were transformed into *E. coli*. Single colonies were transferred to a PCR tube containing 10 µL of HPLC-grade water and mixed by pipetting up and down. Two microliters were transferred to a new LB plate with the appropriate antibiotic and incubated overnight at 37°C, while the remaining 8 µL were used as a template for PCR under the conditions described in Table 2.5. The PCR products were visualized using agarose gel electrophoresis as described below.

Colony PCR for *Streptomyces* was performed by streaking colonies with a sterile wooden toothpick onto a SLB plate with antibiotics as required. The plate was incubated for two days at 28°C, after which one to three colonies were transferred to a sterile 1.5 mL tube containing 20 µL of sterile water. The colonies were crushed with a sterile pipette tip and then incubated at 100°C for 10 minutes. After incubation, the samples were centrifuged at 16873 × *g* for 5 minutes. The supernatant was transferred to a fresh tube and 2.5 µL were used as a template for PCR under the conditions described in Table 2.4. The PCR products were visualized using agarose gel electrophoresis as described below.

2.2.4 Gel electrophoresis and gel extraction

Gel electrophoresis was performed using 0.8-1% w/v agarose gels prepared with 1× Tris Base-Boric Acid-EDTA (TBE) buffer when required. The gels were run at 8-10 V/cm, depending on the length of the gel, from 50-80 minutes using a VWR 300V power source (VWR International, Canada). The gel was then stained in an ethidium bromide solution (2.0 µg/mL in 1× TBE buffer) for 20-25 min, followed by a destaining step in 1× TBE buffer for 15-20 min. For visualization, the gel was exposed to UV light and photographed using a GelDoc38It® TS2 310 Imager (UVP Analytik Jena, USA).

The electrophoresis and staining/destaining steps were the same for gel extraction. After the destaining, gels were placed on a UV transilluminator, and the bands of interest were excised using a scalpel, transferred to a new 2 mL microcentrifuge tube, and stored at -20°C until ready for purification.

DNA purification was done using the Monarch® DNA Gel Extraction Kit (New England Biolabs, Canada), following the manufacturer's protocol.

2.2.5 Restriction enzyme digestion of DNA

Plasmids and PCR-amplified DNA (500-1000 ng) were digested as required using various restriction enzymes (New England Biolabs, Canada) in a total reaction volume of 25 or 50 µL. Digests were conducted following the manufacturer's protocol, except that the incubation time varied from 1 hour to overnight.

Digestion of plasmids for ligation of PCR products included dephosphorylation with Quick CIP (New England Biolabs, Canada) to prevent re-ligation. The Quick CIP was added near the end of the plasmid digestion, incubated, and heat-inactivated as per the manufacturer's guidelines.

2.2.6 DNA ligation

Digested PCR products were ligated together using the T4 DNA Ligase system (New England Biolabs, Canada) following the manufacturer's protocol. In some instances, the addition of 10 mM ATP was required. The mixture was incubated at room temperature overnight and then heat-inactivated at 65°C for 10 minutes. The entire reaction mixture was subjected to gel electrophoresis, and the DNA band with the expected size was excised and purified as described above (Section 2.2.4). The purified ligated PCR products were then ligated into the pCR™-Blunt II-TOPO® plasmid (Table 2.2) using the Zero Blunt® TOPO®

PCR Cloning Kit (Invitrogen, USA) following the manufacturer's instructions, except that the incubation time was increased from 5 minutes to 30 minutes. The ligation reactions were used to transform chemically competent *E. coli* DH5α cells, as described in Section 2.1.5.

The ligation of antibiotic cassettes into plasmids with a single restriction enzyme was performed by digestion and dephosphorylation of the plasmid as described in Section 2.2.5, followed by ligation of the plasmid and antibiotic cassette using the T4 DNA Ligase system (New England Biolabs, Canada) with 1:2 or 1:3 vector:insert ratios. The ligation reaction was used to transform chemically competent *E. coli* DH5α cells, as described before (Section 2.1.5).

2.2.7 Construction of gene deletion plasmids for *Streptomyces* sp. 11-1-2

To delete the *gdmAI*, *nigAI,* and *sigJ* genes from the 11-1-2 genome, 1-1.5 kb regions upstream and downstream of each target gene were amplified by PCR using primers containing engineered restriction sites (Table 2.3). The products for each amplification were gel-extracted, digested with the desired restriction enzyme, and then ligated together. Next, the newly ligated products were cloned into the pCR™-Blunt II-TOPO® plasmid, and clones obtained were screened for the presence of the correct insert by restriction digestion. Colonies were screened for the correct insert using colony PCR and plasmid DNA digestion as previously described; colonies showing the expected results were then prepared and sent for Sanger sequencing at The Center for Applied Genomics (TCAG) at the University of Toronto. Plasmids without mutations were digested with the appropriate restriction enzyme(s), dephosphorylated, and gel-extracted, then ligated to the desired antibiotic resistance cassette previously digested with the same restriction enzyme. The new ligated plasmid was then transformed into chemically competent *E. coli* DH5α cells. Colonies were

screened for the correct insert using colony PCR and plasmid DNA digestion; colonies showing the expected results were then prepared and sent for Sanger sequencing to confirm the integrity of the sequence and directionality of the insert. Finally, glycerol stocks of the sequenced colonies were prepared as described above (Section 2.1.1, Table 2.2).

For construction of plasmids for the deletion of *nigR* and *nigAI*, the Redirect PCR targeting method was used (Gust et al. 2004). For *nigR*, the gene of interest and approximately 1 kb upstream and downstream were PCR-amplified and ligated into the pCR™-Blunt II-TOPO® plasmid using the Zero Blunt® TOPO® PCR Cloning Kit (Invitrogen, USA), and was then transformed into *E. coli* DH5α cells as previously described. The presence of the insert was verified by DNA digestion, and the sequence integrity was confirmed by Sanger sequencing at the TCAG facility. The selected plasmid was then transformed by electroporation into competent *E. coli* BW25113/pIJ790 cells, prepared as described in Section 2.1.4. The [Apra^R+*oriT*] cassette was amplified using pIJ773 as template and the primers GDC75 and GDC76, which contain a 39-nucleotide extension that is homologous to the target gene. The cassette was amplified, gel-extracted, and purified as described in Sections 2.2.3 and 2.2.4.

The Redirect PCR targeting protocol was followed with some modifications. The volume of SOB used for the culture was 50 mL instead of 10 mL. L-arabinose was added to the medium to promote the expression of the *red* genes (final concentration: 10 mM) at the time of inoculation and again after 2 hours of incubation. Following the electroporation, the cells were mixed with 1 mL of ice-cold SOC medium instead of LB. The cells were then plated onto LB agar + kanamycin + apramycin and incubated for 16-20 hours at 37°C to promote the loss of the plasmid pIJ790.

Following the incubation period, colonies with a relatively larger size were diluted in 10 µL of sterile distilled water, from which 8 µL were used for colony PCR using primers ApraR For and ApraR Rev, and the remaining 2 µL were transferred to a new LB agar + kanamycin + apramycin and incubated overnight at 37°C. Colonies showing the expected PCR product after gel electrophoresis were grown overnight at 37°C in liquid culture for plasmid extraction. The plasmids with the desired insert were used to transform *E. coli* DH5α cells and then prepared and sent for Sanger sequencing. Plasmids with the expected insert were kept for further work (Table 2.2).

The Redirect process was also used to change the kanamycin resistance gene in the plasmid pGDC2 backbone for the [Apra^R+*oriT*] cassette from pIJ773. The sequenced plasmid containing the flanking regions to the 11-1-2 *nigAI* and lacking [Hyg^R+*oriT*] was used to transform *E. coli* BW25113/pIJ790 by electroporation, as described above. Primers GDC92 and GDC93, which contain a 39-nucleotide section homologous to the kanamycin resistance gene, were used to amplify the [Apra^R+*oriT*] cassette from pIJ773.

The *E. coli* BW25113/pIJ790 + pGDC2 cells were prepared for a second electroporation with the same modification described above in this section, and the cells were plated on LB + apramycin and were incubated for 16-20 hours at 37°C, which promotes the loss of the plasmid pIJ790. Following the incubation period, colonies with a relatively larger size were diluted in 10 µL of sterile distilled water, from which 8 µL were used for colony PCR using primers ApraR For and ApraR Rev, and the remaining 2 µL were transferred to a new LB agar + apramycin and incubated overnight at 37°C. Colonies showing the expected PCR product after gel electrophoresis were grown overnight at 37°C in liquid culture for plasmid extraction. The plasmids with the desired insert were used to transform *E. coli* DH5α cells and then extracted again. Plasmids with the expected insert were then used to ligate the

kanamycin resistance gene (which was amplified from pGEM-neo 5 using primers GDC94 and GDC95; see Table 2.3) into the SspI restriction site located in between the *nigAI* flanking regions. The plasmid was then transformed into *E. coli* DH5α, and cells presenting resistance to kanamycin were then prepared for plasmid extraction and glycerol stocks. To confirm the directionality of the cassette, the plasmid was digested with the appropriate restriction enzymes. Plasmids with the desired fragmentation pattern were kept for further work (Table 2.2).

2.3 Metabolomics analysis

2.3.1 Organic extraction of *Streptomyces* sp. 11-1-2 cultures

Culture extracts were prepared from whole or half plate cultures of 11-1-2 grown on various agar media as described in Section 2.1.7. Following incubation, the agar was cut into small pieces using a sterile pipettor tip, and the pieces were transferred to a clean 250 mL glass flask or a 50 mL plastic conical tube. If not immediately processed, the agar pieces were stored at -80ºC in glass test tubes or 50 mL conical tubes. ACS grade ethyl acetate or methanol (20 mL) was added to each vessel, and the contents were mixed and left to incubate at room temperature overnight. If the agar pieces had previously been stored at -80ºC, they were first thawed at room temperature before addition of the organic solvent. Following incubation, the extracts were filtered using Whatman® #1 filter paper (GE Healthcare Life Sciences) and transferred into clean flasks or conical tubes. The remaining agar pieces were rinsed with 10 mL of fresh solvent, which was subsequently filtered and combined with the corresponding extract. The solvent was evaporated using a rotary evaporator IKA® RV 10 (IKA Works, USA) or by leaving the flasks uncovered in a fume hood overnight. Methanol extracts were also subjected to freeze-drying for 3 days using a Labconco Freezone 12 Freeze

Dryer (Labconco Corp., MO, USA) to remove the remaining aqueous liquid following rotary evaporation. The dried extracts were resuspended in 1 mL of 50%, 70% or 100% v/v LC-grade methanol and were stored at -80 ºC. Non-inoculated plates of each media were used as controls in all cases. The control plates were prepared, incubated and used for organic extraction in identical conditions as the inoculated media.

2.3.2 LC-MS^2 analysis for untargeted metabolomics

For untargeted metabolomics, two different methods were used. The first method was performed at the University of California San Diego using a Thermo Fisher Scientific Vanquish Ultra High Performance LC System coupled to a Thermo Q Exactive Hybrid Quadrupole-Orbitrap Mass Spectrometer. Metabolite separation was carried out using a Scherzo SM-C18 column (2 × 250 mm, 3 µm, 130 Å; Imtakt, United States) maintained at 40 °C, and utilizing a mobile phase gradient of water/acetonitrile with 0.1% v/v formic acid. Mass spectra were recorded in mixed mode following the MS settings. Then, the raw LC-MS^2 data files were converted into mzXML format using MSConvert (Chambers et al. 2012) for further analysis. Both the raw and the converted files are available in the Mass Spectrometry Interactive Virtual Environment (MassIVE) data repository (massive.ucsd.edu) under the accession number MSV000086628.

The second method was done at the BioZone Mass Spectrometry Facility in the University of Toronto using the Thermo Scientific Ultimate 3000 UHPLC coupled to Thermo Scientific Q-Exactive equipped with a HESI-II probe. Metabolite separation was carried out using a Thermo Scientific Hypersil Gold C18 column (2.1 × 50 mm, 1.9 µm, 175 Å, equipped with guard column) maintained at 40 °C and utilizing a mobile phase gradient of water/acetonitrile with 0.1% v/v formic acid. Mass spectra were recorded using fast polarity

switching. Then, the raw LC-MS^2 data files were converted into mzXML format and separated based on their polarity using MSConvert for further analysis. Both the raw and the converted files are available in the Mass Spectrometry Interactive Virtual Environment (MassIVE) data repository (massive.ucsd.edu) under the accession number MSV000091858.

2.3.3 Targeted detection of *Streptomyces* metabolites

2.3.3.1 Geldanamycin

Detection of geldanamycin in culture extracts was performed by reverse-phase high performance liquid chromatography (RP-HPLC) using an Agilent 1260 Infinity Quaternary LC system (Agilent Technologies Canada Inc., Mississauga, ON). Extracts (5 µl) prepared from triplicate cultures were loaded onto a Poroshell 120 EC-C18 column (4.6 × 50 mm, 2.7 µm particle size; Agilent Technologies Canada Inc.) held at 40 °C. Metabolites were eluted using a linear gradient of acetonitrile and water, each containing 0.1% v/v formic acid. The initial mobile phase consisted of 90% water/10% acetonitrile, and this was held constant for 0.2 min before changing to 0% water/100% acetonitrile over a period of 5.8 min. The mobile phase was maintained at this concentration for 0.4 min, and was then returned to 90% water/10% acetonitrile over 0.6 min. The flow rate was held constant at 1 ml/min. Geldanamycin was monitored using a detection wavelength of 308 nm, and the ChemStation software version B.04.03 (Agilent Technologies Canada Inc.) was used for data acquisition. A standard curve was generated using known amounts of a pure geldanamycin standard dissolved in DMSO (Cayman Chemicals, USA) and was used for metabolite quantification. To confirm the presence of geldanamycin, LC-MS analysis of mMYM and YMS (± 50 mM NAG) culture extracts was performed using an Agilent 1260 Infinity LC-6230 TOF LC-MS system (Agilent Technologies Canada Inc.) with the same column and separation method

described above. Mass spectra were recorded in negative mode between 100 and 3200 *m/z*. Data acquisition was perfomed using Agilent MassHunter version B.08.00 (Agilent Technologies Canada Inc.) and MestReNova version 14.1.2 (Mestrelab Research S.L.) was used for data analysis.

2.3.3.2 Nigericin

Nigericin was detected using a modified version of a previously published protocol (Harvey et al. 2007). Culture extracts were analyzed using an Agilent 1260 Infinity LC-6230 TOF LC-MS system. Extracts (5 µL) from triplicate cultures were loaded onto a Poroshell 120 EC-C18 column (4.6 × 50 mm, 2.7 µm particle size) held at 22°C. The column was equilibrated in 12% ammonium acetate buffer (20 mM)/88% methanol, and compounds were eluted using a linear gradient to 100% methanol over 17 minutes at a constant flow rate of 1 mL/min. Mass spectra were recorded in positive mode between 100 and 3200 *m/z*. Data acquisition was performed using Agilent MassHunter version B.08.00 (Agilent Technologies Canada Inc.) and MestReNova version 14.1.2 (Mestrelab Research S.L.) was used for data analyses. Quantification of nigericin was achieved by generating a standard curve using known amounts of a pure nigericin sodium salt standard dissolved in methanol (Cayman Chemicals, USA).

Another protocol for LC-MS detection of nigericin was as described above, except that a Zorbax SB C-18 column (4.6 × 150 mm, 5 µm particle size) was used for the analysis. The column was equilibrated in 20% ammonium acetate buffer (20 mM)/80% methanol, and compounds were eluted using a linear gradient to 100% methanol over 22.5 minutes at a constant flow rate of 1 mL/min.

2.3.3.3 Elaiophylin

Detection of elaiophylin in culture extracts was performed by RP-HPLC using an Agilent 1260 Infinity Quaternary LC system. Extracts (5 µL) prepared from triplicate cultures were loaded onto a Poroshell 120 EC-C18 column (4.6 × 50 mm, 2.7 µm particle size) held at 40 °C. Metabolites were eluted using a linear gradient of methanol and water. The initial mobile phase consisted of 70% water/30% methanol, and this was held constant for 0.5 min before changing to 0% water/100% methanol over a period of 15 min. The mobile phase was maintained at this concentration for 1 min, and was then returned to 70% water/30% acetonitrile over 1 min. The flow rate was held constant at 1 ml/min. Elaiophylin was monitored using a detection wavelength of 254 nm, and the ChemStation software version B.04.03 was used for data acquisition. A standard curve was generated using known amounts of a pure elaiophylin standard dissolved in DMSO (Cayman Chemicals, USA) and was used for metabolite quantification.

2.3.3.4 Echoside C

Detection of echoside C in culture extracts was performed by RP-HPLC using an Agilent 1260 Infinity Quaternary LC system. Extracts (5 µL) prepared from triplicate cultures were loaded onto a Poroshell 120 EC-C18 column (4.6 × 50 mm, 2.7 µm particle size) held at 40 °C. Metabolites were eluted using a linear gradient of acetonitrile and water with 0.1% v/v formic acid in both phases. The initial mobile phase consisted of 95% water/5% acetonitrile, and this was held constant for 0.5 min before changing to 5% water/95% acetonitrile over a period of 10 minutes. The mobile phase was maintained at this concentration for 1 min, and was then returned to 95% water/5% acetonitrile over 1 min. The flow rate was held constant at 1 mL/min. Echoside C was monitored using a detection

wavelength of 260 nm, and the ChemStation software version B.04.03 was used for data acquisition. A known amount of a pure echoside C standard dissolved in DMSO (Chemspace LLC, USA) was used as a reference.

2.4 Chemoinformatics

2.4.1 Molecular networking

To perform molecular networking, the raw data files were pre-processed using MSConvert (Chambers et al. 2012) with the recommended parameters (https://ccms-ucsd.github.io/GNPSDocumentation/fileconversion/). The files were converted into mzXML files with a 32-bit binary encoding precision and no zlib compression. The Peak Picking filter was selected with the vendor algorithm for MS-Levels 1-2.

The spectral data obtained were analyzed using Feature-Based Molecular Networking (FBMN) (Wang et al. 2016; Nothias et al. 2020). The mzXML files were imported and analyzed using MZmine (version 2.53) (Pluskal et al. 2010; Myers et al. 2017). The parameters used for the analysis are detailed in Table S2.1. The peak area of each ion in the feature quantification table was adjusted by subtracting the area from the corresponding control extract. The spectral summary files (.mgf files) and edited feature quantification tables (.csv files) were then processed using the FBMN workflow within the GNPS web platform (https://gnps.ucsd.edu). The parameters of the FBMN analysis are detailed in Table S2.2. The files were further analyzed using the MolNetEnhancer workflow, which requires the pre-processing of the molecular networks using the Network Annotation Propagation (NAP) and the DEREPLICATOR+ workflows, also available in the GNPS web platform (da Silva et al. 2018; Mohimani et al. 2018; Ernst et al. 2019a). The networks generated were visualized using Cytoscape (Shannon et al. 2003). To further characterize the results in each

network, the spectra of compounds without matches to the GNPS reference libraries were analyzed using MetFrag (Ruttkies et al. 2016), SIRIUS including the CSI:fingerID option (Dührkop et al. 2015, 2019a), and BUDDY with no chemical database restriction (Xing et al. 2023).

The IIMN complement of FBMN was also utilized to analyze untargeted metabolomics data (Schmid et al. 2021). For this, the mzXML files were imported and analyzed using MZmine (version 2.37.corr17.7) (Pluskal et al. 2010). The parameters used for the analysis are detailed in Table S2.3. The peak area of each ion in the feature quantification table was adjusted by subtracting the area from the corresponding control extract. The spectral summary files (.mgf files), edited feature quantification tables (.csv files) and supplementary edge files (.csv files) were then processed using the FBMN workflow (Nothias et al. 2020) within the GNPS web platform (https://gnps.ucsd.edu). The parameters of the FBMN analysis are detailed in Table S2.4. The networks generated were visualized using Cytoscape (Shannon et al. 2003). To further characterize the results in each network, the spectra of compounds without matches to the GNPS reference libraries were analyzed using MetFrag (Ruttkies et al. 2016), SIRIUS, including the CSI:fingerID option (Dührkop et al. 2015, 2019a) and BUDDY with no chemical database restriction (Xing et al. 2023). High confidence predictions were determined as those with an estimated FDR value ≤ 0.05 from BUDDY, or matching the formula prediction from both BUDDY and SIRIUS.

2.5 Bioassays

2.5.1 Potato tuber slice assay

To evaluate the production of phytotoxic compounds, a potato tuber slice bioassay was performed as described before with some modifications (Loria et al. 1995). Whole potato

tubers were peeled, disinfected in a 15% v/v bleach (Clorox) solution for 10 min, and then rinsed twice using sterile distilled water. The tubers were then cut into 1-2 cm thick slices, and four slices were placed into each of three sterile glass Petri dishes (150 mm diameter) containing sterile filter paper pre-wetted with sterile distilled water. Agar cores (8 mm diameter) from 14-day old plate cultures of 11-1-2 were placed on top of each slice, and cores from non-inoculated media were used as controls. When testing organic culture extracts or pure compounds, sterile 6 mm Whatman® filter disks (GE Healthcare Life Sciences) were placed onto the tuber slices, and 20 µL of each extract (or 50%, 70%, or 100% v/v methanol) was added to the center of the disk. For pure compounds, the solutions were prepared to provide the desired concentrations in a final volume of 20 µL, which was then added to the centre of the paper disk. The glass plates were sealed with parafilm and incubated in the dark at room temperature (~22-25ºC) for 7-10 days. Following incubation, the tuber slices were photographed. Each assay was performed twice.

2.5.2 Radish seedling assay

Radish seeds (cv. Cherry Belle; McKenzie Seeds, Canada) were disinfected with 70% v/v ethanol for 5 min and then with 15% v/v of bleach (Chlorox) for 10 min, after which the seeds were rinsed 10 times with sterile distilled water. The seeds were then placed into a sterile deep Petri dish (90 mm diameter) containing pre-wetted sterile filter paper, and they were incubated in the dark at room temperature (~22-25ºC) for 24 hours. Germinated seeds showing good development were selected and placed into wells of a 6-well tissue culture plate (two seeds per well). Each well contained 5 mL of sterile water, and 5 µL of each culture extract or pure compound to the desired concentration was added to three separate wells, while control wells were treated with 5 µL of 50%, 70% or 100% v/v methanol or sterile

water. The tissue culture plates were wrapped with parafilm and were incubated with shaking (100 rpm) at room temperature (~21-23 ºC) under a 16-h photoperiod for five days. The root, shoot and total seedling length were determined for each treatment, and the outliers (namely, highest and lowest recorded length per treatment) were removed, resulting in four data points per treatment. Where indicated, the number of lateral roots was also determined. Each assay was performed three times in total.

2.5.3 Anthocyanin determination assay

The anthocyanin content of radish seedlings treated with culture extracts or pure compounds (Section 2.5.2) was evaluated as described by Uppalapati and collaborators (Uppalapati et al. 2005) with some modifications. Briefly, two representative seedlings per replicate were dried using a paper towel, weighted, and then transferred to a 2-mL tube. Then, 1 mL of 3M HCl:H_2O:methanol (1:3:16) was added to each tube, and the tubes were sealed with parafilm and covered with foil. The tubes were incubated at 15ºC and 110 rpm for 24 hours, after which the solutions were transferred into fresh tubes. An aliquot of 200 µL of each replicate was transferred into a well of a 96-well plate, and absorbances at 530 and 653 nm (A_{530} and A_{653}) were measured using a Synergy H1 Hybrid Reader (BIOTEK, Winooski, Vermont, USA). The anthocyanin content was calculated for each extract using the formula $\frac{(A_{530} - 0.24A_{653})}{\text{fresh weight (g)}}$. The assay was performed twice.

2.5.4 Antimicrobial bioassays

The antimicrobial activity of 11-1-2 agar cores and culture extracts were determined using different microbial indicator organisms (Table 2.1). Cultures of *B. subtilis*, *S. epidermidis* and *P. syringae* pv. *tomato* DC3000 were prepared by inoculating a single

colony into 10 mL of TSB (Appendix 1), while *Saccharomyces cerevisiae* cultures were prepared by inoculating a single colony into 10 mL of YPD broth (Appendix 1). The cultures were incubated overnight at 28ºC (*B. subtilis*, *P. syringae* pv. *tomato*, *S. cerevisiae*) and 37 ºC (*S. epidermidis*), and then 2 mL of each was added to 200 mL of molten TSA (for bacterial cultures) or YPD agar (for yeast cultures). The cells were mixed with the melted agar by swirling, and the agar was then poured into sterile Corning® Square BioAssay dishes (245 mm × 245 mm) and allowed to solidify. Agar cores from 11-1-2 cultures plates, or 6 mm Whatman® filter disks (GE Healthcare Life Sciences) with 20 µL of 11-1-2 culture extract, were placed equidistantly onto the bioassay plates, after which the plates were incubated at the appropriate temperature for 24 hours. The diameter of the zone of inhibition around the agar core or paper disk was recorded after the incubation period.

When testing for antimicrobial activity against *Streptomyces* indicator organisms (Table 2.1), the indicator species were inoculated onto PMA or ISP-4 and were incubated for 10-15 days. The spores and mycelia were then collected using 1.5 mL of sterile water, and 500 µL of the resulting suspension was added to 200 mL of molten TSA. The assay then proceeded as described above.

2.6 Bioinformatics

2.6.1 Multi-locus species tree

The genome of 11-1-2 was previously sequenced (Bown and Bignell 2017). To characterize its phylogenetic placement, an Automated Multi-locus Species Tree was created by submitting the genome sequence to the autoMLST website (Alanjary et al. 2019). Following the *de novo* workflow, a concatenated alignment was built using the Fast alignment mode (MAFFT FFT-NS-2) with 100 genes (Table S2.5), followed by an IQ-TREE

Ultrafast Bootstrap analysis (1000 replicates). The alignment was manually edited to include the most relevant plant-pathogenic *Streptomyces* species and visualized using the R package ggtree v2.2.4 (Yu et al. 2017).

2.6.2 Genomic analyses

To identify specialized metabolite biosynthetic gene clusters in 11-1-2 and other *Streptomyces* species included in the phylogenetic analysis, the genome sequences of these strains (Table S2.6) were analyzed using antiSMASH 6.0 (Blin et al. 2021) with the default parameters, or antiSMASH 7.0 (Blin et al. 2023) with all the extra features available.

The 11-1-2 genome was analyzed and compared using the Biosynthetic Gene Similarity Clustering and Prospecting Engine (BiG-SCAPE) workflow against the MIBiG database with the default parameters (https://git.wur.nl/medema-group/BiG-SCAPE) (Navarro-Muñoz et al. 2020). For the large-scale network and phylogenetic analysis of specific BGCs, 2,136 Streptomycetales genomes (as of November 2022) were downloaded from the National Center for Biotechnology Information (NCBI) and were processed using the command-line version of antiSMASH 5.1.2 with the bacterial setting and otherwise default parameters. Sequence similarity networks and phylogenetic relationships for the nigericin and geldanamycin BGCs were generated using the BiG-SCAPE workflow with the default parameters (https://git.wur.nl/medema-group/BiG-SCAPE) (Navarro-Muñoz et al. 2020). Network files were visualized using Cytoscape version 3.8.2 (Shannon et al. 2003), and the BGCs present within each network were retrieved and compared using Clinker with default parameters and Clustermap.js. was used to visualize the BGC alignment results (Gilchrist and Chooi 2021). Further visualization of selected BGCs was performed using the CAGECAT suite (van den Belt et al. 2023) and Gene Graphics (Harrison et al. 2018).

2.6.3 Prediction of DasR binding sites

The 11-1-2 genome was uploaded to the PREDetector online tool (http://predetector.hedera22.com/) and analyzed to predict the presence of DasR binding sites using the DasR matrix available in the site with the default parameters.

2.6.4 Restriction-methylation systems

Information about the restriction-methylation systems present in the *Streptomyces* sp. 11-1-2, *S. scabiei* 87-22 and *S. hygroscopicus* XM201 genomes was retrieved from the REBASE database (Roberts et al. 2023). When required, amino acid sequences were aligned and compared using the blastp tool available in the NCBI Blast site (https://blast.ncbi.nlm.nih.gov/Blast.cgi).

2.6.5 Domain prediction

The identification of domains present in protein sequences of interest was performed by uploading the amino acid sequences in FASTA format to the InterPro webtool (https://www.ebi.ac.uk/interpro/search/sequence/).

2.6.6 Sequence alignment

Sequence alignments were performed and visualized using the ClustalW alignment within the Geneious version 6.1.2 software (Biomatters Inc., Newark, NJ, USA).

2.7 Statistical analyses

The results of the radish seedling bioassays (seedling length and anthocyanin accumulation) were analyzed using the Student's t-test function in Microsoft Excel 365, or an analysis of variance and Tukey's test using the R package "agricolae", and visualized using "ggplot2" and "ggsignif" (Wickham 2016; Ahlmann-Eltze 2019; de Mendiburu 2020).

The peak areas obtained from RP-HPLC and LC-MS analyses were transformed using the $\log_{10}$ function and analyzed using an ANOVA paired with Dunnett's test in Minitab® version 20.4, or ANOVA paired with Tukey's test as described above. The results were visualized using R packages "ggplot2", "ggsignif" and "patchwork" (Pedersen 2020).

APPENDIX 1.

Media and buffer recipes

2× YT broth: Tryptone 16 g/L, yeast extract 10 g/L, NaCl 5 g/L.

5X Tris Base-Boric Acid-EDTA buffer (TBE): Tris-base 54 g/L, Boric acid 27.5 g/L, EDTA-sodium 4.65 g/L.

AS-1: Yeast extract 1 g/L, L-alanine 0.2 g/L, L-arginine 0.2 g/L, L-asparagine 0.5 g/L, soluble starch 5 g/L, NaCl 2.5 g/L, Na_2SO_4 10 g/L, agar 20 g/L. Final pH 7.5.

GSY: soluble starch 20 g/L, KNO3 1 g/L, NaCl 0.5 g/L, $MgSO_4$ * 7 H_2O 0.2 g/L, K_2HPO_4 0.5 g/L, $FeSO_4$ * 7 H_2O 0.01 g/L, yeast extract 1 g/L, agar 15 g/L. Final pH 7.4. Different $CaCl_2$ and $MgCl_2$ concentrations were added after autoclaving as required.

International *Streptomyces* Project Medium 4: ISP-4 powder (BD Difco) 8 g/L.

LB agar: LB Miller (Fisher Scientific) 25 g/L, agar 15 g/L.

LB broth: LB Miller (Fisher Scientific) 25 g/L.

Low salt LB: 1% w/v tryptone, 0.5% w/v yeast extract, 0.25% sodium chloride.

M4: soybean flour 15 g/L, soluble starch 25 g/L, yeast extract 2g/L, agar 20 g/L. Final pH 7.2.

MMM: $NH_4(SO_4)$ 1g/L, K_2HPO_4 0.5 g/L, $MgSO_4$ * 7 H_2O 0.2 g/L, $FeSO_4$ * 7 H_2O 0.01 g/L, agar 10 g/L. Final pH 7-7.2. 50 mL of 10% mannitol are added after autoclaving.

mMYM: Maltose 4 g/L, yeast extract 4 g/L, malt extract broth 10 g/L, agar 20 g/L.

NA: nutrient broth (BD Difco™) 8g/L, agar 15 g/L.

Nutrient agar (NA): nutrient broth (Difco) 8 g/L, agar 15 g/L.

OBA: Oat bran 20 g/L, Trace Element Solution 2 mL/L, 15 g/L. Final pH 7.2. The oat bran is taken to boiling point in water (half of the desired volume), simmered for 20 minutes in a

microwave, and then let to cool down with stirring for 1 hour. Then, the trace elements are added, followed by pH adjustment and then the agar is incorporated.

P buffer: sucrose 103 g/L, K_2SO_4 0.25 g/L, $MgCl_2$ * 6 H_2O 2.02 g/L, trace element solution 2 ml/L in 800 mL of water. Before use, add 10 ml of 0.5% w/v KH_2PO_4, 100 ml of 3.68% w/v $CaCl_2$ * 2 H_2O and 100 ml of 5.73% w/v TES buffer (pH 7.2) to complete 1 liter.

PMA: Instant mashed potato flakes 50g/L, agar 20 g/L.

Pregermination broth: yeast extract 10 g/L, Difco casaminoacids 10 g/L, 10 mM $CaCl_2$.

R2YE: sucrose 103 g/L, K_2SO_4 0.25 g/L, $MgCl_2$ * 6 H_2O 10.12 g/L, glucose 10 g/L, Difco casaminoacids 0.1 g/L in 800 mL of water. Before use, add 10 ml of 0.5% w/v KH_2PO_4, 80 ml of 3.68% w/v $CaCl_2$ * 2 H_2O, 15 mL of 20% L-proline, 100 ml of 5.73% w/v TES buffer (pH 7.2), trace element solution 2 ml/L, 50 mL of 10% w/v of yeast extract and 5 mL of 1M NaOH to complete 1 liter.

SA: soluble starch 10 g/L, L-asparagine 2 g/L, MOPS 21 g/L, $MgSO_4$ * 7 H_2O 0.6 g/L, K_2HPO_4 4.4 g/L, trace element solution 1mL/L, agar 15 g/L Final pH 6.8

SFM agar: soybean flour 20 g/L, mannitol 20 g/L, 1mL/L. Final pH 6.8

SLB media: sucrose 103 g/L, tryptone 10 g/L, yeast extract 5 g/L, NaCl 5 g/L. Final pH 7.0.

SM liquid media: glucose 10 g/L, yeast extract 4 g/L, peptone 4 g/L, K_2HPO_4 4 g/L, KH_2PO_4 2 g/L, $MgSO_4$ * 7 H_2O 0.5 g/L, sucrose 103 g/L.

SOB: 2% w/v bacto-tryptone, 0.5% w/v yeast extract, 0.05% w/v NaCl.

SOB^{++}: 2% w/v bacto-tryptone, 0.5% w/v yeast extract, 0.05% w/v NaCl, 2.5 mM KCl supplemented with 10 mM of $MgCl_2$ and 10 mM $MgSO_4$ after sterilization.

SOC: 2% w/v bacto-tryptone, 0.5% w/v yeast extract, and 0.05% w/v NaCl supplemented 25 mM KCl with 10 mM of $MgCl_2$, 10 mM $MgSO_4$ and 20 mM of glucose after sterilization.

TB Buffer: 10 mM HEPES pH 6.7, 15 mM $CaCl_2$, 55 mM $MnCl_2$, 250 mM KCl.

Trace element solution for SA: $FeSO_4$ * $7H_2O$ 1 g/L, $MnCl_2$ * $4H_2O$ 1 mg/L $CaCl_2$ * $2H_2O$ 1.3 g/L, ZnSO4 * $7H_2O$ 1 g/L. The solution is mixed, filter sterilized and stored at 4ºC.

Trace element solution for OBA: $ZnCl_2$ 40 mg/L, $FeCl_3$ * $6H_2O$ 200 mg/L, $CuCl_2$ * $2H_2O$ 10 mg/L, $MnCl_2$ * $4H_2O$ 10 mg/L, $Na_2B_4O_7$ * $10H_2O$ 10 mg/L, $(NH_4)_6Mo_7O_{24}$ * $4H_2O$ 10 mg/L.

Trace element solution for P buffer and R2YE: $ZnCl_2$ 40 mg/L, $FeCl_3$ * $6H_2O$ 200 mg/L, $CuCl_2$ * $2H_2O$ 10 mg/L, $MnCl_2$ * $4H_2O$ 10 mg/L, $Na_2B_4O_7$ * $10H_2O$ 10 mg/L, $(NH_4)_6Mo_7O_{24}$ * $4H_2O$ 10 mg/L.

Tryptic soy agar (TSA): tryptic soy broth (BD Biosciences) 30 g/L, agar 15 g/L.

Tryptic soy broth - starch (TSB-S): tryptic soy broth (BD Biosciences) 30 g/L, soluble starch 10 g/L.

Tryptic soy broth (TSB): tryptic soy broth (BD Biosciences) 30 g/L.

YEME: yeast extract 3 g/L, bacto-peptone 5 g/L, malt extract 3 g/L, glucose 10 g/L, sucrose 340 g/L. After autoclaving, add $MgCl_2$, 5 mM final concentration.

YMS: 0.4% w/v Yeast extract, 0.4% w/v soluble starch (Fisher Scientific, Canada), 1% m/v malt extract, 10 mM $CoCl_2$ * $6H_2O$ (final concentration = 0.021 mM), 2% agar. Final pH 7.2.

YPD: yeast extract 10 g/L, peptone 20 g/L, dextrose 20 g/L. For solid medium, agar 20 g/L.

Supplementary Tables

Table S2.1. MZmine parameters used to process untargeted metabolomics files for Feature-Based Molecular Networking.

Parameter		FBMN
Job ID in GNPS		**ID=da29f29c08da44719af6cf811a12ec28 ID=cfc2b152c8cb444e80c3a5a21eaf2107 ID=3939fbbf8b9c4e82a8865baa2647dc68 ID=55298dfedf86472496a3cdb88e098a59**
Mass detection MS1		
	Scans	1
	Mass detector	Centroid; 15000
	Mass list name	masses
Mass detection MS2		
	Scans	2
	Mass detector	Centroid; 1000
	Mass list name	masses
Chromatogram builder - ADAP		
	Scans	5
	Mass list	masses
	Group intensity threshold	500000
	Min height	100000
	m/z tolerance	0.02; 10 ppm
	Suffix	chromatograms
Chromatogram deconvolution		
	Suffix	deconvoluted
	Algorithm	Local Minimum Search: Chromatographic threshold 10%; Search minimum in RT range (min) 0.1 ; Minimum relative height 30%; Minimum absolute height 100000; Min ratio of peak top/edge 1.0; Peak duration range (min) 0.0-3.0
	m/z center calculation	Median
	m/z range for MS2 scan pairing (Da)	0.025
	RT range for MS2 scan pairing (min)	0.15
Isotopic peaks grouper		
	Suffix	deisotoped

	m/z tolerance	0.01 ; 10 ppm
	Retention time tolerance	0.2
	Monotonic shape	Checked
	Maximum charge	2
	Representative isotope	Most intense
Join Aligner		
	Peak list name	Aligned peak lists
	m/z tolerance	0.02; 10 ppm
	Weight for *m/z*	80
	Retention time tolerance	0.2
	Weight for RT	20
	Require same charge state	No
Peak finder (multithreaded)		
	Suffix	gap-filled
	Intensity Tolerance	5%
	m/z tolerance	0.02; 10 ppm
	Retention time tolerance	0.2
Peak list rows filter		
	Suffix	filtered
	Minimum peaks in a row	3
	Minimum peaks in an isotope pattern	2
	Peak duration range (min)	0-3
	Keep or remove rows	Keep all that match criteria
	Keep only peaks with MS2 scan	Checked
	Reset the peak number ID	Checked

Table S2.2. Parameters for Feature-Based Molecular Networking in the GNPS platform.

Parameter		
Basic options		
	Precursor Ion Mass Tolerance	0.02
	Fragment Ion Mass Tolerance	0.02
Advanced Network Options		
	Min pairs Cos	0.7
	Min matched fragment ions	6
Any other parameter not included here was used as the default value from the workflow. The spectra was then compared against the GNPS spectral libraries and only results with a cosine value equal or higher than 0.7 and at least 6 fragment ions were kept.		

Table S2.3. MZmine parameters used to process untargeted metabolomics files for Ion Identity Molecular Networking.

Parameter		**IIN6.2 (2020)**	**IIMN_MeOH and IIMN_EtOAc (2023)**
Job ID in GNPS		**ID=edd7891711114ce6874f0697fc578f83**	**ID=0d9c1a422b544d9ca702919498701dd5 ID=1c940ee0450246829e8d503bee711285**
Mass detection MS1			
	Scans	1	1
	Mass detector	15000	100000
	Mass list name	masses	masses
Mass detection MS2			
	Scans	2	2
	Mass detector	1000	1000
	Mass list name	masses	masses
Chromatogram builder - ADAP			
	Scans	4	4
	Mass list	masses	masses
	Group intensity threshold	500000	500000
	Min height	50000	100000
	m/z tolerance	0.01; 10 ppm	0.01; 10 ppm
	Suffix	chromatograms	chromatograms
Chromatogram deconvolution			
	Suffix	deconvoluted	deconvoluted

	Algorithm	S/N threshold = 10; min feature height 50000; coefficient/area threshold = 60; peak duration range = 0.01-0.5 min, RT wavelet range = 0.01-0.1	Local Minimum Search: Chromatographic threshold 10%; Search minimum in RT range (min) 0.2 ; Minimum relative height 10%; Minimum absolute height 500000.0; Min ratio of peak top/edge 1.0; Peak duration range (min) 0.0-3.0
	m/z center calculation	Median	Median
	m/z range for MS2 scan pairing (Da)	0.02	0.02
	RT range for MS2 scan pairing (min)	0.2	0.2
Isotopic peaks grouper			
	Suffix	deisotoped	deisotoped
	m/z tolerance	0.01 ; 10 ppm	0.01 ; 5 ppm
	Retention time tolerance	0.5	0.15
	Monotonic shape	Checked	Checked
	Maximum charge	4	4
	Representative isotope	Most intense	Most intense
Join Aligner			
	Peak list name	Aligned peak lists	Aligned peak lists
	m/z tolerance	0.01; 10 ppm	0.01; 5 ppm
	Weight for *m/z*	75	75
	Retention time tolerance	0.5	0.25
	Weight for RT	25	25
	Require same charge state	No	No
Peak finder (multithreaded)			
	Suffix	gap-filled	gap-filled
	Intensity Tolerance	5%	5%
	m/z tolerance	0.01; 5 ppm	0.01; 5 ppm
	Retention time tolerance	0.15	0.2
Peak filter			
	Suffix	N/A	filtered
	Duration (min)	N/A	0-3
	# data points	N/A	3-10000
Duplicate Peak filter			
	Suffix	N/A	filtered

	Filter mode	N/A	New average
	m/z tolerance	N/A	0.001 or 5 ppm
	RT tolerance	N/A	0.15
Peak list rows filter			
	Suffix	filtered	filtered
	Minimum peaks in a row	2	3
	Minimum peaks in an isotope pattern	2	1
	Peak duration range	-	-
	Keep or remove rows	Keep all that match criteria	Keep all that match criteria
	Keep only peaks with MS2 scan	Checked	Checked
	Reset the peak number ID	Checked	Checked
Metacorrelate			
	RT tolerance	0.1	0.2
	Min height	10000	100000
	Noise level	1000	10000
	Correlation grouping	Checked; min data points 5, Min data points on edge 2; measure PEARSON; min feature shape correlation 85%	Checked; min data points 5, Min data points on edge 2; measure PEARSON; min feature shape correlation 85%
	Feature height correlation	Checked; min data points 3, measure PEARSON; min correlation 70%	Checked; min data points 3, measure PEARSON; min correlation 70%
Ion identity networking			
	m/z tolerance	0.001; 10 ppm	0.001; 10 ppm
	Check	ONE FEATURE	ONE FEATURE
	Min height	100000	100000
	Annotation refinement	No	No
	Ion identity library	Positive; max charge 2; max mol/cluster 2	Positive; max charge 2; max mol/cluster 2
		Adducts: [M+H]+; [M+Na]+; [M+NH4]+; [M+2H]2+; [M+H+Na]2+	Adducts: [M+H]+; [M+Na]+; [M+K]+; [M+NH4]+; [M+2H]2+; [M+H+Na]2+
		Modifications: [M-H2O]; [M-2H2O]	Modifications: [M-H2O]; [M-2H2O]

	Ion identity library	Negative; max charge 2; max mol/cluster 2	Negative; max charge 2; max mol/cluster 2
		Adducts: [M-H]-; [M+Cl]-	Adducts: [M-H]-; [M+Cl]-; [M+FA]-
		Modifications: [M-H2O]; [M-2H2O]	Modifications: [M-H2O]; [M-2H2O]
Add Ion identities to network	*m/z* tolerance	0.001; 10 ppm	0.001; 10 ppm
	Min height	100000	100000
	Ion identity library	Adducts: [M+H]+; [M+Na]+; [M+K]+; [M+NH4]+; [M+2H]2+; [M+Ca]2+; [M+Fe]2+; [M+H+Na]2+; [M+H+NH4]2+; [M-H+2Na]; [M+Ca-H]+; [M+Fe-H]+	Adducts: [M+H]+; [M+Na]+; [M+K]+; [M+NH4]+; [M+2H]2+; [M+Ca]2+; [M+Fe]2+; [M+H+Na]2+; [M+H+NH4]2+; [M-H+2Na]; [M+Ca-H]+; [M+Fe-H]+; [M+HFA]-
Add Ion identities to network	*m/z* tolerance	0.001; 10 ppm	0.001; 10 ppm
	Min height	100000	100000
	Ion identity library	Adducts: [M-H]-; [M-2H+Na]-; [M+Cl]-; [M+FA]-	Adducts: [M-H]-; [M-2H+Na]-; [M+Cl]-; [M+FA]-
		Modifications: [M-H2O]; [M-2H2O]; [M-NH3]	Modifications: [M-H2O]; [M-2H2O]; [M-NH3]; [M+FA]-

Table S2.4. Parameters for Ion Identity Molecular Networking in the GNPS platform.

Parameter		
Basic options		
	Precursor Ion Mass Tolerance	0.02
	Fragment Ion Mass Tolerance	0.02
Advanced Network Options		
	Min pairs Cos	0.7
	Min matched fragment ions	5
Any other parameter not included here was used as the default value from the workflow. The spectra was then compared against the GNPS spectral libraries and only results with a cosine value equal or higher than 0.7 and at least 5 fragment ions were kept.		

Table S2.5. Genes used in autoMLST to construct the phylogenetic tree.

Accession number	Gene	Function	Description
TIGR00133	gatB	Protein synthesis	aspartyl/glutamyl-tRNA(Asn/Gln) amidotransferase, B subunit
TIGR00132	gatA	Protein synthesis	aspartyl/glutamyl-tRNA(Asn/Gln) amidotransferase, A subunit
TIGR03953	rplD_bact	Protein synthesis	50S ribosomal protein uL4
TIGR01959	nuoF_fam	Energy metabolism	NADH oxidoreductase (quinone), F subunit
TIGR00138	rsmG_gidB	Protein synthesis	16S rRNA (guanine(527)-N(7))-methyltransferase RsmG
TIGR01816	sdhA_forward	Energy metabolism	succinate dehydrogenase, flavoprotein subunit
TIGR01520	FruBisAldo_II_A	Energy metabolism	fructose-bisphosphate aldolase, class II
TIGR00036	dapB	Amino acid biosynthesis	4-hydroxy-tetrahydrodipicolinate reductase
TIGR01529	argR_whole	Regulatory functions	arginine repressor
TIGR00763	lon	Protein fate	endopeptidase La
TIGR00447	pth	Protein synthesis	aminoacyl-tRNA hydrolase
TIGR02692	tRNA_CCA_actino	Protein synthesis	CCA tRNA nucleotidyltransferase
TIGR00331	hrcA	Regulatory functions	heat-inducible transcription repressor HrcA
TIGR01049	rpsJ_bact	Protein synthesis	ribosomal protein uS10
TIGR01044	rplV_bact	Protein synthesis	ribosomal protein uL22
TIGR00338	serB	Amino acid biosynthesis	phosphoserine phosphatase SerB
TIGR00962	atpA	Energy metabolism	ATP synthase F1, alpha subunit
TIGR01127	ilvA_1Cterm	Amino acid biosynthesis	threonine ammonia-lyase
TIGR01966	RNasePH	Transcription	ribonuclease PH
TIGR00459	aspS_bact	Protein synthesis	aspartate--tRNA ligase
TIGR00754	bfr	Transport and binding proteins	bacterioferritin
TIGR02504	NrdJ_Z	Purines, pyrimidines, nucleosides, and nucleotides	ribonucleoside-diphosphate reductase, adenosylcobalamin-dependent
TIGR03594	GTPase_EngA	Protein synthesis	ribosome-associated GTPase EngA
TIGR00088	trmD	Protein synthesis	tRNA (guanine(37)-N(1))-methyltransferase
TIGR00855	L12	Protein synthesis	ribosomal protein bL12
TIGR00615	recR	DNA metabolism	recombination protein RecR
TIGR00244	TIGR00244	Regulatory functions	transcriptional regulator NrdR

TIGR01039	atpD	Energy metabolism	ATP synthase F1, beta subunit
TIGR01134	purF	Purines, pyrimidines, nucleosides, and nucleotides	amidophosphoribosyltransferase
TIGR01137	cysta_beta	Amino acid biosynthesis	cystathionine beta-synthase
TIGR00690	rpoZ	Transcription	DNA-directed RNA polymerase, omega subunit
TIGR01032	rplT_bact	Protein synthesis	ribosomal protein bL20
TIGR00019	prfA	Protein synthesis	peptide chain release factor 1
TIGR00012	L29	Protein synthesis	ribosomal protein uL29
TIGR01978	sufC	Biosynthesis of cofactors, prosthetic groups, and carriers	FeS assembly ATPase SufC
TIGR02673	FtsE	Cellular processes	cell division ATP-binding protein FtsE
TIGR00150	T6A_YjeE	Protein synthesis	tRNA threonylcarbamoyl adenosine modification protein YjeE
TIGR01389	recQ	DNA metabolism	ATP-dependent DNA helicase RecQ
TIGR00090	rsfS_iojap_ybeB	Protein synthesis	ribosome silencing factor
TIGR00554	panK_bact	Biosynthesis of cofactors, prosthetic groups, and carriers	pantothenate kinase
TIGR02127	pyrF_sub2	Purines, pyrimidines, nucleosides, and nucleotides	orotidine 5'-phosphate decarboxylase
TIGR00096	TIGR00096	Protein synthesis	16S rRNA (cytidine(1402)-2'-O)-methyltransferase
TIGR01302	IMP_dehydrog	Purines, pyrimidines, nucleosides, and nucleotides	inosine-5'-monophosphate dehydrogenase
TIGR03800	PLP_synth_Pdx2	Biosynthesis of cofactors, prosthetic groups, and carriers	pyridoxal 5'-phosphate synthase, glutaminase subunit Pdx2
TIGR01022	rpmJ_bact	Protein synthesis	ribosomal protein bL36
TIGR01021	rpsE_bact	Protein synthesis	ribosomal protein uS5
TIGR00065	ftsZ	Cellular processes	cell division protein FtsZ
TIGR00064	ftsY	Protein fate	signal recognition particle-docking protein FtsY
TIGR00060	L18_bact	Protein synthesis	ribosomal protein uL18
TIGR00062	L27	Protein synthesis	ribosomal protein bL27
TIGR01394	TypA_BipA	Regulatory functions	GTP-binding protein TypA/BipA
TIGR00639	PurN	Purines, pyrimidines, nucleosides, and nucleotides	phosphoribosylglycinamide formyltransferase

TIGR00302	TIGR00302	Purines, pyrimidines, nucleosides, and nucleotides	phosphoribosylformylglycinamidine synthase, purS protein
TIGR00431	TruB	Protein synthesis	tRNA pseudouridine(55) synthase
TIGR00263	trpB	Amino acid biosynthesis	tryptophan synthase, beta subunit
TIGR01011	rpsB_bact	Protein synthesis	ribosomal protein uS2
TIGR01855	IMP_synth_hisH	Amino acid biosynthesis	imidazole glycerol phosphate synthase, glutamine amidotransferase subunit
TIGR00409	proS_fam_II	Protein synthesis	proline--tRNA ligase
TIGR03705	poly_P_kin	Central intermediary metabolism	polyphosphate kinase 1
TIGR01169	rplA_bact	Protein synthesis	ribosomal protein uL1
TIGR00482	TIGR00482	Biosynthesis of cofactors, prosthetic groups, and carriers	nicotinate (nicotinamide) nucleotide adenylyltransferase
TIGR01164	rplP_bact	Protein synthesis	ribosomal protein uL16
TIGR01009	rpsC_bact	Protein synthesis	ribosomal protein uS3
TIGR00168	infC	Protein synthesis	translation initiation factor IF-3
TIGR02012	tigrfam_recA	DNA metabolism	protein RecA
TIGR02970	succ_dehyd_cytB	Energy metabolism	succinate dehydrogenase, cytochrome b556 subunit
TIGR00086	smpB	Protein synthesis	SsrA-binding protein
TIGR00048	rRNA_mod_RlmN	Protein synthesis	23S rRNA (adenine(2503)-C(2))-methyltransferase
TIGR00184	purA	Purines, pyrimidines, nucleosides, and nucleotides	adenylosuccinate synthase
TIGR00166	S6	Protein synthesis	ribosomal protein bS6
TIGR02075	pyrH_bact	Purines, pyrimidines, nucleosides, and nucleotides	UMP kinase
TIGR00651	pta	Energy metabolism	phosphate acetyltransferase
TIGR00498	lexA	Regulatory functions	repressor LexA
TIGR03654	L6_bact	Protein synthesis	ribosomal protein uL6
TIGR01171	rplB_bact	Protein synthesis	ribosomal protein uL2
TIGR00959	ffh	Protein fate	signal recognition particle protein
TIGR01455	glmM	Central intermediary metabolism	phosphoglucosamine mutase
TIGR01071	rplO_bact	Protein synthesis	ribosomal protein uL15
TIGR01073	pcrA	DNA metabolism	ATP-dependent DNA helicase PcrA
TIGR00952	S15_bact	Protein synthesis	ribosomal protein uS15
TIGR00700	GABAtrnsam	Central intermediary metabolism	4-aminobutyrate transaminase

TIGR01632	L11_bact	Protein synthesis	ribosomal protein uL11
TIGR00461	gcvP	Energy metabolism	glycine dehydrogenase
TIGR00190	thiC	Biosynthesis of cofactors, prosthetic groups, and carriers	phosphomethylpyrimidine synthase
TIGR00468	pheS	Protein synthesis	phenylalanine--tRNA ligase, alpha subunit
TIGR01736	FGAM_synth_II	Purines, pyrimidines, nucleosides, and nucleotides	phosphoribosylformylglycinamidine synthase II
TIGR01737	FGAM_synth_I	Purines, pyrimidines, nucleosides, and nucleotides	phosphoribosylformylglycinamidine synthase I
TIGR01066	rplM_bact	Protein synthesis	ribosomal protein uL13
TIGR01067	rplN_bact	Protein synthesis	ribosomal protein uL14
TIGR01063	gyrA	DNA metabolism	DNA gyrase, A subunit
TIGR00580	mfd	DNA metabolism	transcription-repair coupling factor
TIGR00228	ruvC	DNA metabolism	crossover junction endodeoxyribonuclease RuvC
TIGR00670	asp_carb_tr	Purines, pyrimidines, nucleosides, and nucleotides	aspartate carbamoyltransferase
TIGR03635	uS17_bact	Protein synthesis	ribosomal protein uS17
TIGR01059	gyrB	DNA metabolism	DNA gyrase, B subunit
TIGR00343	TIGR00343	Biosynthesis of cofactors, prosthetic groups, and carriers	pyridoxal 5'-phosphate synthase, synthase subunit Pdx1
TIGR03631	uS13_bact	Protein synthesis	ribosomal protein uS13
TIGR03632	uS11_bact	Protein synthesis	ribosomal protein uS11
TIGR01051	topA_bact	DNA metabolism	DNA topoisomerase I
TIGR01050	rpsS_bact	Protein synthesis	ribosomal protein uS19

Table S2.6. Genome accessions used for phylogenetic tree and antiSMASH analysis.

Species name	**Accession**
Nocardiopsis dassonvillei subsp. *dassonvillei* DSM 43111	CP002040.1
Streptomyces alboflavus NRRL B-2373	JNXT00000000.1
Streptomyces ambofaciens ATCC 23877	CP012382.1
Streptomyces antioxidans MUSC 164	LAKD00000000
Streptomyces autolyticus CGMCC0516	CP019458
Streptomyces bottropensis ATCC 25435	ARTP00000000
Streptomyces bungoensis DSM 41781	LMWX00000000
Streptomyces caatingaensis CMAA-1322	LFXA00000000
Streptomyces catenulae NRRL B-2342	JODY00000000.1
Streptomyces celluloflavus NRRL B-2493	JOEL00000000
Streptomyces chattanoogensis NRRL ISP-5002	LGKG00000000
Streptomyces corchorusii DSM 40340	LMWP00000000
Streptomyces decoyicus NRRL 2666	LGUU00000000
Streptomyces europaeiscabiei NCPPB-4064	JPPV00000000
Streptomyces fodineus TW1S1	CP017248
Streptomyces himastatinicus ATCC 53653	ACEX00000000.1
Streptomyces hygroscopicus subsp. *hygroscopicus* NBRC 100766	BCAN00000000
Streptomyces hygroscopicus subsp. *hygroscopicus* NBRC 16556	BBOU00000000
Streptomyces hygroscopicus subsp. *hygroscopicus* NRRL B-1477	JOIK00000000.1
Streptomyces hygroscopicus subsp. *hygroscopicus* strain OsiSh-1	MDFG00000000
Streptomyces hygroscopicus XM201	CP018627
Streptomyces iranensis	LK022848
Streptomyces leeuwenhoekii C34 DSM 42122 NRRL B-24963	LN831790.1
Streptomyces luteus TRM 45540	JNFQ00000000
Streptomyces lydicus NRRL ISP-5461	JNZA00000000.1
Streptomyces melanosporofaciens DSM 40318	FNST00000000
Streptomyces niger NRRL B-3857	JOFQ00000000
Streptomyces noursei ATCC 11455	CP011533.1
Streptomyces ochraceiscleroticus NRRL ISP-5594	JOAX00000000.1
Streptomyces platensis DSM 40041	MIGA00000000
Streptomyces rimosus subsp. *rimosus* ATCC 10970	CP023688.1
Streptomyces rimosus subsp. *rimosus* NRRL ISP-5260	JNYR00000000
Streptomyces sp. 11-1-2	CP022545
Streptomyces sp. NBRC 109436	BBON00000000.1
Streptomyces sp. NBRC 110028	BBUZ00000000.1

Streptomyces sp. PRh5	JABQ01000001
Streptomyces sp. SPMA113	BDFA00000000.1
Streptomyces sparsogenes ATCC 25498	MAXF00000000.1
Streptomyces stelliscabiei strain P3825	JPPZ00000000
Streptomyces turgidiscabies T45	BCMN00000000
Streptomyces varsoviensis NRRL B-3589	JOFN00000000
Streptomyces violaceusniger NRLL F-8817	LLZJ00000000
Streptomyces violaceusniger Tu 1443	CP002994
Streptomyces violens NRRL ISP-5597	JOBH00000000
Streptomyces viridosporus ATCC 14672	ABYA00000000
Streptomyces yokosukanensis DSM 40224	LMWN00000000
Streptomyces sp. RTd22	CP015726
Streptomyces bingchenggensis BCW-1	NC_016582
Streptomyces scabiei 87-22	NC_013929
Streptomyces acidiscabies 84-104	AHBF01000001.1

CHAPTER 3

NIGERICIN AND GELDANAMYCIN ARE PHYTOTOXIC SPECIALIZED METABOLITES PRODUCED BY THE PLANT PATHOGEN *STREPTOMYCES* SP. 11-1-2

3.1 Abstract

Streptomyces bacteria are a key source of microbial specialized metabolites with useful applications in medicine and agriculture. In addition, some species are important plant pathogens and cause diseases such as potato scab, which reduces the quality and market value of affected potato crops. Most scab-associated *Streptomyces* spp. produce the phytotoxic metabolite thaxtomin A as the principal pathogenicity factor. However, recent reports have described scab-causing strains that do not produce thaxtomin A, but instead produce other phytotoxins that are thought to contribute to plant host infection and symptom development. *Streptomyces* sp. 11-1-2 is a highly pathogenic strain that was originally isolated from a scab symptomatic potato tuber in Newfoundland, Canada. The strain secretes one or more phytotoxic compounds of unknown identity, and it is hypothesized that these compounds serve as virulence factors for this organism. The genome sequence of *Streptomyces* sp. 11-1-2 was analyzed and biosynthetic gene clusters for producing the known herbicidal compounds nigericin and geldanamycin were found. Phytotoxic culture extracts were analyzed using liquid chromatography-coupled tandem mass spectrometry and molecular networking, and this confirmed the production of both compounds by *Streptomyces* sp. 11-1-2 along with other, potentially related metabolites. The biosynthesis of both metabolites was found to be suppressed by the addition of *N*-acetylglucosamine to the culture medium,

and pure nigericin and geldanamycin were able to exhibit phytotoxic effects against both radish seedlings and potato tuber tissue. Furthermore, the coadministration of the two compounds produced greater phytotoxic effects against potato tuber tissue than administration of each compound alone. As the biological activity of nigericin and geldanamycin is vastly different from the proposed activity of thaxtomin A against plants, the secretion of these compounds may represent a novel mechanism of plant pathogenicity exhibited by some *Streptomyces* species.

3.2 Introduction

Members of the genus *Streptomyces* are widely regarded as one of the main natural sources of antibiotics and other medically relevant compounds, and they also have an important role in microbial communities associated with healthy soils and good plant development (Bakker et al. 2010; Kinkel et al. 2012; Viaene et al. 2016; Rey and Dumas 2017). However, some *Streptomyces* species are capable of causing plant diseases, of which scab disease of potato is considered the most important, due to the negative impact on the quality and market value of the potato crop (Wanner and Kirk 2015; Charkowski et al. 2020). *S. scabiei* was the first species to be described as a causal agent of potato scab, although multiple surveys across the world have resulted in the identification of other relevant species, including *S. turgidiscabies*, *S. acidiscabies* and *S. europaeiscabiei* (Li et al. 2019c).

Like other members of the *Streptomyces* genus, *S. scabiei* has the potential to produce a diverse array of specialized metabolites, but only a few have been determined to exhibit phytotoxic activity. Thaxtomin A, a 2,5-diketopiperazine, has been shown to be essential for scab disease development by *S. scabiei*, thus making it the principal pathogenicity determinant of this organism, as well as in other closely related species (Lawrence et al. 1990;

Goyer et al. 1998; Li et al. 2019c). The biosynthesis of thaxtomin A in these species involves a BGC consisting of seven open reading frames, of which six genes (*txtABCDEH*) play a direct role in metabolite production, and one (*txtR*) functions as a regulator of metabolite biosynthesis (Healy et al. 2000, 2002; Joshi et al. 2007; Barry et al. 2012; Li et al. 2019b). The thaxtomin BGC is highly conserved among scab-causing pathogens (Huguet-Tapia et al. 2016; Zhang et al. 2016b) and is widely used for the detection and quantification of scab pathogens in soils using polymerase chain reaction (PCR) (Wang and Lazarovits 2004; Wanner 2006, 2007; Qu et al. 2008; St-Onge et al. 2008). However, recent reports suggest that *Streptomyces* spp. that do not produce thaxtomin A are capable of causing scab disease symptoms on potato tubers, and this has been attributed to the production of other specialized metabolites with phytotoxic activity. Notably, *Streptomyces* sp. GK18 produces borrelidin (Cao et al. 2012), while a *S. niveiscabiei* strain was shown to produce the polyketide desmethylmensacarcin (Lapaz et al. 2017, 2018). Moreover, a survey conducted in Central Europe reported pathogenic isolates missing the *txtAB* genes from the thaxtomin BGC, suggesting that other unidentified factors are responsible for scab development (Pánková et al. 2012).

A survey conducted in Newfoundland, Canada between 2011 and 2012 (Fyans et al. 2016) reported the isolation of multiple pathogenic *Streptomyces* strains from scab-infected potatoes, one of which (*Streptomyces* sp. 11-1-2, herein referred to as 11-1-2) was found to produce one or more highly phytotoxic metabolites that were not thaxtomin A or borrelidin (Fyans et al. 2016). The objective of this research chapter was to further investigate the phytotoxic compound(s) produced by 11-1-2 using genomic analyses, LC-MS, and untargeted LC-MS^2-based metabolomics analysis. Using this approach, nigericin and geldanamycin were identified in 11-1-2 extracts, both of which are phytotoxic at low amounts

and exhibit synergistic effects in promoting damage to potato tuber tissue. Further, there is evidence that compounds related to these metabolites are also produced by *Streptomyces* sp. 11-1-2 and may contribute to the phytotoxic activity of this strain.

3.3 Results and Discussion

3.3.1 *Streptomyces* sp. 11-1-2 is phylogenetically and metabolically distinct from other plant pathogenic *Streptomyces* spp.

Initial work on the characterization of the 11-1-2 strain revealed that it is not closely related to the known scab pathogens *S. scabiei*, *S. acidiscabies, S. turgidiscabies* or *S. europaeiscabiei*, suggesting that it belongs to a novel group of pathogenic species (Fyans et al. 2016). To further elucidate the phylogenetic placement of 11-1-2, a multilocus species tree was constructed using the online tool autoMLST (Alanjary et al. 2019). The analysis revealed that 11-1-2 is highly similar to *Streptomyces hygroscopicus* strain XM201 (Fig. 3.1), sharing over 98% of the average nucleotide identity (Table S3.1). *S. hygroscopicus* XM201 was isolated from soil in China and has been reported as a source of different specialized metabolites (Wu et al. 2009; Meng et al. 2017; Wang et al. 2017). Other closely related strains include the soil-isolated *Streptomyces violaceusniger* Tü 4113 (Höltzel et al. 1998), *Streptomyces melanosporofaciens* DSM 40318, and *S. violaceusniger* NRRL F-8817. Type strains for these species have been grouped in the *S. violaceusniger* subclade, which in turn is part of the larger *S. hygroscopicus* clade (Rong and Huang 2012, 2014). Recently, an analysis of the *Streptomyces* pan-genome confirmed that 11-1-2 and *S. hygroscopicus* XM201 are closely related to each other, and that both strains share more similarity at the genomic level with *S. violaceusniger* than *S. hygroscopicus,* suggesting that they should be re-classified as *S. violaceusniger* (Caicedo-Montoya et al. 2021). Plant pathogenic

Streptomyces strains are usually located within or near the *S. scabiei* clade. They often share some genomic traits such as thaxtomin A biosynthesis and the presence of other virulence genes such as *nec1* and/or *tomA* (Labeda 2011, 2016; Labeda et al. 2012). In contrast, 11-1-2 does not contain any of these markers (Fyans et al. 2016), and it is not closely phylogenetically related to the classic scab-inducing strains (Fig. 3.1), which suggests that 11-1-2 is the first member of the *S. violaceusniger* subclade with plant pathogenic capabilities.

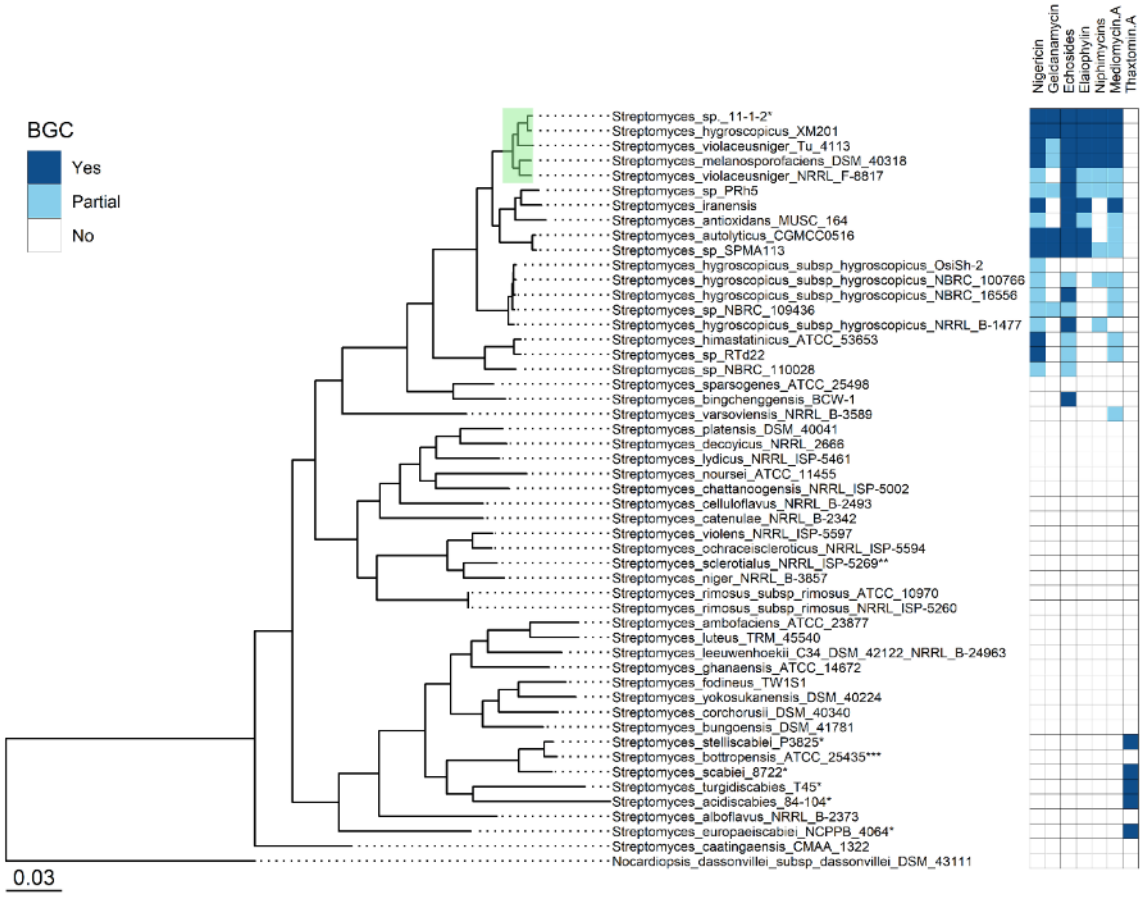

Figure 3.1. Maximum-likelihood multilocus species tree showing the phylogenetic relationship between *Streptomyces* sp. 11-1-2 and other *Streptomyces* species. *Streptomyces* sp. 11-1-2 localized to the clade that is highlighted in green and consists of strains with an average nucleotide identity >95%. Plant-pathogenic strains are indicated with "*". Strains for which the antiSMASH analysis did not show results are indicated with "**". For *S. bottropensis*, only some strains of this species are plant pathogenic, "***". The presence, absence and partial presence of selected biosynthetic gene clusters is indicated in the heatmap. "Partial" correspond to BGCs not fully detected by antiSMASH due to genome

completeness level or partial matches (< 85% of similarity) to the BGC of the respective compound.

To determine the potential metabolites responsible for the phytotoxic activity previously recorded, the genome sequence of 11-1-2 (Bown and Bignell 2017) was analyzed for the presence of specialized metabolite BGCs using antiSMASH 6.0 (Blin et al. 2021). The analysis determined the presence of 51 regions with varying degrees of similarity to known BGCs (Table S3.2). Six of the regions are highly similar (≥85%) to BGCs that produce compounds with known antifungal, antimicrobial and/or cytotoxic activities, i.e. nigericin, geldanamycin, echosides, elaiophylin, niphimycins, and mediomycin A (DeBoer and Dietz 1976; Heisey and Putnam 1986; Grabley et al. 1990; Allen and Ritchie 1994; Trejo-Estrada et al. 1998; Fang et al. 2000; Cai et al. 2007; Deng et al. 2014; Zhu et al. 2014). Interestingly, two of these, nigericin and geldanamycin, have been reported to exhibit herbicidal activity against some plants, including garden cress, cucumber, tomato, soybean and wheat (Heisey and Putnam 1986, 1990). The other strains in the phylogenetic tree were also evaluated using antiSMASH to determine the presence of these six BGCs in their genomes (accession numbers available in Table S2.6). The comparison provided further evidence for the close relationship between 11-1-2 and *S. hygroscopicus* XM201, given that these strains both harbour all six of the BGCs (Fig. 3.1). Furthermore, the BGCs for production of nigericin, echosides, elaiophylin, niphimycins and mediomycin A appear to constitute a "core" of BGCs that are conserved in the species that are most closely related to the 11-1-2 strain (Fig. 3.1). It has been reported that strains of *S. hygroscopicus* can produce different combinations of these compounds, with geldanamycin and nigericin being commonly co-produced (DeBoer and Dietz 1976; Heisey and Putnam 1986; Grabley et al. 1990; Allen and Ritchie 1994; Trejo-Estrada et al. 1998; Fang et al. 2000). When considering

the presence of BGCs across the *Streptomyces* genus, geldanamycin and geldanamycin-like clusters are often found associated with nigericin clusters; however, neither of these clusters are found in genomes containing the thaxtomin BGC (Fig. S3.1).

To further explore the conservation and evolution of the nigericin and geldanamycin BGCs among *Streptomyces* spp., the BiG-SCAPE computational tool was employed (Navarro-Muñoz et al. 2020). BiG-SCAPE (Biosynthetic Gene Similarity Clustering And Prospecting Engine) uses anti-SMASH-detected BGCs to generate sequence similarity networks and group them into gene cluster families (GCFs) along with reference BGCs from the MIBiG (Minimum Information about a Biosynthetic Gene cluster) database, and it elucidates the evolutionary relationships of the BGCs within each GCF. Using BGCs obtained from 2,136 *Streptomyces* genomes, BiG-SCAPE generated a similarity network for the *Streptomyces* sp. 11-1-2 region 012 (the predicted nigericin BGC; Table S3.2) that consisted of 28 BGCs (Fig. 3.2A), and these 28 BGCs were grouped into two distinct GCFs. Phylogenetic analysis of the GCF containing the predicted 11-1-2 nigericin BGC (Fig. 3.2A) showed that this gene cluster is most closely related to the *Streptomyces* sp. NEAU-YJ-81 region 001 and the known nigericin BGC (BGC0000114) from *S. violaceusniger* Tu 4113. An alignment of the BGCs from the GCF tree revealed that the gene content and architecture of the nigericin BGC is highly conserved among different *Streptomyces* spp., including the 11-1-2 strain (Fig. 3.2B). This supports the notion that the 11-1-2 strain is capable of biosynthesizing nigericin. It should be pointed out that the nigericin BGC comparison was affected by the assembly level of the genome sequences available in the public database. Although the BGC appears to be incomplete in some strains (Fig. 3.2B), this is most likely due to the presence of gaps in the genome sequences of these organisms.

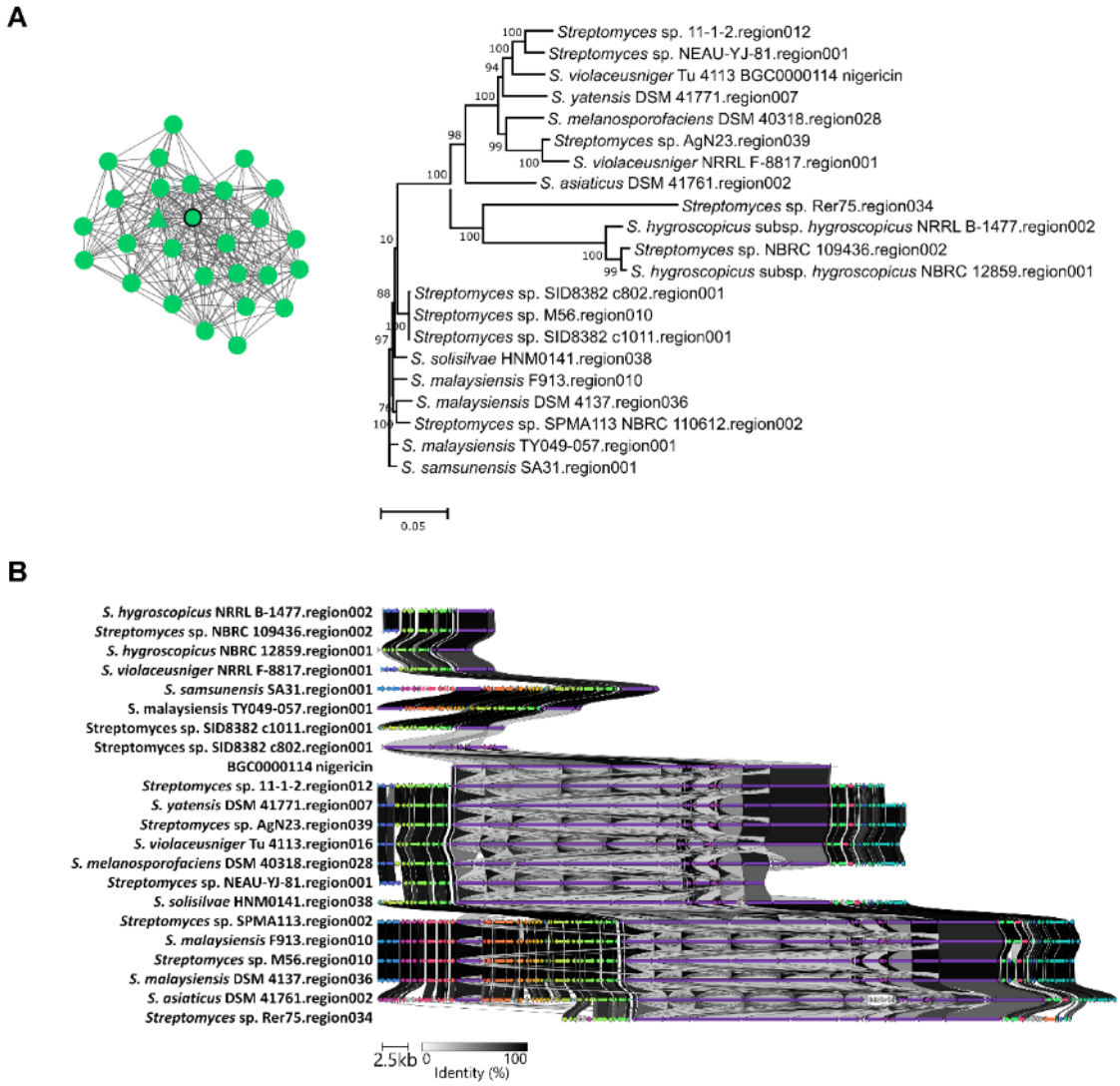

Figure 3.2. Large-scale analysis of nigericin BGCs from *Streptomyces* spp. (A) The similarity network of *Streptomyces* sp. 11-1-2 region 012 (nigericin BGC) and BGCs from other *Streptomyces* species (left), and their evolutionary relationships within the GCF (right). The triangular node within the network represents *Streptomyces* sp. 11-1-2 region 012, and the circular nodes represent known BGCs from the MIBiG database (outlined in thick black) and BGCs from other *Streptomyces* spp. Bootstrap values of ≥ 50% are shown at the respective branch points and are based on 1000 repetitions. (B) Alignment of the *Streptomyces* sp. 11-1-2 region 012 with the known nigericin BGC (BGC0000114) from *S. violaceusniger* Tu 4113 and other BGCs within the same GCF. Genes coloured the same belong to the same functional group, and homologues are linked by shaded areas that indicate the % identity.

The similarity network for the 11-1-2 region 045 (the predicted geldanamycin BGC; Table S3.2) consisted of 12 BGCs that were grouped into a single GCF, and phylogenetic analysis revealed that the 11-1-2 BGC does not cluster with the other BGCs in the GCF (Fig. 3.3A). A comparison of the gene content and organization (Fig. 3.3B) revealed that the 11-1-2 BGC is most similar to the geldanamycin BGC from *S. hygroscopicus* XM201 (region 042). Notably, the 11-1-2 BGC contains a gene (*CGL_43245*) that is homologous to *gdmM* from the *S. hygroscopicus* geldanamycin BGC (BGC0000066.1). This gene is absent from the closely related herbimycin BGC (BGC0000074.1) (Fig. 3.3B) and is proposed to function in an oxidation step that occurs during geldanamycin biosynthesis but not during herbimycin biosynthesis (Rascher et al. 2005). Thus, the presence of this gene in the 11-1-2 BGC suggests that 11-1-2 produces geldanamycin rather than herbimycin.

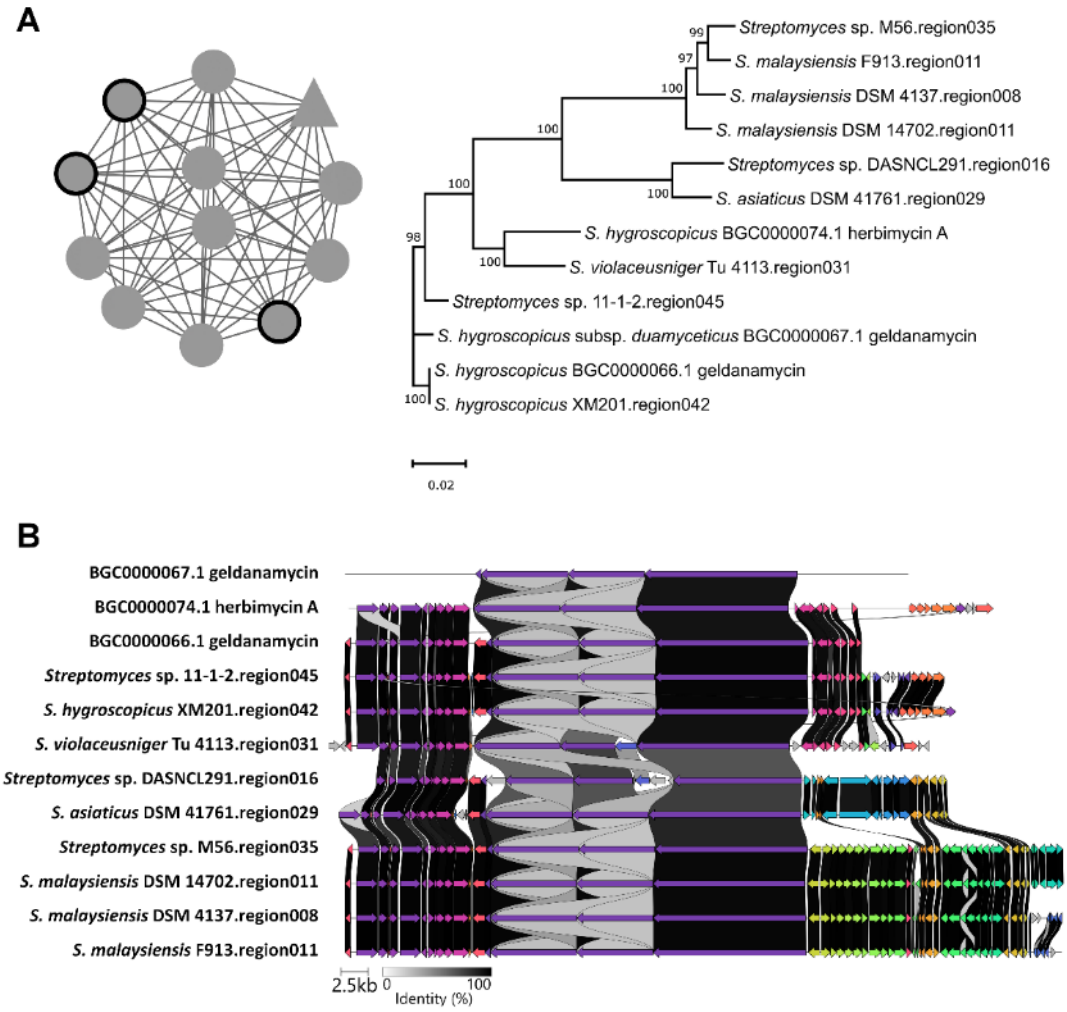

Figure 3.3. Large-scale analysis of geldanamycin BGCs from *Streptomyces* spp. (A) The similarity network of *Streptomyces* sp. 11-1-2 region 045 (geldanamycin BGC) and BGCs from other *Streptomyces* species (left), and their evolutionary relationships within the GCF (right). The triangular node within the network represents *Streptomyces* sp. 11-1-2 region 045, and the circular nodes represent known BGCs from the MIBiG database (outlined in thick black) and BGCs from other *Streptomyces* spp. Bootstrap values of ≥ 50% are shown at the respective branch points and are based on 1000 repetitions. (B) Alignment of *Streptomyces* sp. 11-1-2 region 045 with the known geldanamycin BGC (BGC0000066.1) and the known herbimycin BGC (BGC0000074.1) from *S. hydroscopicus,* and other BGCs within the same GCF. Genes coloured the same belong to the same functional group, and homologues are linked by shaded areas that indicate the % identity. The *gdmM* gene from the geldanamycin BGC that is conserved in the 11-1-2 region 045 and is missing from the herbimycin BGC is indicated with a red asterisk above the gene.

3.3.2 The production of phytotoxic compounds by *Streptomyces* sp. 11-1-2 is dependent on medium composition

To identify the conditions that promote the production of phytotoxic compounds by the 11-1-2 strain, the strain was cultured on four different agar media containing or lacking *N*-acetylglucosamine (NAG). The addition of NAG to culture media has differential effects on *Streptomyces* morphological development and specialized metabolite production, depending on the type of medium used. Specifically, addition to nutrient-rich culture media typically results in disruption of sporulation in favour of a vegetative state, and the production of specialized metabolites can either be stimulated or suppressed (Rigali et al. 2008; Zhang et al. 2016c). In contrast, addition of NAG to nutrient-poor media generally enables sporulation and stimulates specialized metabolite production (Rigali et al. 2006). Two of the media used, modified maltose-yeast extract-malt extract agar [mMYM; (Liu et al. 2021a)] and yeast extract-malt extract-starch agar [YMS; (Ikeda et al. 1988)] are nutrient-rich media and have been used for the production of specialized metabolites by other *Streptomyces* spp. Oat bran agar [OBA; (Johnson et al. 2007)] is a plant-based medium previously shown to support phytotoxin production by the 11-1-2 strain (Fyans et al. 2016), and minimal medium with mannitol [(MMM; (Kieser et al. 2000)] is a simple, defined medium that supports growth and sporulation by *Streptomyces* spp. and has been used in other studies to characterize the effects of NAG on morphology and specialized metabolite production (Rigali et al. 2006, 2008). Following incubation of the 11-1-2 strain on the different media, agar cores were removed from the plates and were placed onto potato tuber tissue slices, after which the slices were incubated in a moist chamber for 7 days. As shown in Figure 3.4A, the cores from the 11-1-2 - inoculated plates caused pitting, softening, and browning of the tuber

tissue around the contact area, while cores from the uninoculated control plates had no effect. The OBA and YMS cores from the inoculated plates caused similar tissue damage regardless of whether or not NAG was present in the medium. In contrast, cores from the mMYM and MMM plates lacking NAG caused greater damage than those from plates containing NAG, suggesting that NAG influences the production of the phytotoxic compounds in these media.

Next, the agar plates were extracted with ethyl acetate, and the resulting culture extracts were evaluated for phytotoxicity using the potato tuber slice bioassay. As shown in Figure 3.4B, the extracts prepared from the 11-1-2 - inoculated OBA and YMS ± NAG plates all caused pitting and browning of the tuber tissue in a similar manner as the corresponding agar cores (Fig. 3.4A), though the browning was darker in appearance with the extracts. The extract from the inoculated mMYM - NAG medium showed some pitting and browning, though the effect was less severe than with the OBA and YMS extracts. In contrast, the extracts prepared from the mMYM + NAG and MMM ± NAG plates did not cause any damage that differed from the control extracts prepared from the uninoculated media (Fig. 3.4B).

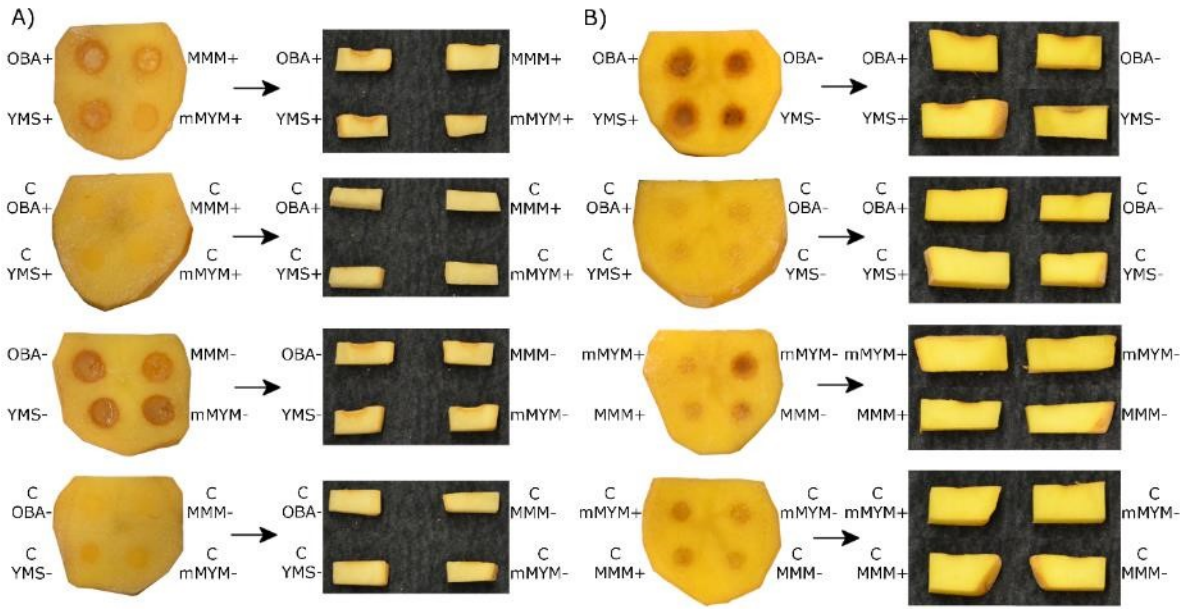

Figure 3.4. Phytotoxic activity of agar cores (A) and organic culture extracts (B) on excised potato tuber tissue. Each tuber slice contained four agar cores or four disks wetted with 20 µl of culture extract. The 11-1-2 strain was cultured on OBA, YMS, MMM and mMYM media, with (+) and without (-) 50 mM NAG for 14 days. The agar cores were obtained directly from the agar plates, while the extracts were prepared from one whole plate of each medium. Names of culture media preceded by a "C" are cores or extracts from control (non-inoculated) media. Photos were taken at 7 days after inoculation and show the top and side view of the tuber slices at the inoculation sites. Each slice had three replicates per experiment. The assay was performed twice with three biological replicates per treatment in each assay, with similar results obtained each time.

The organic culture extracts were also evaluated using a radish seedling bioassay, since such an assay was previously used to detect the phytotoxic activity of the 11-1-2 strain (Fyans et al. 2016). The results of the assay were in agreement with those of the potato tuber tissue assay in that the OBA and YMS extracts showed greater phytotoxic activity than the mMYM and MMM extracts (Fig. 3.5). The OBA and YMS extracts all caused severe stunting of the radish seedlings as compared to the water and solvent controls, and interestingly, the presence of NAG in the YMS medium caused a significant reduction in activity compared to the same medium without NAG. NAG also had a suppressive effect on the phytotoxic activity

when the 11-1-2 strain was cultured on mMYM and MMM, with the NAG+ extracts showing little effect on the seedlings as compared to the water and solvent controls (Fig. 3.5).

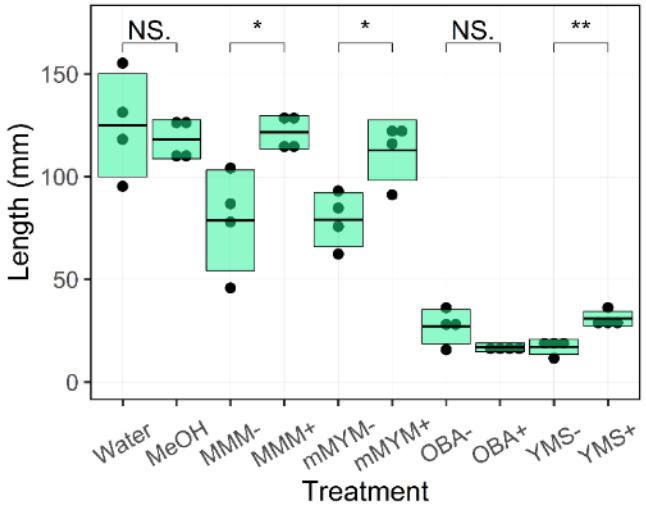

Figure 3.5. Phytotoxic activity of organic culture extracts on radish seedlings. Extracts were prepared from 14-day old plate cultures of 11-1-2 grown on OBA, YMS, MMM and mMYM media, with (+) and without (-) 50 mM NAG. Each box represents the average length of four seedlings ± one standard deviation. To evaluate how the addition of NAG to the culture medium affected the phytotoxic activity against the seedlings, the treatments were analyzed using the Student's t-test in pairs (N.S.= not significant; * = $p \leq 0.05$; ** = $p \leq 0.01$). The assay was performed three times, with similar results obtained each time.

Overall, the results of the two bioassays demonstrate that YMS and OBA both promote the production of high levels of the phytotoxic compound(s) by the 11-1-2 strain as compared to MMM and mMYM, and that NAG has a negative regulatory effect on the phytotoxic activity in some media, as well as on morphological development (Fig. S3.2). It has been reported that NAG acts as a signal for the activation of the global regulator DasR, which in turn can either activate (under nutrient-poor conditions) or repress (under nutrient-rich conditions) the expression of genes associated with morphological development and specialized metabolite production (Rigali et al. 2008). The DNA binding site of DasR has

been experimentally characterized, and *in silico* analysis of the 11-1-2 genome sequence identified several possible binding sites (Table S3.3). Among the predicted sites are ones upstream of chitinase and NAG metabolism-associated genes, which are known targets of DasR in other *Streptomyces* spp. (Colson et al. 2006; Rigali et al. 2006). Some of the predicted binding sites are associated with genes encoding GntR, TetR/AraC, LysR and LuxR transcriptional regulators, whereas none are located within the BGCs identified in the antiSMASH results. Therefore, it is possible that DasR indirectly regulates the production of the phytotoxic compounds through one or more global regulatory proteins, and future studies will aim to further investigate this.

3.3.3 *Streptomyces* sp. 11-1-2 produces the herbicidal compounds geldanamycin and nigericin

To identify the phytotoxic compounds produced by 11-1-2, organic extracts were prepared from YMS and mMYM (± NAG) plate cultures and subjected to untargeted LC-MS^2 analysis. The organic extracts from these media were selected based on the general differences in phytotoxic activity recorded in previous bioassays. The resulting MS^2 spectral data were analyzed using the Ion Identity Molecular Networking (IIMN) module of the Feature-Based Molecular Networking (FBMN) workflow within the Global Natural Products Social Molecular Networking (GNPS) web platform (Wang et al. 2016; Nothias et al. 2020; Schmid et al. 2021). With this analysis, molecular networks of fragmentation spectra for the detected ion adducts can be generated, with nodes (each representing a single fragmentation spectrum) linked based on similarity in retention time, peak shape, and fragmentation patterns. The MS^2 spectra obtained were annotated by performing a GNPS spectral library search, which compares the experimental spectral data to a library of MS^2 reference spectra

for known metabolites (Wang et al. 2016). Spectra with no matches to the library were analyzed using SIRIUS (Dührkop et al. 2015, 2019b), which provides a prediction of the molecular formula, and MetFrag, which compares the fragmentation pattern and molecular formula to annotate and classify molecule candidates by comparing them to the PubChem database (Ruttkies et al. 2016).

Given that nigericin and geldanamycin are predicted to be produced by the 11-1-2 strain, and that these compounds have known herbicidal activity, IIMN was employed to analyze the MS^2 data for the presence of these metabolites in the extracts. Using this approach, one molecular network containing a node with a spectral match to nigericin in the GNPS libraries was annotated (Fig. 3.6; Table 3.1). For nigericin, three different ion adducts were detected. Another network with nodes having spectral matches to geldanamycin in the GNPS libraries was annotated (Fig. 3.7; Table 3.1).

Along with nigericin and geldanamycin, the accumulation of biosynthetic intermediates or derivatives of these compounds has been reported in other studies, and the presence of some of these in the analyzed extracts was also predicted based on the MS^2 data obtained (Table 3.1; Figs. 3.6 and 3.7). For example, abierixin and grisorixin are compounds that are closely related to nigericin and are co-produced with nigericin (Oikawa et al. 1992; Mouslim and David 1995; Harvey et al. 2007). Studies in other *Streptomyces* spp. suggest that these molecules along with *O*-demethylabierixin, which was also predicted to be present in the samples of the present study (Table 3.1; Fig. 3.6), may be intermediates in the biosynthesis of nigericin (Kim et al. 1996). Other nigericin-related compounds predicted from the current data include 29-*O*-methylabierixin, which was first detected in *S. hygroscopicus* XM201 (Wu et al. 2009), and mutalomycin, initially detected in *Streptomyces mutabilis* NRRL 8088 (Table 3.1; Fig. 3.6) (Fehr et al. 1977). Among the

detected molecules that are predicted to be structurally related to geldanamycin is the antibiotic TAN-420B, which was originally obtained from strains of *S. hygroscopicus* and was reported to have weak antimicrobial activity (Table 3.1; Fig. 3.7) (Tanida et al. 1983). Other geldanamycin-related compounds annotated in the analyzed samples (Table 3.1; Fig. 3.7) have been previously obtained by fermentation of *Streptomyces* strains (Liu et al. 2011; Kitson et al. 2013; Ni et al. 2014). Two smaller, separate networks also contained geldanamycin-related compounds. The first one is predicted to match 15-hydroxygeldanamycin (Hu et al. 2004), while the other network contains EH21A2 (or Autolytimycin) (Onodera et al. 2008).

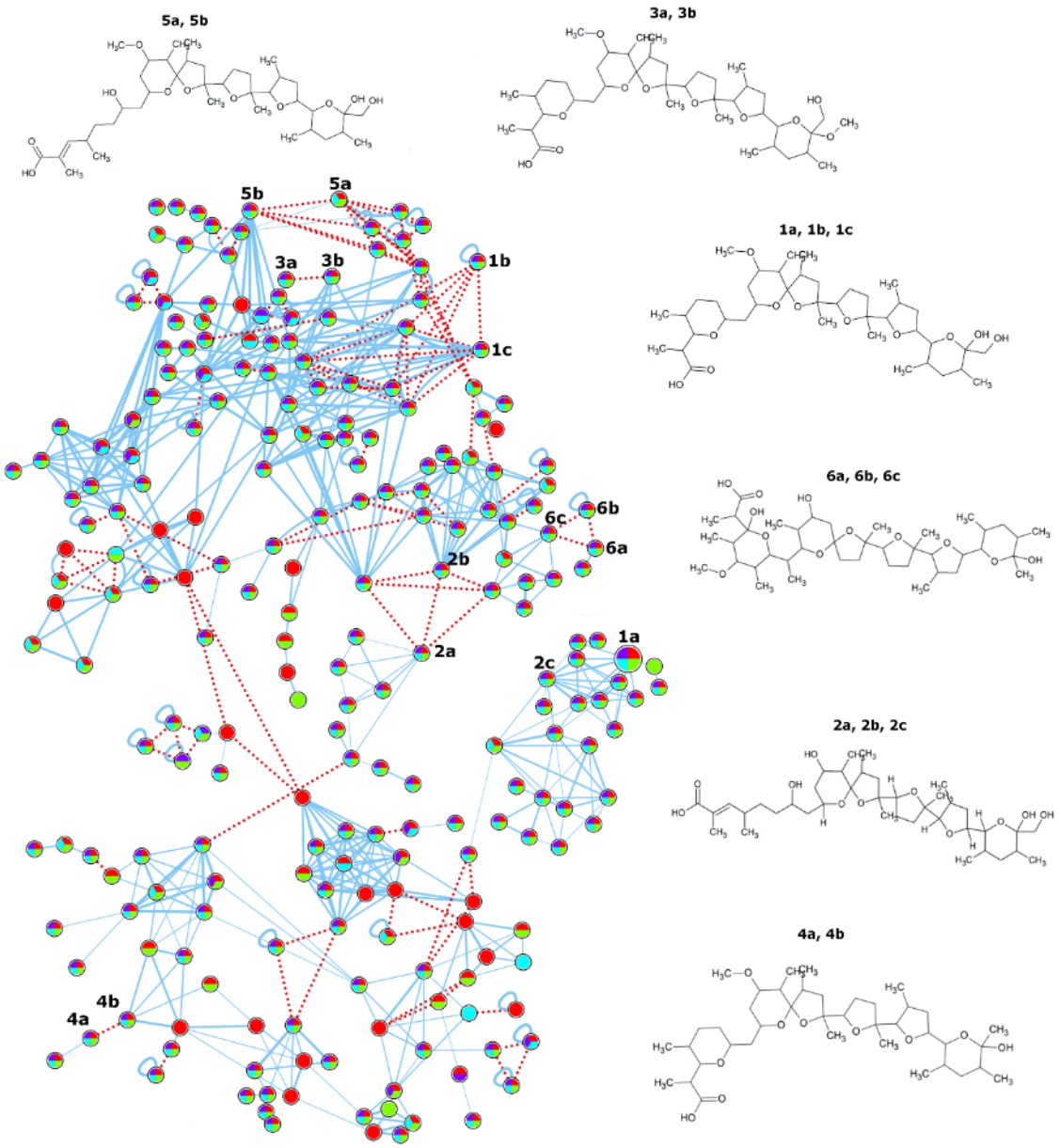

Figure 3.6. Molecular network for nigericin. Organic culture extracts were prepared from plate cultures of 11-1-2 grown on YMS and mMYM (± 50 mM NAG) for 14 days. The extracts were evaluated using LC-MS^2, and the resulting sepctral data were analyzed using Ion Identity Molecular Networking. Each node in the network represents one fragmentation spectrum, and the structures of the predicted compounds listed in Table 1 are shown and numbered to match the corresponding nodes. Nodes are linked by a blue line if the cosine score is >0.7 and there are at least six matched fragment ions, thus sharing MS^2 identity. The width of the line represents the score between two nodes (0.7-1.0). Nodes linked by a red dotted line share MS^1 identity. Each node shows a pie chart that represents the presence of the compound in extracts obtained from the different culture media. Pie chart legend: Purple: mMYM + NAG; Red: mMYM – NAG; Green: YMS + NAG; Teal: YMS – NAG. Nodes larger in size represent matches to the GNPS spectral libraries.

Table 3.1. Summary of compounds associated with nigericin and geldanamycin obtained from the IIMN-FBMN analysis.

Molecular formula[1]	Compound Name[2]	Calculated molecular weight (g/mol)	Adduct	*m/z*	Retention time (min)	Figure label[3]
$C_{40}H_{68}O_{11}$	Nigericin*	725.0	$[M-H]^-$	723.4683	13.6815	1a
			$[M+Na]^+$	747.4641	13.6341	1b
			$[M+NH_4]^+$	742.5091	13.6315	1c
$C_{39}H_{66}O_{11}$	*O*-demethylabierixin	710.9	$[M+Na]^+$	733.4486	13.2231	2a
			$[M+NH_4]^+$	728.4932	13.2162	2b
			$[M-H]^-$	709.4504	13.1907	2c
$C_{41}H_{70}O_{11}$	29-*O*-methylabierixin	739.0	$[M+Na]^+$	761.4821	13.9350	3a
			$[M+NH_4]^+$	756.5280	13.9400	3b
$C_{40}H_{68}O_{10}$	Grisorixin	709.0	$[M+Na]^+$	731.4717	12.8333	4a
			$[M+NH_4]^+$	726.5145	12.8081	4b
$C_{40}H_{68}O_{11}$	Abierixin	725.0	$[M+Na]^+$	747.4647	15.4556	5a
			$[M+NH_4]^+$	742.5098	15.5002	5b
$C_{41}H_{70}O_{12}$	Mutalomycin	755.0	$[M-H]^-$	753.4796	13.7183	6a
			$[M+Na]^+$	777.4760	12.7979	6b
			$[M-H_2O+H]^+$	737.4870	12.7643	6c
$C_{29}H_{40}N_2O_9$	Geldanamycin*	560.6	$[M-H]^-$	559.2657	11.2173	7a
			$[M-H]^-$	559.2654	11.1868	7b
			$[M-H]^-$	559.2656	9.6200	7c
			$[M+Cl]^-$	595.2423	11.2024	7d
$C_{28}H_{38}N_2O_9$	Antibiotic TAN-420B	546.6	$[M-H]^-$	545.2506	10.8291	8
$C_{28}H_{42}N_2O_9$	[(4E,6Z,8S,9S,10E,12S,13R,14S,16S,17R)-13,14,20,22-Tetrahydroxy-8,17-dimethoxy-4,10,12,16-tetramethyl-3-oxo-2-azabicyclo[16.3.1]docosa-1(21),4,6,10,18-pentaen-9-yl] carbamate	550.6	$[M-H]^-$	549.2806	9.3509	9
$C_{29}H_{44}N_2O_8$	[(8R,9R,12S,13R,14R,16S,17R)-13,17,20-Trihydroxy-8,14-bis(hydroxymethyl)-4,10,12,16,19-pentamethyl-3-oxo-2-azabicyclo[16.3.1]docosa-1(22),4,10,18,20-pentaen-9-yl] carbamate	548.7	$[M-H]^-$	547.3027	9.4444	10a
			$[M-H_2O+Cl]^-$	565.2744	9.2727	10b
			$[M+FA]^-$	593.3081	9.4809	10c
$C_{29}H_{40}N_2O_{10}$	[(8S,9S,12S,13R,14S)-13,20,22-Trihydroxy-10-(hydroxymethyl)-8,14,19-trimethoxy-4,12,16-trimethyl-3-oxo-2-azabicyclo[16.3.1]docosa-1(21),4,6,10,16,18(22),19-heptaen-9-yl] carbamate	576.6	$[M-H]^-$	575.2594	10.9951	11
$C_{30}H_{42}N_2O_9$	19-Methylgeldanamycin	574.7	$[M-H]^-$	573.2798	9.5806	12a
$C_{30}H_{42}N_2O_9S$	19-S-Methylgeldanamycin	606.7	$[M-H]^-$	605.2524	9.9423	12b
$C_{29}H_{40}N_2O_8$	6-demethoxy-6-methylgeldanamycin	544.6	$[M-H]^-$	543.2723	11.8121	13
$C_{28}H_{39}NO_8$	7-*O*-descarbamoyl-7-hydroxygeldanamycin	517.6	$[M-H]^-$	516.2596	11.1875	14

$C_{30}H_{42}N_2O_{10}$	8,9-Epoxyherbimycin A	590.7	$[M-H]^-$	589.2768	11.1210	15
$C_{29}H_{40}N_2O_{10}$	15-Hydroxygeldanamycin	576.6	$[M-H]^-$	575.2605	10.3256	16
$C_{28}H_{42}N_2O_7$	EH21A2/Autolytimycin*	518.6	$[M-H]^-$	517.2915	9.3496	17

1 The molecular formulas were obtained from analysis of the spectra using SIRIUS and MetFrag.
2 Names with "*" were a match to the GNPS database. Names without "*" are the PubChem entry for the predictions estimated by MetFrag.
3 The numbers in this column refer to the nodes label in Figures 3.6 and 3.7.

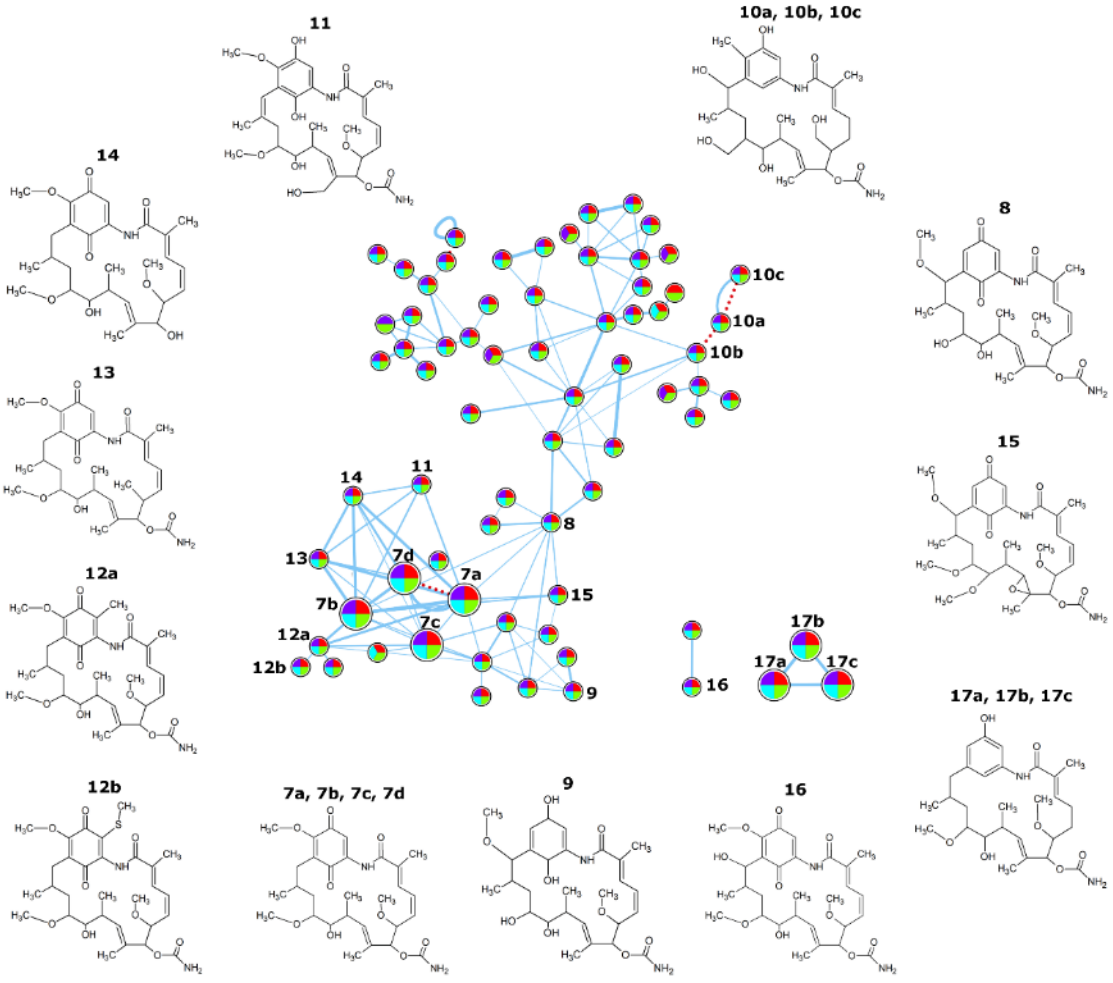

Figure 3.7. Molecular network for geldanamycin. Organic culture extracts were prepared from plates cultures of 11-1-2 grown on YMS and mMYM (± 50 mM NAG) for 14 days. The extracts were evaluated using LC-MS^2, and the resulting spectral data were analyzed using Ion Identity Molecular Networking. The features of the network are as described in the Figure 3.6 figure legend. The structures of the predicted compounds are shown.

Since the phytotoxic activity of the 11-1-2 strain was found to be suppressed by NAG in some media, the effect of NAG in suppressing production of nigericin and geldanamycin by this strain was explored. Thus, the effects of different concentrations of NAG on the production of these metabolites in mMYM and YMS were tested. In the case of nigericin, NAG concentrations of 50 and 100 mM in mMYM significantly reduced the metabolite production level, while production in YMS was significantly decreased starting at 20 mM NAG (Fig. 3.8A). Interestingly, a much smaller peak with the same *m/z* (742.5, $[M+NH_4]^+$) as nigericin but having a different retention time was also detected in the culture extracts (Fig. S3.3). A similar peak was previously observed in the culture extracts of the nigericin producer *Streptomyces* sp. DSM4137 and is presumed to be abierixin (Harvey et al. 2007), which was also predicted to be present based on the IIMN analysis (Fig. 3.6; Table 3.1). The peak area for this compound was much less than that of nigericin in both the mMYM and YMS culture extracts, but it showed a similar trend in terms of the suppressive effects of NAG (Fig. 8A). For geldanamycin, the addition of NAG significantly reduced the metabolite production levels starting at 20 mM NAG in both mMYM and YMS (Fig. 3.8B). Moreover, the addition of NAG to YMS yielded another prominent peak with a different retention time than that of geldanamycin (Fig. S3.4). LC-MS analysis of this peak revealed an *m/z* of 575.2 ($[M-H]^-$), which together with the IIMN results (Fig. 3.7; Table 3.1) suggests the presence of 15-hydroxygeldanamycin, a geldanamycin derivative previously obtained by the bioconversion of geldanamycin (Hu et al. 2004). Interestingly, the analysis revealed that this compound is only present when NAG is added to YMS, and the amount produced remained relatively constant at NAG concentrations of 10-50 mM and decreased only at higher NAG concentrations (Fig. 3.8B). Quantification of the nigericin and geldanamycin production levels demonstrated that the 11-1-2 strain produces significantly higher amounts of nigericin

than geldanamycin in both mMYM and YMS (Table 3.2, fig. S3.5 and S3.6). Furthermore, in the absence of NAG, the level of nigericin in the YMS culture extract was almost three times that in the mMYM extract, and this appeared to correlate with the relative phytotoxicity of these extracts in the bioassays (Fig. 3.4 and 3.5), suggesting that nigericin is a major contributor to the observed phytotoxicity of the 11-1-2 culture extracts.

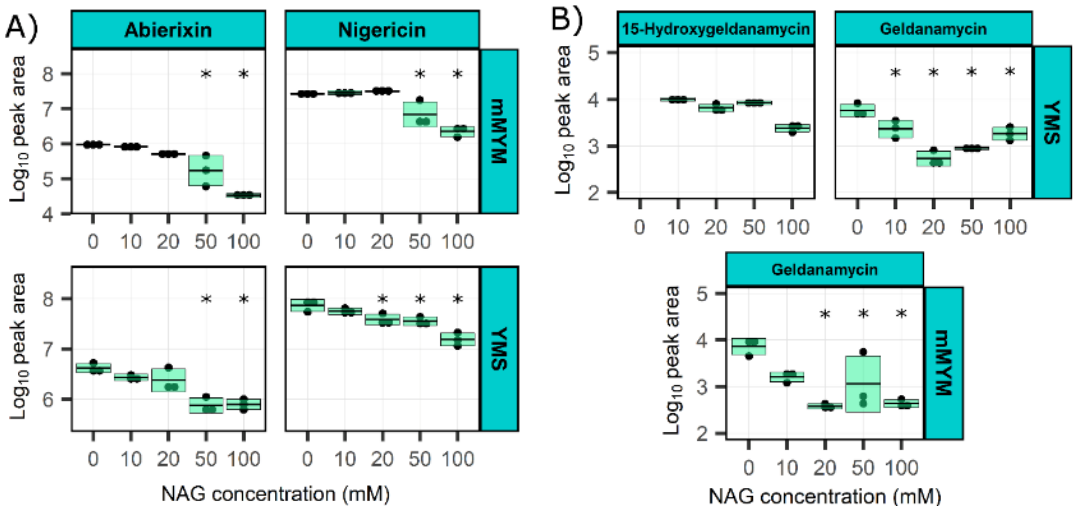

Figure 3.8. Effects of NAG on the production of nigericin and the related molecule abierixin (A), and of geldanamycin and the related molecule 15-hydroxygeldanamycin (B). Organic culture extracts were prepared from plate cultures of 11-1-2 grown for 14 days on YMS and mMYM supplemented with different concentrations of NAG. The extracts were evaluated using LC-MS (nigericin and abierixin) and RP-HPLC (geldanamycin and 15-hydroxygeldanamycin). The areas of the nigericin/abierixin and geldanamycin/15-hydroxygeldanamycin peaks were obtained using MestReNova and Chemstation, respectively, and were transformed using the $\log_{10}$ function. An ANOVA paired with Dunnett's test was performed in Minitab®, and media without NAG were used as control treatments for statistical analysis. Data boxes showing an asterisk (*) are statistically different from their respective control ($p<0.05$). Each box represents the average peak area of three extracts ± one standard deviation. The RP-HPLC analysis did not show a peak for 15-hydroxygeldanamcyin in extracts from YMS (0 mM NAG); thus, no statistical analysis was performed. A peak for 15-hydroxygeldanamycin was not observed for any of the mMYM ± NAG extracts, and thus this graph was not included.

Table 3.2. Quantification of nigericin and geldanamycin obtained from organic culture extracts.

Media	NAG (mM)	Nigericin (mM)[1]	Geldanamycin (mM) [1]
mMYM	0	11.90 ± 0.58	0.25 ± 0.09
	10	13.00 ± 1.92	0.05 ± 0.01
	20	14.02 ± 0.88	0.01 ± 0.00
	50	3.88 ± 3.42	0.07 ± 0.09
	100	1.02 ± 0.31	0.01 ± 0.00
YMS	0	33.44 ± 8.81	0.19 ± 0.06
	10	25.28 ± 3.71	0.08 ± 0.03
	20	17.40 ± 4.46	0.02 ± 0.01
	50	15.98 ± 3.25	0.03 ± 0.00
	100	7.07 ± 2.14	0.06 ± 0.02

[1] The values correspond to the average of three replicates ± one standard deviation.

3.3.4 Geldanamycin and nigericin exhibit phytotoxic activity against potato tissue and radish seedlings

Although nigericin and geldanamycin have been reported to exhibit herbicidal activity against different plants, their phytotoxic effects on radish seedlings and potato tuber tissue have not been previously studied. Therefore, the phytotoxic activity of different concentrations of pure nigericin and geldanamycin were evaluated in potato tuber slice and radish seedlings bioassays. A pure standard of thaxtomin A, the main phytotoxin produced by *S. scabiei* and other scab-causing pathogens, was included as a positive control in the bioassays. As shown in Figure 3.9, the pure geldanamycin caused shallow necrosis of the potato tuber tissue, and the severity of tissue damage increased with increasing amounts of the compound. On the other hand, nigericin did not present significant necrosis like geldanamycin; instead, the inoculation sites showed pitting of the tissue. This effect was also more pronounced with higher amounts of the compound. To determine if the two compounds

have a synergistic effect, the tuber tissue was treated with equimolar amounts of both compounds. This resulted in both pitting and necrosis of the tissue that was more severe when compared to treatment with the individual compounds. Notably, the effects of geldanamycin and nigericin were distinct from that of thaxtomin A, which caused dark brown necrosis of the potato tissue without pitting (Fig. 3.9). Furthermore, the effects of the pure compounds seem relatively less severe than those of the agar cores but more similar to the organic extracts. In the radish seedling bioassay, nigericin had a more significant impact on the growth of the seedlings than geldanamycin at the same concentration (Fig. 3.10A). The combination treatment (10 nmol of each compound) caused seedling stunting like that caused by the 10 nmol amount of nigericin alone, suggesting that nigericin is primarily responsible for the observed effect (Fig. 3.10A). This result is in contrast to a previous study that reported that geldanamycin and nigericin have additive effects on the radicle length of different plant species, though this study did not test the effects of these compounds on radish seedlings (Heisey and Putnam 1990). Notably, neither compound could cause the same degree of seedling stunting as similar amounts of thaxtomin A, indicating that they are less toxic than thaxtomin A against radish seedlings.

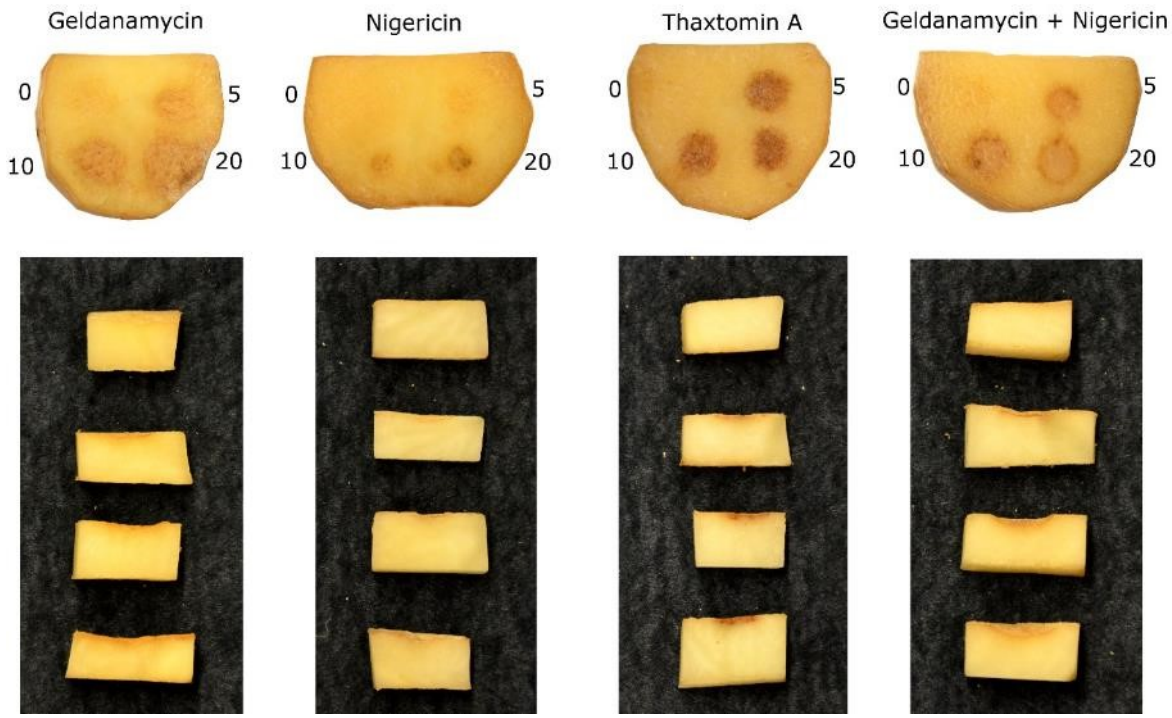

Figure 3.9. Phytotoxic effects of pure geldanamycin, nigericin and thaxtomin A on potato tuber tissue. Each tuber slice contained four disks inoculated with 0 (control), 5, 10 and 20 nmol of the respective compound in a fixed volume of 20 µl. For the combination of geldanamycin + nigericin, each compound provided half of the amount reported, i.e., 5, 10 and 20 nmol had 2.5, 5 and 10 nmol of each compound. The assay was performed twice with three biological replicates per treatment in each assay, with similar results obtained each time.

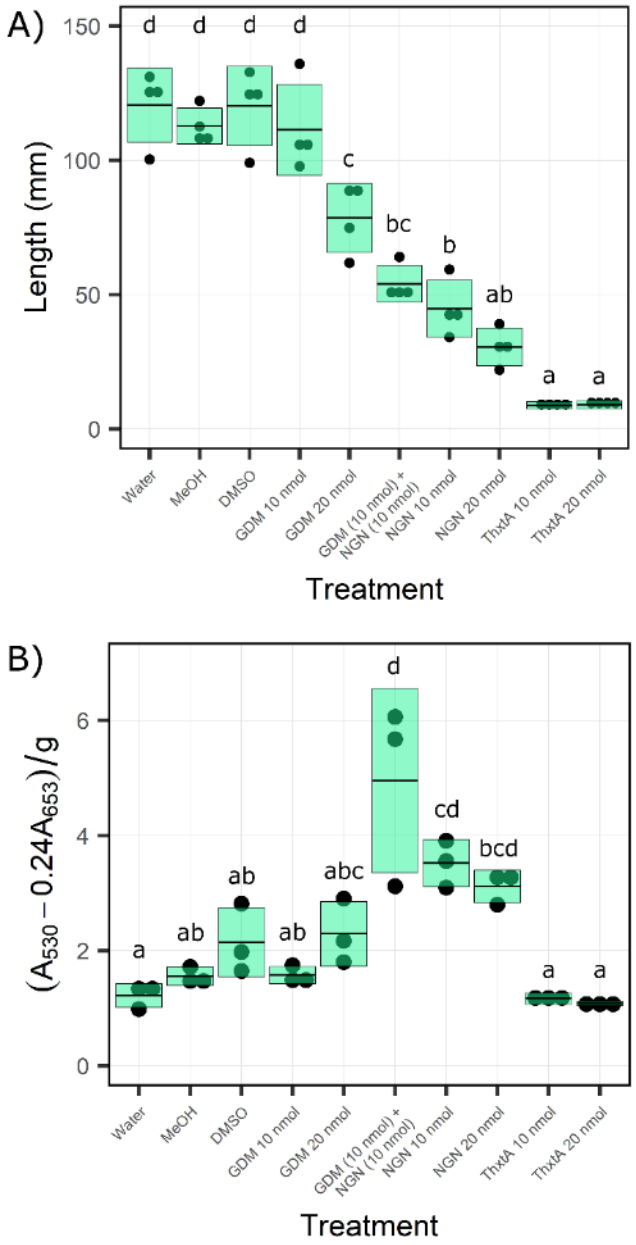

Figure 3.10. (A) Phytotoxic effect of pure nigericin (NGN), geldanamycin (GDM) and thaxtomin A (ThxtA) on the growth of radish seedlings. Seedlings were treated with 10 or 20 nmol of each compound, or a combination of 10 nmol of each compound. Each box represents the average length of four seedlings ± one standard deviation. (B) Relative quantification of anthocyanin accumulation in radish seedlings treated with nigericin, geldanamycin and thaxtomin A. Seedlings were treated with 10 or 20 nmol of each compound, or a combination of 10 nmol of each compound. Each box represents the average anthocyanin amount from three pairs of seedlings ± one standard deviation. For both experiments, the treatments were analyzed using an ANOVA test with Tukey's test. Values with different letter are statistically different ($p < 0.05$). Each assay was performed three times with similar results.

The appearance of the seedlings treated with the pure nigericin was notably distinct from that of seedlings subjected to the other treatments. The seedlings exhibited areas of distinct red pigmentation, especially along the edges of the cotyledons. As red pigmentation is an indicator of anthocyanin accumulation (Grotewold 2006), the levels of anthocyanins in the seedlings subjected to the different treatments were evaluated. Interestingly, only nigericin caused a significant increase in the level of anthocyanins in the radish seedlings at both test concentrations, while geldanamycin and thaxtomin A did not have a significant effect (Fig. 3.10B). Treatment with both nigericin and geldanamycin caused the accumulation of an even greater amount of anthocyanins, though the level was not significantly different from the treatment with nigericin alone. Based on review of the current literature, this is the first report of nigericin impacting anthocyanin accumulation in plants, and further work will be required to determine how nigericin and anthocyanin accumulation are connected. Anthocyanin accumulation has been associated to different abiotic and biotic stresses, suggesting a response to preserve the plant development under unfavourable conditions (Kovinich et al. 2014). Overall, these results demonstrate that both nigericin and geldanamycin display toxic effects against potato tuber tissue and radish seedlings in low amounts, and that their effects are distinct from that of thaxtomin A.

3.4 Conclusions

This study demonstrated for the first time that nigericin and geldanamycin are biosynthesized by the plant pathogen *Streptomyces* sp. 11-1-2, which is closely related to strains within the *S. violaceusniger* subclade. The production of these metabolites was shown to be influenced by the amino sugar NAG, and both compounds were phytotoxic at low quantities against both potato tubers and radish seedlings. Other related compounds were also

predicted to be produced by the 11-1-2 strain under the culturing conditions used. The biosynthetic pathways for nigericin and geldanamycin are rich in intermediates and naturally occurring analogues that have been shown to retain or enhance the biological activity of the final products (Wu et al. 2009; Lee et al. 2017). Under this context, it is hypothesized that the spectrum of molecules closely related to nigericin and geldanamycin play a role in enhancing the pathogenicity of 11-1-2. Geldanamycin is a benzoquinone ansamycin that acts as an inhibitor of the heat shock protein 90 (HSP90) chaperone (Stebbins et al. 1997), and nigericin is a polyether ionophore that facilitates the transport of different ions across membranes (Kevin II et al. 2009). Importantly, HSP90 plays a critical role in different plant mechanisms, including resistance to diseases and abiotic disorders (Kadota and Shirasu 2012), and this protein is known to serve as a target for the HopBF1 virulence effector produced by the plant pathogen *Pseudomonas syringae* pv. *syringae* (Lopez et al. 2019). Nigericin has been shown to disrupt different mechanisms in plants, including the uncoupling of photophosphorylation in the presence of K^+ ions (Shavit and San Pietro 1967; Shavit et al. 1968), redirecting of vicilin in pea cotyledons (Craig and Goodchild 1984), inhibition of protein import into the chloroplast (Cline et al. 1985), and reduction of photosynthesis (Quick et al. 1989). Thus, these molecules may contribute to the pathogenicity of *Streptomyces* sp. 11-1-2 by affecting different plant targets and processes. Future work will focus on the construction of geldanamycin and nigericin biosynthetic mutants of *Streptomyces* sp. 11-1-2 so that the role of each compound in plant-pathogen interactions can be further assessed. Given that strains of *S. violaceusniger* and *S. hygroscopicus* have been reported by others as potential biological control agents for the management of fungal plant diseases and potato common scab (Sarwar et al. 2019b; Xu et al. 2019; Mitrović et al. 2021), the present study

additionally highlights the need for potential biological control agents to undergo a thorough assessment for the presence of BGCs that could produce highly phytotoxic compounds.

APPENDIX 2.

Supplementary tables

Table S3.1. Estimated average nucleotide identity (ANI) of multiple strains to *Streptomyces* sp. 11-1-2 as calculated by autoMLST.

Species name	Estimated ANI
*Streptomyces_hygroscopicus*_XM201	0.9866
*Streptomyces_violaceusniger*_Tu_4113	0.9626
Streptomyces_melanosporofaciens	0.9573
Streptomyces_violaceusniger	0.9538
Streptomyces_autolyticus	0.9304
*Streptomyces*_sp._PRh5	0.9297
Streptomyces_iranensis	0.928
Streptomyces_antioxidans	0.9215
*Streptomyces*_sp._NBRC_109436	0.9143
*Streptomyces_hygroscopicus*_subsp._*hygroscopicus*	0.9141
*Streptomyces_hygroscopicus*_subsp._*hygroscopicus*	0.9141
*Streptomyces*_sp._NBRC_110028	0.8756
*Streptomyces_himastatinicus*_ATCC_53653	0.8738
*Streptomyces*_sp._RTd22	0.8734
*Streptomyces_bingchenggensis*_BCW-1	0.8583
Streptomyces_sparsogenes	0.8548
Streptomyces_sclerotialus	0.821
Streptomyces_violens	0.821
Streptomyces_niger	0.8206
Streptomyces_ochraceiscleroticus	0.8194
Streptomyces_lydicus	0.8186
Streptomyces_catenulae	0.8182
Streptomyces_celluloflavus	0.8173
*Streptomyces_rimosus*_subsp._*rimosus*_ATCC_10970	0.8173
Streptomyces_varsoviensis	0.8173
Streptomyces_platensis	0.8151
Streptomyces_decoyicus	0.8142
Streptomyces_bungoensis	0.8132
Streptomyces_yokosukanensis	0.8132
Streptomyces_leeuwenhoekii	0.8128
Streptomyces_chattanoogensis	0.8118
Streptomyces_corchorusii	0.8113
*Streptomyces_ghanaensis*_ATCC_14672	0.8108
Streptomyces_caatingaensis	0.8098

Streptomyces_luteus	0.8093
*Streptomyces_noursei*_ATCC_11455	0.8093
Streptomyces_alboflavus	0.8088
*Streptomyces_ambofaciens*_ATCC_23877	0.8088
Streptomyces_fodineus	0.805
Streptomyces_stelliscabiei	0.8039
*Streptomyces_bottropensis*_ATCC_25435	0.7997
*Streptomyces_scabiei*_87.22	0.7997
Streptomyces_europaeiscabiei	0.7971
Streptomyces_turgidiscabies	0.7891
*Streptomyces_acidiscabies*_84-104	0.7841
*Nocardiopsis_dassonvillei*_subsp._*dassonvillei*_DSM_43111	0.72

Table S3.2. Biosynthetic gene clusters predicted in the genome of *Streptomyces* sp. 11-1-2 using antiSMASH 6.0.

Region	Type	From	To	Most similar known cluster		Similarity
Region 1	lanthipeptide-class-i	244467	267372	mycotrienin I	NRP + Polyketide	7%
Region 2	terpene	304965	327957	isorenieratene	Terpene	85%
Region 3	arylpolyene,ladderane,NRPS	457599	529895	RP-1776	Polyketide + NRP:Cyclic depsipeptide	22%
Region 4	NRPS-like	571719	614054	echoside A / echoside B / echoside C / echoside D / echoside E	NRP	11%
Region 5	PKS-like,terpene	658010	705793	rustmicin	Polyketide:Iterative type I	20%
Region 6	terpene	824320	845259	tiancilactone	Terpene	17%
Region 7	NRPS	884096	962151	dechlorocuracomycin	NRP	8%
Region 8	RiPP-like,T1PKS,hglE-KS	974268	1097025	A83543A	Polyketide	21%
Region 9	NRPS-like	1160316	1200586	herboxidiene	Polyketide	3%
Region 10	T1PKS,NRPS	1277766	1393079	meridamycin	NRP + Polyketide	63%
Region 11	NAPAA	1541803	1572879	paulomycin	Other	7%
Region 12	T1PKS	1575870	1705961	nigericin	Polyketide:Modular type I	100%
Region 13	T1PKS	1709681	1754690	salinomycin	Polyketide:Modular type I	8%
Region 14	T1PKS,hglE-KS	2077385	2128172	asukamycin	Polyketide:Type II	11%
Region 15	T1PKS,NRPS-like	2322627	2402967	naphthomycin A	Polyketide	50%
Region 16	NRPS,nucleoside	2436317	2481506	toyocamycin	Other	30%
Region 17	NRPS	2541367	2594739	glycinocin A	NRP	11%

Region 18	terpene	2943967	2964259	BE-43547A1 / BE-43547A2 / BE-43547B1 / BE-43547B2 / BE-43547B3 / BE-43547C1 / BE-43547C2	NRP:Cyclic depsipeptide + Polyketide:Modular type I	20%
Region 19	T1PKS,siderophore	2991613	3045502	apoptolidin	Polyketide	25%
Region 20	ectoine	3210416	3220820	ectoine	Other	100 %
Region 21	terpene	3719051	3738277			
Region 22	lanthipeptide-class-i	3920406	3943726			
Region 23	T1PKS	4304490	4484508	mediomycin A	Polyketide	68%
Region 24	RRE-containing	4623525	4643578	granaticin	Polyketide:Type II	10%
Region 25	ladderane	4658207	4697921	atratumycin	NRP	31%
Region 26	NRPS	4753653	4795917	ochronotic pigment	Other	50%
Region 27	indole	5011258	5032403	5-isoprenylindole-3-carboxylate β-D-glycosyl ester	Other	61%
Region 28	terpene	5596461	5615957	geosmin	Terpene	100 %
Region 29	siderophore	6759041	6769871	desferrioxamin B	Other	100 %
Region 30	NRPS-like	7294519	7335806	echoside A / echoside B / echoside C / echoside D / echoside E	NRP	100 %
Region 31	siderophore	7921967	7933880			
Region 32	ladderane,arylpolyene,NRPS,aminocoumarin	7996321	8069356	atratumycin	NRP	57%
Region 33	RiPP-like	8166050	8177396			

Region 34	T1PKS	8239229	8295520	totopotensamide A / totopotensamide B	NRP + Polyketide	5%
Region 35	T2PKS	8421342	8493857	spore pigment	Polyketide	83%
Region 36	terpene	8870148	8892706	hopene	Terpene	76%
Region 37	lanthipeptide-class-i	9096140	9120593	steffimycin D	Polyketide:Type II + Saccharide:Hybrid/tailoring	16%
Region 38	terpene	9210479	9230310	lasalocid	Polyketide	3%
Region 39	T1PKS	9358088	9405558			
Region 40	NRPS,transAT-PKS,NRPS-like	9419881	9495386	meilingmycin	Polyketide	7%
Region 41	butyrolactone	9654449	9665381			
Region 42	hserlactone	9675690	9696448	daptomycin	NRP	3%
Region 43	redox-cofactor	9815666	9837784	lankacidin C	NRP + Polyketide	13%
Region 44	T1PKS	9877490	9945918	elaiophylin	Polyketide	87%
Region 45	T1PKS,NRPS-like	10159131	10240039	herbimycin A	Polyketide	83%
Region 46	terpene	10383924	10403386	pristinol	Terpene	100%
Region 47	terpene	10508385	10529722	ebelactone	Polyketide	8%
Region 48	T1PKS	10696374	10842668	niphimycins C-E	Polyketide	87%
Region 49	NAPAA	10939213	10973346			
Region 50	NRPS,T1PKS	11092881	11205821	coelichelin	NRP	90%
Region 51	betalactone	11367403	11392789			

Table S3.3. DasR binding sites predicted in the genome of *Streptomyces* sp. 11-1-2 as calculated by PREDetector

Gene locus	Gene product	Sequence	Position	Score	Region	Co-transcribed locus	Co-transcribed gene product	Region name
CGL27_RS07365 [CGL27_07235]	chitinase	ACTGGTCTAGTCCTGT	-112	16.6	regulatory			UPS1216
CGL27_RS22220 [CGL27_21915]	ROK family protein	AGTGGACTAGACCTCT	-44	16.5	regulatory	CGL27_RS22225 [CGL27_21920] (nagA)	N-acetylglucosamine-6-phosphate deacetylase	UPS3746
CGL27_RS22215 [CGL27_21910]	extracellular solute-binding protein	AGTGGACTAGACCTCT	-264	16.5	regulatory			UPS3746
CGL27_RS31315 [CGL27_30985]	ATPase	TCTGGACTAGACCACT	-85	16.1	regulatory			UPS5280
CGL27_RS19705 [CGL27_19420]	PTS lactose transporter subunit IIC	ACAGGTCTACACCACA	-80	15.5	regulatory			UPS3309
CGL27_RS19700 [CGL27_19415]	PTS sugar transporter	ACAGGTCTACACCACA	-146	15.5	regulatory			UPS3309
CGL27_RS25640 [CGL27_25340]	tRNA-Gly	AGAGGTCTAGACAACA	36	15	terminator			UPS4324
CGL27_RS25635 [CGL27_25335]	site-specific integrase	AGAGGTCTAGACAACA	1	15	terminator			UPS4324
CGL27_RS19705 [CGL27_19420]	PTS lactose transporter subunit IIC	AATGGTCTACACCATT	-163	14.9	regulatory			UPS3309

CGL27_RS19700 [CGL27_19415]	PTS sugar transporter	AATGGTCTACACCATT	-63	14.9	regulatory			UPS3309
CGL27_RS17585 [CGL27_17285] (leuA)	2-isopropylmalate synthase	GGAGGTGTAGACCAGA	1085	14.5	coding			CGL27_RS17585 [CGL27_17285] (leuA)
CGL27_RS31290 [CGL27_30960]	extracellular solute-binding protein	ACTGGTCTGGACCATT	-49	14.5	regulatory	CGL27_RS31295 [CGL27_30965]; CGL27_RS31300 [CGL27_30970]; CGL27_RS31305 [CGL27_30975]	sugar ABC transporter permease; carbohydrate ABC transporter permease; glycoside hydrolase family 3 protein	UPS5276
CGL27_RS31285 [CGL27_30955]	GntR family transcriptional regulator	ACTGGTCTGGACCATT	-228	14.5	regulatory			UPS5276
CGL27_RS39880 [CGL27_39435]	acyl-CoA dehydrogenase	GAAGGACTAGACCAGT	-290	13.7	regulatory			UPS6714
CGL27_RS39875 [CGL27_39430]	glycoside hydrolase family 18 protein	GAAGGACTAGACCAGT	-111	13.7	regulatory			UPS6714
CGL27_RS04780 [CGL27_04740]	sugar hydrolase	ACTGGTCTAGACATAC	-113	13.3	regulatory	CGL27_RS04775 [CGL27_04735]	glycosyl hydrolase	UPS0793
CGL27_RS04785 [CGL27_04745]	TetR/AcrR family transcriptional regulator	ACTGGTCTAGACATAC	-446	13.3	upstream			UPS0793
CGL27_RS36175 [CGL27_35785]	peptide ABC transporter substrate-binding protein	AGTGGACTGGACCAGT	-65	13.2	regulatory	CGL27_RS36180 [CGL27_35790]; CGL27_RS36185 [CGL27_35795]; CGL27_RS36190 [CGL27_35800];	M20/M25/M40 family metallo-hydrolase; S9 family peptidase; 4'-phosphopantetheinyl transferase superfamily protein; N-acetyltransferase	UPS6119

						CGL27_RS36195 [CGL27_35805]		
CGL27_RS18555 [CGL27_18270]	sugar ABC transporter substrate-binding protein	TCAGGTCTAGACGTGT	-213	12.9	regulatory	CGL27_RS18560 [CGL27_18275]; CGL27_RS18565 [CGL27_18280]	ABC transporter permease; sugar ABC transporter ATP-binding protein	UPS3111
CGL27_RS18550 [CGL27_18265] (iolC)	5-dehydro-2-deoxygluconokinase	TCAGGTCTAGACGTGT	-84	12.9	regulatory			UPS3111
CGL27_RS34965 [CGL27_34620] (ngcE)	carbohydrate ABC transporter N-acetylglucosamine/diacetylchitobiose-binding protein	AGTGGACTATACCTGT	-209	12.9	regulatory			UPS5911
CGL27_RS34960 [CGL27_34615]	hypothetical protein	AGTGGACTATACCTGT	-106	12.9	regulatory			UPS5911
CGL27_RS12990 [CGL27_12765]	CTP synthase	GGTGGAGTAGACCTGT	278	12.7	coding			CGL27_RS12990 [CGL27_12765]
CGL27_RS34310 [CGL27_33980]	GNAT family N-acetyltransferase	TGTTGTCTAGACCAAA	-162	12.7	regulatory			UPS5814
CGL27_RS34305 [CGL27_33975]	HPr family phosphocarrier protein	TGTTGTCTAGACCAAA	-44	12.7	regulatory			UPS5814
CGL27_RS47585 [CGL27_47080]	alpha-mannosidase	ACTGGTCCACACCACA	314	12.6	coding			CGL27_RS47585 [CGL27_47080]

CGL27_RS23245 [CGL27_22930] (acs)	acetate--CoA ligase	ACAGGTCTAAACCAAT	-103	12.4	regulatory			UPS3916
CGL27_RS32530 [CGL27_32195]	DinB family protein	ACTGGACTCGACCTGT	-110	12.4	regulatory			UPS5498
CGL27_RS32525 [CGL27_32190]	M4 family peptidase	ACTGGACTCGACCTGT	-285	12.4	regulatory			UPS5498
CGL27_RS25565 [CGL27_25265]	ATP-binding protein	CGTGGTCTAGACAACA	-2468	12.3	upstream			UPS4312
CGL27_RS30200 [CGL27_29870]	hypothetical protein	AGTGGTCCAGACCAAT	-202	12.3	regulatory	CGL27_RS30205 [CGL27_29875] (cpaB); CGL27_RS30210 [CGL27_29880]	Flp pilus assembly protein CpaB; ParA family protein	UPS5088
CGL27_RS30195 [CGL27_29865]	chitinase	AGTGGTCCAGACCAAT	-95	12.3	regulatory			UPS5088
CGL27_RS21320 [CGL27_21025]	hypothetical protein	ACTGGTCCAGACCTGC	-98	11.8	regulatory			UPS3585
CGL27_RS33065 [CGL27_32735]	tRNA-Gln	ACTGGTCTATACCATG	-14	11.7	regulatory			CGL27_RS33065 [CGL27_32735]
CGL27_RS33060 [CGL27_32730]	tRNA-Glu	ACTGGTCTATACCATG	72	11.7	coding			CGL27_RS33065 [CGL27_32735]
CGL27_RS21150 [CGL27_20855]	alpha/beta hydrolase	AGTGGAGTACACCAAT	-36	11.7	regulatory			UPS3560

CGL27_RS21145 [CGL27_20850]	adenosine deaminase	AGTGGAGTACACCAAT	-83	11.7	regulatory			UPS3560
CGL27_RS39605 [CGL27_39175]	FAD-dependent oxidoreductase	ACTGGTCTGCACCTCC	773	11.6	coding			CGL27_RS39605 [CGL27_39175]
CGL27_RS45830 [CGL27_45345]	hypothetical protein	ACAGGTCTACACGACC	1700	11.6	coding			CGL27_RS45830 [CGL27_45345]
CGL27_RS08795 [CGL27_08645]	sugar hydrolase	CCAGGTCTAGACCAAT	-194	11.6	regulatory			UPS1449
CGL27_RS25590 [CGL27_25290]	hypothetical protein	ACTCATCTACACAACT	-48	11.5	regulatory	CGL27_RS25595 [CGL27_25295]	conjugal transfer protein TraS	UPS4316
CGL27_RS01490 [CGL27_01440]	alpha-L-rhamnosidase	ACTGGTCCATACCTGT	-321	11.4	regulatory			UPS0254
CGL27_RS19705 [CGL27_19420]	PTS lactose transporter subunit IIC	TGTGGTTTAGACCATA	-64	11.4	regulatory			UPS3309
CGL27_RS19700 [CGL27_19415]	PTS sugar transporter	TGTGGTTTAGACCATA	-162	11.4	regulatory			UPS3309
CGL27_RS33775 [CGL27_33445] (eccCa)	type VII secretion protein EccCa	AGTGGTGTCCACAACT	490	11.3	coding			CGL27_RS33775 [CGL27_33445] (eccCa)
CGL27_RS22135 [CGL27_21830]	copper homeostasis protein CutC	ATTGGTCTAGACATGG	-2	11.2	regulatory			UPS3732

CGL27_RS22300 [CGL27_21995]	DNA-binding response regulator	ACTGGTCGAGACCGGT	-792	11.1	upstream			UPS3761
CGL27_RS43500 [CGL27_43040]	chitin-binding protein	AGTGGACCAGACCACA	-201	11.1	regulatory			UPS7305
CGL27_RS19970 [CGL27_19680]	extracellular solute-binding protein	AGAGGTCTGAACCACT	-110	11	regulatory	CGL27_RS19965 [CGL27_19675]; CGL27_RS19960 [CGL27_19670]	sugar ABC transporter permease; carbohydrate ABC transporter permease	UPS3352
CGL27_RS31080 [CGL27_30755]	hypothetical protein	AAGGGTGTACTCCACT	-123	10.9	regulatory			UPS5239
CGL27_RS26245 [CGL27_25940]	XRE family transcriptional regulator	ACAGGTCGAGACAACC	480	10.8	coding	CGL27_RS26240 [CGL27_25935]	DUF397 domain-containing protein	CGL27_RS26245 [CGL27_25940]
CGL27_RS48995 [CGL27_48460]	FAD-dependent oxidoreductase	ACTGGTGTAAACCAGG	-238	10.8	regulatory			UPS8206

Supplementary figures

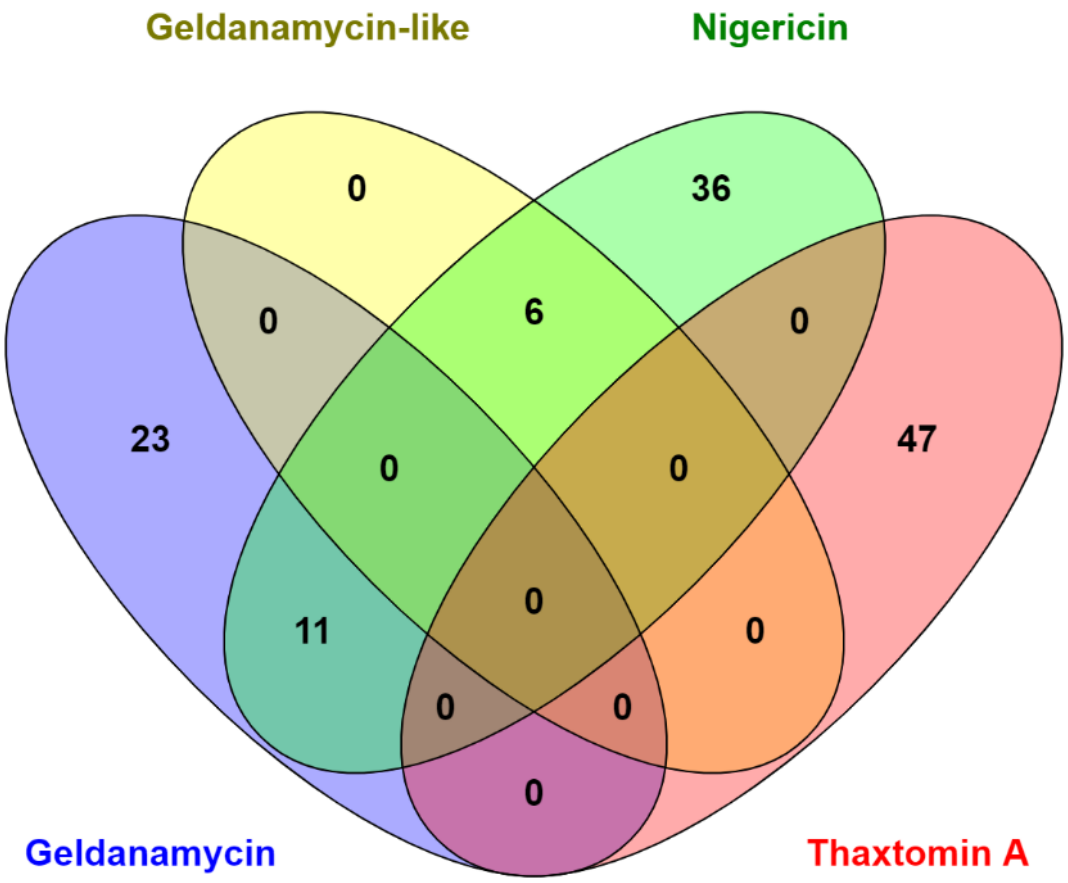

Figure S3.1. Venn diagram for the distribution of BGCs across the *Streptomyces* genus. The BGC for geldanamycin (GenBank accession AY179507.1.), nigericin (GenBank accession DQ354110.1.) and thaxtomin A (extracted from NC_013929.1) were used to search *Streptomyces* genome sequences on NCBI using the online BLASTn tool with the following parameters: database refseq_genomes, ≥70% identity, ≥70% coverage, and E-values < 10-6. Matches to the geldanamycin BGC were refined by searching for the presence of genes *gdmF* and *gdmM*. BGCs lacking *gdmF* and *gdmM* but with similarity to the geldanamycin gene cluster were labeled as "Geldanamycin-like". The diagram was prepared using Venny 2.1 (https://bioinfogp.cnb.csic.es/tools/venny/).

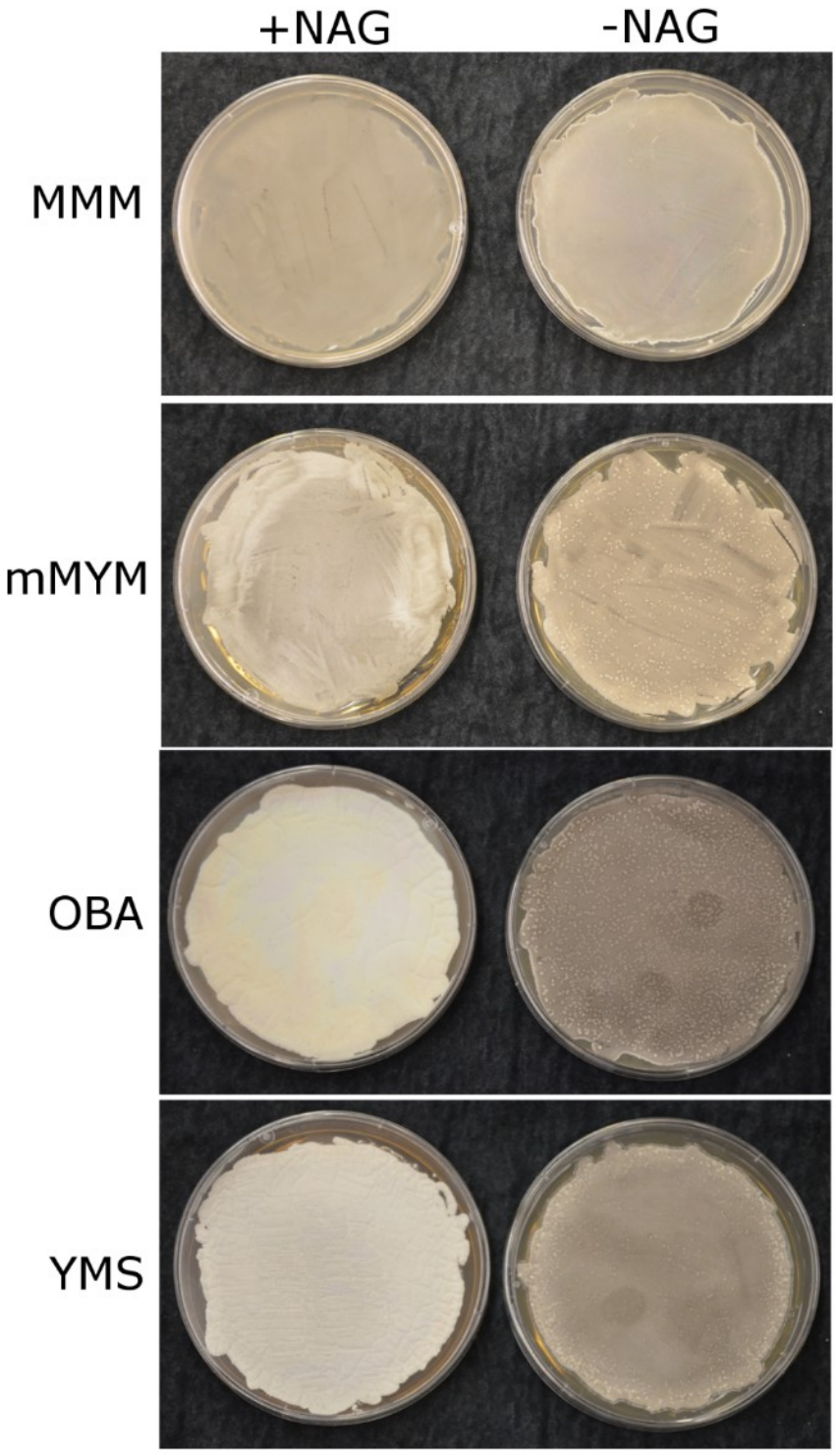

Figure S3.2. Morphological development of *Streptomyces* sp. 11-1-2 on different culture media containing (+) or lacking (-) 50 mM NAG. Photos were taken 14 days after inoculation and incubation at 28°C.

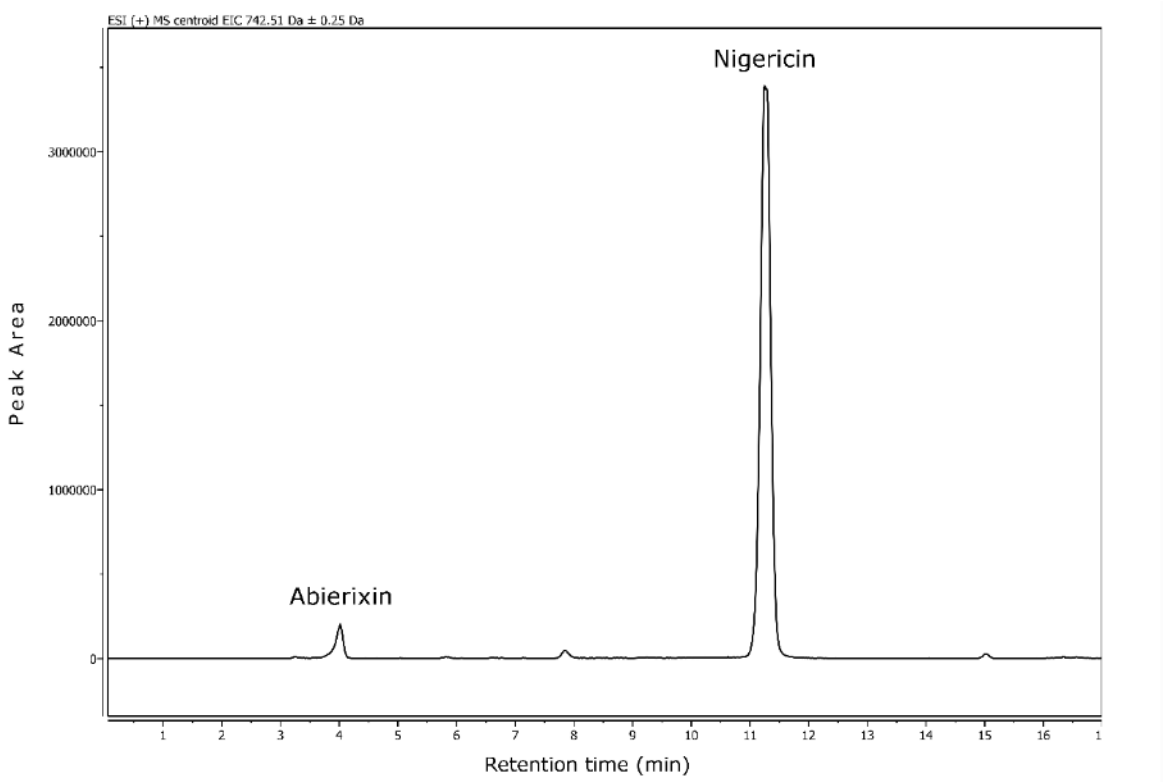

Figure S3.3. Representative extracted ion chromatogram for nigericin and abierixin. The chromatogram was obtained by analyzing a YMS - NAG extract for the m/z 742.51 ([M+NH_4]+) using MestReNova version 14.1.2 (Mestrelab Research S.L.).

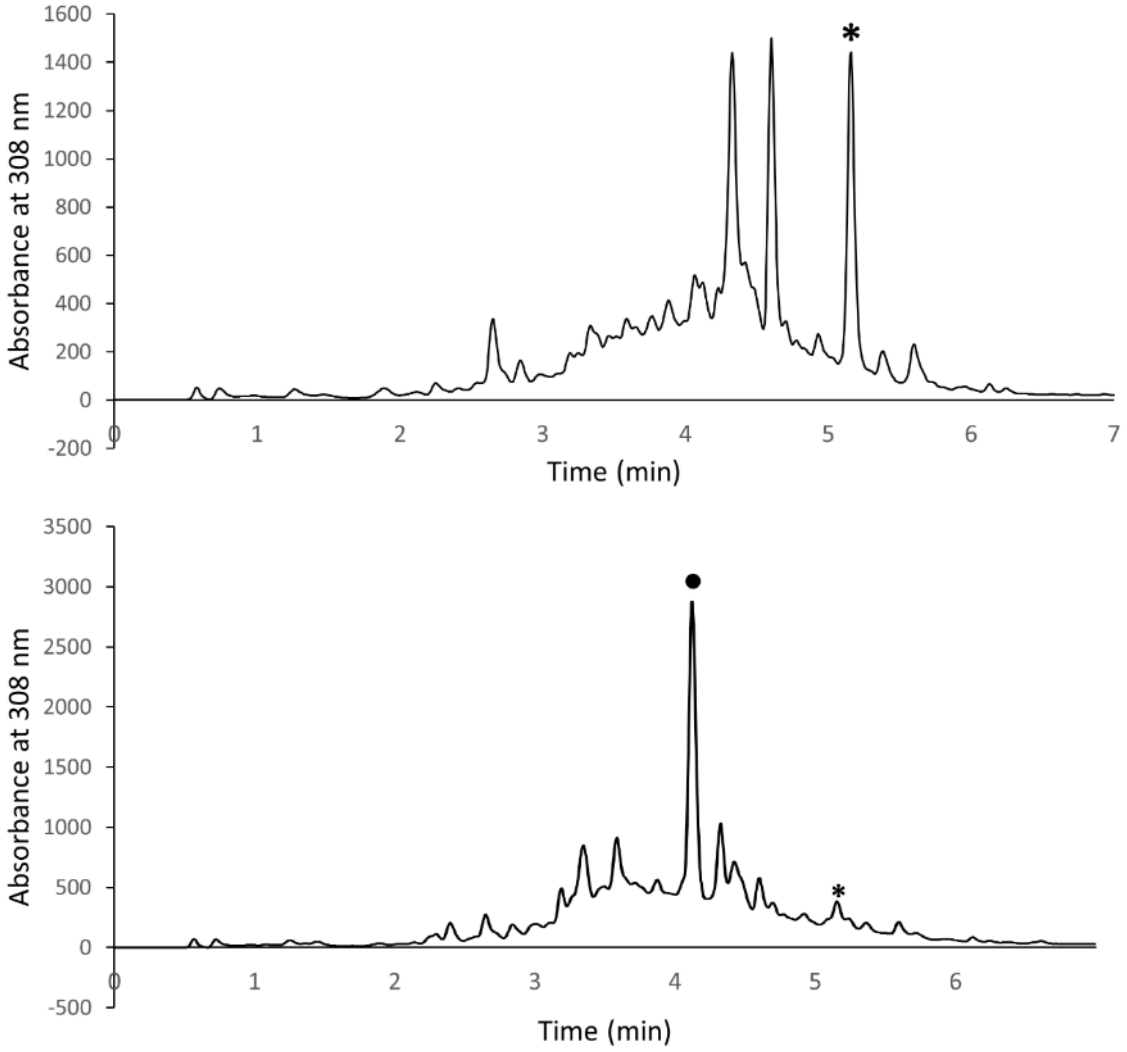

Figure S3.4. Representative chromatograms for geldanamycin detection using RP-HPLC. The chromatograms correspond to extracts from a plate culture of strain 11-1-2 on YMS - NAG (top) and YMS + 50 mM NAG (bottom). The geldanamycin peak is indicated by *, and the predicted 15-hydroxygeldanamycin peak is indicated by ●.

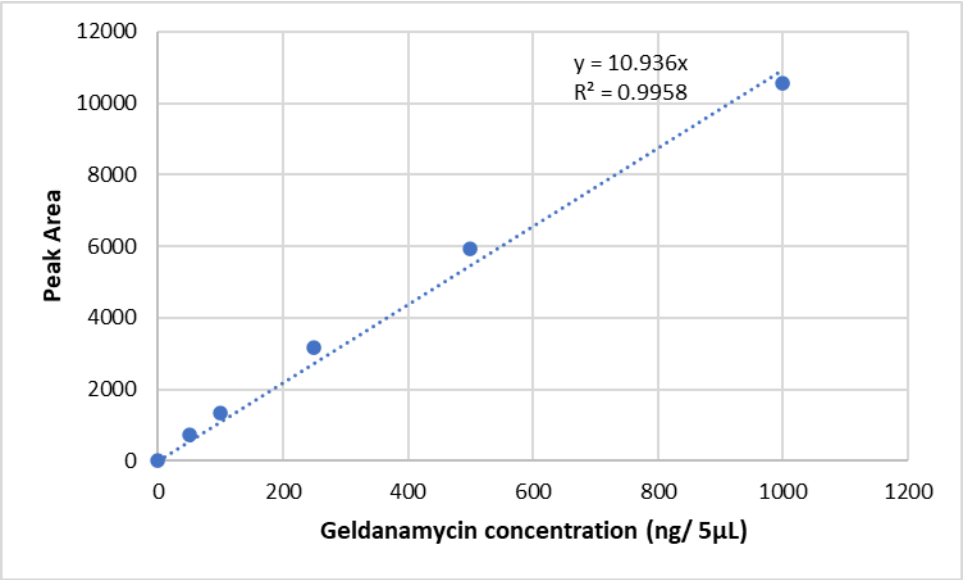

Figure S3.5. Geldanamycin standard curve used for quantification of organic culture extracts using RP-HPLC. The concentration represents the amount of geldanamycin in a 5 µL injection. The peak area was calculated using ChemStation software version B.04.03 (Agilent Technologies Canada Inc.).

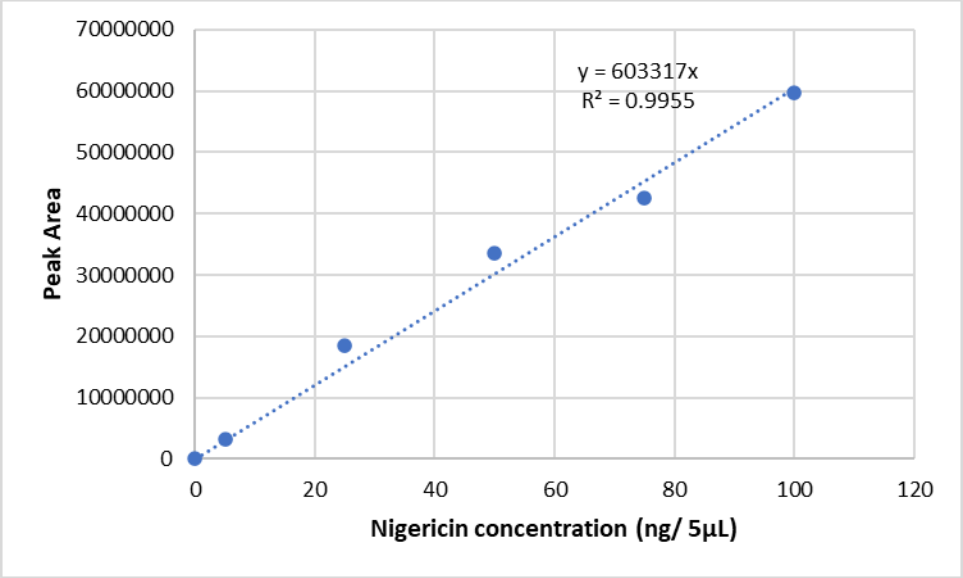

Figure S3.6. Nigericin standard curve used for quantification of organic culture extracts using LC-MS. The concentration represents the amount of nigericin in a 5 µL injection. The peak area was calculated using MestReNova version 14.1.2 (Mestrelab Research S.L.).

CHAPTER 4

EXPLORING THE SPECIALIZED METABOLOME OF THE PLANT PATHOGENIC *STREPTOMYCES* SP. 11-1-2

4.1 Abstract

Members of the *Streptomyces* genus are renowned for their ability to produce a diverse array of specialized metabolites (SMs) with various bioactivities, including antimicrobial and phytotoxic activities. The production of SMs is highly regulated and depends in part on the growth conditions of the organism. The chemical elicitor *N*-acetylglucosamine (NAG) and the 'One Strain Many Compounds' (OSMAC) approach were used to characterize the metabolic potential of the plant pathogen *Streptomyces* sp. 11-1-2. Genome mining revealed that in addition to producing the phytotoxic compounds nigericin and geldanamycin, 11-1-2 has the potential to produce at least 49 other specialized metabolites, some of which are not widely distributed among *Streptomyces* species. Organic extracts were prepared using two different organic solvents and plate cultures of *Streptomyces* sp. 11-1-2 grown on different culture media and media containing or lacking the chemical elicitor NAG. The extracts were tested in bioassays to assess the presence of compounds with antimicrobial and phytotoxic activities, and they were subjected to untargeted metabolomics and molecular networking analyses. Differences were observed in the phytotoxicity of the extracts, and this was due in part to differences in the levels of nigericin and geldanamycin. Moreover, the antimicrobial activity against Gram-positive bacteria and yeast was very consistent among extracts, but no activity against Gram-negative bacteria was detected. The use of untargeted metabolomics predicted the presence of elaiophylin, guanidylfungin A, echosides and other related compounds, in accordance with

the BGCs present in the 11-1-2 genome. Furthermore, this study determined for the first time that elaiophylin might be involved in pathogen-host interactions, and other predicted and detected molecules could also take part in the interaction. Overall, this is the first specialized metabolome characterization of a non-thaxtomin producing pathogenic *Streptomyces* and should provide the basis for further studies with *Streptomyces* sp. 11-1-2.

4.2 Introduction

Streptomyces bacteria are ubiquitous in terrestrial and aquatic environments where they interact with various organisms (Seipke et al. 2012; Viaene et al. 2016; Rey and Dumas 2017; Chevrette et al. 2019; Zhao et al. 2020a; Besaury et al. 2021; Duangupama et al. 2021). These interactions can be mutualistic, parasitic or competitive and are thought to be primarily mediated by the production of specialized metabolites with diverse bioactivities (O'Brien and Wright 2011). The SMs can protect or inflict damage on a host or other microorganisms in the community in order to compete for nutritional resources, or they can act as signaling molecules in inter- and intra-species communication (Scott et al. 2008; Oh et al. 2009; Cornforth and Foster 2013; Vaz Jauri and Kinkel 2014; Traxler and Kolter 2015; Kim et al. 2019).

In *Streptomyces*, the production of SMs is facilitated by BGCs that can be categorized based on the core biosynthetic enzymes that are present and the class of metabolite(s) produced. For example, there are BGCs for the production of peptides, phenazines, polyketides, terpenes, lanthipeptides, non-ribosomal peptides, etc. (Nett et al. 2009; Hwang et al. 2014; Lee et al. 2020a). SM BGCs also usually contain pathway-specific regulatory genes that are also known as cluster-situated regulatory (CSR) genes. These encode regulators that act as a switch, either activating or repressing the biosynthesis of the specific

metabolite that is produced by the BGC. CSRs are also often regulated by environmental cues via global regulators (Van Wezel and McDowall 2011; Hoskisson and Fernández-Martínez 2018), which control multiple SM biosynthetic pathways rather than individual pathways (Hoskisson and Fernández-Martínez 2018). For example, the amino sugar *N*-acetylglucosamine (NAG) acts as an elicitor of SMs in different *Streptomyces* strains. NAG addition to culture media is a tested strategy to activate the expression of genes associated with different *Streptomyces* specialized metabolites such as actinorhodin (Rigali et al. 2008), siderophores (Craig et al. 2012), monensin (Zhang et al. 2016c), bleomycin (Chen et al. 2020), among others. NAG binds to the DasR regulator, impeding it from attaching to specific DNA sequences that are involved in the regulation of specialized metabolite BGCs.

Not all SMs are produced at the same time or under the same environmental conditions, and this has led to the implementation of strategies such as the One Strain-Many Compounds (OSMAC) approach for exploring the metabolic diversity of microorganisms. With this approach, growth conditions such as nutrient content, temperature and rate of aeration are altered in order to promote the activation of different SM biosynthetic pathways and yield potentially novel compounds (Bode et al. 2002; Romano et al. 2018). This strategy is complemented by easy access to genome sequencing and genome mining bioinformatics tools such as antiSMASH and the MIBiG database. Likewise, the use of untargeted metabolomics and the establishment of open specialized databases and cheminformatics tools such as the Global Natural Products Social Molecular Networking (GNPS) platform and associated workflows has greatly facilitated and improved compound annotation (Wu et al. 2015; Wang et al. 2016; Kind et al. 2018; Chaleckis et al. 2019; Nothias et al. 2020; van

Bergeijk et al. 2020; Blin et al. 2021; Schmid et al. 2021; Bayona et al. 2022; Terlouw et al. 2022).

The plant pathogen *Streptomyces* sp. 11-1-2, isolated in 2011 from a CS-infected potato in Newfoundland, produces at least two phytotoxic compounds, geldanamycin and nigericin; the detection of these compounds was discussed in Chapter 3. The objective of this chapter was to characterize the metabolic profile of *Streptomyces* sp. 11-1-2 and explore the production of specialized metabolites that could participate in microbe-microbe and plant-pathogen interactions by combining genomics and metabolomics approaches.

4.3 Results and Discussion

4.3.1 *Streptomyces* sp. 11-1-2 encodes for several specialized metabolites of interest

Compared to the initial analysis (see Section 3.3.1 and Table S3.2), the updated antiSMASH analysis (Table 4.1) predicted the same total number of BGCs (51), but the annotation of several clusters had changed, as discussed in more detail below. Overall, the analysis predicted a diverse array of BGC classes, including many PKs, NRPs and terpenes, while six regions (22, 23, 32, 39, 41, and 51) were still uncharacterized and cannot be assigned to a known BGC with the information available.

Table 4.1. Biosynthetic gene clusters predicted in the genome of *Streptomyces* sp. 11-1-2 using antiSMASH 7.0.

Region	Type	From	To	Most similar known cluster		Similarity
1	lanthipeptide -class-i	244467	267372	mycotrienin I	NRP+ Polyketide	7%
2	terpene	304965	327957	isorenieratene	Terpene	85%
3	arylpolyene,l adderane,NR PS	457599	529895	coprisamide C/coprisamide D	NRP	95%
4	NRPS-like	571719	614054	Echosides A-E	NRP	11%
5	PKS-like,terpene	658010	705793	rustmicin	Polyketide: Iterative type I polyketide	20%
6	terpene	824320	845259	brasilicardin A	Terpene+ Saccharide	38%
7	NRPS	884096	962151	cyclofaulknamy cin	Polyketide	8%
8	RiPP-like,T1PKS,h glE-KS	974268	1097025	hexacosalactone A	Other	79%
9	NRPS-like	1160316	1200586	meilingmycin	Polyketide	2%
10	2dos	1237882	1273203	Hygrocin A-B	Polyketide	67%
11	T1PKS,NRP S	1277766	1393079	meridamycin	NRP+ Polyketide	65%
12	NAPAA	1541803	1572879	paulomycin	Other	7%
13	T1PKS	1575870	1705961	nigericin	Polyketide: Modular type I polyketide	100%
14	T1PKS	1709681	1754690	salinomycin	Polyketide: Modular type I polyketide	8%
15	T1PKS,hglE-KS	2077385	2128172	hexacosalactone A	Other	11%
16	2dos,T1PKS, NRPS-like	2317281	2402967	naphthomycin A	Polyketide	50%
17	NRPS,nucleo side	2436317	2481506	toyocamycin	Other	30%
18	NRPS	2541367	2594739	glycinocin A	NRP	11%
19	terpene	2943967	2964259	aurachin C/aurachin D/aurachin SS	Polyketide+ Terpene	20%
20	T1PKS,NI-siderophore	2991613	3045502	peucechelin	NRP	20%
21	ectoine	3210416	3220820	ectoine	Other	100%
22	terpene	3719051	3738277			
23	lanthipeptide -class-i	3920406	3943726			
24	T1PKS	4304490	4484508	desulfoclethram ycin/clethramyci n	Other	61%

25	RiPP-like	4627469	4639844	granaticin	Polyketide: Type II polyketide	10%
26	ladderane	4658207	4697921	o-dialkylbenzene 1/o-dialkylbenzene 2	Polyketide+ NRP	58%
27	NRPS	4753653	4795917	ochronotic pigment	Other	50%
28	indole	5011258	5032403	5-isoprenylindole-3-carboxylate β-D-glycosyl ester	Other	61%
29	terpene	5596461	5615957	geosmin	Terpene	100%
30	NI-siderophore	6759041	6769871	legonoxamine A/desferrioxamine B/legonoxamine B	Other	83%
31	NRPS-like	7294519	7335806	Echosides A-E	NRP	100%
32	NI-siderophore	7921967	7933880			
33	ladderane,arylpolyene,NRPS,aminocoumarin	7996321	8069356	cinnapeptin	NRP	82%
34	T1PKS	8239229	8295520	notonesomycin A	Other	18%
35	T2PKS	8421342	8493857	spore pigment	Polyketide	83%
36	terpene	8870148	8892706	hopene	Terpene	76%
37	lanthipeptide-class-i	9096140	9120593	steffimycin D	Polyketide: Type II polyketide+ Saccharide: Hybrid/tailoring saccharide	16%
38	terpene	9210479	9230310	lasalocid	Polyketide	3%
39	T1PKS	9358088	9405558			
40	NRPS,transAT-PKS,NRPS-like	9419881	9495386	meilingmycin	Polyketide	9%
41	butyrolactone	9654449	9665381			
42	hserlactone	9675690	9696448	Heronamide A-F	NRP+ Polyketide	8%
43	redox-cofactor	9815666	9837784	lankacidin C	NRP+ Polyketide	13%
44	T1PKS	9877490	9945918	efomycin K-L	Polyketide	100%
45	T1PKS,NRPS-like	10159131	10240039	geldanamycin	Polyketide	100%
46	terpene	10383924	10403386	pristinol	Terpene	100%
47	terpene	10508385	10529722	ebelactone	Polyketide	11%
48	T1PKS	10696374	10842668	niphimycins C-E	Polyketide	87%

49	NAPAA	10939213	10973346	γ-poly-L-2,4-diaminobutyric acid	NRP	25%
50	NRP-metallophore,NRPS,T1PKS	11085502	11205821	coelichelin	NRP	90%
51	betalactone	11367403	11392789			

Analysis of the 11-1-2 genome against the MIBiG database using BiG-SCAPE revealed a majority of BGCs from different classes with no similarity to reported clusters (Fig. 4.1). In contrast, other BGCs were successfully placed into gene cluster families (GCF). Nigericin (region 013), elaiophylin/efomycins (region 044), geldanamycin (region 045), niphimycins (region 048) and coelichelin (region 050) have at least one match to the database using a 0.3 cutoff value (Fig. 4.1).

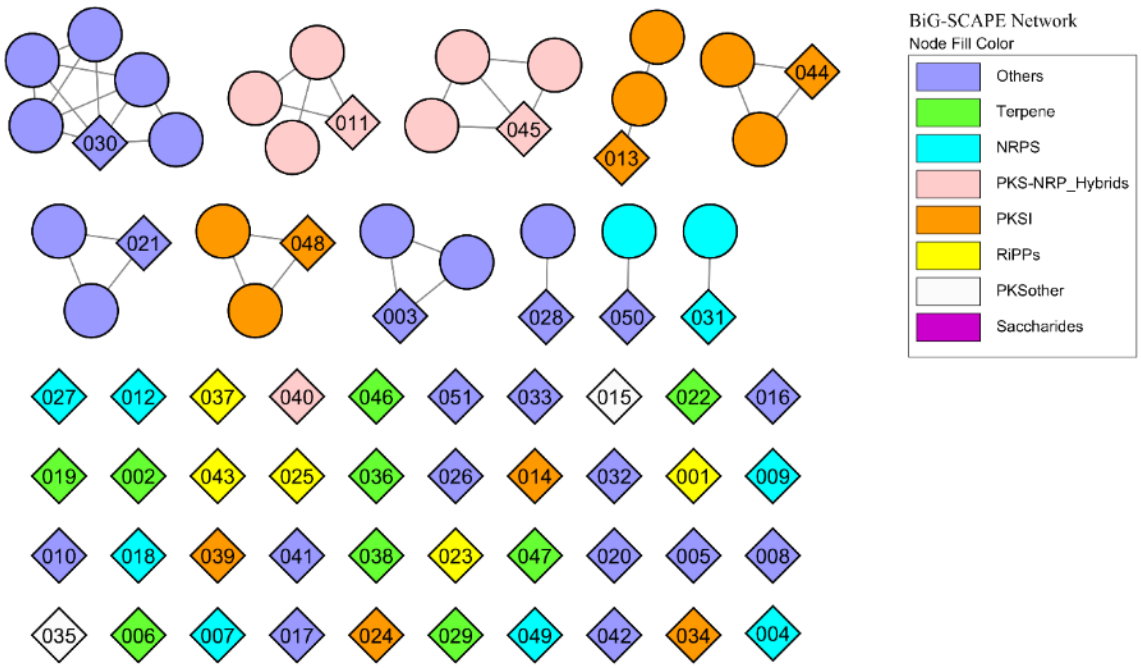

Figure 4.1. BiG-SCAPE analysis of 11-1-2. The network shows the correlation between predicted BGCs in the 11-1-2 genome (diamonds) and the MIBiG database (circles) using a cutoff of 0.3. Diamonds are labeled with their region number as defined by antiSMASH and presented in Table 4.1. The colour of the nodes represents the BGC class as determined by BiG-SCAPE.

Two regions in the 11-1-2 genome, regions 4 and 31, match the BGC for echosides A-E with 11 and 100% similarity, respectively (Table 4.1). Echosides A-E are *para*-therphenyl compounds produced by *Streptomyces*, and some of them possess DNA topoisomerase inhibition activity and weak antibacterial activity (Deng et al. 2014). The echoside BGC was described as containing a NRPS-like polyporic acid synthase (encoded by *echA*) that is essential for biosynthesis of these metabolites, along with a number of genes with putative regulatory and tailoring functions (Zhu et al. 2014). According to the BiG-SCAPE analysis, the echosides BGC and closely related BGCs can be subdivided into three gene cluster families (GCFs); moreover, the BGC network suggests that echosides and similar metabolites might be widespread among *Streptomyces* (Fig. 4.2). Interestingly, a

comparison between the BGC predicted at region 31 and the terfestatin/echoside BGC from *Streptomyces* sp. RM-5-8 showed important differences both upstream and downstream of the proposed core genes of the BGC (Fig. 4.2). These differences might account for the production of different echoside analogs, as previously proposed (Clinger et al. 2021). Previously, terfestatin A, an auxin signaling inhibitor, was isolated from *Streptomyces* sp. F40 (Yamazoe et al. 2004), and it shares structural similarities with the echosides. However, it is currently not known if this compound is produced by the same BGC that is responsible for echoside biosynthesis, and the genome of the strain is not available.

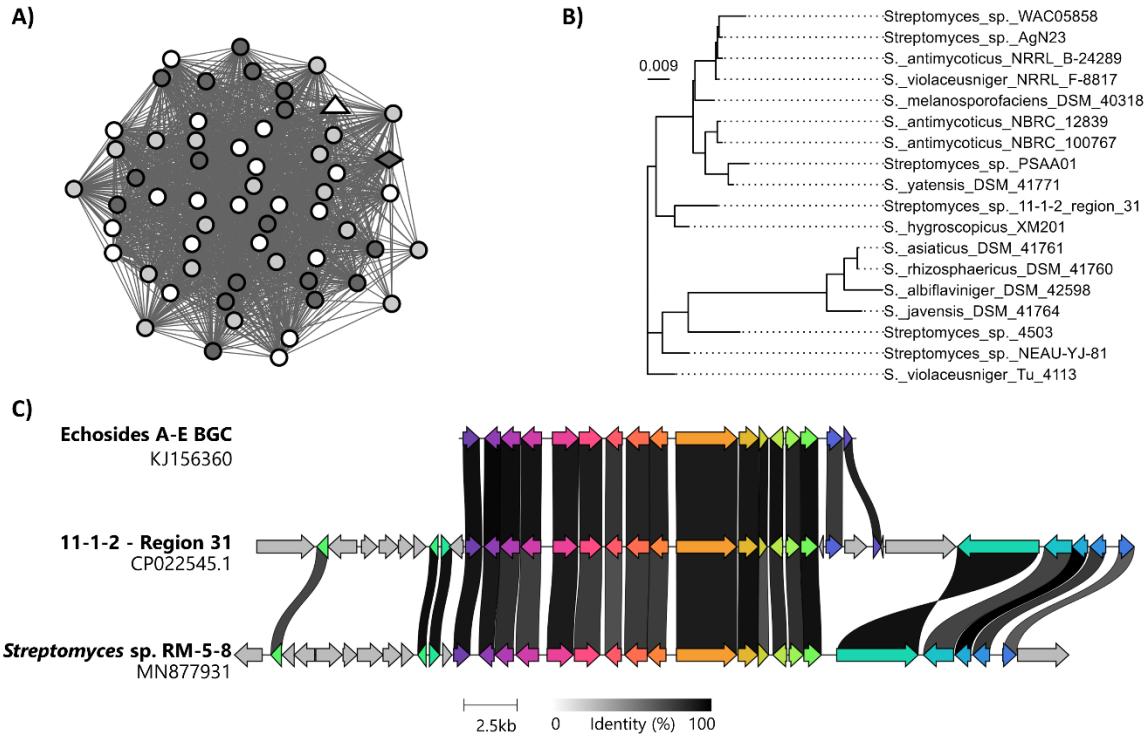

Figure 4.2. Genomic analysis of region 31 in the 11-1-2 genome. **A)** BiG-SCAPE network. The diamond represents the 11-1-2 region 31, the triangle represents the MIBiG BGC, and the colour of the nodes represents different gene cluster families (GCFs). **B)** Phylogenetic tree showing the GCF containing region 31 and closely related BGCs in the custom *Streptomyces* BGC database. **C)** Alignment of the Echosides A-E BGC with a similar BGC from *Streptomyces* sp. RM-5-8 and the predicted echoside BGC at region 31 in 11-1-2. Genes coloured the same belong to the same functional group, and homologues are linked by shaded areas that indicate the % amino acid identity of the corresponding protein products.

The BGC predicted in region 4 from 11-1-2 contains homologues of the *echA* and *echB* genes from the echoside BGC (Fig. 4.3), but no other significant matches to the echoside BGC are present. The NRPS EchA is a tri-domain module protein, and each domain contains signature motifs for substrate specificity: adenylation (VAEFSGAASK), thiolation (LGGTSL), and thioesterase (GYSYG) domains (Zhu et al. 2014). The EchA homologue from region 4 has identical domain for thiolation and thioesterase domain, but not for the adenylation domain (Fig. S4.1), where a valine is replaced by an isoleucine, which is believed to modify the substrate specificity (Zhu et al. 2014). Moreover, the amino acid alignment of the EchB homologue from region 4 with EchB reveals that both proteins contain an N-terminal nucleotide binding motif TGxxGxxA (Fig. S4.2), typical of short-chain dehydrogenase/reductases (Zhu et al. 2021). The protein EchB interacts with EchC, a dehydratase, to modify the polyporic acid molecule assembled by EchA during the biosynthesis of echosides in *Streptomyces* sp. LZ35 (Zhu et al. 2021), and a similar finding was reported for the EchB/EchC homologues TerB and TerC in *Streptomyces* sp. R-M-5-8 (Clinger et al. 2021); yet, no *echC/terC* region is present in region 4. This suggests that the compound produced by the BGC in region 4 might have some basic structural features that are shared with the echosides, but it is likely a different molecule.

Interestingly, two BGCs in the MIBiG database, o-dialkylbenzene 1/o-dialkylbenzene 2 (BGC0002441) and kitacinnamycins (BGC0002109), also contain homologues of *echA* and *echB*, although it remains unclear what their role is in the production of the corresponding compounds (Shi et al. 2019; Zhang et al. 2021). Notably, it was recently shown that the deletion of the *echA* homologue from the globisporamic acid BGC in

Streptomyces globisporus C-1027 did not affect the biosynthesis of that compound (Li et al. 2022).

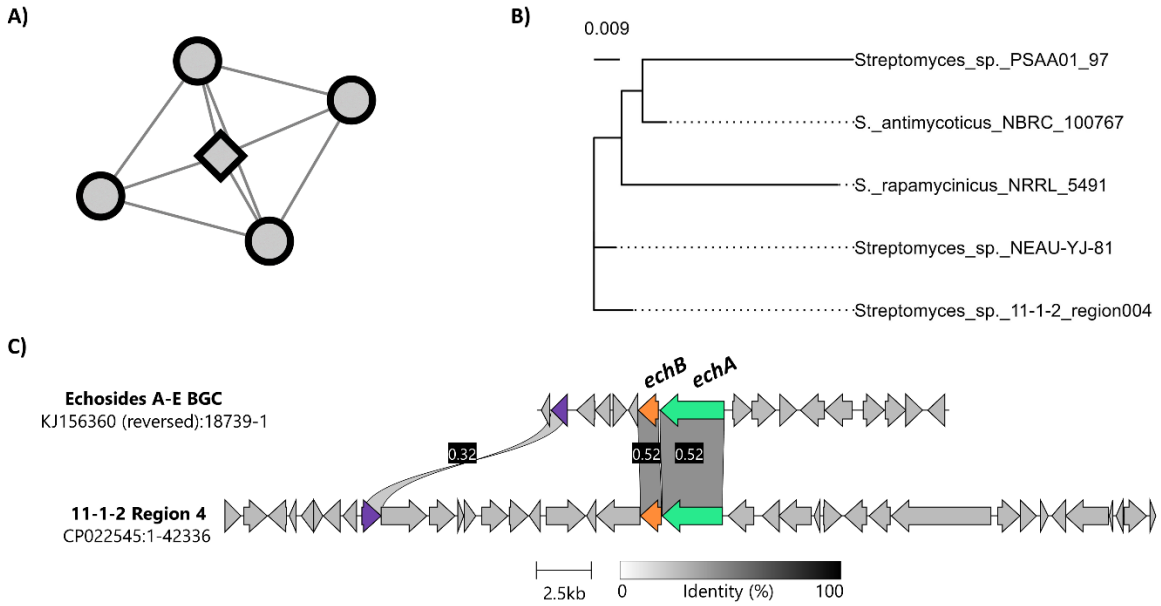

Figure 4.3. Genomic analysis of region 4 in the 11-1-2 genome. **A)** BiG-SCAPE network. The diamond represents the 11-1-2 region 4. **B)** Phylogenetic tree showing closely related BGCs in the custom *Streptomyces* BGC database. **C)** Alignment of the Echosides A-E BGC with the BGC predicted for the 11-1-2 region 4. The colouring and linking of genes in each cluster are as described in the Figure 4.2 figure legend. The *echA* and *echB* genes in the echoside BGC are labeled.

Region 5 in the 11-1-2 genome is predicted by antiSMASH to contain a BGC with 20% similarity to the known rustmicin BGC (Table 4.1). Rustmicin is also known as galbonolide A, and the related compound neorustmicin is also known as galbonolide B; both molecules are 14-membered macrolides with antifungal activity (Karki et al. 2010). The rustmicin BGC from *Streptomyces galbus* contains 30 genes, and it is separated into two operons. Genes *galA-E* are sufficient for the production of neorustmicin/galbonolide B (Liu et al. 2015), while genes *galGHIJK* are required for production of rustmicin/galbonolide A

(Karki et al. 2010). The role of the remaining genes is unclear, but it is speculated that they are tailoring enzymes (Karki et al. 2010; Zhang et al. 2016a). The *galA-E* core is present in region 5 of 11-1-2, suggesting that this strain could at least produce galbonolide B, while the flanking genes could serve as post-PKS tailoring enzymes yielding novel galbonolides (Fig. 4.4).

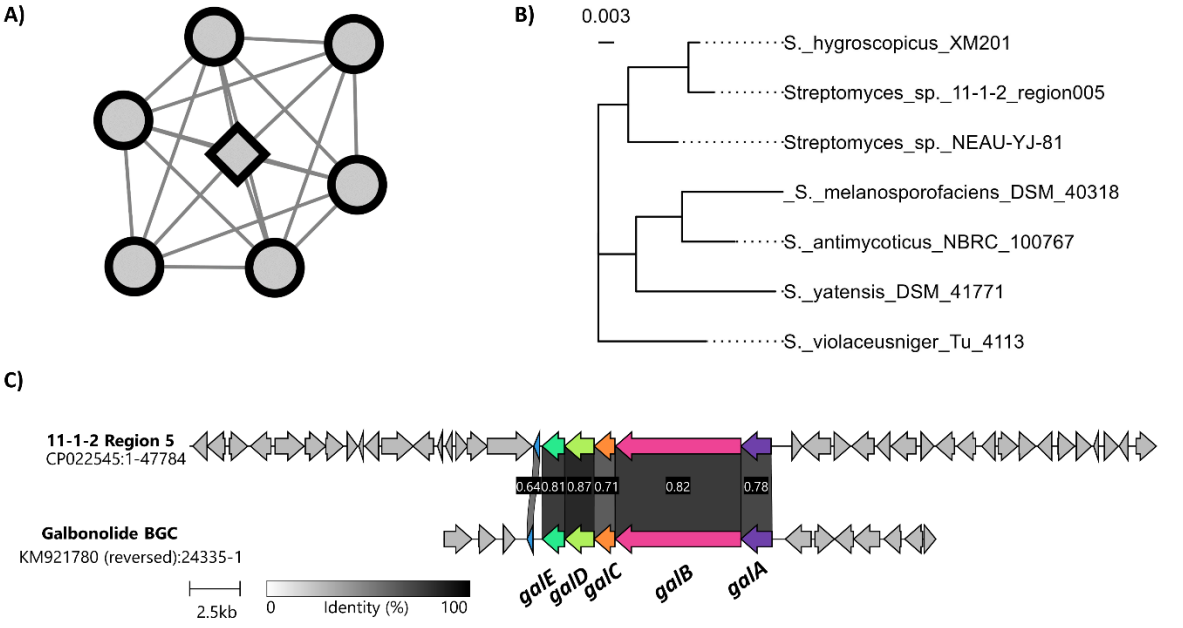

Figure 4.4. Genomic analysis of region 5 in the 11-1-2 genome. **A)** BiG-SCAPE network. The diamond represents the 11-1-2 region. **B)** Phylogenetic tree showing closely related BGCs in the custom *Streptomyces* BGC database. **C)** Alignment of the galbonolide BGC with the BGC predicted for the 11-1-2 region 5. The colouring and linking of genes in each cluster are as described in the Figure 4.2 figure legend.

Region 11 of the 11-1-2 genome partially matches the reported meridamycin BGC. This compound is a 27-membered macrolide with neuroprotective activity (Salituro et al. 1995; He et al. 2006; Sun et al. 2006). Other closely related molecules, meridamycins A-E, have also been described in *Streptomyces* sp. LZ35 and are likely to be produced by the same

BGC (Liu et al. 2016). The meridamycin BGC has been characterized as a hybrid NRP-PKS cluster in *Streptomyces* sp. NRRL 30748 and *Streptomyces* sp. DSM 4137 (syn: *Streptomyces malaysiensis* DSM 4137) (He et al. 2006; Sun et al. 2006). The 11-1-2 cluster shows some significant differences compared to other reported clusters (Fig. 4.5). Firstly, the homologue for *merC* is split into three PKSs and two discrete domains, while the homologue for *merD* is expanded. Secondly, a group of four genes consisting of two regulatory genes (LysR and TetR transcriptional regulators), one transporter (major facilitator superfamily, MFS transporter) and a DNA polymerase III subunit alpha is located upstream of the PKS genes in 11-1-2, while they are downstream of the PKS genes in *S. malaysiensis*, and are absent from the *Streptomyces* sp. NRRL 30748 cluster. Thirdly, three genes located downstream from the PKS genes in 11-1-2 are not present in the other clusters. These genes include a homologue to a sensor histidine kinase followed by a LuxR transcriptional regulator, resembling a two-component system operon. The third gene is a protein of unknown function. It remains unclear how these changes might affect the production of meridamycins in 11-1-2.

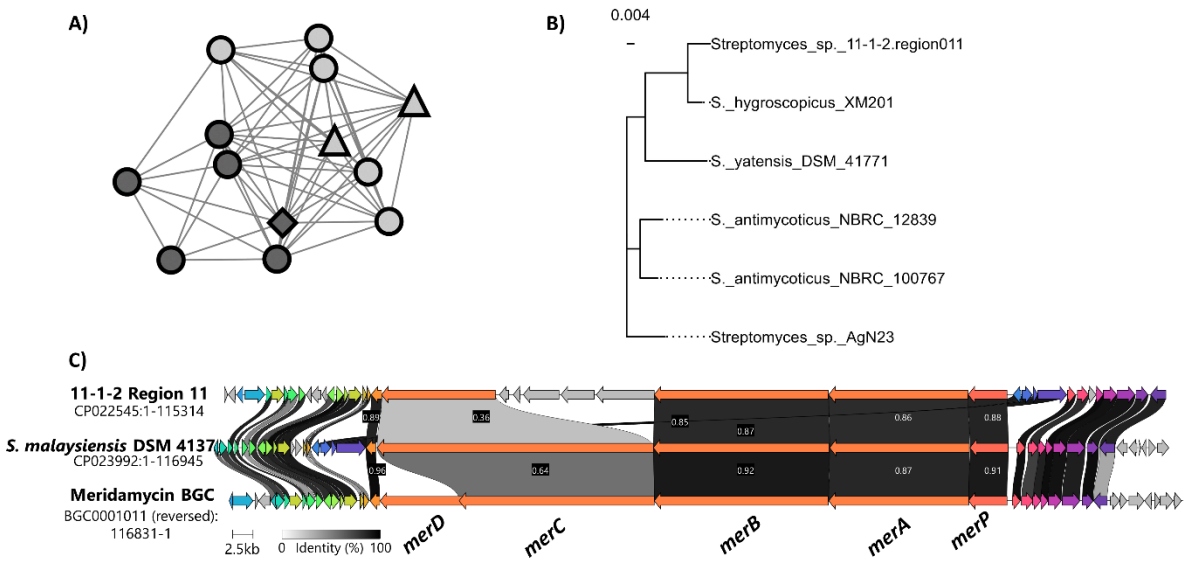

Figure 4.5. Genomic analysis of region 11 in the 11-1-2 genome. **A)** BiG-SCAPE network. The diamond represents the 11-1-2 region, the triangles represent the MIBiG BGCs, and the colour of the nodes represents the gene cluster family. **B)** Phylogenetic tree showing the GCF containing region 11 and related BGCs in the custom *Streptomyces* BGC database. **C)** Alignment of the meridamycin BGC, a similar cluster from *S. malaysiensis* DSM 4137 and the BGC predicted for the 11-1-2 region 11. The colouring and linking of genes in the clusters are as described in the Figure 4.2 figure legend.

Region 28 of the 11-1-2 genome partially matches the reported 6-isoprenylindole-3-carboxylate β-D-glycosyl ester BGC. BiG-SCAPE analysis showed a network with a large number of nodes, suggesting that similar regions are widespread among *Streptomyces* (Fig. 4.6). This compound does not present significant antimicrobial activity, and it was first described as being co-produced with two terfestatins (B and C), all of which contain a novel unsaturated hexuronic acid (4-deoxy-α-L-threo-hex-4-enopyranuronate) attached to the main core (Wang et al. 2015). The biosynthesis of the molecule is proposed to be initiated by L-tryptophan, which is sequentially modified by the products of *priABCD* until the compound is obtained. The 11-1-2 cluster contains homologues of *priABCDEFG* and some hypothetical genes, but it also shows some differences (Fig. 4.6), suggesting the potential production of a related molecule by 11-1-2.

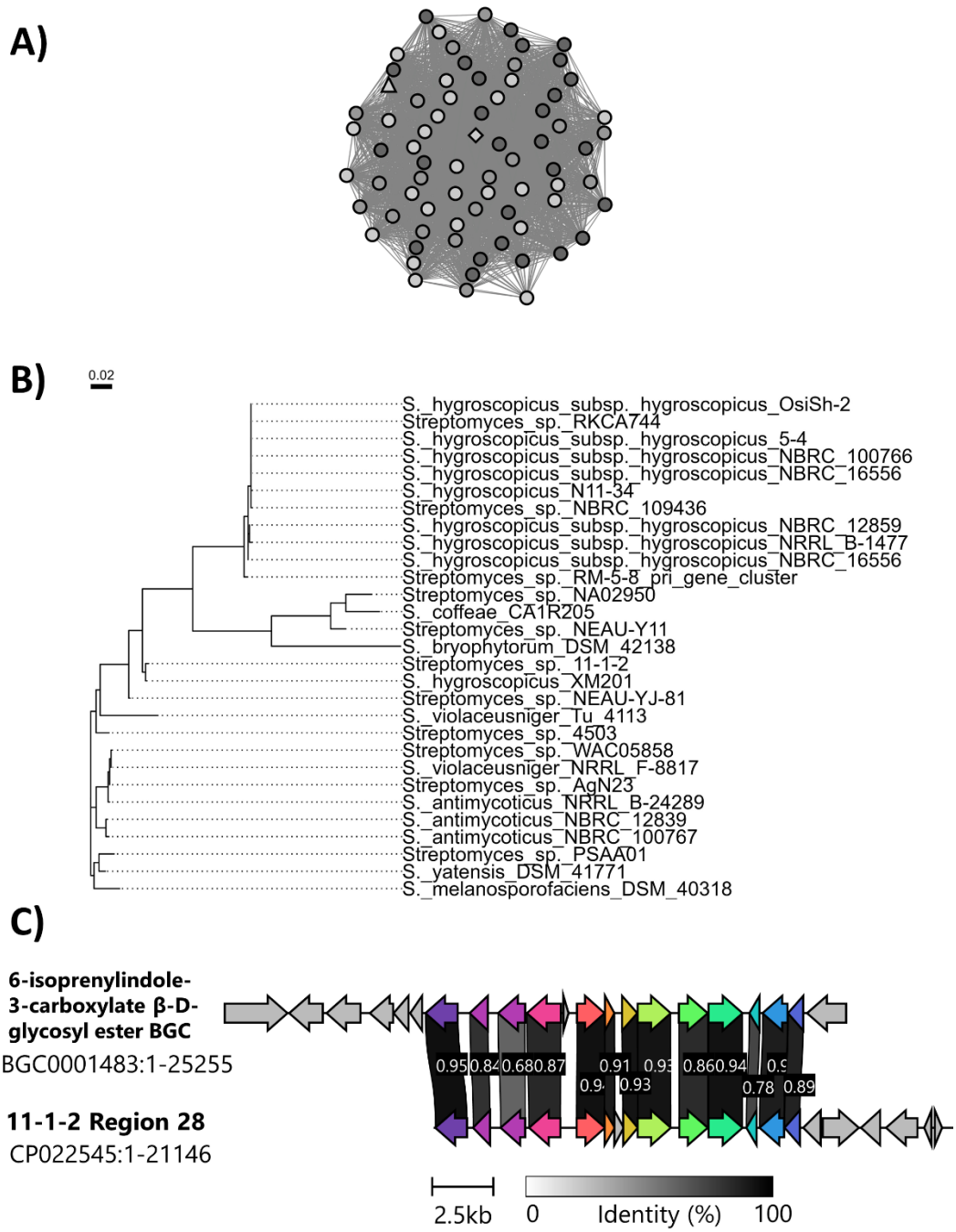

Figure 4.6. Genomic analysis of region 28 in the 11-1-2 genome. **A)** BiG-SCAPE network. The diamond represents the 11-1-2 region, the triangles represent the MIBiG BGCs, and the colour of the nodes represents the gene cluster family. **B)** Phylogenetic tree showing the GCF containing region 28 and closely related BGCs in the custom *Streptomyces* BGC database. **C)** Alignment of the 6-isoprenylindole-3-carboxylate β-D-glycosyl ester BGC and the BGC predicted for the 11-1-2 region 28. The colouring and linking of genes in each cluster are as described in the Figure 4.2 figure legend.

4.3.2 Agar cores and organic culture extracts from 11-1-2 have differential antimicrobial and phytotoxic activity

Previously, *Streptomyces* sp. 11-1-2 was shown to produce the phytotoxic compounds nigericin and geldanamycin, and other compounds related to these molecules were also predicted to be produced (see Chapter 3). Given the number of putative specialized metabolites that are predicted to be encoded by the 11-1-2 genome (Table 4.1), it is expected that this strain may produce other metabolites that could play a role in mediating plant-pathogen interactions as well as microbe-microbe interactions. To investigate this further, the OSMAC approach was employed in order to activate the production of as many compounds as possible. This was achieved by culturing the 11-1-2 strain in triplicate on different solid media (Section 2.1.7), including one (PMA) that is derived from potato tuber tissue and is expected to at least partially mimic the nutritional conditions encountered during tuber colonization. In addition, the chemical elicitor NAG was used in some media to determine the impact of this molecule on the specialized metabolism of 11-1-2 (Section 2.1.7). Agar cores from the culture plates were tested for phytotoxic activity on potato tuber slice assays (Section 2.5.1) and for antimicrobial activity against different Gram-positive and Gram-negative bacteria and yeast (Section 2.5.4). In addition, the cultures were subjected to extraction using two different organic solvents (EtOAc, MeOH) (Section 2.3.1), and the resulting extracts were also evaluated for antimicrobial activity and phytotoxic activity against both potato tuber tissue and radish seedlings.

4.3.2.1 Antimicrobial assays

Figure 4.7 show the results of the antimicrobial bioassays using agar cores and organic extracts from plate cultures of 11-1-2 grown on four different media (OBA, MMM,

YMS and mMYM) with and without (+/-) the addition of 50 mM NAG. In general, the cores and organic extracts from all of the media exhibited good activity against the three Gram-positive bacterial indicator organisms used (*B. subtilis, S. epidermidis, S. scabiei*). In contrast, there was no observable antimicrobial activity with any of the cores or organic extracts against the Gram-negative bacterial indicator organisms *E. coli* and *Pseudomonas syringae* (not shown). The cores and methanol extracts also exhibited antifungal activity against *S. cerevisiae,* whereas this activity was mainly absent from the ethyl acetate extracts, with the exception of the YMS-NAG extract (Fig. 4.7).

As discussed in Chapter 3, the addition of NAG to culture media was shown to suppress the production of geldanamycin and nigericin by the 11-1-2 strain (Fig. 3.8 and Table 3.2). In the case of 11-1-2, the addition of NAG to the mMYM medium reduced the activity of the agar cores and extracts against the bacterial indicators to a greater extent than in the other media (Fig. 4.7). Furthermore, NAG appears to suppress the production of one or more methanol-soluble antifungal compounds in OBA, while some stimulatory effects of NAG were observed in OBA when assessing the antibacterial activity of agar cores against *B. subtilis* and *S. epidermidis* (Fig. 4.7).

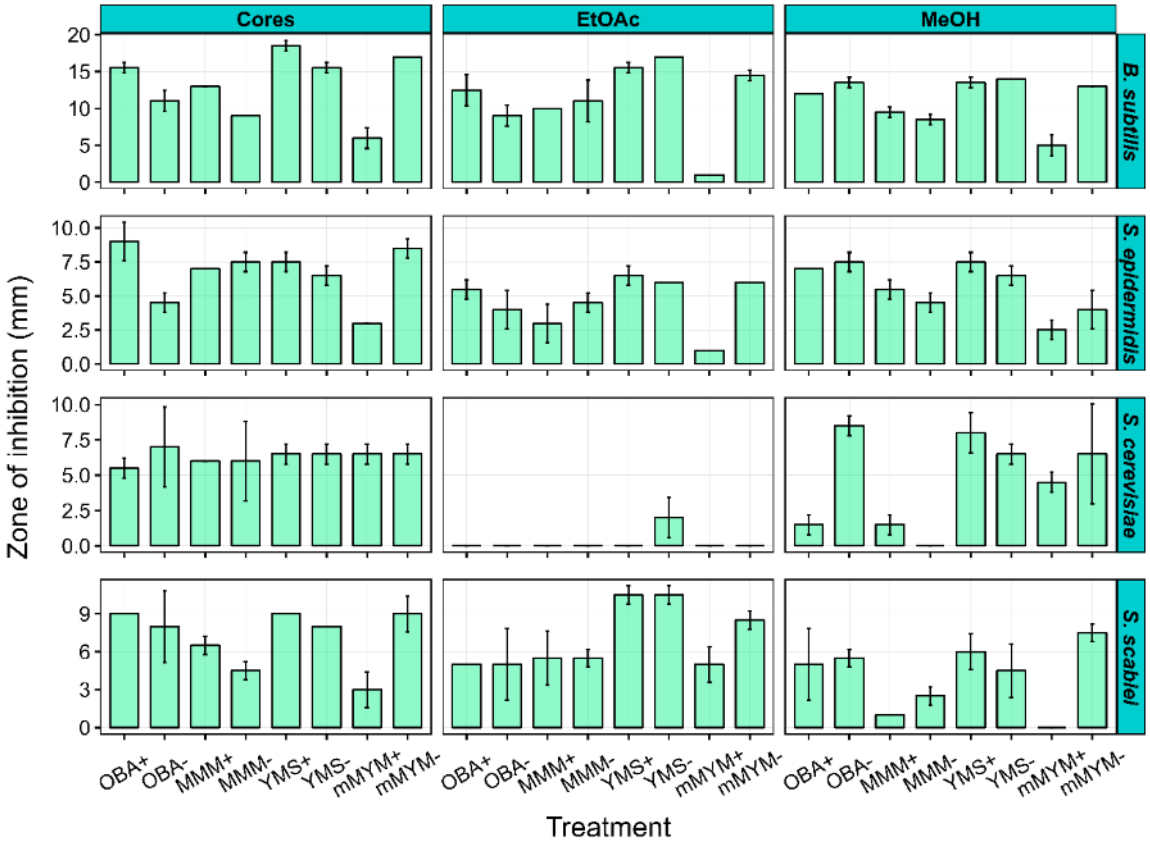

Figure 4.7. Antimicrobial assay with agar cores and organic culture extracts. Each bar represents the average of the diameter of the zone of inhibition of two disks or cores ± standard deviation after removing the core or disk diameter. The assay was repeated twice with similar results.

Given the observed antibacterial activity of the 11-1-2 agar cores and extracts against *S. scabiei,* I conducted additional antimicrobial assays against other *Streptomyces* strains, including two other plant pathogenic species (*S. turgidiscabies, S. acidiscabies*). As shown in Figure 4.8, the observed antibacterial activity of the agar cores varied depending on the test strain, with greater inhibitory activity generally observed against *S. turgidiscabies*, and less inhibitory activity against *S. coelicolor*. The effect of NAG on the inhibitory activity varied depending on the medium used and indicator test strain. In the case of *S. clavuligerus,* NAG had a suppressive effect on the inhibitory activity against this organism in three of the

four media tested (Fig. 4.8). In the context of the plant pathogenic *Streptomyces*, it remains unknown if the 11-1-2 strain has an advantage when colonizing plant tissues and competing against other plant pathogenic species like *S. scabiei*, *S. acidiscabies* or *S. turgidiscabies*, due to their susceptibility to the compounds produced by 11-1-2. Antibiotic susceptibility might be involved in competition among *Streptomyces* strains in the environment. For example, the production of streptomycin by *S. griseus* conferred an advantage against streptomycin-susceptible *S. coelicolor* in short-term interactions (Westhoff et al. 2020). Moreover, the production of antibiotics in cocultures and mixed populations is dependant on the phylogenetic relatedness of the organisms in the community (Westhoff et al. 2021). None of the tested strains are closely related to 11-1-2 (Caicedo-Montoya et al. 2021), and specific microbe-microbe interactions were not evaluated in this work to determine the effects on specialized metabolites. Overall, further investigation is required to characterize the interactions between 11-1-2 and other soil-borne *Streptomyces* and their effects on metabolite production.

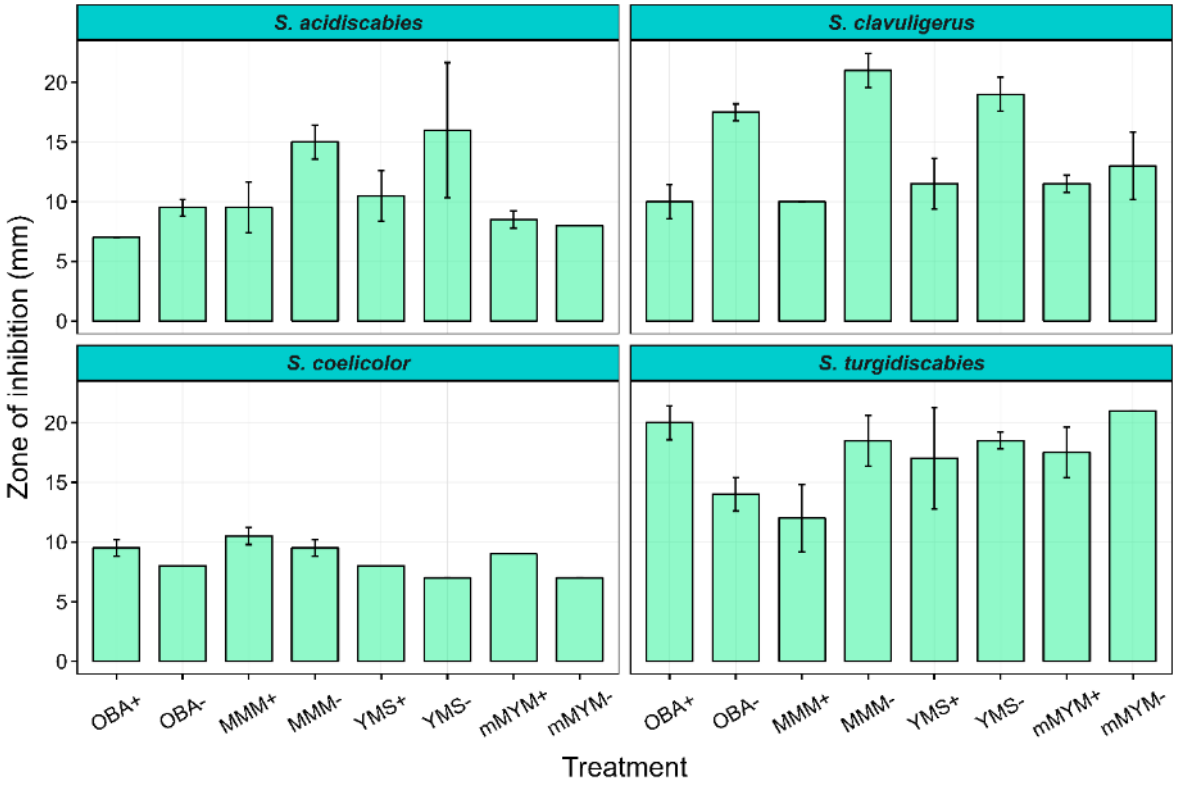

Figure 4.8. Antimicrobial assay with agar cores against different *Streptomyces* spp. Each bar represents the average of the diameter of the zone of inhibition of two disks or cores ± standard deviation after removing the core diameter.

The antimicrobial assays were also conducted using cores and organic extracts of the 11-1-2 strain grown on four additional agar media – M4, PMA, SA and SFM - in addition to two previously tested media (OBA, YMS). Again, no antibacterial activity against the Gram-negative bacterial indicator organisms was detected (not shown), but the cores and extracts all exhibited inhibitory activity against the two Gram-positive indicator organisms tested (Fig. 4.9). Notably, the ethyl acetate extracts from the tested media all exhibited antifungal activity, with the exception of the OBA culture extract (Fig. 4.9). This is consistent with the results shown in Fig. 4.7, in which only the YMS – NAG ethyl aetate extract exhibited inhibitory activity against *S. cerevisiae.* Overall, these results show that 11-1-2 produces specialized metabolites in the culture media tested, and that agar cores have activity against

Gram-positive bacteria and antifungal activity against *S. cerevisiae*. This activity was retained after extraction from the agar plates with organic solvents.

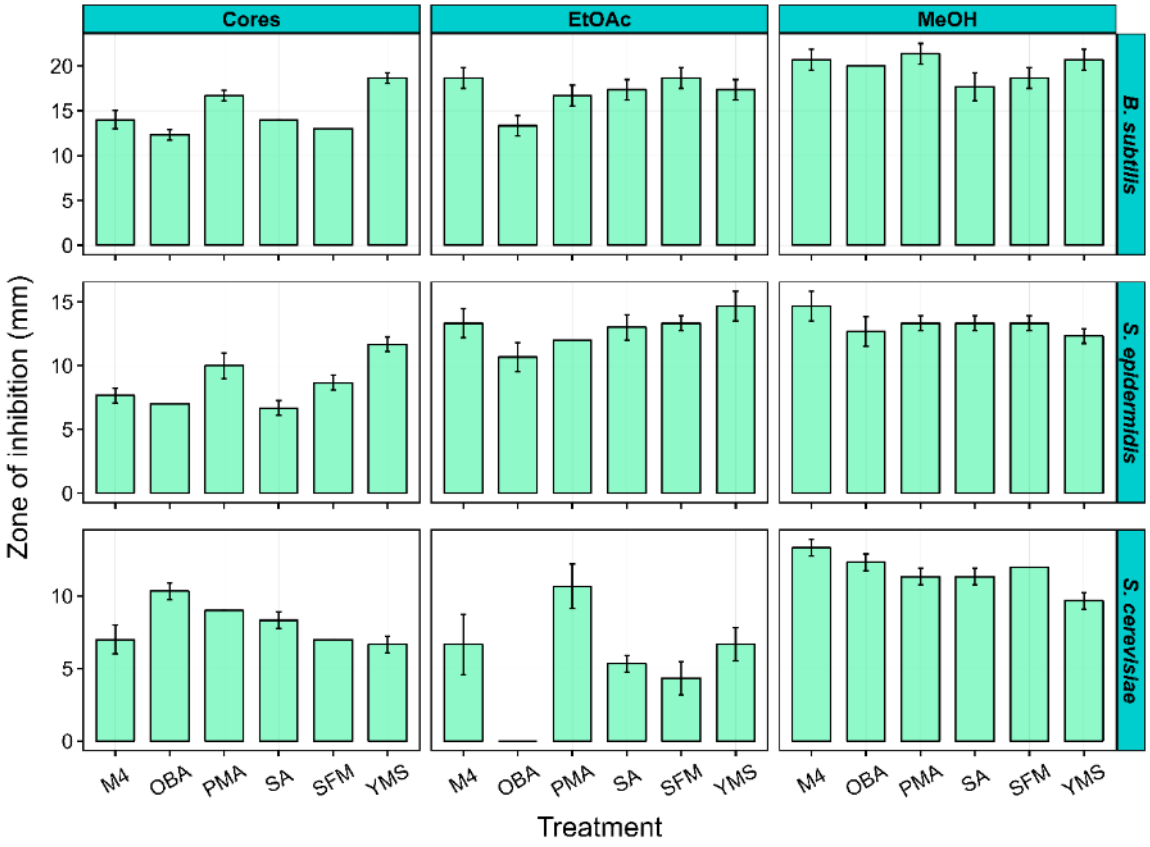

Figure 4.9. Antimicrobial assay with agar cores and organic culture extracts. Each bar represents the average of the diameter of the zone of inhibition of two disks or cores ± standard deviation after removing the core or disk diameter.

4.3.2.2 Plant bioassays

Considering the role of 11-1-2 as a plant pathogen, the production of phytotoxic compounds by this strain was of particular interest. The effect of NAG on the phytotoxic activity of agar cores and organic culture extracts was examined previously (See Chapter 3), and so the discussion here will focus on the activity observed for the cores and extracts from

the M4, PMA, OBA, SA, SFM and YMS solid cultures. As shown in Figure 4.10, the cores from all of these media showed different levels of phytotoxicity against potato tuber tissue; notably, the PMA and SFM cores were highly phototoxic, whereas the SA cores had minimal effect on the plant tissue. The organic culture extracts also had differential effects on the potato tissue. Generally, the phytotoxic activity from the extracts was seen as necrosis and pitting of the tissue that extended beyond the inoculation site. The ethyl acetate extracts from M4, SFM and YMS cultures caused less necrosis than the methanol extracts from the same cultures (Fig. 4.10). Extracts from PMA were more severe and consistent for both solvents, while extracts from the SA cultures only showed some pitting and with minimum necrosis. The control cores from the uninoculated media and the solvent controls showed no effects on the tissue (Fig. S4.3).

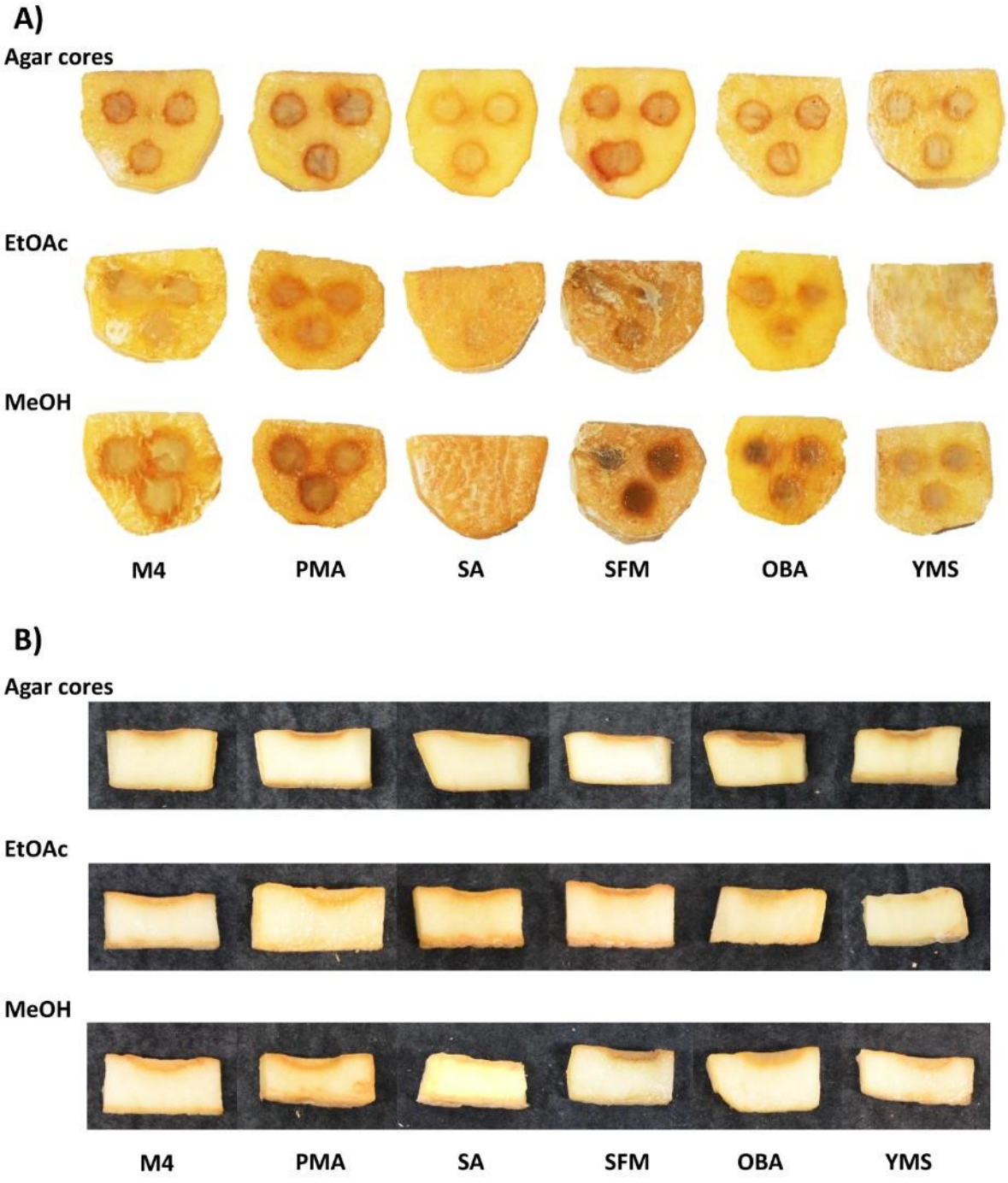

Figure 4.10. Potato tuber slice assay with agar cores and organic culture extracts. A) Top view and B) side view of a representative slice for each treatment. Each slice was treated with three cores or disks from the same media or extract, and three slices per treatment were used. The assay was repeated twice with similar results.

When tested against radish seedlings, the extracts differentially affected the development of the shoot, but the effects on root length and total length were more pronounced (Figs. 4.11-4.13). Both the EtOAc and MeOH extracts from the PMA cultures as well as the M4 ethyl acetate extract caused considerable stunting of the seeding roots as compared to the other extracts, while the SA extracts did not reduce the seedling length.

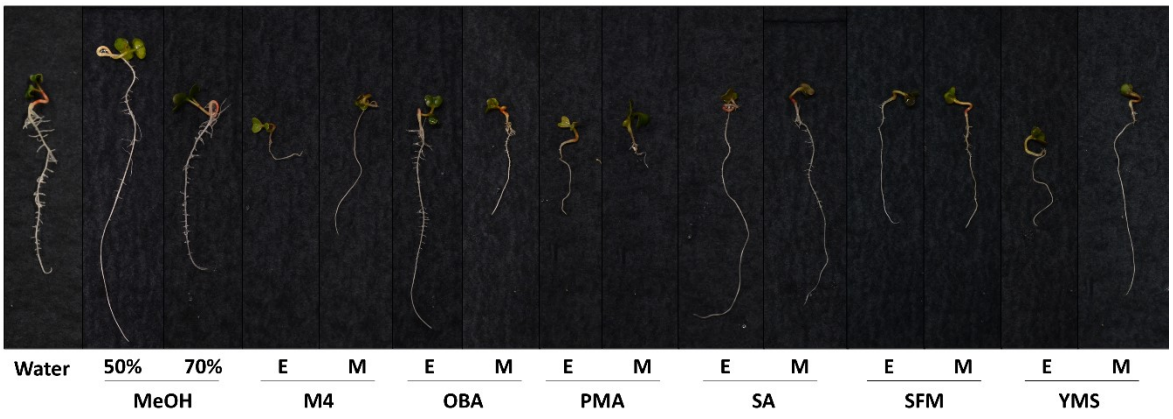

Figure 4.11. Representative radish seedlings treated with different organic culture extracts. E: ethyl acetate; M: methanol. The photos were taken after five days of incubation.

It was observed that the seedlings for some treatments had long roots but the development of lateral roots was affected (Fig. 4.11); thus, the lateral roots/cm was determined for the seedlings (Fig. 4.13). Interestingly, seedlings that were treated with the M4 EtOAc extract, which had caused a severe reduction in the root length (Fig. 4.13), had similar numbers of lateral roots as the control plants, whereas the SA ethyl acetate extract-treated seedlings had a reduction in the number of lateral roots despite having an average root length similar to the control plants (Fig. 4.13). Lateral root development is controlled by the presence of the indole-3-acetic acid (IAA) auxin, which promotes cell division and maintains cell viability (Celenza et al. 1995; Du and Scheres 2018). It is possible that auxin signaling

interference by specialized metabolites recovered with the organic solvents are responsible for the phenotype seen in specific extracts. Auxin activity can be regulated or inhibited by a number of synthetic and natural products (Hayashi 2021), some of which include cytokinins (Stoeckle et al. 2018), tryptophan conjugates of jasmonic acid and IAA (Staswick 2009), and most notably, *Streptomyces*-produced terfestatin A (Yamazoe et al. 2005) and yokonolides A and B (Hayashi et al. 2001, 2003).

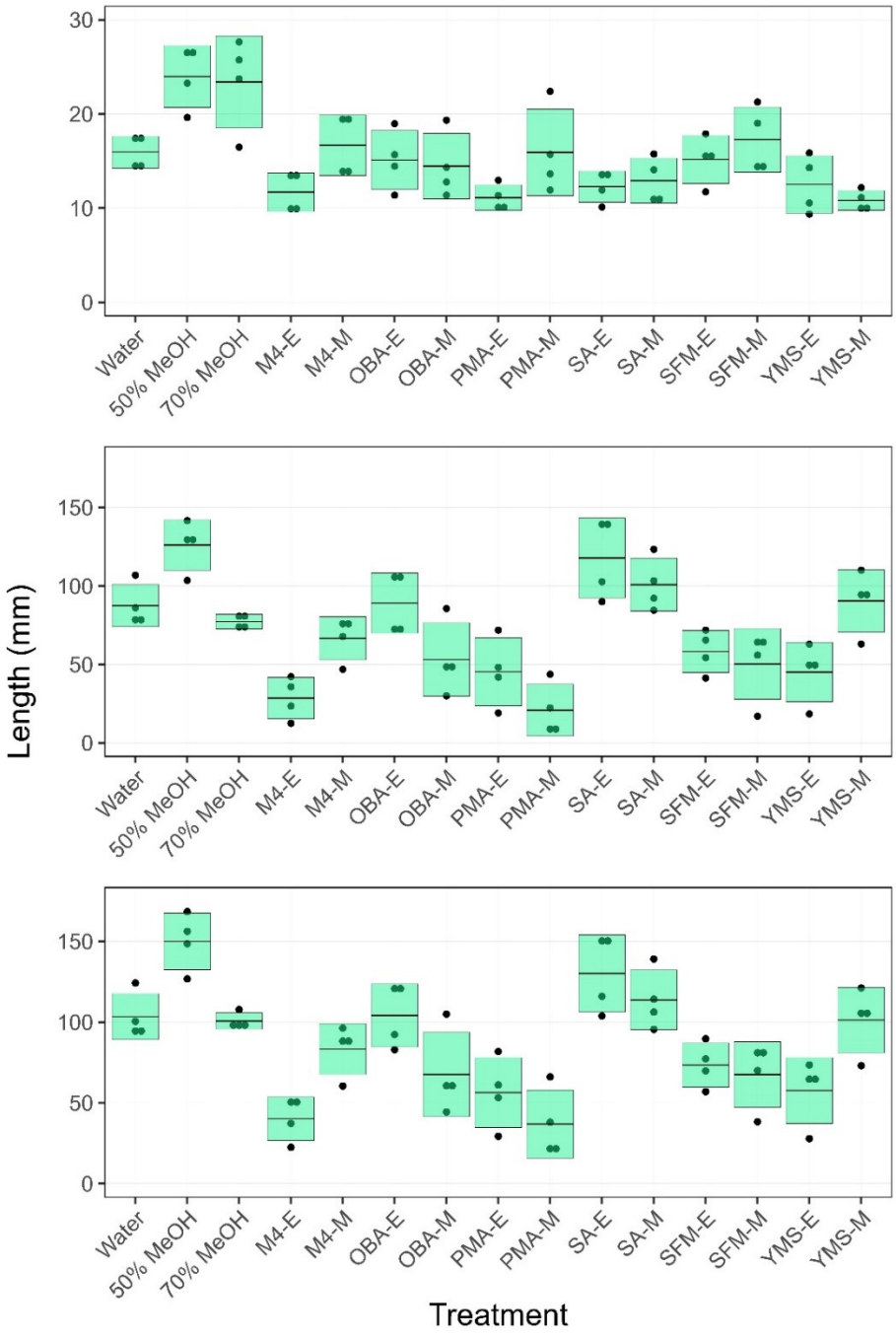

Figure 4.12. Effect of different organic culture extracts on radish seedlings. The shoot (top), root (middle) and total length (bottom) of the seedlings were evaluated. Each box represents the average of the measurement ± standard deviation. The assay was repeated twice with similar results. The name of the media is preceded by E (ethyl acetate) or M (methanol) according to the organic solvent used for the metabolite extraction. 50% MeOH served as the control for the methanol extracts while 70% MeOH was the control for the ethyl acetate extracts.

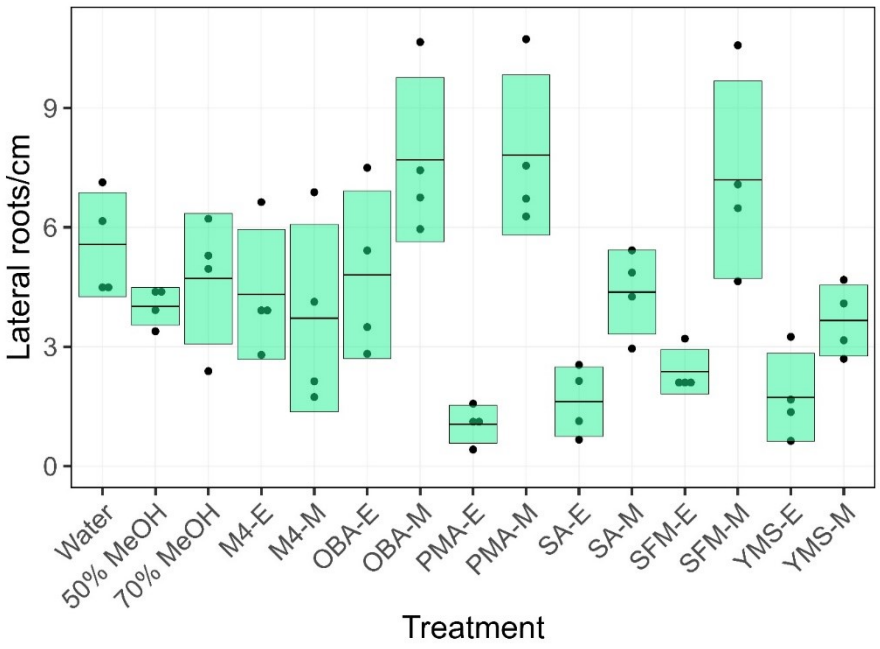

Figure 4.13. Effect of different organic culture extracts on the number of lateral roots/cm of root length in radish seedlings. Each box represents the average ± standard deviation. The assay was repeated twice with similar results. The name of the media is preceded by E (ethyl acetate) or M (methanol) according to the organic solvent used for the metabolite extraction. 50% MeOH served as the control for the methanol extracts while 70% MeOH was the control for the ethyl acetate extracts.

4.3.3 *Streptomyces* sp. 11-1-2 produces a diverse array of specialized metabolites

To gain further insights into the specialized metabolites that may be responsible for the observed bioactivities, organic culture extracts were analyzed using untargeted LC-MS^2 (Section 2.3.2) and the resulting files were processed using MZmine ion identity molecular networking in the GNPS environment, aided by SIRIUS (Dührkop et al. 2019b) and BUDDY (Xing et al. 2023) for prediction and annotation of compounds (Section 2.4).

Two LC-MS^2 datasets were used for the analysis in this study. The first one was generated as part of the work described in Chapter 3, where EtOAc extracts prepared from

YMS and mMYM ± 50 mM NAG plate cultures were subjected to untargeted LC-MS^2 . The second dataset was generated in the work described in this chapter using the EtOAc and MeOH extracts prepared from the M4, OBA, PMA, SA, SFM and YMS plate cultures.

When analyzing the first dataset, the number of unique features was found to be higher in media without NAG for both media types, suggesting a significant suppresive effect on specialized metabolites biosynthesis due to NAG, and mMYM showed more unique features when including both conditions (Fig. 4.14). For the second LC-MS^2 dataset, the number of unique features was found to be higher in the methanol extracts, and for both EtOAc and MeOH; the SA extracts had more unique features than the other media (Fig. 4.15). The hits to the GNPS library and the general networks are included in Appendix 3 (Tables S4.1-4.3 and Figures S4.4-4.6).

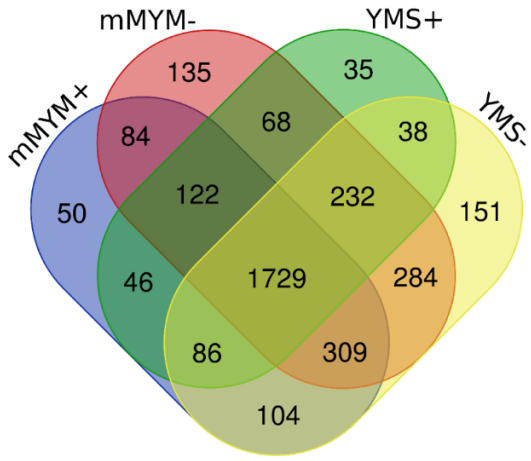

Figure 4.14. Venn diagram showing the number of shared features detected by the IIMN analysis for the first dataset. The comparison shows organic culture extracts from the mMYM and YMS plate cultures with (+) and without (-) NAG. The diagram was prepared using the precursor mass obtained from the quantification table after processing in the GNPS website.

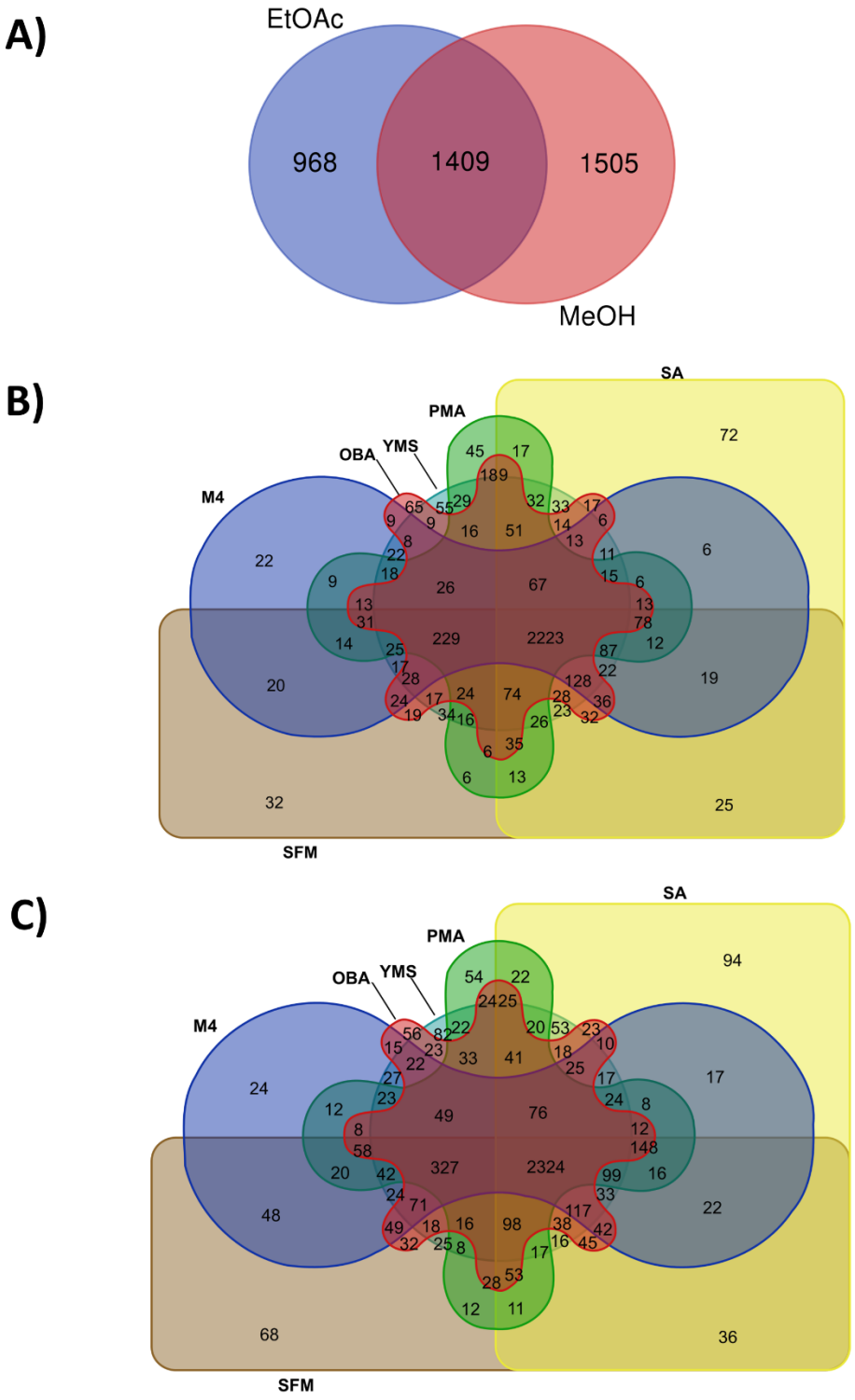

Figure 4.15. Venn diagrams showing the number of shared features detected by the IIMN analysis for the second dataset. The comparison was made by organic solvent (**A**) and by media for ethyl acetate (**B**) and methanol (**C**) extracts. The diagram was prepared using the precursor mass obtained from the quantification table after processing in the GNPS website.

Searching the datasets for known metabolites, the presence of three echosides was determined in the EtOAc extracts from different media only in the second dataset. Echoside C (**1**; *m*/*z* 453.1191, $[M-H]^-$) was detected in all of the EtOAc media extracts but the relative peak area in the PMA extract was greater than in the extracts from the other media (Fig. 4.16). Two other echosides, D and E (**2** and **3**; *m*/*z* 494.0914 $[M-H]^-$ and *m/z* 524.1019 $[M-H]^-$, respectively) were also predicted in the same network. The production of the different echosides is performed by the same BGC, therefore, it is expected to find them being coproduced (Deng et al. 2014). Other features in the same network include two matches to the GNPS library for the plant metabolites baicalin (**4**) and chrysin-7-O-glucoronide (**5**), and two more features annotated by SIRIUS and BUDDY with high confidence, the structures of which remains unclear. The echosides were not detected in the other extracts evaluated in this study. The fragmentation pattern comparison plots for echosides are shown in Fig. S4.7.

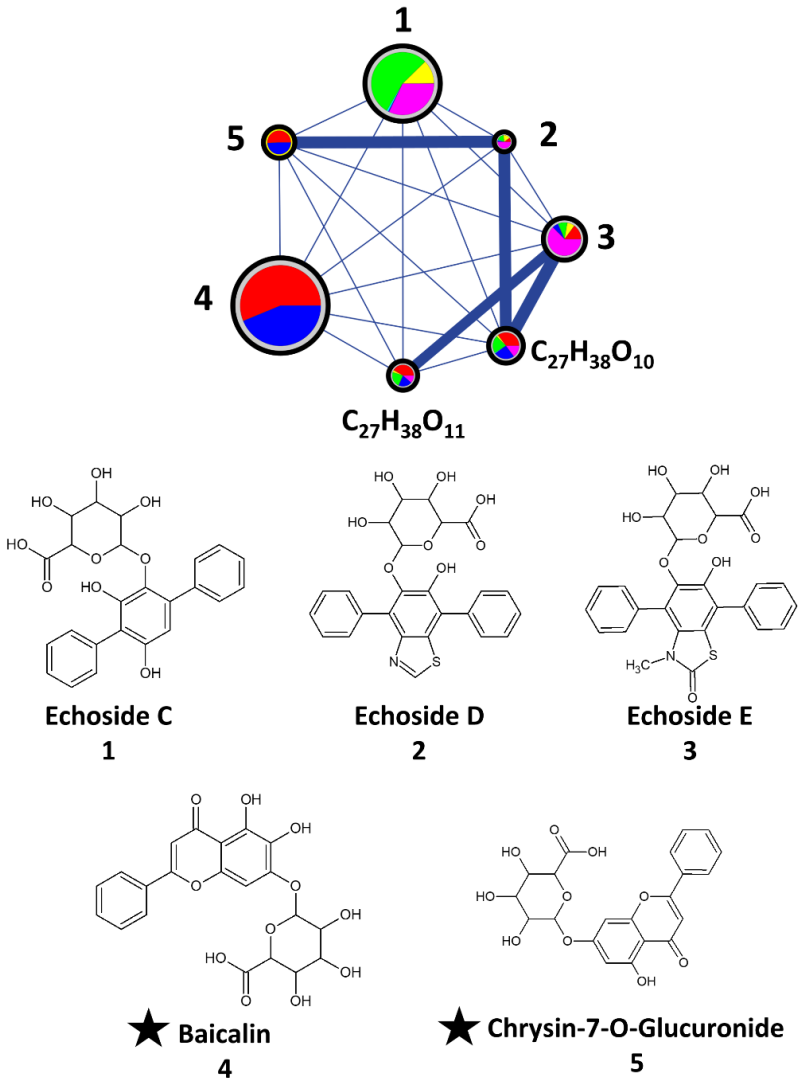

Figure 4.16. Echosides network obtained from untargeted LC-MS^2 of organic culture extracts after analysis using Ion Identity Molecular Networking. Each node in a network represents a metabolite. The ★ represent matches to the GNPS library. Nodes are linked by a similarity cosine score (>0.7), and the width thickness increases at higher values. The size of the nodes is relative to the sum of the peak areas for all media. The pie chart represents a relative distribution of the peak area for six different media: Red = M4, Yellow = OBA, Light green = PMA, Teal = SA, Blue = SFM, Violet = YMS.

Another compound that was predicted in the extracts is galbonolide B. In the first dataset, a feature predicted as galbonolide B (**6**) was detected in mMYM-NAG but not in mMYM+NAG (*m/z* 365.2315, $[M+H]^+$) (Fig. 4.17 and Fig. S4.8). In contrast, the same

feature appeared to be present in higher amounts in the YMS+NAG extract as compared to the YMS-NAG extract (Fig. 4.17A). Intriguingly, the node representing galbonolide B is linked to another feature (**7**) predicted to have a formula of $C_{23}H_{38}O_6$ (*m/z* 411.2728, $[M+H]^+$). To date, none of the known galbonolide analogues reported match this molecular formula (Zhang et al. 2016a), and the structure for this compound remains unknown. Both compounds were also detected in the EtOAc and MeOH extracts from the second dataset, and these networks also included other nodes (**8-11**) that represent potential intermediates or derived molecules (Fig. 4.17B and C).

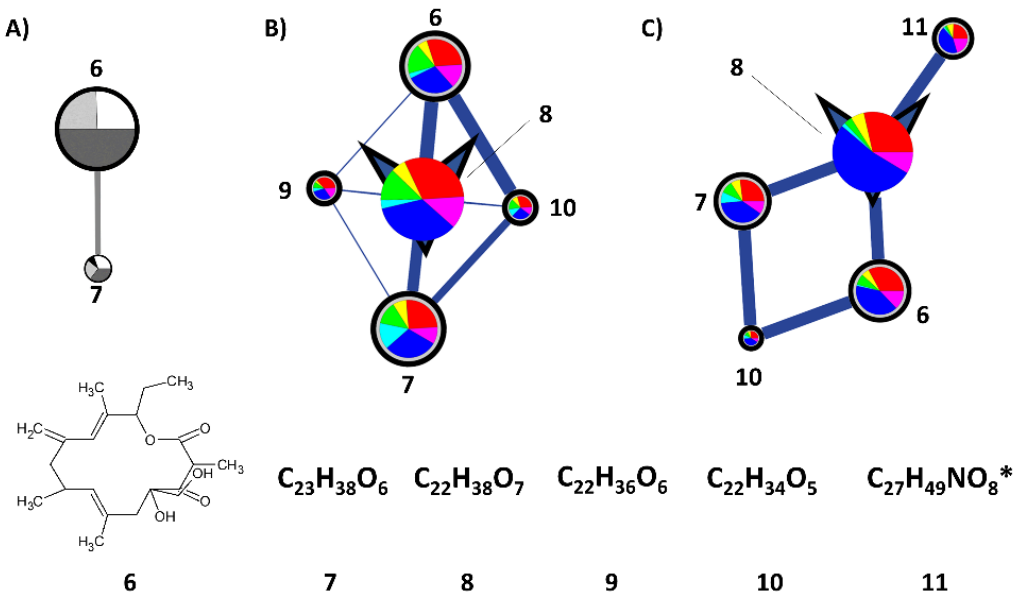

Figure 4.17. Galbonolide B (5) networks obtained from untargeted LC-MS^2 of organic culture extracts after analysis using Ion Identity Molecular Networking. The networks for media ± NAG (A), ethyl acetate (B) and methanol (C) extracts are shown. Each node in a network represents a metabolite and the number refers to the best prediction. Nodes are linked by a similarity cosine score (>0.7), and the width thickness increases at higher values. The size of the nodes is relative to the sum of the peak areas for all media in each network. An inverted triangle behind a node represents the combination of adducts into one node. The pie chart represents a relative distribution of the peak area for different media: white = mMYM-, black = mMYM+, light grey = YMS-, dark grey = YMS+, Red = M4, Yellow = OBA, Light green = PMA, Teal = SA, Blue = SFM, Violet = YMS. * = low confidence prediction.

Given the presence of a BGC with high similarity to the meridamycin BGC, the presence of this compound was also investigated (Fig. 4.18). A feature consistent with meridamycin (**12**; *m*/*z* 822.5375, $[M+H]^+$ and Fig. S4.9A) was predicted in the first dataset, and the addition of NAG drastically reduced the relative levels of the feature in YMS, while the levels in mMYM ± NAG remained very similar (Fig. 4.198A). The feature was also predicted in the EtOAc (820.5217, $[M-H]^-$) extracts from the second dataset (Fig. 4.18B). In this network, the meridamycin feature was linked to a second feature (*m/z* 866.5272, $[M-H]^-$) of larger peak area, which may be a new intermediate or derivative (Fig. 4.18B).

The analogue meridamycin A (**13**; *m*/*z* 838.5326, $[M-H]^-$ and Fig. S4.9B) was predicted in extracts from both datasets, but the relative amount varied depending on the medium. Notably, the feature was absent from the YMS-NAG extract (Fig. 4.18C), and the SA EtOAc and MeOH extracts recorded the lowest levels from the second dataset (Fig. 4.18D-E). Other nodes in the network are assumed to represent related compounds due to the similarity of their molecular formula and the high confidence prediction, but their structures remain unknown.

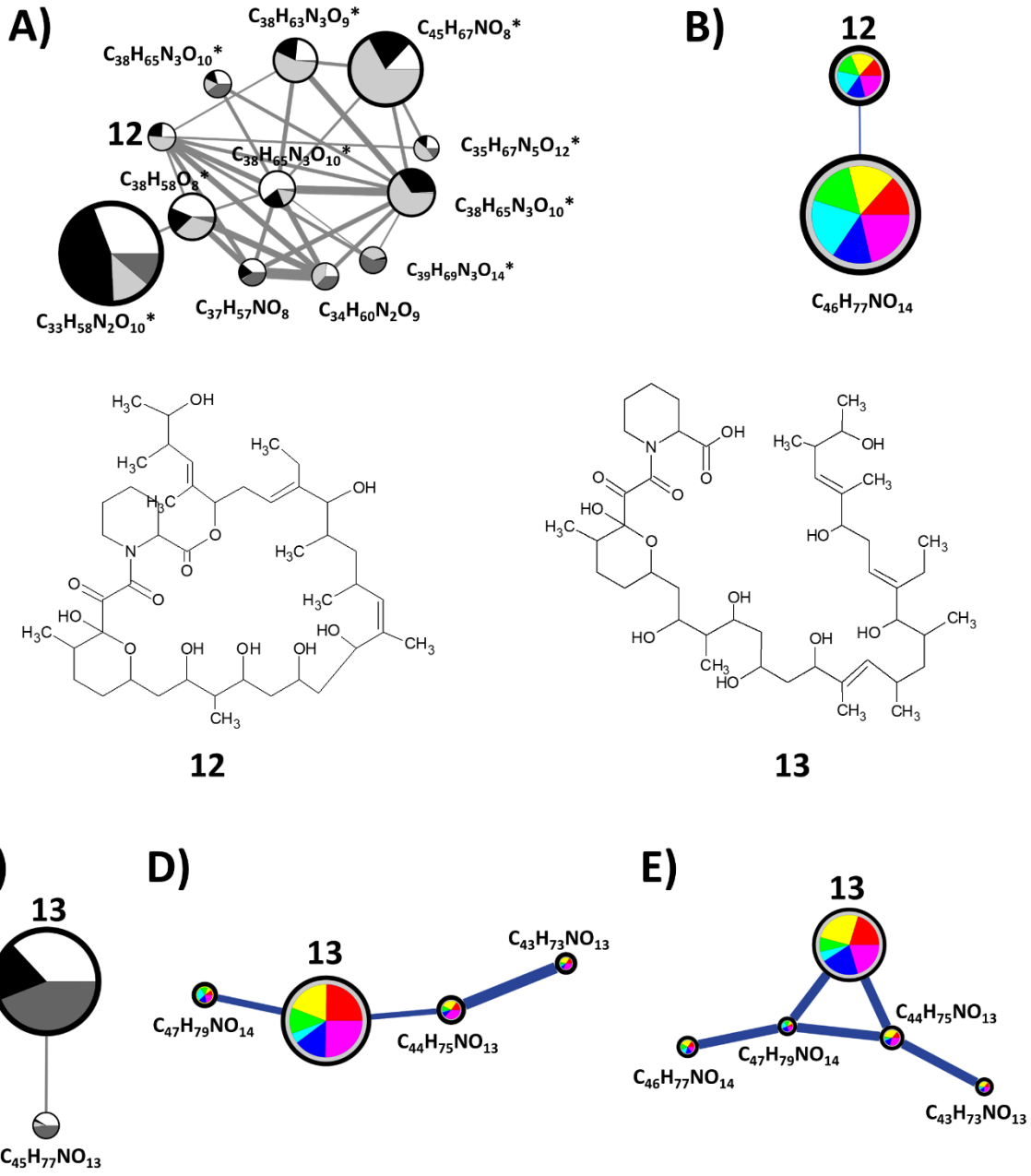

Figure 4.18. Meridamycin (12) and meridamycin A (13) networks obtained from untargeted LC-MS^2 of organic culture extracts after analysis using Ion Identity Molecular Networking. The networks for media ± NAG (A and C), ethyl acetate (B and D) and methanol (E) extracts are shown. The components of the networks are the same as described for Fig. 4.17.

Other compounds of interest are the niphimycins, which are macrolides with structural resemblance to azalomycins and guanidylfungins, all of which have antifungal activity (Ivanova et al. 1998; Usuki et al. 2006; Hu et al. 2018; Chen et al. 2022). The analysis of the different extracts (Fig. 4.19) identified a niphimycin-like compound that was a match to the GNPS library in the majority of the extracts (**14**; *m*/*z* 1130.7292, $[M+H]^+$; *m*/*z* 1128.7141, $[M-H]^-$). This compound is likely to be guanidylfungin A, a molecule with antimicrobial activity against fungi and Gram-positive bacteria and it is co-produced with guanidylfungin B (Takesako and Beppu 1984). Guanidylfungin B was also predicted to be present in some of the extracts, although with low confidence (**16**, $C_{57}H_{101}N_3O_{18}$).

In the first dataset, the production of guanidylfungins seemed to be reduced in the presence of NAG, based on the relative peak area (Fig. 4.19A and D). In the second dataset, extracts from PMA generally showed higher amounts, while the levels in SA were very low or completely absent. Notably, the compound was detected in both positive and negative ionization, although the molecular networking suggests that the positive ionization is capable of detecting more related molecules and, subsequently, creating larger networks (Fig. 4.19B-C and E-F).

To date, there is no BGC assigned specifically for the production of guanidylfungins in *Streptomyces*. Given the structural similarities between niphimycins and guanidylfungins, the cluster in region 48 (87% similarity to the niphimycins C-E cluster, Table 4.1) of the 11-1-2 genome is most likely responsible for the production of this compound.

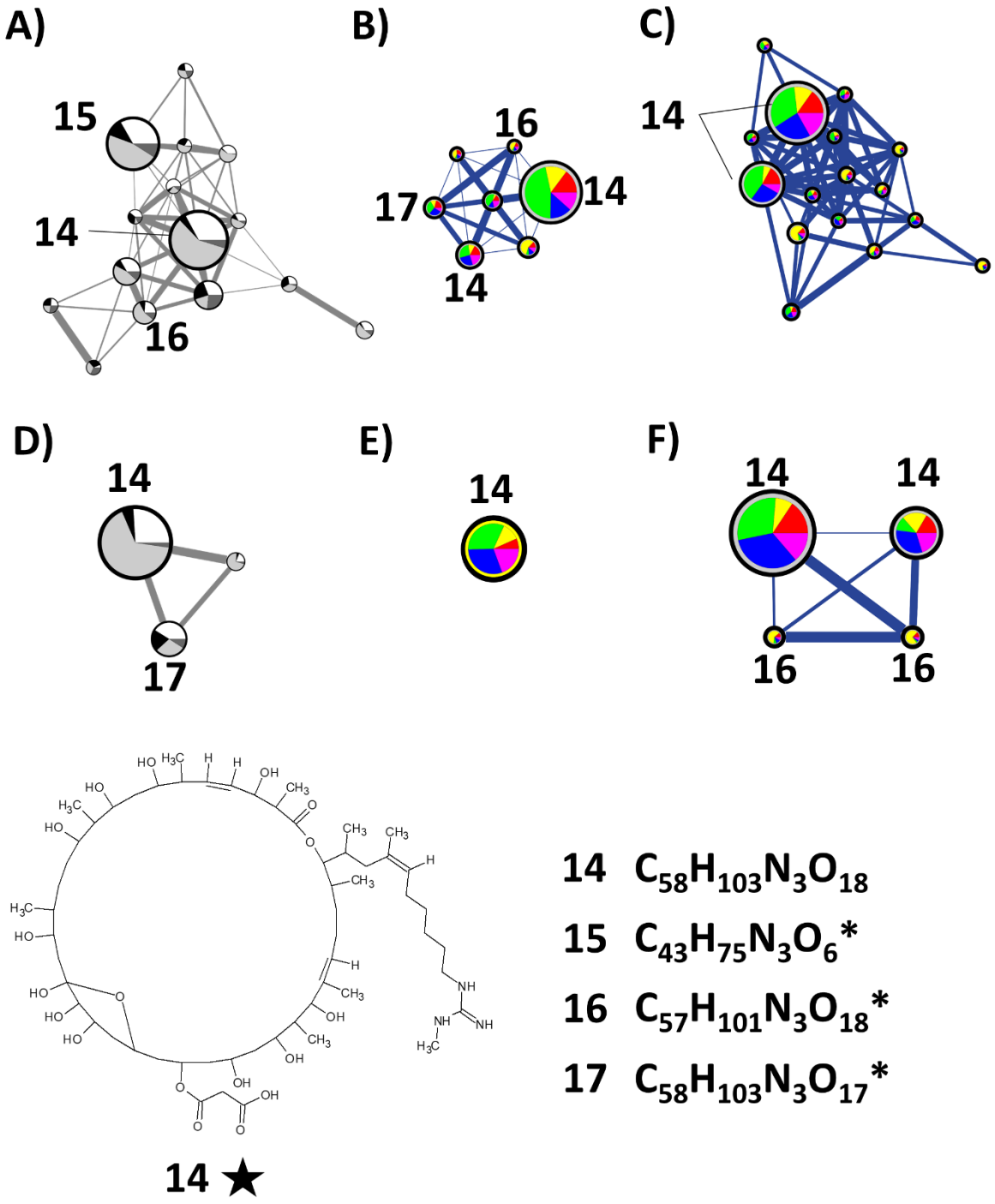

Figure 4.19. Guanidylfungin A (14) networks obtained from untargeted LC-MS^2 of organic culture extracts after analysis using Ion Identity Molecular Networking. The networks for media ± NAG (A and D), ethyl acetate (B and E) and methanol (C and F) extracts are shown. The ★ represent matches to the GNPS library. The components of the networks are the same as described for Fig. 4.17.

Elaiophylin is a macrolide with diverse bioactivities that is often co-produced with geldanamycin and nigericin, and several analogues have been identified from different *Streptomyces* strains of diverse origins, like efomycins and halichoblelides (Lee et al. 1996; Wu et al. 2013; Sheng et al. 2015; Han et al. 2016; Gui et al. 2019; Klassen et al. 2019). The production of elaiophylins and efomycins is likely performed by the same BGC, and some discrete differences may account for the production of the different analogues, as previously suggested (Klassen et al. 2019).

The organic extracts were analyzed for the presence of elaiophylin, and a feature consistent with this molecule was predicted from the analysis in negative mode (**18**; *m*/*z* 1023.5900, $[M-H]^-$ and Fig. S4.10A). The relative level of the feature was not affected by the presence of NAG in either mMYM and YMS (Fig. 4.20A), while the second dataset revealed a larger amount of the feature in the PMA extracts as compared to the other extracts (Fig. 4.20B and C). A number of related features were detected in each case, most notably, efomycin G (**19**; *m*/*z* 1009.5739, $[M-H]^-$ and Fig. S4.10B), which possesses antimicrobial activity against Gram-positive bacteria (Supong et al. 2016; Gui et al. 2019). Intriguingly, other features predicted with high confidence in these networks do not match the known elaiophylin analogues (**20-23**), which suggests the possible presence of novel elaiophylin derivatives being produced by 11-1-2.

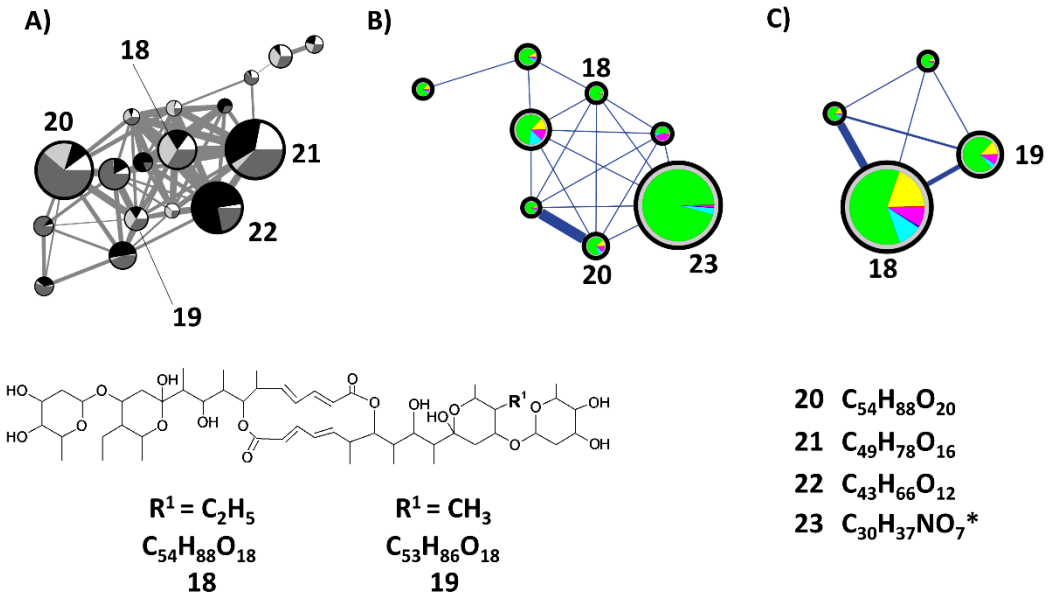

Figure 4.20. Elaiophylin (18) networks obtained from untargeted LC-MS^2 of organic culture extracts after analysis using Ion Identity Molecular Networking. The networks for media ± NAG (A), ethyl acetate (B) and methanol (C) extracts are shown. The components of the networks are the same as described for Fig. 4.17.

A feature in the EtOAc extracts from the second dataset matched with 12-hydroxyjasmonic acid (**24**, *m/z* 227.1280 $[M+H]^+$) in the GNPS library (Fig. 4.21). However, the same match did not occur in the methanol extracts or the first dataset. Instead, the feature was predicted by BUDDY and SIRIUS with high confidence. The extracts from mMYM- had the largest peak area in the first dataset for **24**, while M4 showed larger peak areas in the second dataset.

Notably, tuberonic acid, a compound that promotes the tuberization in potato plants, is often referred to as a synonym of 12-hydroxyjasmonic acid due to their structural similarity, but they are separate isomers (Miyawaki et al. 2021). It has been reported that 12-hydroxyjasmonic acid can be bioconverted from jasmonic acid by the fungal pathogen *Magnaporthe oryzae* as a method to evade host defences and enhance pathogenicity after

tissue penetration (Patkar et al. 2015). With the current data, it is not possible to conclude that 11-1-2 is capable of producing 12-hydroxyjasmonic acid, and what role it may have in the pathogenicity of the strain. Thus, further research is required to confirm the presence of the compound and elucidate the biosynthesis pathway.

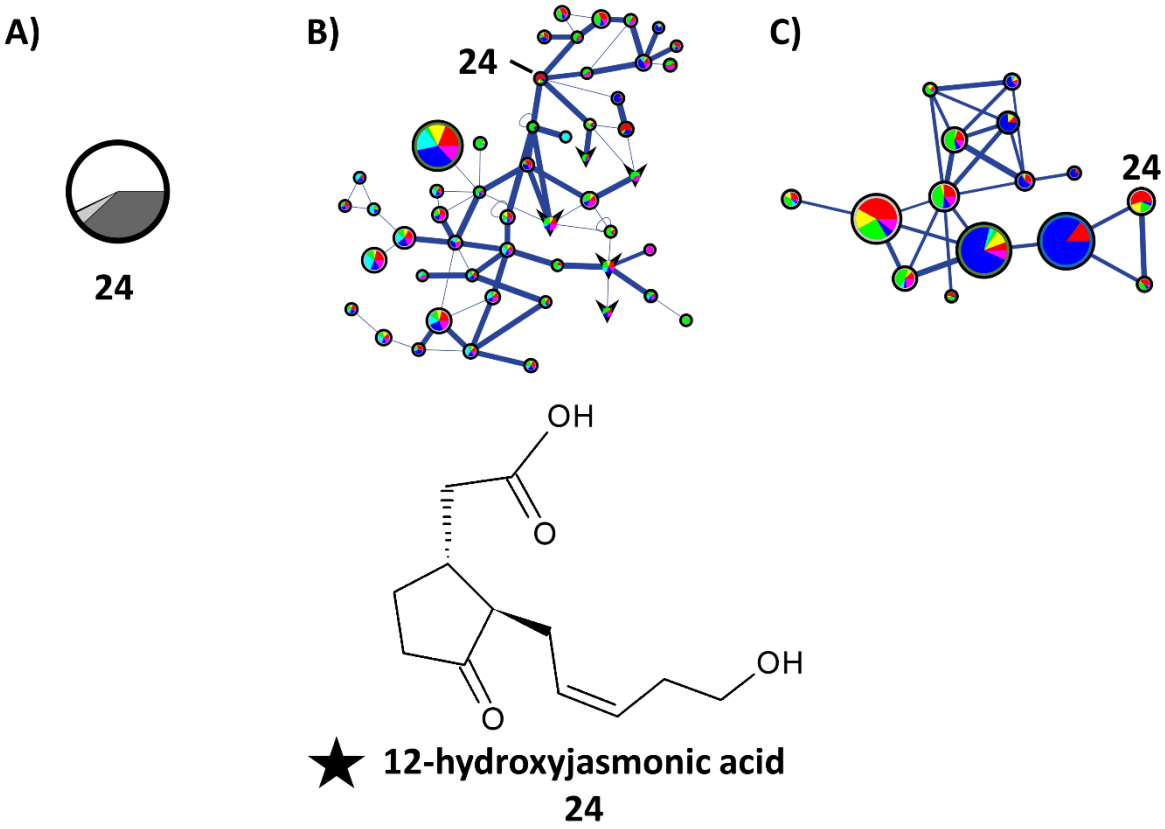

Figure 4.21. 12-hydroxyjasmonic acid (24) networks obtained from untargeted LC-MS^2 of organic culture extracts after analysis using Ion Identity Molecular Networking. The networks for media ± NAG (A), ethyl acetate (B) and methanol (C) extracts are shown. The components of the networks are the same as described for Fig. 4.17.

A prominent feature found in all datasets (Fig. 4.22) was predicted to be musacin D (**25**, *m*/*z* 155.0706 $[M+H]^+$ and Fig. S4.11). The extracts from YMS+ had the largest peak area in the first dataset for **25** (Fig. 4.22A), while PMA and YMS showed larger peak areas in the second dataset for both EtOAc and MeOH extracts (Fig. 4.22B and C).

Musacin D is part of several musacins first detected in *Streptomyces griseoviridis*, all of which were initially reported as having no significant bioactivity (Burkhardt et al. 1996; Schneider et al. 1996). Later, it was determined that the plant pathogen *Nigrospora sacchari* produces a phytotoxic compound with identical structure to musacin D except for a different stereochemical configuration of the hydroxy group in carbon number five (Fukushima et al. 1998). The stereochemichal configuration of many compounds affect their bioactivity to different levels, as previously reviewed (Evidente et al. 2013). With the current information, it is not possible to conclude if the feature predicted as musacin D has a role in the phytotoxicity of the extracts, or if its identity truly corresponds to musacin D or the phytotoxin from *N. sacchari*. Further purification and characterization of the feature is necessary to establish its significance for the pathogenic phenotype of 11-1-2.

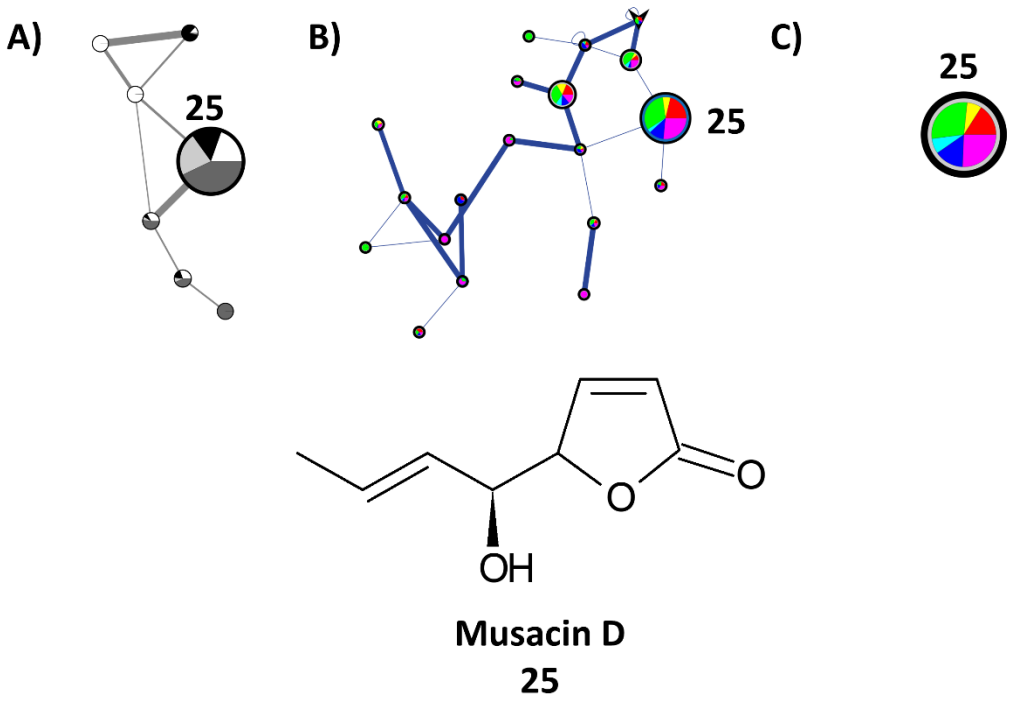

Figure 4.22. Musacin D (25) networks obtained from untargeted LC-MS^2 of organic culture extracts after analysis using Ion Identity Molecular Networking. The networks for media ± NAG (A), ethyl acetate (B) and methanol (C) extracts are shown. The components of the networks are the same as described for Fig. 4.17.

Other features of interest in the organic extracts include three molecules of unknown structure with relative large peak areas (Fig. 4.23), which are predicted to have the formulas $C_{27}H_{33}NO_6$ (**26**, *m/z* 468.2376 $[M+H]^+$), $C_{27}H_{33}NO_7$ (**27**, *m/z* 484.2324 $[M+H]^+$) and $C_{27}H_{37}NO_6$ (**28**, *m/z* 472.2671 $[M+H]^+$). While the first compound is common across all the extracts, the second compound is only present in the media ± NAG, which could be due to its solubility in the resuspension solvent during the metabolite extraction process. Moreover, the molecular networking analysis revealed a number of related nodes. However, the current data does not allow a conclusive identity for these compounds to be determined, thus, more detailed work is required.

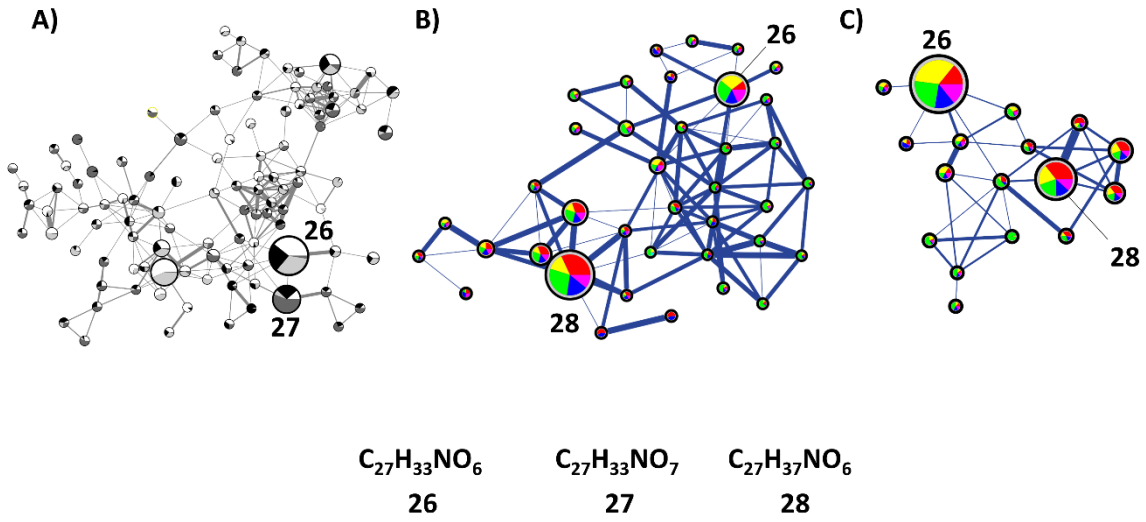

Figure 4.23. Molecular networks of three unknown compounds obtained from untargeted LC-MS^2 of organic culture extracts after analysis using Ion Identity Molecular Networking. The networks for media ± NAG (A), ethyl acetate (B) and methanol (C) extracts are shown. The components of the networks are the same as described for Fig. 4.17.

4.3.4 Culture media composition affects the production of different specialized metabolites of interest

In the previous study (see Chapter 3), geldanamycin and nigericin were shown to be produced by 11-1-2 in both mMYM and YMS, and the presence of NAG in the culture media had a suppressive effect on the production of both metabolites. Features consistent with these molecules were also identified in the untargeted metabolomics analysis conducted in the current study (Tables S4.2 and S4.3), and targeted detection and quantification was conducted in order to confirm the presence of the metabolites and to compare their relative levels in the different culture extracts (Fig. S4.12).

The analysis revealed that in all of the culture media tested, the nigericin production levels were significantly greater than that of geldanamycin (Table 4.2), and this is consistent with what was observed in the previous study for the YMS and mMYM media (Table 3.2).

When comparing the metabolite levels in the extracts prepared using the two different organic solvents, both compounds were detected in both sets of extracts, but the EtOAc extracts contained higher amounts of both compounds than the MeOH extracts. Looking at the levels of each compound produced in the different media, PMA was found to contain high amounts of both compounds, while the SA medium generally contained lower concentrations of each (Table 4.2).

Table 4.2. Nigericin, geldanamycin and elaiophylin quantification in different organic culture extracts.

Extraction solvent	Culture medium	Nigericin[1] (mM)	Geldanamycin[1] (mM)	Elaiophylin[1] (mM)
Ethyl acetate	M4	6.931 ± 0.549	0.191 ± 0.019	0.001 ± 0.000
	OBA	0.824 ± 0.280	0.219 ± 0.020	0.023 ± 0.007
	PMA	9.441 ± 2.258	0.506 ± 0.036	1.212 ± 0.111
	SA	1.579 ± 0.172	0.011 ± 0.001	0.021 ± 0.008
	SFM	4.532 ± 0.366	0.149 ± 0.020	N.D.[2]
	YMS	8.479 ± 0.663	0.154 ± 0.013	0.018 ± 0.004
Methanol	M4	2.927 ± 0.499	0.032 ± 0.040	0.001 ± 0.000
	OBA	0.983 ± 0.427	0.149 ± 0.094	0.033 ± 0.012
	PMA	3.793 ± 2.323	0.180 ± 0.042	0.271 ± 0.044
	SA	0.996 ± 0.227	0.002 ± 0.002	0.007 ± 0.002
	SFM	1.418 ± 0.326	0.052 ± 0.023	0.001 ± 0.001
	YMS	4.098 ± 0.890	0.055 ± 0.008	0.010 ± 0.004

[1] The values shown correspond to the average of three replicates ± one standard deviation.
[2] Not detected.

Elaiophylin is often co-produced with geldanamycin and nigericin, and the untargeted LC-MS^2 analysis predicted its presence in the organic extracts from 11-1-2 (Fig. 4.20). Although it is a known metabolite with some antimicrobial activity, its structural similarity with concanamycin A, a known phytotoxin from *S. scabiei* (Natsume et al. 2017; Li et al. 2019c), made it an interesting target to study its bioactivity against plants. First, to confirm the prediction from the molecular networking analysis, the MeOH and EtOAc organic

extracts prepared from the six different media were analyzed for the presence of elaiophylin using HPLC with an authentic elaiophylin standard. A peak with the identical retention time and absorbance spectrum as the standard was detected in both the EtOAc and MeOH extracts (Fig. S4.12 and S4.13). When comparing the relative amount of the compound in the different media, the levels were highest in the PMA extracts, in accordance with the untargeted LC-MS^2 data (Fig. 4.20B and C), while no elaiophylin was detected in the EtOAc extracts of SFM. When compared to nigericin and geldanamycin, the elaiophylin levels were lower in all of the media with the exception of PMA, where they exceeded the geldanamycin production levels (Table 4.2).

To determine whether elaiophylin exhibits any bioactivity against plants, a potato tuber slice bioassay was conducted using different concentrations of the pure standard. Figure 4.24 shows that 10 nmol of elaiophylin caused some minor necrosis and pitting to the tissue; the damage was more severe when the concentration of the compound was increased and resembled the effects of geldanamycin. The combination of elaiophylin with geldanamycin or nigericin increased the severity of the damage caused by each compound independently, especially the nigericin. As with geldanamycin and nigericin, the effects of elaiophylin were distinct from the damage caused by the thaxtomin A phytotoxin at the same concentrations (Fig. 4.24).

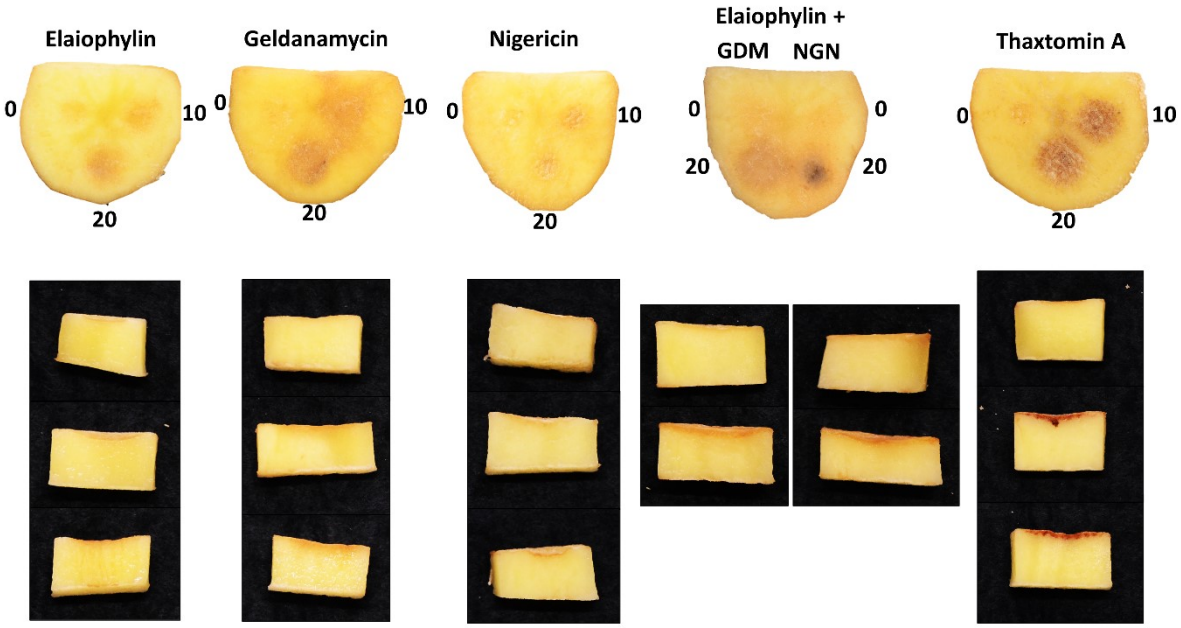

Figure 4.24. Top and side view of potato tuber slice assay treated with pure compounds. Each tuber slice contained disks inoculated with 0 (control), 10, and 20 nmol of the respective compound in a fixed volume of 20 µL. For the combination of elaiophylin with geldanamycin or nigericin, each compound provided half of the amount reported, i.e., 20 nmol had 10 nmol of each compound. The assay was performed twice with three biological replicates per treatment in each assay, with similar results obtained each time.

The bioactivity of elaiophylin was also tested against radish seedlings alongside geldanamycin, nigericin and thaxtomin A (Fig. 4.25). The shoot length was generally increased in the presence of elaiophylin as compared to the control plants, while the other compounds seemed to have more of an effect on shoot development (Fig. 4.26, top panel). In contrast, the root length was reduced in presence of higher concentrations of elaiophylin when compared to the DMSO-treated control plant, though the results were not statistically significant (Fig. 4.26, middle panel). The combination of elaiophylin with geldanamycin or nigericin did not affect the root length when compared to the same concentrations of each compound separately. For the total length, the treatments had the same trend as the root length values (Fig. 4.26, bottom panel).

Figure 4.25. Representative radish seedlings treated with different pure compounds. The photos were taken after five days of incubation.

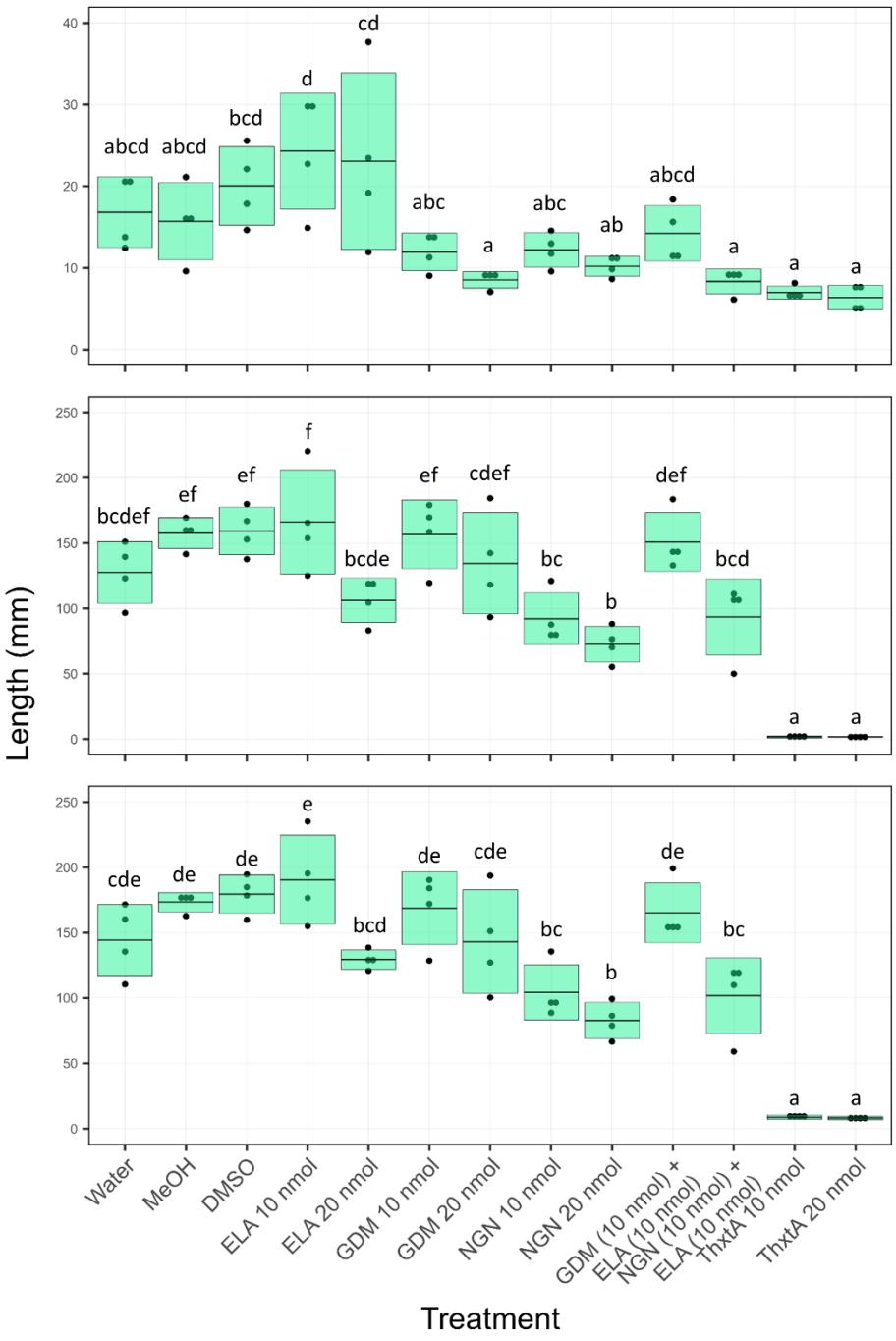

Figure 4.26. Effect of different pure compounds on radish seedlings. Elaiophylin (ELA), geldanamycin (GDM), nigericin (NGN) and thaxtomin A (ThxtA) were tested for their effects on shoot (top), root (middle) and total length (bottom) of radish seedlings. Seedlings were treated with 10 or 20 nmol of each compound, or a combination of 10 nmol of each compound. Each box represents the average of the measurement ± standard deviation. The data was analyzed using an ANOVA with Tukey's test. Values with different letters are statistically different ($P < 0.05$).

The development of lateral roots on the radish seedling was also evaluated following treatment with the pure compounds. The addition of elaiophylin did not have a negative impact on this variable, but it slightly improved the number of roots when combined with geldanamycin (Fig. 4.27 and 4.28). Interestingly, the use of nigericin alone or in combination caused a clear reduction in the number of lateral roots/cm of root length, an effect also seen with some organic extracts (Fig. 4.13); however, low numbers of lateral roots/cm were also obtained with organic extracts containing much lower amounts of nigericin (e.g. SA-E), which may be due to the presence of another compound with similar effects. This role of nigericin and other compounds in lateral root development requires further investigation.

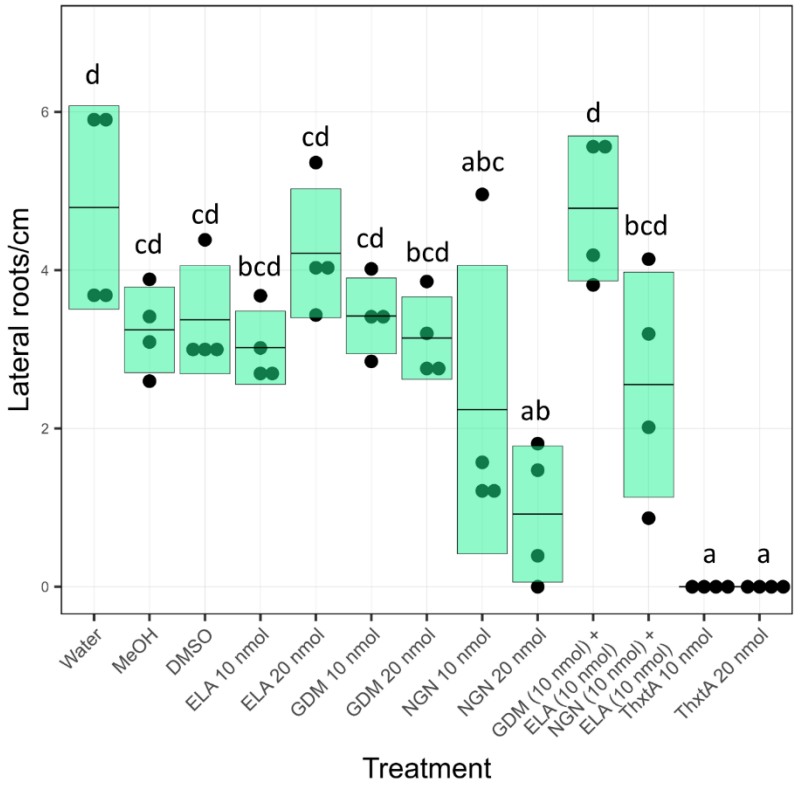

Figure 4.27. Effect of different compounds on the number of lateral roots/cm of root length in radish seedlings. Elaiophylin (ELA), geldanamycin (GDM), nigericin (NGN) and thaxtomin A (ThxtA) were tested. Each box represents the average of the measurement ± standard deviation. The data was analyzed using an ANOVA with Tukey's test. Values with different letter are statistically different ($P < 0.05$)

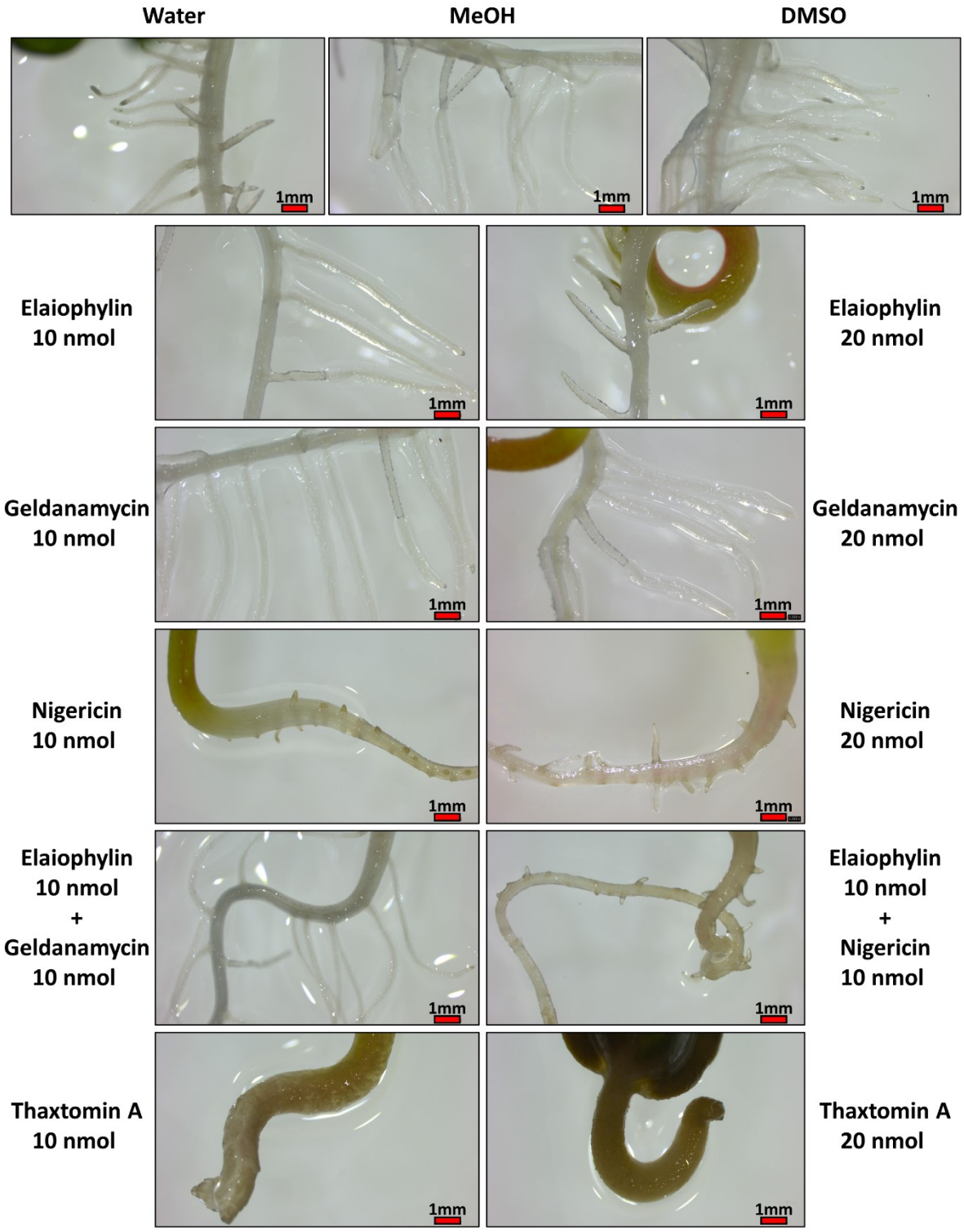

Figure 4.28. Effect of elaiophylin (ELA), geldanamycin (GDM), nigericin (NGN) and thaxtomin A (ThxtA) on the lateral roots of radish seedlings. A 1-mm scale bar is located in the lower right corner of each photo.

The quantification and bioactivity of echoside C was also investigated in this study. An RP-HPLC method was tested using an echoside C commercial standard (Section 2.3.3.4); however, the metabolite could not be detected in the extracts using this method. More work is required to find the suitable conditions for the targeted detection and quantification of this molecule.

The bioactivity of this compound was evaluated using plant bioassays. The potato tuber slice assay did not show any pitting, necrosis, oxidation, or any other symptoms associated with phytotoxic activity at the concentrations tested (Fig. S4.14). When evaluated using radish seedlings, the molecule did not exhibit any significant effect compared to the water and solvent controls (Fig. S4.15-S4.17). Given the structural similarity of echoside C with the auxin-signaling inhibitor terfestatin A, including the active core that is involved in this activity (Hayashi et al. 2008), it was considered a metabolite of interest that may contribute to the pathogenic phenotype of 11-1-2. However, under the conditions of this work, echoside C showed no phytotoxic activity, and its role in plant-pathogen interactions remains unclear.

4.4 Conclusions

This study provides new insights into the specialized metabolome of the novel plant pathogenic *Streptomyces* sp. 11-1-2. Genomic analyses revealed that 11-1-2 has the potential to produce at least 51 different specialized metabolites, and bioassays conducted using agar cores and extracts from 11-1-2 plate cultures demonstrated that the organism can produce compounds with inhibitory activity against Gram-positive bacteria (including other *Streptomyces* spp.), fungi and plants. Of the different culture media used in this study, PMA was the best supporting the production of the phytotoxic compounds geldanamycin and

nigericin, and agar cores and extracts from this medium were very bioactive in all the assays performed. Considering that 11-1-2 was originally isolated from a CS-diseased potato tuber, it is likely that the strain has adapted its metabolism to enable colonization of the nutrient-dense tuber tissues, thereby providing a selective advantage over other microbes in the soil environment.

The untargeted LC-MS^2 and molecular networking analysis suggests that 11-1-2 produces many known specialized metabolites and closely related compounds with unknown structure and bioactivity. The identification of guanidylfungin A, an antifungal compound, suggests that this compound is at least partially responsible for the activity seen against *S. cerevisiae*. However, the absence of antifungal activity in the OBA EtOAc extract contradicts this, as guanidylfungin A was detected in this extract. Targeted detection and quantification of this compound in the different extracts is therefore necessary to further investigate the contribution of the metabolite to the observed antifungal activity.

It is noteworthy that some prominent compounds in the organic culture extracts could not be identified, and their role in the plant pathogenic and/or antimicrobial phenotype remains unknown. Furthermore, the metabolites expected from some BGCs were not detected in this study, suggesting that the conditions used do not promote their biosynthesis, or that other strategies are required to recover them during the extraction process.

This study additionally showed that elaiophylin is produced by 11-1-2, and it has some phytotoxicity against potato tuber tissue, though not as much as the other phytotoxins tested. Importantly, elaiophylin appeared to enhance the tuber tissue damage caused by geldanamycin and nigericin, suggesting that it exhibits synergistic effects with these compounds. The elaiophylin precursors pteridic acids A and B, and related pteridic acids H

and F have been tested in plants and show protective effects against abiotic stress and auxin-like effects (Igarashi et al. 2002; Yang et al. 2022) but the effects of elaiophylin had not been previously evaluated in plant bioassays until now.

Another known effect of elaiophylin is enhancing the antifungal activity of rapamycin (Fang et al. 2000), and it has good antibacterial activity against Gram-positive bacteria along with efomycin G, which was also predicted to be present in the organic extracts (Wu et al. 2013). Thus, it is possible that elaiophylin and related molecules contributed to the antimicrobial activity recorded in this study.

An interesting result from this study was the observation that nigericin is able to cause a reduction in lateral root development, an effect not previously recorded for this compound. The mechanism for how this occurs remains unclear and warrants further investigation. Considering that the nigericin concentrations were much higher than other compounds in the tested extracts, this compound likely plays a major role in the phytotoxic phenotype of the 11-1-2 strain. It is notable, however, that the SA EtOAc extract contained low nigericin amounts and yet caused a considerable reduction in lateral root development of the radish seedings, whereas the M4 EtOAc extract had significantly higher levels of nigericin but was not as effective in reducing lateral root development. This suggests that at least one other compound with inhibitory activity against lateral root development may be produced by the 11-1-2 strain, an idea that should be further explored.

Overall, 11-1-2 produces an array of specialized metabolites and their biosynthesis is affected by the composition of the culture media. Some of the metabolites detected and predicted in the organic extracts, like geldanamycin, nigericin and elaiophylin, are likely to be involved in mediating plant-pathogen interactions, while other like guanidylfungin A are

probably involved in microbe-microbe interactions. This study will also serve as the basis for further research in the elucidation of novel phytotoxins, as it is the first metabolome analysis of a non-thaxtomin producing plant pathogenic *Streptomyces*.

APPENDIX 3.

Supplementary tables

Table S4.1. Hits to the GNPS library for the first dataset (media ± NAG, IIMN 6.2).

SpectrumID	Compound_Name	Adduct	Precursor_MZ	Cosine_score	RT_Query	LibMZ
CCMSLIB00006707365	1-({[2-(2-furylmethyl)-5-methylpyrrolidinyl]amino}methylene)-7-[8-({[2-(2-furylmethyl)pyrrolidinyl]amino}methylene)-1,6-dihydroxy-3-methyl-5-(methylethyl)-7 -oxo(2-naphthyl)]-3,8-dihydroxy-6-methyl-4-(methylethyl)naphthalen-2-one	M+2H]	415.212	0.99282	670.093	415.212
CCMSLIB00005466072	16-hydroxypalmitic acid	M-H	271.227	0.704737	738.073	271.227
CCMSLIB00004708392	3-[3-[3,4-dihydroxy-5-(6-oxo-3H-purin-9-yl)oxolan-2-yl]propanoyl]benzoic acid	[M+H]+	415.125	0.923941	509.639	415.125
CCMSLIB00004714368	3-oxo-3-[[(10E,20E)-5,7,9,19,23,25,27,31,33,34,35-undecahydroxy-8,10,14,18,22,26,30-heptamethyl-15-[(Z)-4-methyl-10-[(N'-methylcarbamimidoyl)amino]dec-4-en-2-yl]-17-oxo-16,37-dioxabicyclo[31.3.1]heptatriaconta-10,20-dien-3-yl]oxy]propanoic acid	[M-H]-	1128.72	0.848826	559.02	1128.72
CCMSLIB00004714381	3-oxo-3-[[(10E,20E)-5,7,9,19,23,25,27,31,33,34,35-undecahydroxy-8,10,14,18,22,26,30-heptamethyl-15-[(Z)-4-methyl-10-[(N'-methylcarbamimidoyl)amino]dec-4-en-2-yl]-17-oxo-16,37-dioxabicyclo[31.3.1]heptatriaconta-10,20-dien-3-yl]oxy]propanoic acid	[M+H]+	1130.73	0.768016	564.913	1130.73
CCMSLIB00006704450	3-phenyl-2-pyrrolylpropanoic acid	M+H	216.102	0.960239	675.787	216.102
CCMSLIB00006679090	4-HYDROXYPHENYL ACETIC ACID	M-H	151.04	0.971207	513.028	151.04
CCMSLIB00006704816	6-Gingerol	M-H	293.176	0.928866	647.313	293.176
CCMSLIB00006708625	7,2'-DIHYDROXYFLAVONE	M-H	253.051	0.829595	948.953	253.051
CCMSLIB00006697418	AC1L1X1Z	M+Na	637.302	0.928117	810.938	637.302
CCMSLIB00005724311	Andrachcinidine	M+H	228.196	0.990965	599.521	228.196
CCMSLIB00005724311	Andrachcinidine	M+H	228.196	0.929429	532.826	228.196
CCMSLIB00006708720	aphidicolin	M+H-H2O	321.242	0.708142	591.551	321.242

CCMSLIB00006701464	azelaic acid	M-H	187.098	0.938872	542.64	187.098
CCMSLIB00005463949	BETAINE	2M+Na	257.147	0.984108	67.494	257.147
CCMSLIB00005724304	Bisucaberin	M+H	401.239	0.906606	512.313	401.239
CCMSLIB00005724300	Bottromycin A2 Acid	M+H	809.434	0.970977	522.477	809.434
CCMSLIB00005724283	C-14 dehydrated analogs of thaxtomin A	M+H	421.151	0.975839	566.233	421.151
CCMSLIB00005724290	C-7-methyl substituted CFA-Ile	M+H	308.189	0.983625	621.692	308.189
CCMSLIB00005723293	CFA-L-isoleucine	M+H	320.186	0.948777	946	320.186
CCMSLIB00005724296	Concanamycin A	M+Na	888.507	0.97998	778.911	888.507
CCMSLIB00005724295	Concanamycin B	M+Na	874.491	0.973976	732.967	874.491
CCMSLIB00005723292	Concanamycin B	M+Na	874.491	0.862875	675.752	874.491
CCMSLIB00000007069	cyclo(D-Trp-L-Pro)	M+Na	284.139	0.944738	527.763	284.139
CCMSLIB00000007069	cyclo(D-Trp-L-Pro)	M+Na	284.139	0.933101	541.665	284.139
CCMSLIB00000081186	cyclo-(Leu-Leu)	M+H	227.174	0.784057	562.216	227.174
CCMSLIB00000007136	cyclo(L-Phe-D-Pro)	M+H	245.128	0.945052	521.974	245.128
CCMSLIB00000007135	cyclo(L-Phe-D-Pro)	M+H	245.128	0.761459	535.796	245.128
CCMSLIB00000007146	cyclo(L-Val-L-Pro)	M+H	197.129	0.946655	485.46	197.129
CCMSLIB00000007145	cyclo(L-Val-L-Pro)	M+H	197.129	0.860576	490.158	197.129
CCMSLIB00000007145	cyclo(L-Val-L-Pro)	M+H	197.129	0.828	943.586	197.129
CCMSLIB00000007063	cyclo(Phe-Leu)	M+H	261.159	0.826311	567.114	261.159
CCMSLIB00000007063	cyclo(Phe-Leu)	M+H	261.159	0.826311	566.544	261.159
CCMSLIB00006706712	Cyclopiazonic acid///alpha-cyclopiazonic acid	M+H	337.155	0.959902	752.038	337.155
CCMSLIB00006706713	Cyclopiazonic acid///alpha-cyclopiazonic acid	M-H	335.14	0.93366	748.907	335.14
CCMSLIB00006701569	daidzein	M-H	253.051	0.993975	568.807	253.051
CCMSLIB00006552895	Daidzein	[M+H]+	255.07	0.951733	568.682	255.07
CCMSLIB00006694440	Daidzin	M+H	417.118	0.965919	507.14	417.118
CCMSLIB00005724303	Desferrioxamine E	M+H	601.353	0.984528	509.751	601.353
CCMSLIB00005723980	Geldanamycin	M-H	559.266	0.960421	673.035	559.266
CCMSLIB00005723980	Geldanamycin	M-H	559.266	0.960421	671.209	559.266

CCMSLIB00005723980	Geldanamycin	M-H	559.266	0.757534	577.202	559.266
CCMSLIB00004704403	Genistein	[M-H]-	269.046	0.930811	598.335	269.046
CCMSLIB00006417999	Glycitein	[M+H]+	285.076	0.938942	571.848	285.076
CCMSLIB00004694138	HYDROQUINIDINE	[M-H]-	325.192	0.765848	812.843	325.192
CCMSLIB00006679025	INDOLELACTIC ACID	M-H	204.067	0.86588	562.771	204.067
CCMSLIB00004680136	Loliolide	M+H	197.117	0.757889	545.549	197.117
CCMSLIB00006700055	lumichrome	M+H	243.088	0.981036	546.014	243.088
CCMSLIB00006678147	Lyso PC (16:1)	M+H	494.324	0.913091	714.123	494.324
CCMSLIB00004691207	maltotriose	[M+Na]+	527.158	0.878666	71.858	527.158
CCMSLIB00005884958	MANNITOL - 40.0 eV	M+H	183.086	0.815968	945.169	183.086
CCMSLIB00005734817	Massbank:EQ368253 Nigericin|2-{6-[(2-{5`-[6-hydroxy-6-(hydroxymethyl)-3,5-dimethyltetrahydro-2h-pyran-2-yl]-2,3`-dimethyloctahydro-2,2`-bifuran-5-yl}-9-methoxy-2,4,10-trimethyl-1,6-dioxaspiro[4.5]dec-7-yl)methyl]-3-met	M-H	723.469	0.907685	820.892	723.469
CCMSLIB00005766542	Massbank:LU130903 Sulfamethazine|4-amino-N-(4,6-dimethylpyrimidin-2-yl)benzenesulfonamide	M+H	279.091	0.772281	84.307	279.091
CCMSLIB00005746967	Massbank:PR309108 FA 18:1+3O	M-H	329.231	0.870342	595.319	329.231
CCMSLIB00005747189	Massbank:PR310844 LPC 18:2	M+H	520.341	0.821921	737	520.341
CCMSLIB00005739084	Massbank:PR311142 Cyclo(leucylprolyl)	M+H	211.144	0.943615	521.647	211.144
CCMSLIB00005738467	Massbank:RP030602 N6-Isopentenyladenosine|Riboprine|(2R,3S,4R,5R)-2-(hydroxymethyl)-5-[6-(3-methylbut-2-enylamino)purin-9-yl]oxolane-3,4-diol	M+H	336.167	0.868199	519.092	336.167
CCMSLIB00005726877	Massbank:UA005501 L-Phenylalanine|(2S)-2-Azaniumyl-3-phenylpropanoate	M+H	166.086	0.977041	558.595	166.086
CCMSLIB00005726877	Massbank:UA005501 L-Phenylalanine|(2S)-2-Azaniumyl-3-phenylpropanoate	M+H	166.086	0.959742	543.187	166.086
CCMSLIB00005726623	Massbank:UF416201 Genistein|5,7-Dihydroxy-3-(4-hydroxyphenyl)chromen-4-one	M+H	271.06	0.940468	597.505	271.06
CCMSLIB00005883731	METHYLTHIOADENOSINE - 30.0 eV	M+H	298.097	0.892919	458.923	298.097

CCMSLIB00000424739	MS_Contaminant_Sodium_Formate_Cluster	M+H	838.835	0.754169	56.589	838.835
CCMSLIB00006679916	N-ACETYLMURAMIC ACID	M+H	294.118	0.972449	208.848	294.118
CCMSLIB00006679916	N-ACETYLMURAMIC ACID	M+H	294.118	0.910894	161.395	294.118
CCMSLIB00006679116	N-ACETYL-PHENYLALANINE	M-H	206.082	0.93142	558.866	206.082
CCMSLIB00000851993	NCGC00015088-09_C12H14N2O_N-[2-(1H-Indol-3-yl)ethyl]acetamide	M+H	203.118	0.839308	560.648	203.118
CCMSLIB00005723208	NCGC00178646-02!2,4-dihydroxyheptadecyl acetate [IIN-based: Match]	[M-H2O+H]+	313.273	0.746837	827.529	313.273
CCMSLIB00000853006	NCGC00380668-01_C48H78O18_(3beta,5xi,9xi,22beta)-22,24-Dihydroxyolean-12-en-3-yl 6-deoxy-alpha-L-mannopyranosyl-(1->2)-beta-D-galactopyranosyl-(1->2)-beta-D-glucopyranosiduronic acid	M+H	943.526	0.823226	765.236	943.526
CCMSLIB00000849791	NCGC00380976-01_C28H42N2O7_(4E,10E)-13,20-Dihydroxy-8,14-dimethoxy-4,10,12,16-tetramethyl-3-oxo-2-azabicyclo[16.3.1]docosa-1(22),4,10,18,20-pentaen-9-yl carbamate	M+FA-H	563.297	0.916236	559.61	563.297
CCMSLIB00000849791	NCGC00380976-01_C28H42N2O7_(4E,10E)-13,20-Dihydroxy-8,14-dimethoxy-4,10,12,16-tetramethyl-3-oxo-2-azabicyclo[16.3.1]docosa-1(22),4,10,18,20-pentaen-9-yl carbamate	M+FA-H	563.297	0.916236	560.566	563.297
CCMSLIB00000849788	NCGC00380976-01_C28H42N2O7_(4E,10E)-13,20-Dihydroxy-8,14-dimethoxy-4,10,12,16-tetramethyl-3-oxo-2-azabicyclo[16.3.1]docosa-1(22),4,10,18,20-pentaen-9-yl carbamate	M-H	517.292	0.864627	560.974	517.292
CCMSLIB00000848996	NCGC00381071-01!1,12-dihydroxy-1,6,12,17,23,28-hexazacyclotritriacontane-2,5,13,16,24,27-hexone	M+H	585.36	0.851688	505.214	585.36
CCMSLIB00005724289	N-coronafacoyl-L-isoleucine	M-H	320.186	0.997708	636.294	320.186
CCMSLIB00006702883	Nigericin sodium salt	M+H	747.465	0.886984	900.187	747.465
CCMSLIB00006678144	OL (32:0)	M+H	625.551	0.782472	845.506	625.551
CCMSLIB00005724298	O-Methylconcanamycin A	M+Na	902.523	0.986886	786.009	902.523
CCMSLIB00004716667	Pantethine	[M+Na]+	577.234	0.873574	500.185	577.234
CCMSLIB00003138526	Spectral Match to 1-(9Z-Octadecenoyl)-sn-glycero-3-phosphocholine from NIST14	M+H	522.36	0.937284	818.552	522.36

CCMSLIB00003136454	Spectral Match to 1H-Indole-3-carboxylic acid from NIST14	M+H	162.05	0.931721	547.598	162.05
CCMSLIB00003139406	Spectral Match to 20-Hydroxy-(5Z,8Z,11Z,14Z)-eicosatetraenoic acid from NIST14	M+H-H2O	303.231	0.725842	803.462	303.231
CCMSLIB00003139406	Spectral Match to 20-Hydroxy-(5Z,8Z,11Z,14Z)-eicosatetraenoic acid from NIST14	M+H-H2O	303.231	0.716815	804.62	303.231
CCMSLIB00003139413	Spectral Match to 9-Octadecenamide, (Z)- from NIST14	M+H	282.279	0.733986	868.106	282.279
CCMSLIB00003136308	Spectral Match to 9-Oxo-10E,12Z-octadecadienoic acid from NIST14	M+H-H2O	277.216	0.778413	754.073	277.216
CCMSLIB00003139019	Spectral Match to 9-OxoOTrE from NIST14	M+H-H2O	275.201	0.832945	614.764	275.201
CCMSLIB00003137125	Spectral Match to 9Z,11E,13E-Octadecatrienoic acid methyl ester from NIST14	M+H	293.247	0.865659	794.552	293.247
CCMSLIB00003139168	Spectral Match to Abrine from NIST14	M+H-CH3NH2	188.07	0.978705	454.628	188.07
CCMSLIB00003140066	Spectral Match to Arg-Ile from NIST14	M+H	288.202	0.745147	103.939	288.202
CCMSLIB00003137753	Spectral Match to Asp-Leu from NIST14	M+H	247.128	0.728634	269.326	247.128
CCMSLIB00003135694	Spectral Match to Bolasterone from NIST14	203.1	203.107	0.865515	585.863	203.107
CCMSLIB00003139085	Spectral Match to D-(+)-Trehalose from NIST14	M+NH4	360.149	0.976055	70.528	360.149
CCMSLIB00003139752	Spectral Match to D-Fructose from NIST14	M+NH4-H2O	180.086	0.877147	68.246	180.086
CCMSLIB00003135580	Spectral Match to Dibutyl phthalate from NIST14	M+H	279.159	0.982644	757.296	279.159
CCMSLIB00003135367	Spectral Match to Dioctyl phthalate from NIST14	M+H	391.285	0.990589	886.036	391.285
CCMSLIB00003138783	Spectral Match to Farnesol from NIST14	M+H	223.205	0.808523	760.817	223.205
CCMSLIB00003137247	Spectral Match to Guanosine from NIST14	M+H	284.093	0.98864	207.945	284.093
CCMSLIB00003139533	Spectral Match to Guanosine, 2'-deoxy- from NIST14	M+H	268.105	0.887238	265.157	268.105
CCMSLIB00003135348	Spectral Match to His-Ile from NIST14	M+H	269.164	0.858447	98.907	269.164
CCMSLIB00003134833	Spectral Match to His-Pro from NIST14	M+H-H2O	235.119	0.978167	75.333	235.119
CCMSLIB00003138069	Spectral Match to His-Pro from NIST14	M+H-H2O	235.119	0.974245	104.253	235.119
CCMSLIB00003138103	Spectral Match to Ile-Arg from NIST14	M+H	288.197	0.889094	75.003	288.197
CCMSLIB00003138103	Spectral Match to Ile-Arg from NIST14	M+H	288.197	0.889094	69.686	288.197
CCMSLIB00003134776	Spectral Match to Ile-Glu from NIST14	M+H	261.148	0.923474	110.566	261.148
CCMSLIB00003136121	Spectral Match to Ile-Pro-Ile from NIST14	M+H	342.239	0.987638	484.26	342.239
CCMSLIB00003137975	Spectral Match to Ile-Tyr from NIST14	M+H	295.159	0.958001	445.808	295.159

CCMSLIB00003137975	Spectral Match to Ile-Tyr from NIST14	M+H	295.159	0.880029	459.48	295.159
CCMSLIB00003138608	Spectral Match to Leu-Gly from NIST14	M+H-H2O	171.113	0.832066	471.649	171.113
CCMSLIB00003137659	Spectral Match to Leu-Pro from NIST14	M+H	229.155	0.77575	440.021	229.155
CCMSLIB00003138645	Spectral Match to L-Saccharopine from NIST14	M+H-H2O	259.129	0.970584	163.446	259.129
CCMSLIB00003137628	Spectral Match to L-Tryptophan from NIST14	M+H	205.097	0.946265	453.383	205.097
CCMSLIB00003136698	Spectral Match to Lys-Leu from NIST14	M+H	260.197	0.95397	102.55	260.197
CCMSLIB00003135346	Spectral Match to Lyso-PC(16:0) from NIST14	M+H	496.329	0.960255	790.654	496.329
CCMSLIB00003138028	Spectral Match to N-Acetyl-D-glucosamine from NIST14	M+H-H2O	204.082	0.979852	75.08	204.082
CCMSLIB00003137584	Spectral Match to N-Acetyl-D-glucosamine from NIST14	M+H-H2O	204.087	0.979116	904.046	204.087
CCMSLIB00003137937	Spectral Match to Palmitamide from NIST14	M+H	256.264	0.91249	867.612	256.264
CCMSLIB00003137162	Spectral Match to Phe-Thr from NIST14	M+H	267.134	0.941396	173.987	267.134
CCMSLIB00003134979	Spectral Match to Phe-Trp from NIST14	M+H	352.166	0.834784	499.901	352.166
CCMSLIB00003137316	Spectral Match to Pinolenic acid from NIST14	M+H	279.231	0.780112	770.049	279.231
CCMSLIB00003135124	Spectral Match to Pro-Ile from NIST14	M+H	229.155	0.887748	266.104	229.155
CCMSLIB00003139616	Spectral Match to Ser-Leu from NIST14	M+H	219.134	0.825264	178.244	219.134
CCMSLIB00003139078	Spectral Match to Ser-Leu from NIST14	M+H	219.134	0.822319	176.497	219.134
CCMSLIB00003140084	Spectral Match to Thr-Leu from NIST14	M+H	233.149	0.931987	210.195	233.149
CCMSLIB00003139119	Spectral Match to Tris(2-butoxyethyl) phosphate from NIST14	M+Na	421.233	0.954021	739.824	421.233
CCMSLIB00003135481	Spectral Match to Val-Arg from NIST14	M+H	274.187	0.761709	65.478	274.187
CCMSLIB00003137129	Spectral Match to Val-Gly-Val from NIST14	M+H	274.176	0.908695	439.615	274.176
CCMSLIB00003137123	Spectral Match to Val-Phe from NIST14	M+H	265.155	0.822634	462.624	265.155
CCMSLIB00003136202	Spectral Match to Val-Trp from NIST14	M+H	304.165	0.889819	473.415	304.165
CCMSLIB00005724284	Thaxtomin A	M-H	437.147	0.982155	567.665	437.147
CCMSLIB00005724275	Thaxtomin A	M+H	439.16	0.926941	566.487	439.16

Table S4.2. Hits to the GNPS library for the ethyl acetate extracts in the second dataset (IIMN_EtOAc).

SpectrumID	Compound_Name	Adduct	Precursor_MZ	Cosine_score	RT_Query	LibMZ
CCMSLIB00010107375	"(+)-Nootkatone, crystalline, 98+% CollisionEnergy:102040"	M+H-H2O	201.164	0.951883	305.853	201.164
CCMSLIB00010107375	"(+)-Nootkatone, crystalline, 98+% CollisionEnergy:102040"	M+H-H2O	201.164	0.716624	328.653	201.164
CCMSLIB00010113136	"1-({[2-(2-furylmethyl)-5-methylpyrrolidinyl]amino}methylene)-7-[8-({[2-(2-furylmethyl)pyrrolidinyl]amino}methylene)-1,6-dihydroxy-3-methyl-5-(methylethyl)-7 -oxo(2-naphthyl)]-3,8-dihydroxy-6-methyl-4-(methylethyl)naphthalen-2-one CollisionEnergy:102040"	M+2H]	415.212	0.979447	420.806	415.212
CCMSLIB00006681076	"1,6-ANHYDRO-B-GLUCOSE"	M-H	161.046	0.852404	201.621	161.046
CCMSLIB00006681076	"1,6-ANHYDRO-B-GLUCOSE"	M-H	161.046	0.852404	212.242	161.046
CCMSLIB00006681076	"1,6-ANHYDRO-B-GLUCOSE"	M-H	161.046	0.837785	806.889	161.046
CCMSLIB00006678983	"1,6-ANHYDRO-B-GLUCOSE"	M-H	161.046	0.804784	343.945	161.046
CCMSLIB00006681076	"1,6-ANHYDRO-B-GLUCOSE"	M-H	161.046	0.800044	868.521	161.046
CCMSLIB00006681076	"1,6-ANHYDRO-B-GLUCOSE"	M-H	161.046	0.791371	438.288	161.046
CCMSLIB00006681076	"1,6-ANHYDRO-B-GLUCOSE"	M-H	161.046	0.741704	88.52	161.046
CCMSLIB00006678983	"1,6-ANHYDRO-B-GLUCOSE"	M-H	161.046	0.71044	121.782	161.046
CCMSLIB00006681076	"1,6-ANHYDRO-B-GLUCOSE"	M-H	161.046	0.707156	421.448	161.046
CCMSLIB00006678983	"1,6-ANHYDRO-B-GLUCOSE"	M-H	161.046	0.701514	142.208	161.046
CCMSLIB00006678983	"1,6-ANHYDRO-B-GLUCOSE"	M-H	161.046	0.696152	359.507	161.046
CCMSLIB00006678983	"1,6-ANHYDRO-B-GLUCOSE"	M-H	161.046	0.681488	472.463	161.046
CCMSLIB00006678983	"1,6-ANHYDRO-B-GLUCOSE"	M-H	161.046	0.681488	462.942	161.046
CCMSLIB00006678983	"1,6-ANHYDRO-B-GLUCOSE"	M-H	161.046	0.647479	370.925	161.046
CCMSLIB00006678983	"1,6-ANHYDRO-B-GLUCOSE"	M-H	161.046	0.639074	276.573	161.046
CCMSLIB00006678983	"1,6-ANHYDRO-B-GLUCOSE"	M-H	161.046	0.634898	402.922	161.046
CCMSLIB00006678983	"1,6-ANHYDRO-B-GLUCOSE"	M-H	161.046	0.632815	775.532	161.046
CCMSLIB00006678983	"1,6-ANHYDRO-B-GLUCOSE"	M-H	161.046	0.627809	158.948	161.046

CCMSLIB00010106627	"6-aminododecanedioic acid, chloride CollisionEnergy:102040"	M+H	246.17	0.600618	289.555	246.17
CCMSLIB00010104459	"methyl 3-oxo-2-[(3,4,5-trimethoxyphenyl)methylene]benzo[b]furan-5-carboxylate CollisionEnergy:102040"	M+2Na]	208.042	0.909429	24.866	208.042
CCMSLIB00010115794	"methyl 3-oxo-2-[(3,4,5-trimethoxyphenyl)methylene]benzo[b]furan-5-carboxylate CollisionEnergy:205060"	M+2Na]	208.042	0.899921	771.799	208.042
CCMSLIB00005724857	(10E,15E)-9,12,13-trihydroxyoctadeca-10,15-dienoic acid	M-H	327.218	0.764158	355.237	327.218
CCMSLIB00005724857	(10E,15E)-9,12,13-trihydroxyoctadeca-10,15-dienoic acid	M-H	327.218	0.764158	371.993	327.218
CCMSLIB00010114577	(1R)-(-)-Nopol CollisionEnergy:102040	M+H-H2O	149.132	0.842309	453.488	149.132
CCMSLIB00006718004	(2E)-3-[4-Hydroxy-3-[(1E)-2-(4-hydroxy-3-methoxyphenyl)ethenyl]-5-methoxyphenyl]-2-propenoic acid = poacic acid	M-H	341.103	0.851401	332.528	341.103
CCMSLIB00004703112	(2S,3S,4S,5R,6S)-3,4,5-trihydroxy-6-(5-hydroxy-4-oxo-2-phenylchromen-7-yl)oxyoxane-2-carboxylic acid	[M-H]-	429.083	0.888006	275.254	429.083
CCMSLIB00005725152	(4E,8E)-7-hydroxy-10-(hydroxymethyl)-4,8,11,15-tetramethylbicyclo[11.2.0]pentadeca-4,8,14-trien-6-one	M+H	319.227	0.618043	289.701	319.227
CCMSLIB00006124728	.alpha.-D-Glucopyranose - 40.0 eV	Unknown	225.062	0.812234	204.462	225.062
CCMSLIB00006124728	.alpha.-D-Glucopyranose - 40.0 eV	Unknown	225.062	0.811068	815.972	225.062
CCMSLIB00006124728	.alpha.-D-Glucopyranose - 40.0 eV	Unknown	225.062	0.805826	117.491	225.062
CCMSLIB00006124728	.alpha.-D-Glucopyranose - 40.0 eV	Unknown	225.062	0.79457	880.173	225.062
CCMSLIB00006124728	.alpha.-D-Glucopyranose - 40.0 eV	Unknown	225.062	0.791528	108.459	225.062
CCMSLIB00006124728	.alpha.-D-Glucopyranose - 40.0 eV	Unknown	225.062	0.778424	11.747	225.062
CCMSLIB00005724597	1-methyl-4-(6-methylhept-5-en-2-yl)-2,3-dioxabicyclo[2.2.2]oct-5-ene	M+H	237.185	0.700147	355.705	237.185
CCMSLIB00005724597	1-methyl-4-(6-methylhept-5-en-2-yl)-2,3-dioxabicyclo[2.2.2]oct-5-ene	M+H	237.185	0.677544	328.822	237.185
CCMSLIB00005724597	1-methyl-4-(6-methylhept-5-en-2-yl)-2,3-dioxabicyclo[2.2.2]oct-5-ene	M+H	237.185	0.638366	310.578	237.185
CCMSLIB00005724598	1-methyl-4-(6-methylhept-5-en-2-yl)-2,3-dioxabicyclo[2.2.2]oct-5-ene	M-H2O+H	219.174	0.624139	302.671	219.174

CCMSLIB00005724598	1-methyl-4-(6-methylhept-5-en-2-yl)-2,3-dioxabicyclo[2.2.2]oct-5-ene	M-H2O+H	219.174	0.60813	356.162	219.174
CCMSLIB00005725033	1-methyl-4-methylidene-7-(propan-2-yl)-1,2,3,3a,4,5,6,8a-octahydroazulen-1-ol	M-H2O+H	203.179	0.956589	365.287	203.179
CCMSLIB00005725033	1-methyl-4-methylidene-7-(propan-2-yl)-1,2,3,3a,4,5,6,8a-octahydroazulen-1-ol	M-H2O+H	203.179	0.860758	390.459	203.179
CCMSLIB00005725033	1-methyl-4-methylidene-7-(propan-2-yl)-1,2,3,3a,4,5,6,8a-octahydroazulen-1-ol	M-H2O+H	203.179	0.75188	348.013	203.179
CCMSLIB00005725033	1-methyl-4-methylidene-7-(propan-2-yl)-1,2,3,3a,4,5,6,8a-octahydroazulen-1-ol	M-H2O+H	203.179	0.745388	418.247	203.179
CCMSLIB00005725033	1-methyl-4-methylidene-7-(propan-2-yl)-1,2,3,3a,4,5,6,8a-octahydroazulen-1-ol	M-H2O+H	203.179	0.668093	309.91	203.179
CCMSLIB00005725033	1-methyl-4-methylidene-7-(propan-2-yl)-1,2,3,3a,4,5,6,8a-octahydroazulen-1-ol	M-H2O+H	203.179	0.649213	270.047	203.179
CCMSLIB00005883983	2-DEOXY-D-GLUCOSE - 40.0 eV	M+H	165.076	0.900356	798.79	165.076
CCMSLIB00005883983	2-DEOXY-D-GLUCOSE - 40.0 eV	M+H	165.076	0.900356	787.452	165.076
CCMSLIB00005883983	2-DEOXY-D-GLUCOSE - 40.0 eV	M+H	165.076	0.875226	248.832	165.076
CCMSLIB00005883983	2-DEOXY-D-GLUCOSE - 40.0 eV	M+H	165.076	0.875226	259.549	165.076
CCMSLIB00005883983	2-DEOXY-D-GLUCOSE - 40.0 eV	M+H	165.076	0.874314	4.358	165.076
CCMSLIB00005883983	2-DEOXY-D-GLUCOSE - 40.0 eV	M+H	165.076	0.839281	204.831	165.076
CCMSLIB00005883983	2-DEOXY-D-GLUCOSE - 40.0 eV	M+H	165.076	0.836509	854.957	165.076
CCMSLIB00005883983	2-DEOXY-D-GLUCOSE - 40.0 eV	M+H	165.076	0.829129	183.484	165.076
CCMSLIB00005883983	2-DEOXY-D-GLUCOSE - 40.0 eV	M+H	165.076	0.818038	823.166	165.076
CCMSLIB00005883983	2-DEOXY-D-GLUCOSE - 40.0 eV	M+H	165.076	0.80349	69.855	165.076
CCMSLIB00005883983	2-DEOXY-D-GLUCOSE - 40.0 eV	M+H	165.076	0.793662	107.587	165.076
CCMSLIB00005883983	2-DEOXY-D-GLUCOSE - 40.0 eV	M+H	165.076	0.781383	13.426	165.076
CCMSLIB00005883983	2-DEOXY-D-GLUCOSE - 40.0 eV	M+H	165.076	0.781154	228.942	165.076
CCMSLIB00005883983	2-DEOXY-D-GLUCOSE - 40.0 eV	M+H	165.076	0.761123	870.887	165.076
CCMSLIB00004708653	3-[(1-Carboxyvinyl)oxy]benzoic acid	[M-H]-	207.03	0.818399	304.473	207.03

CCMSLIB00004714368	3-oxo-3-[[(10E,20E)-5,7,9,19,23,25,27,31,33,34,35-undecahydroxy-8,10,14,18,22,26,30-heptamethyl-15-[(Z)-4-methyl-10-[(N'-methylcarbamimidoyl)amino]dec-4-en-2-yl]-17-oxo-16,37-dioxabicyclo[31.3.1]heptatriaconta-10,20-dien-3-yl]oxy]propanoic acid	[M-H]-	1128.72	0.834574	384.148	1128.72
CCMSLIB00004714380	3-oxo-3-[[(10E,20E)-5,7,9,19,23,25,27,31,33,34,35-undecahydroxy-8,10,14,18,22,26,30-heptamethyl-15-[(Z)-4-methyl-10-[(N'-methylcarbamimidoyl)amino]dec-4-en-2-yl]-17-oxo-16,37-dioxabicyclo[31.3.1]heptatriaconta-10,20-dien-3-yl]oxy]propanoic acid	[M+H]+	1130.73	0.709411	369.105	1130.73
CCMSLIB00004714380	3-oxo-3-[[(10E,20E)-5,7,9,19,23,25,27,31,33,34,35-undecahydroxy-8,10,14,18,22,26,30-heptamethyl-15-[(Z)-4-methyl-10-[(N'-methylcarbamimidoyl)amino]dec-4-en-2-yl]-17-oxo-16,37-dioxabicyclo[31.3.1]heptatriaconta-10,20-dien-3-yl]oxy]propanoic acid	[M+H]+	1130.73	0.70939	385.799	1130.73
CCMSLIB00006717995	8-5'-Benzofuran-diferulic acid	M-H	385.094	0.818744	304.306	385.094
CCMSLIB00010114511	AC1L1X1Z CollisionEnergy:102040	M+Na	637.302	0.712055	527.463	637.302
CCMSLIB00006125720	alpha,alpha-Trehalose - 40.0 eV	Unknown	387.115	0.754041	28.794	387.115
CCMSLIB00010107223	azelaic acid CollisionEnergy:102040	M+H	189.112	0.904803	307.359	189.112
CCMSLIB00010114544	CARVEOL CollisionEnergy:102040	M+H-H2O	135.117	0.879795	313.772	135.117
CCMSLIB00005435823	Contaminant vial septum ThermoFisher C5000-44B	M+NH4	628.196	0.816781	569.032	628.196
CCMSLIB00004709698	Curcumenol	[M+H]+	235.169	0.743209	342.563	235.169
CCMSLIB00000081186	cyclo-(Leu-Leu)	M+H	227.174	0.655795	326.903	227.174
CCMSLIB00000081165	cyclo-(Leu-Phe)	M+H	261.159	0.881619	334.624	261.159
CCMSLIB00000007145	cyclo(L-Val-L-Pro)	M+H	197.129	0.900814	174.385	197.129
CCMSLIB00006113174	D-Galactitol - 40.0 eV	M-H	181.072	0.929307	382.462	181.072
CCMSLIB00006113174	D-Galactitol - 40.0 eV	M-H	181.072	0.929084	395.867	181.072
CCMSLIB00006113174	D-Galactitol - 40.0 eV	M-H	181.072	0.929084	406.252	181.072
CCMSLIB00006113174	D-Galactitol - 40.0 eV	M-H	181.072	0.917876	143.869	181.072
CCMSLIB00006114355	dl-3-Indolelactic acid - 30.0 eV	M-H	204.066	0.713567	287.527	204.066
CCMSLIB00005719626	D-Mannitol	[M-H+HCOOH]	227.077	0.93542	328.183	227.077

CCMSLIB00005719626	D-Mannitol	[M-H+HCOOH]	227.077	0.925783	386.83	227.077
CCMSLIB00005719017	D-Mannitol	[M-H+HCOOH]	227.077	0.922154	494.86	227.077
CCMSLIB00005719626	D-Mannitol	[M-H+HCOOH]	227.077	0.921885	143.283	227.077
CCMSLIB00005719626	D-Mannitol	[M-H+HCOOH]	227.077	0.918668	634.793	227.077
CCMSLIB00005719626	D-Mannitol	[M-H+HCOOH]	227.077	0.916321	411.323	227.077
CCMSLIB00005719626	D-Mannitol	[M-H+HCOOH]	227.077	0.916321	397.517	227.077
CCMSLIB00005719626	D-Mannitol	[M-H+HCOOH]	227.077	0.911877	461.295	227.077
CCMSLIB00005719017	D-Mannitol	[M-H+HCOOH]	227.077	0.910012	479.486	227.077
CCMSLIB00005719626	D-Mannitol	[M-H+HCOOH]	227.077	0.909038	87.29	227.077
CCMSLIB00005719017	D-Mannitol	[M-H+HCOOH]	227.077	0.908089	308.209	227.077
CCMSLIB00005719017	D-Mannitol	[M-H+HCOOH]	227.077	0.907032	30.044	227.077
CCMSLIB00005719017	D-Mannitol	[M-H+HCOOH]	227.077	0.905359	851.841	227.077
CCMSLIB00005719017	D-Mannitol	[M-H+HCOOH]	227.077	0.903839	183.691	227.077
CCMSLIB00005719017	D-Mannitol	[M-H+HCOOH]	227.077	0.901514	4.826	227.077
CCMSLIB00005719017	D-Mannitol	[M-H+HCOOH]	227.077	0.899337	253.263	227.077
CCMSLIB00005719017	D-Mannitol	[M-H+HCOOH]	227.077	0.89556	267.924	227.077
CCMSLIB00005719017	D-Mannitol	[M-H+HCOOH]	227.077	0.893641	239.619	227.077
CCMSLIB00005719017	D-Mannitol	[M-H+HCOOH]	227.077	0.893493	449.787	227.077
CCMSLIB00005719017	D-Mannitol	[M-H+HCOOH]	227.077	0.891948	97.273	227.077
CCMSLIB00005719017	D-Mannitol	[M-H+HCOOH]	227.077	0.890266	862.013	227.077
CCMSLIB00005719017	D-Mannitol	[M-H+HCOOH]	227.077	0.889314	765.062	227.077
CCMSLIB00005719017	D-Mannitol	[M-H+HCOOH]	227.077	0.887188	428.155	227.077
CCMSLIB00005719017	D-Mannitol	[M-H+HCOOH]	227.077	0.886311	810.435	227.077
CCMSLIB00005719017	D-Mannitol	[M-H+HCOOH]	227.077	0.886311	783.933	227.077
CCMSLIB00005719965	D-Mannitol	[M+H]	183.087	0.872693	487.525	183.087
CCMSLIB00005719626	D-Mannitol	[M-H+HCOOH]	227.077	0.854145	505.023	227.077
CCMSLIB00005719626	D-Mannitol	[M-H+HCOOH]	227.077	0.841404	515.515	227.077
CCMSLIB00005719965	D-Mannitol	[M+H]	183.087	0.804943	449.959	183.087

CCMSLIB00005719965	D-Mannitol	[M+H]	183.087	0.793454	466.782	183.087
CCMSLIB00005719626	D-Mannitol	[M-H+HCOOH]	227.077	0.778367	276.569	227.077
CCMSLIB00010102807	D-mannitol CollisionEnergy:102040	M-H	181.072	0.958763	483.523	181.072
CCMSLIB00010102807	D-mannitol CollisionEnergy:102040	M-H	181.072	0.945993	28.355	181.072
CCMSLIB00010102807	D-mannitol CollisionEnergy:102040	M-H	181.072	0.936136	764.269	181.072
CCMSLIB00010102807	D-mannitol CollisionEnergy:102040	M-H	181.072	0.935708	107.11	181.072
CCMSLIB00010102807	D-mannitol CollisionEnergy:102040	M-H	181.072	0.927991	469.804	181.072
CCMSLIB00010102807	D-mannitol CollisionEnergy:102040	M-H	181.072	0.921722	310.663	181.072
CCMSLIB00005884962	D-SORBITOL - 20.0 eV	M+H	183.086	0.782933	893.644	183.086
CCMSLIB00005884962	D-SORBITOL - 20.0 eV	M+H	183.086	0.770445	102.374	183.086
CCMSLIB00005884962	D-SORBITOL - 20.0 eV	M+H	183.086	0.751298	200.678	183.086
CCMSLIB00005884962	D-SORBITOL - 20.0 eV	M+H	183.086	0.744254	10.766	183.086
CCMSLIB00005884962	D-SORBITOL - 20.0 eV	M+H	183.086	0.728505	145.985	183.086
CCMSLIB00005884962	D-SORBITOL - 20.0 eV	M+H	183.086	0.727241	187.781	183.086
CCMSLIB00005884962	D-SORBITOL - 20.0 eV	M+H	183.086	0.71157	877.072	183.086
CCMSLIB00005884962	D-SORBITOL - 20.0 eV	M+H	183.086	0.709624	36.74	183.086
CCMSLIB00005884962	D-SORBITOL - 20.0 eV	M+H	183.086	0.692328	121.494	183.086
CCMSLIB00005884962	D-SORBITOL - 20.0 eV	M+H	183.086	0.688508	172.043	183.086
CCMSLIB00005884962	D-SORBITOL - 20.0 eV	M+H	183.086	0.6876	229.306	183.086
CCMSLIB00005884962	D-SORBITOL - 20.0 eV	M+H	183.086	0.686261	84.849	183.086
CCMSLIB00005884962	D-SORBITOL - 20.0 eV	M+H	183.086	0.682646	218.8	183.086
CCMSLIB00005884962	D-SORBITOL - 20.0 eV	M+H	183.086	0.679721	261.755	183.086
CCMSLIB00005884962	D-SORBITOL - 20.0 eV	M+H	183.086	0.674761	315.192	183.086
CCMSLIB00005884962	D-SORBITOL - 20.0 eV	M+H	183.086	0.672318	857.625	183.086
CCMSLIB00005884962	D-SORBITOL - 20.0 eV	M+H	183.086	0.654866	250.078	183.086
CCMSLIB00005884962	D-SORBITOL - 20.0 eV	M+H	183.086	0.640809	268.154	183.086
CCMSLIB00005884962	D-SORBITOL - 20.0 eV	M+H	183.086	0.640809	270.572	183.086
CCMSLIB00005884963	D-SORBITOL - 30.0 eV	M+H	183.086	0.738576	132.745	183.086

CCMSLIB00010102811	D-Sorbitol CollisionEnergy:102040	M-H	181.072	0.980228	619.619	181.072
CCMSLIB00010102811	D-Sorbitol CollisionEnergy:102040	M-H	181.072	0.948466	222.892	181.072
CCMSLIB00010102811	D-Sorbitol CollisionEnergy:102040	M-H	181.072	0.939324	652.018	181.072
CCMSLIB00010102811	D-Sorbitol CollisionEnergy:102040	M-H	181.072	0.923288	339.808	181.072
CCMSLIB00010102811	D-Sorbitol CollisionEnergy:102040	M-H	181.072	0.920491	45.94	181.072
CCMSLIB00010102811	D-Sorbitol CollisionEnergy:102040	M-H	181.072	0.910986	517.679	181.072
CCMSLIB00010102811	D-Sorbitol CollisionEnergy:102040	M-H	181.072	0.907432	499.095	181.072
CCMSLIB00006679960	ELAIDIC ACID	M+H	283.263	0.742775	527.652	283.263
CCMSLIB00006679960	ELAIDIC ACID	M+H	283.263	0.740875	506.331	283.263
CCMSLIB00006682427	FRUCTOSE	M-H	179.056	0.672771	253.606	179.056
CCMSLIB00005464191	GALACTITOL	M-H	181.072	0.917719	62.552	181.072
CCMSLIB00005464191	GALACTITOL	M-H	181.072	0.917254	183.652	181.072
CCMSLIB00005464191	GALACTITOL	M-H	181.072	0.917254	169.077	181.072
CCMSLIB00005464191	GALACTITOL	M-H	181.072	0.917154	125.659	181.072
CCMSLIB00005464191	GALACTITOL	M-H	181.072	0.914965	197.688	181.072
CCMSLIB00005464191	GALACTITOL	M-H	181.072	0.914631	6.987	181.072
CCMSLIB00005464191	GALACTITOL	M-H	181.072	0.913659	863.827	181.072
CCMSLIB00005464191	GALACTITOL	M-H	181.072	0.913219	273.825	181.072
CCMSLIB00005464191	GALACTITOL	M-H	181.072	0.913219	263.859	181.072
CCMSLIB00005464191	GALACTITOL	M-H	181.072	0.903401	817.739	181.072
CCMSLIB00005464191	GALACTITOL	M-H	181.072	0.903401	777.209	181.072
CCMSLIB00006679570	GALACTITOL	M+H	183.086	0.895449	511.314	183.086
CCMSLIB00000578174	GALACTITOL	M-H	181.071	0.874078	704.605	181.071
CCMSLIB00000578174	GALACTITOL	M-H	181.071	0.874078	686.668	181.071
CCMSLIB00000578174	GALACTITOL	M-H	181.071	0.864066	326.329	181.071
CCMSLIB00005464191	GALACTITOL	M-H	181.072	0.844755	423.591	181.072
CCMSLIB00005883994	GALACTITOL - 30.0 eV	M+H	183.086	0.608982	839.005	183.086
CCMSLIB00010102810	galactitol CollisionEnergy:102040	M-H	181.072	0.857178	358.979	181.072

CCMSLIB00010102810	galactitol CollisionEnergy:102040	M-H	181.072	0.855826	290.183	181.072
CCMSLIB00010102810	galactitol CollisionEnergy:102040	M-H	181.072	0.854899	85.873	181.072
CCMSLIB00010102810	galactitol CollisionEnergy:102040	M-H	181.072	0.839052	438.057	181.072
CCMSLIB00010102810	galactitol CollisionEnergy:102040	M-H	181.072	0.830914	895.212	181.072
CCMSLIB00010102810	galactitol CollisionEnergy:102040	M-H	181.072	0.830914	881.937	181.072
CCMSLIB00010102810	galactitol CollisionEnergy:102040	M-H	181.072	0.825803	593.976	181.072
CCMSLIB00010102810	galactitol CollisionEnergy:102040	M-H	181.072	0.792423	459.264	181.072
CCMSLIB00005723980	Geldanamycin	M-H	559.266	0.806727	421.949	559.266
CCMSLIB00005723980	Geldanamycin	M-H	559.266	0.657189	364.891	559.266
CCMSLIB00005788066	Glochidone	M+H	423.362	0.647996	506.005	423.362
CCMSLIB00010011444	Gly-C14:1	M+H	284.222	0.670201	355.1	284.222
CCMSLIB00006115517	isopropylmalic acid - 40.0 eV	M-H	175.061	0.740571	145.313	175.061
CCMSLIB00010102464	maltose CollisionEnergy:102040	M+Cl	377.086	0.883662	33.338	377.086
CCMSLIB00006679572	MANNITOL	M+H	183.086	0.951695	532.421	183.086
CCMSLIB00006679572	MANNITOL	M+H	183.086	0.951145	758.424	183.086
CCMSLIB00005884956	MANNITOL - 20.0 eV	M+H	183.086	0.763148	800.422	183.086
CCMSLIB00005884956	MANNITOL - 20.0 eV	M+H	183.086	0.754924	825.78	183.086
CCMSLIB00005727227	Massbank:AC000282 Walleminone|(1R,4S,5S,6R,9R)-5,6-dihydroxy-4,11,11-trimethyl-8-methylidenebicyclo[7.2.0]undecan-3-one	M+H	253.179	0.668583	324.446	253.179
CCMSLIB00005727227	Massbank:AC000282 Walleminone|(1R,4S,5S,6R,9R)-5,6-dihydroxy-4,11,11-trimethyl-8-methylidenebicyclo[7.2.0]undecan-3-one	M+H	253.179	0.603504	346.104	253.179
CCMSLIB00005727227	Massbank:AC000282 Walleminone|(1R,4S,5S,6R,9R)-5,6-dihydroxy-4,11,11-trimethyl-8-methylidenebicyclo[7.2.0]undecan-3-one	M+H	253.179	0.603279	396.105	253.179
CCMSLIB00005727227	Massbank:AC000282 Walleminone|(1R,4S,5S,6R,9R)-5,6-dihydroxy-4,11,11-trimethyl-8-methylidenebicyclo[7.2.0]undecan-3-one	M+H	253.179	0.603279	412.027	253.179
CCMSLIB00005731255	Massbank:EQ331603 Linoleic acid|(9Z,12Z)-octadeca-9,12-dienoic acid	M+H	281.247	0.671073	499.453	281.247

CCMSLIB00005733662	Massbank:EQ368252 Nigericin|2-{6-[(2-{5`-[6-hydroxy-6-(hydroxymethyl)-3,5-dimethyltetrahydro-2h-pyran-2-yl]-2,3`-dimethyloctahydro-2,2`-bifuran-5-yl}-9-methoxy-2,4,10-trimethyl-1,6-dioxaspiro[4.5]dec-7-yl)methyl]-3-met	M-H	723.469	0.910027	584.563	723.469
CCMSLIB00005740058	Massbank:PR309076 FA 18:4+2O	M-H	307.19	0.820168	388.807	307.19
CCMSLIB00005739084	Massbank:PR311142 Cyclo(leucylprolyl)	M+H	211.144	0.709915	276.796	211.144
CCMSLIB00005738288	Massbank:RP022811 D-Galactose|alpha-D-galactose|(2S,3R,4S,5R,6R)-6-(hydroxymethyl)oxane-2,3,4,5-tetrol	M-H	179.056	0.934958	299.742	179.056
CCMSLIB00000567955	MoNA:790536 Linoleic acid	M+H	281.247	0.811224	441.304	281.247
CCMSLIB00000567923	MoNA:790553 Linoleic acid	[M+H]+	281.247	0.832717	535.466	281.247
CCMSLIB00000568813	MoNA:947057 2-{6-[(2-{5`-[6-hydroxy-6-(hydroxymethyl)-3,5-dimethyltetrahydro-2h-pyran-2-yl]-2,3`-dimethyloctahydro-2,2`-bifuran-5-yl}-9-methoxy-2,4,10-trimethyl-1,6-dioxaspiro[4.5]dec-7-yl)methyl]-3-methyltetrahydro-2h-pyran-2-yl}propanoic acid	M-H	723.469	0.858703	519.297	723.469
CCMSLIB00010102814	N-Acetyl-D-tryptophan CollisionEnergy:102040	M-H	245.093	0.922622	301.428	245.093
CCMSLIB00005464448	N-ACETYLPHENYLALANINE	M+H	208.097	0.986405	279.741	208.097
CCMSLIB00006679116	N-ACETYL-PHENYLALANINE	M-H	206.082	0.95609	282.721	206.082
CCMSLIB00010105222	naringenin CollisionEnergy:102040	M+H	273.076	0.947641	293.743	273.076
CCMSLIB00000852864	NCGC00380867-01_C27H46O9_9,12,15-Octadecatrienoic acid, 3-(hexopyranosyloxy)-2-hydroxypropyl ester, (9Z,12Z,15Z)-	M+NH4	532.348	0.749853	458.461	532.348
CCMSLIB00000849791	NCGC00380976-01_C28H42N2O7_(4E,10E)-13,20-Dihydroxy-8,14-dimethoxy-4,10,12,16-tetramethyl-3-oxo-2-azabicyclo[16.3.1]docosa-1(22),4,10,18,20-pentaen-9-yl carbamate	M+FA-H	563.297	0.875108	337.13	563.297
CCMSLIB00000849788	NCGC00380976-01_C28H42N2O7_(4E,10E)-13,20-Dihydroxy-8,14-dimethoxy-4,10,12,16-tetramethyl-3-oxo-2-azabicyclo[16.3.1]docosa-1(22),4,10,18,20-pentaen-9-yl carbamate	M-H	517.292	0.79784	336.344	517.292

CCMSLIB00000852714	NCGC00380976-01_C28H42N2O7_(4E,10E)-13,20-Dihydroxy-8,14-dimethoxy-4,10,12,16-tetramethyl-3-oxo-2-azabicyclo[16.3.1]docosa-1(22),4,10,18,20-pentaen-9-yl carbamate	M+NH4	536.333	0.773365	337.885	536.333
CCMSLIB00000848247	NCGC00381248-01!4-oxododecanedioic acid	M+NH4	262.165	0.733742	324.633	262.165
CCMSLIB00005722220	NCGC00381425-01!8-hydroxy-8-(3-octyloxiran-2-yl)octanoic acid [IIN-based on: CCMSLIB00000846585]	[M-3H2O+H]+	261.222	0.700334	429.131	261.222
CCMSLIB00005722010	NCGC00384809-01!5-[5-hydroxy-3-(hydroxymethyl)pentyl]-8a-(hydroxymethyl)-5,6-dimethyl-3,4,4a,6,7,8-hexahydronaphthalene-1-carboxylic acid [IIN-based on: CCMSLIB00000847958]	[M-H2O+H]+	337.238	0.706884	289.701	337.238
CCMSLIB00000856124	NCGC00385243-01_C12H18O4_{(1R,2R)-2-[(2Z)-5-Hydroxy-2-penten-1-yl]-3-oxocyclopentyl}acetic acid	M+H	227.128	0.641699	268.662	227.128
CCMSLIB00000848373	NCGC00385558-01!(2R,3S,4S,5R,6R)-2-[[(2R,3R,4R)-3,4-dihydroxy-4-(hydroxymethyl)oxolan-2-yl]oxymethyl]-6-oct-1-en-3-yloxyoxane-3,4,5-triol	M+NH4	440.249	0.608048	330.381	440.249
CCMSLIB00005463544	PSICOSE	M-H	179.056	0.806776	160.56	179.056
CCMSLIB00005436164	PSICOSE	M-H	179.056	0.769987	862.511	179.056
CCMSLIB00005463544	PSICOSE	M-H	179.056	0.76377	807.099	179.056
CCMSLIB00003137219	Spectral Match to (-)-Isolongifolol from NIST14	M+H-H2O	205.2	0.867861	491.332	205.2
CCMSLIB00003138515	Spectral Match to .alpha.-Linolenoyl ethanolamide from NIST14	M+H	322.274	0.941666	478.438	322.274
CCMSLIB00003138070	Spectral Match to .alpha.-Linolenoyl ethanolamide from NIST14	M+H	322.273	0.901513	428.079	322.273
CCMSLIB00003136823	Spectral Match to .beta.-Eudesmol from NIST14	M+H-H2O	205.195	0.868491	471.415	205.195
CCMSLIB00003137820	Spectral Match to 12(13)-Epoxy-9Z-octadecenoic acid from NIST14	M+H-H2O	279.232	0.929758	425.038	279.232
CCMSLIB00003134969	Spectral Match to 12,13-DiHOME from NIST14	M+H-H2O	297.242	0.816501	427.768	297.242
CCMSLIB00003134933	Spectral Match to 12,13-DiHOME from NIST14	M+H	315.252	0.694548	426.732	315.252
CCMSLIB00003138554	Spectral Match to 12,13-DiHOME from NIST14	M-H	313.239	0.619582	428.435	313.239
CCMSLIB00003134514	Spectral Match to 13-Docosenamide, (Z)- from NIST14	M+H	338.341	0.871382	600.054	338.341

CCMSLIB00003136232	Spectral Match to 13-Keto-9Z,11E-octadecadienoic acid from NIST14	M+H-H2O	277.216	0.898191	448.09	277.216
CCMSLIB00003136232	Spectral Match to 13-Keto-9Z,11E-octadecadienoic acid from NIST14	M+H-H2O	277.216	0.886028	383.79	277.216
CCMSLIB00003136232	Spectral Match to 13-Keto-9Z,11E-octadecadienoic acid from NIST14	M+H-H2O	277.216	0.726811	365.802	277.216
CCMSLIB00003137992	Spectral Match to 13-Keto-9Z,11E-octadecadienoic acid from NIST14	M+H	295.227	0.652651	369.99	295.227
CCMSLIB00003137992	Spectral Match to 13-Keto-9Z,11E-octadecadienoic acid from NIST14	M+H	295.227	0.652651	392.105	295.227
CCMSLIB00003138475	Spectral Match to 1-Linoleoylglycerol from NIST14	M+H	355.284	0.706244	528.035	355.284
CCMSLIB00003136741	Spectral Match to 2,6-Di-tert-butyl-4-hydroxymethylphenol from NIST14	M+H-H2O	219.175	0.643292	331.682	219.175
CCMSLIB00003135997	Spectral Match to 3,5-Dimethyladamantan-1-amine from NIST14	M+H-NH3	163.148	0.901225	349.279	163.148
CCMSLIB00003134812	Spectral Match to 9(10)-EpOME from NIST14	M+H-H2O	279.231	0.929876	464.655	279.231
CCMSLIB00003134812	Spectral Match to 9(10)-EpOME from NIST14	M+H-H2O	279.231	0.889058	519.072	279.231
CCMSLIB00003135516	Spectral Match to 9,10-Dihydroxy-12Z-octadecenoic acid from NIST14	M+H	315.253	0.694259	397.72	315.253
CCMSLIB00003137723	Spectral Match to 9,12-Octadecadiynoic Acid from NIST14	M+H	277.215	0.759971	429.894	277.215
CCMSLIB00003139147	Spectral Match to 9-Octadecenamide, (Z)- from NIST14	M+H	282.278	0.805676	537.295	282.278
CCMSLIB00003135615	Spectral Match to 9-Oxo-10E,12Z-octadecadienoic acid from NIST14	M+H	295.227	0.698303	411.898	295.227
CCMSLIB00003139019	Spectral Match to 9-OxoOTrE from NIST14	M+H-H2O	275.201	0.743346	410.965	275.201
CCMSLIB00003135863	Spectral Match to 9-OxoOTrE from NIST14	M+H-H2O	275.2	0.64829	373.532	275.2
CCMSLIB00003135863	Spectral Match to 9-OxoOTrE from NIST14	M+H-H2O	275.2	0.64829	352.423	275.2
CCMSLIB00003138563	Spectral Match to Baicalin from NIST14	M-H	445.078	0.929878	305.374	445.078
CCMSLIB00003136526	Spectral Match to cis-9-Hexadecenoic acid from NIST14	M+H	255.232	0.795215	530.266	255.232
CCMSLIB00003136374	Spectral Match to Conjugated linoleic Acid (10E,12Z) from NIST14	M+H-H2O	263.236	0.679078	536.407	263.236
CCMSLIB00003135049	Spectral Match to Didodecyl 3,3'-thiodipropionate oxide from NIST14	M+H	531.408	0.957619	637.251	531.408

CCMSLIB00003139396	Spectral Match to Dihydrokaempferol from NIST14	M+H	289.071	0.622513	261.408	289.071
CCMSLIB00003136083	Spectral Match to D-Sorbitol from NIST14	M+H	183.086	0.657845	298.323	183.086
CCMSLIB00003139527	Spectral Match to Dulcitol from NIST14	M-H	181.071	0.857821	636.171	181.071
CCMSLIB00003135635	Spectral Match to Glycerol 1-myristate from NIST14	M+H	303.253	0.91044	504.77	303.253
CCMSLIB00003137498	Spectral Match to L-Arginine from NIST14	M+H	175.119	0.853483	23.318	175.119
CCMSLIB00003138141	Spectral Match to Linoleoyl ethanolamide from NIST14	M+H	324.29	0.895946	500.115	324.29
CCMSLIB00003138418	Spectral Match to Monolinolenin (9c,12c,15c) from NIST14	M+H	353.269	0.938122	499.846	353.269
CCMSLIB00003138418	Spectral Match to Monolinolenin (9c,12c,15c) from NIST14	M+H	353.269	0.830151	474.21	353.269
CCMSLIB00003138418	Spectral Match to Monolinolenin (9c,12c,15c) from NIST14	M+H	353.269	0.816114	412.815	353.269
CCMSLIB00003138418	Spectral Match to Monolinolenin (9c,12c,15c) from NIST14	M+H	353.269	0.729625	464.4	353.269
CCMSLIB00003137660	Spectral Match to Monolinolenin (9c,12c,15c) from NIST14	M+H	353.27	0.677535	445.08	353.27
CCMSLIB00003137976	Spectral Match to Myristoleic acid from NIST14	M+H	227.2	0.687697	425.231	227.2
CCMSLIB00003139765	Spectral Match to N-Oleoylethanolamine from NIST14	M+H	326.306	0.913924	518.162	326.306
CCMSLIB00003139733	Spectral Match to Palatinose from NIST14	M+NH4	360.15	0.978899	32.566	360.15
CCMSLIB00003138556	Spectral Match to Palmitoyl ethanolamide from NIST14	M+H	300.289	0.821356	511.898	300.289
CCMSLIB00003135107	Spectral Match to Perillaldehyde from NIST14	M+H+H2O	169.122	0.806697	358.26	169.122
CCMSLIB00003140162	Spectral Match to Stearidonic acid from NIST14	M+H	277.215	0.802967	411.362	277.215
CCMSLIB00003138520	Spectral Match to Syringic acid from NIST14	M+H	199.06	0.919264	243.55	199.06
CCMSLIB00003138602	Spectral Match to Val-Leu from NIST14	M+H-H2O	213.16	0.904536	305.182	213.16
CCMSLIB00006679047	THYMIDINE	M+H	243.098	0.929374	56.066	243.098
CCMSLIB00005464529	TREHALOSE	M-H	341.109	0.950972	28.503	341.109
CCMSLIB00005464337	URIDINE	M-H	243.062	0.865674	29.829	243.062
CCMSLIB00010112940	VITAMIN K1 CollisionEnergy:102040	M+2H]	226.182	0.783614	550.365	226.182

Table S4.3. Hits to the GNPS library for the methanol extracts in the second dataset (IIMN_MeOH).

SpectrumID	Compound_Name	Adduct	Precursor_MZ	Cosine_score	RT_Query	LibMZ
CCMSLIB00006681076	"1,6-ANHYDRO-B-GLUCOSE"	M-H	161.046	0.889403	242.016	161.046
CCMSLIB00006681076	"1,6-ANHYDRO-B-GLUCOSE"	M-H	161.046	0.871341	86.391	161.046
CCMSLIB00006681076	"1,6-ANHYDRO-B-GLUCOSE"	M-H	161.046	0.82995	843.009	161.046
CCMSLIB00006681076	"1,6-ANHYDRO-B-GLUCOSE"	M-H	161.046	0.790049	382.829	161.046
CCMSLIB00006681076	"1,6-ANHYDRO-B-GLUCOSE"	M-H	161.046	0.790049	401.999	161.046
CCMSLIB00006681076	"1,6-ANHYDRO-B-GLUCOSE"	M-H	161.046	0.765418	143.038	161.046
CCMSLIB00006681076	"1,6-ANHYDRO-B-GLUCOSE"	M-H	161.046	0.765418	152.324	161.046
CCMSLIB00006678983	"1,6-ANHYDRO-B-GLUCOSE"	M-H	161.046	0.764602	119.951	161.046
CCMSLIB00006681076	"1,6-ANHYDRO-B-GLUCOSE"	M-H	161.046	0.763139	174.962	161.046
CCMSLIB00006681076	"1,6-ANHYDRO-B-GLUCOSE"	M-H	161.046	0.76308	351.455	161.046
CCMSLIB00006681076	"1,6-ANHYDRO-B-GLUCOSE"	M-H	161.046	0.757871	775.77	161.046
CCMSLIB00006681076	"1,6-ANHYDRO-B-GLUCOSE"	M-H	161.046	0.752887	451.372	161.046
CCMSLIB00006681076	"1,6-ANHYDRO-B-GLUCOSE"	M-H	161.046	0.747664	890.288	161.046
CCMSLIB00006678983	"1,6-ANHYDRO-B-GLUCOSE"	M-H	161.046	0.73593	271.224	161.046
CCMSLIB00006681076	"1,6-ANHYDRO-B-GLUCOSE"	M-H	161.046	0.718501	511.438	161.046
CCMSLIB00006678983	"1,6-ANHYDRO-B-GLUCOSE"	M-H	161.046	0.702252	492.92	161.046
CCMSLIB00006681076	"1,6-ANHYDRO-B-GLUCOSE"	M-H	161.046	0.655458	440.681	161.046
CCMSLIB00010125158	"3-(2-methylpropyl)-3a,4,5,6-tetrahydro-2-benzofuran-1(3h)-one CollisionEnergy:205060"	M+H	195.138	0.672592	429.042	195.138
CCMSLIB00005724857	(10E,15E)-9,12,13-trihydroxyoctadeca-10,15-dienoic acid	M-H	327.218	0.742738	354.043	327.218
CCMSLIB00010114577	(1R)-(-)-Nopol CollisionEnergy:102040	M+H-H2O	149.132	0.856168	452.251	149.132
CCMSLIB00010114577	(1R)-(-)-Nopol CollisionEnergy:102040	M+H-H2O	149.132	0.836709	364.362	149.132

CCMSLIB00004715952	(2S,3R,4R,5R,6S)-2-{[(2R,3S,4R,5R,6S)-6-{[(2R,3R,4S,5S,6R)-4,5-dihydroxy-6-(hydroxymethyl)-2-[(1'S,2S,4'S,5S,7'R,9'S,13'R,16'S)-5,7',9',13'-tetramethyl-5-({[(2R,3R,4S,5S,6R)-3,4,5-trihydroxy-6-(hydroxymethyl)oxan-2-yl]oxy}methyl)-5'-oxaspiro[oxolane-2,6'-pentacyclo[10.8.0.0ï¿½,?.0?,?.0ï¿½ï¿½,ï¿½?]icosan]-18'-eneoxy]oxan-3-yl]oxy}-4,5-dihydroxy-2-(hydroxymethyl)oxan-3-yl]oxy}-6-methyloxane-3,4,5-triol	[M+H]+	1063.53	0.888214	348.244	1063.53
CCMSLIB00004710948	(2S,3S,4S,5R,6R)-6-(3-benzoyloxy-2-hydroxypropoxy)-3,4,5-trihydroxyoxane-2-carboxylic acid	[M-H]-	371.098	0.894562	273.034	371.098
CCMSLIB00004706806	(2S,3S,4S,5R,6R)-6-[[(3S,4S,6aR,6bS,8aR,9R,12aS,14bR)-9-hydroxy-4-(hydroxymethyl)-4,6a,6b,8a,11,11,14b-heptamethyl-1,2,3,4a,5,6,7,8,9,10,12,12a,14,14a-tetradecahydropicen-3-yl]oxy]-5-[(2S,3R,4S,5R,6R)-4,5-dihydroxy-6-(hydroxymethyl)-3-[(2S,3R,4R,5R,6S)-3,4,5-trihydroxy-6-methyloxan-2-yl]oxyoxan-2-yl]oxy-3,4-dihydroxyoxane-2-carboxylic acid	[M+H]+	943.526	0.80118	397.784	943.526
CCMSLIB00005724697	(2Z,6S)-6-[(1S,3aS,9aR,11aS)-3a,6,6,9a,11a-pentamethyl-7-oxo-1H,2H,3H,3aH,5H,5aH,6H,7H,8H,9H,9aH,9bH,10H,11H,11aH-cyclopenta[a]phenanthren-1-yl]-2-methylhept-2-enoic acid	M-H2O+H	437.341	0.609237	363.631	437.341

CCMSLIB00006124728	.alpha.-D-Glucopyranose - 40.0 eV	Unknown	225.062	0.902928	111.971	225.062
CCMSLIB00006124728	.alpha.-D-Glucopyranose - 40.0 eV	Unknown	225.062	0.884524	13.016	225.062
CCMSLIB00006124728	.alpha.-D-Glucopyranose - 40.0 eV	Unknown	225.062	0.877834	47.222	225.062
CCMSLIB00006124728	.alpha.-D-Glucopyranose - 40.0 eV	Unknown	225.062	0.872116	72.264	225.062
CCMSLIB00006124728	.alpha.-D-Glucopyranose - 40.0 eV	Unknown	225.062	0.872116	30.309	225.062
CCMSLIB00006124728	.alpha.-D-Glucopyranose - 40.0 eV	Unknown	225.062	0.868448	306.959	225.062
CCMSLIB00006124728	.alpha.-D-Glucopyranose - 40.0 eV	Unknown	225.062	0.868448	287.488	225.062
CCMSLIB00006124728	.alpha.-D-Glucopyranose - 40.0 eV	Unknown	225.062	0.857676	892.753	225.062
CCMSLIB00006124728	.alpha.-D-Glucopyranose - 40.0 eV	Unknown	225.062	0.857149	839.954	225.062
CCMSLIB00006124728	.alpha.-D-Glucopyranose - 40.0 eV	Unknown	225.062	0.838526	353.372	225.062
CCMSLIB00006124728	.alpha.-D-Glucopyranose - 40.0 eV	Unknown	225.062	0.838186	366.369	225.062
CCMSLIB00006124728	.alpha.-D-Glucopyranose - 40.0 eV	Unknown	225.062	0.836557	149.586	225.062
CCMSLIB00006124728	.alpha.-D-Glucopyranose - 40.0 eV	Unknown	225.062	0.832274	243.843	225.062
CCMSLIB00006124728	.alpha.-D-Glucopyranose - 40.0 eV	Unknown	225.062	0.825963	122.07	225.062
CCMSLIB00006124728	.alpha.-D-Glucopyranose - 40.0 eV	Unknown	225.062	0.825097	222.592	225.062
CCMSLIB00006124728	.alpha.-D-Glucopyranose - 40.0 eV	Unknown	225.062	0.82065	259.63	225.062
CCMSLIB00006124728	.alpha.-D-Glucopyranose - 40.0 eV	Unknown	225.062	0.816355	480.087	225.062
CCMSLIB00006124728	.alpha.-D-Glucopyranose - 40.0 eV	Unknown	225.062	0.815742	272.395	225.062
CCMSLIB00006124728	.alpha.-D-Glucopyranose - 40.0 eV	Unknown	225.062	0.807788	459.569	225.062
CCMSLIB00006124728	.alpha.-D-Glucopyranose - 40.0 eV	Unknown	225.062	0.806075	871.84	225.062
CCMSLIB00006124728	.alpha.-D-Glucopyranose - 40.0 eV	Unknown	225.062	0.78498	323.723	225.062
CCMSLIB00006124728	.alpha.-D-Glucopyranose - 40.0 eV	Unknown	225.062	0.77938	807.062	225.062
CCMSLIB00006124728	.alpha.-D-Glucopyranose - 40.0 eV	Unknown	225.062	0.776248	93.333	225.062
CCMSLIB00006124728	.alpha.-D-Glucopyranose - 40.0 eV	Unknown	225.062	0.754792	197.53	225.062
CCMSLIB00006124728	.alpha.-D-Glucopyranose - 40.0 eV	Unknown	225.062	0.750502	390.349	225.062
CCMSLIB00006124728	.alpha.-D-Glucopyranose - 40.0 eV	Unknown	225.062	0.745217	518.7	225.062
CCMSLIB00006124728	.alpha.-D-Glucopyranose - 40.0 eV	Unknown	225.062	0.742908	791.588	225.062
CCMSLIB00006124728	.alpha.-D-Glucopyranose - 40.0 eV	Unknown	225.062	0.742908	777.029	225.062

CCMSLIB00000579680	0055_Triethylcitrate	M+H	277.128	0.88805	351.691	277.128
CCMSLIB00005467655	1-beta-D-Glucopyranosyl-L-tryptophan	M+H	367.15	0.656263	88.282	367.15
CCMSLIB00005724601	1-methyl-4-(6-methylhept-5-en-2-yl)-2,3-dioxabicyclo[2.2.2]oct-5-ene	M-2H2O+H	201.164	0.936838	304.049	201.164
CCMSLIB00005725033	1-methyl-4-methylidene-7-(propan-2-yl)-1,2,3,3a,4,5,6,8a-octahydroazulen-1-ol	M-H2O+H	203.179	0.883698	365.317	203.179
CCMSLIB00005725033	1-methyl-4-methylidene-7-(propan-2-yl)-1,2,3,3a,4,5,6,8a-octahydroazulen-1-ol	M-H2O+H	203.179	0.831559	388.246	203.179
CCMSLIB00005725033	1-methyl-4-methylidene-7-(propan-2-yl)-1,2,3,3a,4,5,6,8a-octahydroazulen-1-ol	M-H2O+H	203.179	0.811458	348.908	203.179
CCMSLIB00010120723	2-(3-carboxypropanoylamino)hexanoic acid CollisionEnergy:205060	M+H	232.118	0.870157	266.575	232.118
CCMSLIB00005883983	2-DEOXY-D-GLUCOSE - 40.0 eV	M+H	165.076	0.970204	111.107	165.076
CCMSLIB00005883983	2-DEOXY-D-GLUCOSE - 40.0 eV	M+H	165.076	0.943108	89.109	165.076
CCMSLIB00005883983	2-DEOXY-D-GLUCOSE - 40.0 eV	M+H	165.076	0.93905	79.795	165.076
CCMSLIB00005883983	2-DEOXY-D-GLUCOSE - 40.0 eV	M+H	165.076	0.93905	42.546	165.076
CCMSLIB00005883983	2-DEOXY-D-GLUCOSE - 40.0 eV	M+H	165.076	0.906686	131.45	165.076
CCMSLIB00005883983	2-DEOXY-D-GLUCOSE - 40.0 eV	M+H	165.076	0.895641	893.075	165.076
CCMSLIB00005883983	2-DEOXY-D-GLUCOSE - 40.0 eV	M+H	165.076	0.888106	175.043	165.076
CCMSLIB00005883983	2-DEOXY-D-GLUCOSE - 40.0 eV	M+H	165.076	0.876774	744.501	165.076
CCMSLIB00005883983	2-DEOXY-D-GLUCOSE - 40.0 eV	M+H	165.076	0.873492	216.453	165.076
CCMSLIB00005883983	2-DEOXY-D-GLUCOSE - 40.0 eV	M+H	165.076	0.865006	61.011	165.076
CCMSLIB00005883983	2-DEOXY-D-GLUCOSE - 40.0 eV	M+H	165.076	0.83461	847.851	165.076
CCMSLIB00005883983	2-DEOXY-D-GLUCOSE - 40.0 eV	M+H	165.076	0.80154	203.999	165.076
CCMSLIB00005883983	2-DEOXY-D-GLUCOSE - 40.0 eV	M+H	165.076	0.75902	16.435	165.076
CCMSLIB00006682458	2-ISOPROPYLMALIC ACID	M-H	175.061	0.85045	124.009	175.061
CCMSLIB00004692351	2-methyl-3-[(2S,3R,4S,5S,6R)-3,4,5-trihydroxy-6-(hydroxymethyl)oxan-2-yl]oxypyran-4-one	[M+H]+	289.092	0.8858	60.317	289.092

CCMSLIB00004708653	3-[(1-Carboxyvinyl)oxy]benzoic acid	[M-H]-	207.03	0.966901	302.368	207.03
CCMSLIB00004708392	3-[3-[3,4-dihydroxy-5-(6-oxo-3H-purin-9-yl)oxolan-2-yl]propanoyl]benzoic acid	[M+H]+	415.125	0.947425	275.279	415.125
CCMSLIB00004708380	3-[3-[3,4-dihydroxy-5-(6-oxo-3H-purin-9-yl)oxolan-2-yl]propanoyl]benzoic acid	[M-H]-	413.11	0.943486	272.79	413.11
CCMSLIB00010123099	32449-99-3 CollisionEnergy:205060	M-H	289.083	0.85287	273.326	289.083
CCMSLIB00004714368	3-oxo-3-[[(10E,20E)-5,7,9,19,23,25,27,31,33,34,35-undecahydroxy-8,10,14,18,22,26,30-heptamethyl-15-[(Z)-4-methyl-10-[(N'-methylcarbamimidoyl)amino]dec-4-en-2-yl]-17-oxo-16,37-dioxabicyclo[31.3.1]heptatriaconta-10,20-dien-3-yl]oxy]propanoic acid	[M-H]-	1128.72	0.889571	379.394	1128.72
CCMSLIB00004714368	3-oxo-3-[[(10E,20E)-5,7,9,19,23,25,27,31,33,34,35-undecahydroxy-8,10,14,18,22,26,30-heptamethyl-15-[(Z)-4-methyl-10-[(N'-methylcarbamimidoyl)amino]dec-4-en-2-yl]-17-oxo-16,37-dioxabicyclo[31.3.1]heptatriaconta-10,20-dien-3-yl]oxy]propanoic acid	[M-H]-	1128.72	0.774325	367.09	1128.72

CCMSLIB00004714380	3-oxo-3-[[(10E,20E)-5,7,9,19,23,25,27,31,33,34,35-undecahydroxy-8,10,14,18,22,26,30-heptamethyl-15-[(Z)-4-methyl-10-[(N'-methylcarbamimidoyl)amino]dec-4-en-2-yl]-17-oxo-16,37-dioxabicyclo[31.3.1]heptatriaconta-10,20-dien-3-yl]oxy]propanoic acid	[M+H]+	1130.73	0.709862	370.816	1130.73
CCMSLIB00004714380	3-oxo-3-[[(10E,20E)-5,7,9,19,23,25,27,31,33,34,35-undecahydroxy-8,10,14,18,22,26,30-heptamethyl-15-[(Z)-4-methyl-10-[(N'-methylcarbamimidoyl)amino]dec-4-en-2-yl]-17-oxo-16,37-dioxabicyclo[31.3.1]heptatriaconta-10,20-dien-3-yl]oxy]propanoic acid	[M+H]+	1130.73	0.673074	382.214	1130.73
CCMSLIB00005467915	4-O-Caffeoylquinic acid	M-H	353.09	0.842651	223.276	353.09
CCMSLIB00005467668	5'-Deoxy-5'-(methylsulfinyl)adenosine	M+H	314.09	0.918501	37.805	314.09
CCMSLIB00004720085	7-hydroxy-2-(4-hydroxyphenyl)-5-[(2S,3R,4S,5S,6R)-3,4,5-trihydroxy-6-(hydroxymethyl)oxan-2-yl]oxy-2,3-dihydrochromen-4-one	[M-H]-	433.114	0.918251	307.421	433.114
CCMSLIB00006717995	8-5'-Benzofuran-diferulic acid	M-H	385.094	0.711977	303.292	385.094
CCMSLIB00010114511	AC1L1X1Z CollisionEnergy:102040	M+Na	637.302	0.66412	530.756	637.302
CCMSLIB00004721671	ACARBOSE	[M+K]+	684.211	0.761446	729.707	684.211
CCMSLIB00006125720	alpha,alpha-Trehalose - 40.0 eV	Unknown	387.115	0.863522	25.504	387.115
CCMSLIB00006125720	alpha,alpha-Trehalose - 40.0 eV	Unknown	387.115	0.804176	48.744	387.115
CCMSLIB00006684604	ASP-PHE	M-H	279.099	0.86843	97.646	279.099
CCMSLIB00006684604	ASP-PHE	M-H	279.099	0.86843	79.628	279.099

CCMSLIB00006684604	ASP-PHE	M-H	279.099	0.820568	123.645	279.099
CCMSLIB00006684929	ASP-PHE	M+H	281.113	0.760378	102.056	281.113
CCMSLIB00006684929	ASP-PHE	M+H	281.113	0.734286	130.979	281.113
CCMSLIB00011427783	BAICALIN	M-H	445.078	0.943585	301.96	445.078
CCMSLIB00010113651	CHLOROGENIC ACID CollisionEnergy:102040	M+H	355.102	0.966854	222.217	355.102
CCMSLIB00006679584	CITRIC ACID	M-H	191.02	0.983188	288.319	191.02
CCMSLIB00005436263	Contaminants septum vial Thermo C4000-53 and C4000-54 serie	M+H	610.184	0.689031	684.863	610.184
CCMSLIB00005436264	Contaminants septum vial Thermo C4000-53 and C4000-54 serie	M+H	536.165	0.655019	649.398	536.165
CCMSLIB00005436265	Contaminants septum vial Thermo C4000-53 and C4000-54 serie	M+H	758.222	0.653972	665.563	758.222
CCMSLIB00011430184	cryptochlorogenic acid	M-H	353.089	0.885074	245.594	353.089
CCMSLIB00006113174	D-Galactitol - 40.0 eV	M-H	181.072	0.928927	288.665	181.072
CCMSLIB00006113174	D-Galactitol - 40.0 eV	M-H	181.072	0.928927	300.891	181.072
CCMSLIB00005719626	D-Mannitol	[M-H+HCOOH]	227.077	0.938027	400.54	227.077
CCMSLIB00005719017	D-Mannitol	[M-H+HCOOH]	227.077	0.93666	596.171	227.077
CCMSLIB00005719626	D-Mannitol	[M-H+HCOOH]	227.077	0.933502	890.964	227.077
CCMSLIB00005719966	D-Mannitol	[M+NH4]	200.113	0.932795	40.328	200.113
CCMSLIB00005719017	D-Mannitol	[M-H+HCOOH]	227.077	0.932576	762.304	227.077
CCMSLIB00005719626	D-Mannitol	[M-H+HCOOH]	227.077	0.928404	188.743	227.077
CCMSLIB00005719626	D-Mannitol	[M-H+HCOOH]	227.077	0.92829	458.79	227.077
CCMSLIB00005719626	D-Mannitol	[M-H+HCOOH]	227.077	0.92829	529.202	227.077

CCMSLIB00005719626	D-Mannitol	[M-H+HCOOH]	227.077	0.92753	799.398	227.077
CCMSLIB00005719017	D-Mannitol	[M-H+HCOOH]	227.077	0.926874	476.084	227.077
CCMSLIB00005719017	D-Mannitol	[M-H+HCOOH]	227.077	0.92607	11.377	227.077
CCMSLIB00005719626	D-Mannitol	[M-H+HCOOH]	227.077	0.925384	340.739	227.077
CCMSLIB00005719626	D-Mannitol	[M-H+HCOOH]	227.077	0.922889	313.768	227.077
CCMSLIB00005719626	D-Mannitol	[M-H+HCOOH]	227.077	0.922721	353.836	227.077
CCMSLIB00005719626	D-Mannitol	[M-H+HCOOH]	227.077	0.922705	172.138	227.077
CCMSLIB00005719626	D-Mannitol	[M-H+HCOOH]	227.077	0.92264	263.073	227.077
CCMSLIB00005719626	D-Mannitol	[M-H+HCOOH]	227.077	0.92264	280.066	227.077
CCMSLIB00005719626	D-Mannitol	[M-H+HCOOH]	227.077	0.919383	368.009	227.077
CCMSLIB00005719626	D-Mannitol	[M-H+HCOOH]	227.077	0.917651	776.119	227.077
CCMSLIB00005719017	D-Mannitol	[M-H+HCOOH]	227.077	0.914469	633.237	227.077
CCMSLIB00005719017	D-Mannitol	[M-H+HCOOH]	227.077	0.914469	643.972	227.077
CCMSLIB00005719017	D-Mannitol	[M-H+HCOOH]	227.077	0.904716	433.101	227.077
CCMSLIB00005719017	D-Mannitol	[M-H+HCOOH]	227.077	0.903777	835.577	227.077
CCMSLIB00005719017	D-Mannitol	[M-H+HCOOH]	227.077	0.900275	216.235	227.077
CCMSLIB00005719966	D-Mannitol	[M+NH4]	200.113	0.899301	177.18	200.113
CCMSLIB00005719017	D-Mannitol	[M-H+HCOOH]	227.077	0.898894	297.38	227.077

CCMSLIB00005719017	D-Mannitol	[M-H+HCOOH]	227.077	0.895382	390.587	227.077
CCMSLIB00005719017	D-Mannitol	[M-H+HCOOH]	227.077	0.894696	850.765	227.077
CCMSLIB00005719017	D-Mannitol	[M-H+HCOOH]	227.077	0.893691	419.423	227.077
CCMSLIB00005719017	D-Mannitol	[M-H+HCOOH]	227.077	0.892862	489.827	227.077
CCMSLIB00005719017	D-Mannitol	[M-H+HCOOH]	227.077	0.88957	207.035	227.077
CCMSLIB00005719017	D-Mannitol	[M-H+HCOOH]	227.077	0.889544	663.763	227.077
CCMSLIB00005719017	D-Mannitol	[M-H+HCOOH]	227.077	0.884776	55.848	227.077
CCMSLIB00005719017	D-Mannitol	[M-H+HCOOH]	227.077	0.884776	75.119	227.077
CCMSLIB00005719017	D-Mannitol	[M-H+HCOOH]	227.077	0.884776	32.08	227.077
CCMSLIB00005719966	D-Mannitol	[M+NH4]	200.113	0.876411	142.143	200.113
CCMSLIB00005719017	D-Mannitol	[M-H+HCOOH]	227.077	0.869275	874.406	227.077
CCMSLIB00005719626	D-Mannitol	[M-H+HCOOH]	227.077	0.828416	234.15	227.077
CCMSLIB00005719965	D-Mannitol	[M+H]	183.087	0.826453	184.04	183.087
CCMSLIB00005719626	D-Mannitol	[M-H+HCOOH]	227.077	0.818211	104.948	227.077
CCMSLIB00010102807	D-mannitol CollisionEnergy:102040	M-H	181.072	0.951635	786.669	181.072
CCMSLIB00010102807	D-mannitol CollisionEnergy:102040	M-H	181.072	0.951253	653.778	181.072
CCMSLIB00010102807	D-mannitol CollisionEnergy:102040	M-H	181.072	0.951253	664.514	181.072
CCMSLIB00010102807	D-mannitol CollisionEnergy:102040	M-H	181.072	0.944974	478.903	181.072
CCMSLIB00010102807	D-mannitol CollisionEnergy:102040	M-H	181.072	0.944843	893.184	181.072
CCMSLIB00010102807	D-mannitol CollisionEnergy:102040	M-H	181.072	0.943247	131.262	181.072
CCMSLIB00010102807	D-mannitol CollisionEnergy:102040	M-H	181.072	0.926956	878.671	181.072

CCMSLIB00005884962	D-SORBITOL - 20.0 eV	M+H	183.086	0.769253	392.093	183.086
CCMSLIB00005884962	D-SORBITOL - 20.0 eV	M+H	183.086	0.766002	871.18	183.086
CCMSLIB00005884962	D-SORBITOL - 20.0 eV	M+H	183.086	0.746849	820.549	183.086
CCMSLIB00005884962	D-SORBITOL - 20.0 eV	M+H	183.086	0.738694	848.591	183.086
CCMSLIB00005884962	D-SORBITOL - 20.0 eV	M+H	183.086	0.737873	10.783	183.086
CCMSLIB00005884962	D-SORBITOL - 20.0 eV	M+H	183.086	0.720844	328.529	183.086
CCMSLIB00005884962	D-SORBITOL - 20.0 eV	M+H	183.086	0.69769	792.524	183.086
CCMSLIB00005884962	D-SORBITOL - 20.0 eV	M+H	183.086	0.691414	892.884	183.086
CCMSLIB00010102811	D-Sorbitol CollisionEnergy:102040	M-H	181.072	0.979074	490.632	181.072
CCMSLIB00010102811	D-Sorbitol CollisionEnergy:102040	M-H	181.072	0.97079	710.689	181.072
CCMSLIB00010102811	D-Sorbitol CollisionEnergy:102040	M-H	181.072	0.963725	67.813	181.072
CCMSLIB00010102811	D-Sorbitol CollisionEnergy:102040	M-H	181.072	0.961654	838.961	181.072
CCMSLIB00010102811	D-Sorbitol CollisionEnergy:102040	M-H	181.072	0.955316	336.424	181.072
CCMSLIB00010102811	D-Sorbitol CollisionEnergy:102040	M-H	181.072	0.953522	468.044	181.072
CCMSLIB00010102811	D-Sorbitol CollisionEnergy:102040	M-H	181.072	0.936859	598.572	181.072
CCMSLIB00010102811	D-Sorbitol CollisionEnergy:102040	M-H	181.072	0.935195	51.422	181.072
CCMSLIB00010102811	D-Sorbitol CollisionEnergy:102040	M-H	181.072	0.923746	641.934	181.072
CCMSLIB00010102811	D-Sorbitol CollisionEnergy:102040	M-H	181.072	0.922891	199.76	181.072
CCMSLIB00010102811	D-Sorbitol CollisionEnergy:102040	M-H	181.072	0.920409	385.444	181.072
CCMSLIB00010102811	D-Sorbitol CollisionEnergy:102040	M-H	181.072	0.912134	501.26	181.072
CCMSLIB00010102811	D-Sorbitol CollisionEnergy:102040	M-H	181.072	0.908952	772.981	181.072
CCMSLIB00010102811	D-Sorbitol CollisionEnergy:102040	M-H	181.072	0.888271	371.062	181.072
CCMSLIB00010102811	D-Sorbitol CollisionEnergy:102040	M-H	181.072	0.884154	447.818	181.072
CCMSLIB00010102811	D-Sorbitol CollisionEnergy:102040	M-H	181.072	0.876649	117.243	181.072
CCMSLIB00006679960	ELAIDIC ACID	M+H	283.263	0.796219	507.023	283.263
CCMSLIB00006679960	ELAIDIC ACID	M+H	283.263	0.767402	521.248	283.263
CCMSLIB00006126861	Formylkynurenine	M+H	237.087	0.677175	57.28	237.087
CCMSLIB00005464191	GALACTITOL	M-H	181.072	0.899188	855.149	181.072

CCMSLIB00005464191	GALACTITOL	M-H	181.072	0.86618	9.705	181.072
CCMSLIB00005464191	GALACTITOL	M-H	181.072	0.849164	624.621	181.072
CCMSLIB00005464191	GALACTITOL	M-H	181.072	0.845158	687.399	181.072
CCMSLIB00005464191	GALACTITOL	M-H	181.072	0.820859	800.631	181.072
CCMSLIB00010102810	galactitol CollisionEnergy:102040	M-H	181.072	0.950579	167.87	181.072
CCMSLIB00010102810	galactitol CollisionEnergy:102040	M-H	181.072	0.950579	180.927	181.072
CCMSLIB00010102810	galactitol CollisionEnergy:102040	M-H	181.072	0.946514	279.639	181.072
CCMSLIB00010102810	galactitol CollisionEnergy:102040	M-H	181.072	0.935704	85.625	181.072
CCMSLIB00010102810	galactitol CollisionEnergy:102040	M-H	181.072	0.930481	586.796	181.072
CCMSLIB00010102810	galactitol CollisionEnergy:102040	M-H	181.072	0.927953	149.855	181.072
CCMSLIB00010102810	galactitol CollisionEnergy:102040	M-H	181.072	0.923985	430.423	181.072
CCMSLIB00010102810	galactitol CollisionEnergy:102040	M-H	181.072	0.920075	244.469	181.072
CCMSLIB00010102810	galactitol CollisionEnergy:102040	M-H	181.072	0.913925	260.011	181.072
CCMSLIB00010102810	galactitol CollisionEnergy:102040	M-H	181.072	0.894604	357.028	181.072
CCMSLIB00010102810	galactitol CollisionEnergy:102040	M-H	181.072	0.894604	316.854	181.072
CCMSLIB00010102810	galactitol CollisionEnergy:102040	M-H	181.072	0.871624	829.36	181.072
CCMSLIB00010102810	galactitol CollisionEnergy:102040	M-H	181.072	0.858368	512.559	181.072
CCMSLIB00010102810	galactitol CollisionEnergy:102040	M-H	181.072	0.795193	749.983	181.072
CCMSLIB00010102810	galactitol CollisionEnergy:102040	M-H	181.072	0.714044	418.006	181.072
CCMSLIB00004683268	Glc-Glc-octadecatrienoyl-sn-glycerol (isomer 1) (PUT) - 45.8016eV	M-H	721.361	0.724997	437.058	721.361
CCMSLIB00005788066	Glochidone	M+H	423.362	0.677196	405.425	423.362
CCMSLIB00010102601	gluconic acid CollisionEnergy:102040	M-H	195.051	0.970915	32.278	195.051
CCMSLIB00010102601	gluconic acid CollisionEnergy:102040	M-H	195.051	0.81431	43.116	195.051
CCMSLIB00000479622	Glucose	M-H	179.063	0.976854	31.534	179.063
CCMSLIB00006553955	linoleic acid	[M+Na]+	303.23	0.614522	509.72	303.23
CCMSLIB00006124011	Maltotriose - 40.0 eV	Unknown	549.168	0.785992	27.583	549.168
CCMSLIB00006679572	MANNITOL	M+H	183.086	0.953244	79.955	183.086

CCMSLIB00006679572	MANNITOL	M+H	183.086	0.953244	104.732	183.086
CCMSLIB00006679572	MANNITOL	M+H	183.086	0.952789	38.002	183.086
CCMSLIB00006679572	MANNITOL	M+H	183.086	0.935926	272.607	183.086
CCMSLIB00006679572	MANNITOL	M+H	183.086	0.918042	156.57	183.086
CCMSLIB00006679572	MANNITOL	M+H	183.086	0.917664	62.549	183.086
CCMSLIB00006679572	MANNITOL	M+H	183.086	0.905709	749.453	183.086
CCMSLIB00006679572	MANNITOL	M+H	183.086	0.898728	291.906	183.086
CCMSLIB00006679572	MANNITOL	M+H	183.086	0.898514	481.958	183.086
CCMSLIB00006679572	MANNITOL	M+H	183.086	0.890024	547.164	183.086
CCMSLIB00006679572	MANNITOL	M+H	183.086	0.881946	120.887	183.086
CCMSLIB00006679572	MANNITOL	M+H	183.086	0.875748	147.437	183.086
CCMSLIB00006679572	MANNITOL	M+H	183.086	0.869585	518.97	183.086
CCMSLIB00006680924	MANNITOL	M+H	183.086	0.820014	224.285	183.086
CCMSLIB00006680924	MANNITOL	M+H	183.086	0.777597	209.935	183.086
CCMSLIB00006680924	MANNITOL	M+H	183.086	0.750813	352.506	183.086
CCMSLIB00006684047	MANNITOL	M+H	183.086	0.724129	261.391	183.086
CCMSLIB00005884956	MANNITOL - 20.0 eV	M+H	183.086	0.729788	780.829	183.086
CCMSLIB00005726579	Massbank: Lauramidopropyl betaine|3-(Dodecanoylamino)propyl(carboxymethyl)dimethylammonium|carboxymethyl-[3-(dodecanoylamino)propyl]-dimethylazanium	M	343.296	0.951167	400.843	343.296
CCMSLIB00005731255	Massbank:EQ331603 Linoleic acid|(9Z,12Z)-octadeca-9,12-dienoic acid	M+H	281.247	0.750611	535.839	281.247
CCMSLIB00005732848	Massbank:EQ367252 Diethyl-phthalate|Diethyl phthalate|Diethyl benzene-1,2-dicarboxylate	M-H	221.082	0.817245	376.5	221.082

CCMSLIB00005760659	Massbank:LU052302 Acetyl tributyl citrate|tributyl 2-acetyloxypropane-1,2,3-tricarboxylate	M+H	403.233	0.930061	501.84	403.233
CCMSLIB00000221707	Massbank:PB000416 Tryptophan|2-amino-3-(1H-indol-3-yl)propanoic acid	[M+H]+	205.098	0.818149	90.735	205.098
CCMSLIB00005739405	Massbank:PR308349 Soyasaponin Ba	M-H	957.506	0.771791	392.545	957.506
CCMSLIB00005740058	Massbank:PR309076 FA 18:4+2O	M-H	307.19	0.777294	389.189	307.19
CCMSLIB00005746967	Massbank:PR309108 FA 18:1+3O	M-H	329.231	0.8031	361.494	329.231
CCMSLIB00005740091	Massbank:PR309201 Coumaroyl + C6H9O8 (isomer of 843, 844, 846)	M-H	355.066	0.709291	97.464	355.066
CCMSLIB00005746433	Massbank:PR309340 12:4+3O fatty acyl hexoside	M-H	387.166	0.633121	263.415	387.166
CCMSLIB00005739356	Massbank:PR310846 LPC 18:1	M+H	522.356	0.769107	508.33	522.356
CCMSLIB00005748443	Massbank:PR311013 Feruloyl putrescine (isomer of 1173)	M+H	265.155	0.809876	164.256	265.155
CCMSLIB00005739084	Massbank:PR311142 Cyclo(leucylprolyl)	M+H	211.144	0.746827	273.615	211.144
CCMSLIB00005738623	Massbank:RP030402 ?-linolenic acid|linolenic acid|(9Z,12Z,15Z)-octadeca-9,12,15-trienoic acid	M+H	279.232	0.662896	518.19	279.232
CCMSLIB00000567955	MoNA:790536 Linoleic acid	M+H	281.247	0.635426	438.209	281.247
CCMSLIB00000568813	MoNA:947057 2-{6-[(2-{5`-[6-hydroxy-6-(hydroxymethyl)-3,5-dimethyltetrahydro-2h-pyran-2-yl]-2,3`-dimethyloctahydro-2,2`-bifuran-5-yl}-9-methoxy-2,4,10-trimethyl-1,6-dioxaspiro[4.5]dec-7-yl)methyl]-3-methyltetrahydro-2h-pyran-2-yl}propanoic acid	M-H	723.469	0.892811	519.817	723.469
CCMSLIB00006684384	N-ACETYLTRYPTOPHAN	M-H	245.093	0.926712	290.262	245.093

CCMSLIB00000850011	NCGC00168953-02_C47H76O17_(3beta,5xi,9xi,22beta)-22,24-Dihydroxyolean-12-en-3-yl 6-deoxy-alpha-L-mannopyranosyl-(1->2)-alpha-L-arabinopyranosyl-(1->2)-beta-D-glucopyranosiduronic acid	M+H	913.516	0.753354	402.292	913.516
CCMSLIB00000848957	NCGC00169122-02!2-oct-1-en-3-yloxy-6-[(3,4,5-trihydroxyoxan-2-yl)oxymethyl]oxane-3,4,5-triol	M+NH4	440.249	0.655273	323.434	440.249
CCMSLIB00000853933	NCGC00380376-01_C22H40O3_1-Naphthalenepentanol, decahydro-2-hydroxy-gamma,2,5,5,8a-pentamethyl-, alpha-acetate	M-H2O+H	335.294	0.785621	398.76	335.294
CCMSLIB00000853933	NCGC00380376-01_C22H40O3_1-Naphthalenepentanol, decahydro-2-hydroxy-gamma,2,5,5,8a-pentamethyl-, alpha-acetate	M-H2O+H	335.294	0.747295	386.562	335.294
CCMSLIB00000851506	NCGC00380522-01_C20H30O4_1-Phenanthrenecarboxylic acid, 1,2,3,4,4a,4b,5,6,7,9,10,10a-dodecahydro-7-hydroxy-1,4a-dimethyl-7-(1-methylethyl)-9-oxo-	M-H2O+H	317.211	0.608048	445.162	317.211
CCMSLIB00000852268	NCGC00380878-01_C18H28O9_Cyclopentaneacetic acid, 2-[(2Z)-5-(hexopyranosyloxy)-2-penten-1-yl]-3-oxo-, (1R,2R)-	M+NH4	406.207	0.621225	264.208	406.207
CCMSLIB00000852714	NCGC00380976-01_C28H42N2O7_(4E,10E)-13,20-Dihydroxy-8,14-dimethoxy-4,10,12,16-tetramethyl-3-oxo-2-azabicyclo[16.3.1]docosa-1(22),4,10,18,20-pentaen-9-yl carbamate	M+NH4	536.333	0.777354	337.938	536.333

CCMSLIB00000851295	NCGC00381308-01_C47H76O17_(3beta,5xi,9xi,18xi,22beta)-22,25-Dihydroxyolean-12-en-3-yl 6-deoxy-alpha-L-mannopyranosyl-(1->2)-beta-D-xylopyranosyl-(1->2)-beta-D-glucopyranosiduronic acid	M-H	911.501	0.725936	405.823	911.501
CCMSLIB00000854306	NCGC00385106-01_C18H26O10_beta-D-Glucopyranoside, phenylmethyl 6-O-[(2R,3R,4R)-tetrahydro-3,4-dihydroxy-4-(hydroxymethyl)-2-furanyl]-	M+NH4	420.186	0.699108	254.153	420.186
CCMSLIB00000855491	NCGC00385952-01_C15H26O_1,7-Dimethyl-7-(4-methyl-3-penten-1-yl)bicyclo[2.2.1]heptan-2-ol	M-H2O+H	205.195	0.700096	457.132	205.195
CCMSLIB00010099321	PC(18:2/0:0); [M+H]+ C26H51N1O7P1	M+H	520.34	0.94987	480.235	520.34
CCMSLIB00010099315	PE(18:2/0:0); [M+H]+ C23H45N1O7P1	M+H	478.293	0.811195	462.844	478.293
CCMSLIB00006684394	RIBOFLAVIN	M+H	377.146	0.918556	265.609	377.146
CCMSLIB00004702149	Salidroside	[M+NH4]+	318.155	0.89282	131.588	318.155
CCMSLIB00006112641	Sorbitol - 30.0 eV	M-H	181.072	0.85512	407.901	181.072
CCMSLIB00006112641	Sorbitol - 30.0 eV	M-H	181.072	0.808789	219.24	181.072
CCMSLIB00003136757	Spectral Match to .alpha.-L-Asp-L-Phe from NIST14	M+H	281.112	0.66815	121.762	281.112
CCMSLIB00003138070	Spectral Match to .alpha.-Linolenoyl ethanolamide from NIST14	M+H	322.273	0.887435	425.916	322.273
CCMSLIB00003137471	Spectral Match to 1-(9Z-Octadecenoyl)-sn-glycero-3-phosphocholine from NIST14	M+Na	544.337	0.973119	533.541	544.337
CCMSLIB00003137820	Spectral Match to 12(13)-Epoxy-9Z-octadecenoic acid from NIST14	M+H-H2O	279.232	0.89533	424.163	279.232
CCMSLIB00003134969	Spectral Match to 12,13-DiHOME from NIST14	M+H-H2O	297.242	0.849298	425.401	297.242

CCMSLIB00003137023	Spectral Match to 13-Keto-9Z,11E-octadecadienoic acid from NIST14	M+H-H2O	277.216	0.902924	430.785	277.216
CCMSLIB00003134668	Spectral Match to 13-Keto-9Z,11E-octadecadienoic acid from NIST14	M+H	295.226	0.725462	430.16	295.226
CCMSLIB00003134668	Spectral Match to 13-Keto-9Z,11E-octadecadienoic acid from NIST14	M+H	295.226	0.725462	442.734	295.226
CCMSLIB00003137868	Spectral Match to 13-Keto-9Z,11E-octadecadienoic acid from NIST14	M+H	295.227	0.702886	366.238	295.227
CCMSLIB00003137992	Spectral Match to 13-Keto-9Z,11E-octadecadienoic acid from NIST14	M+H	295.227	0.600545	391.526	295.227
CCMSLIB00003136761	Spectral Match to 13S-Hydroxy-9Z,11E,15Z-octadecatrienoic acid from NIST14	M+H-H2O	277.216	0.930717	449.719	277.216
CCMSLIB00003136761	Spectral Match to 13S-Hydroxy-9Z,11E,15Z-octadecatrienoic acid from NIST14	M+H-H2O	277.216	0.880876	476.135	277.216
CCMSLIB00003139504	Spectral Match to 1-Hexadecanoyl-sn-glycero-3-phosphocholine from NIST14	M+Na	518.321	0.972804	516.431	518.321
CCMSLIB00003138475	Spectral Match to 1-Linoleoylglycerol from NIST14	M+H	355.284	0.757779	455.935	355.284
CCMSLIB00003138475	Spectral Match to 1-Linoleoylglycerol from NIST14	M+H	355.284	0.645589	518.744	355.284
CCMSLIB00003138475	Spectral Match to 1-Linoleoylglycerol from NIST14	M+H	355.284	0.60102	483.493	355.284
CCMSLIB00003139823	Spectral Match to 1-Myristoyl-sn-glycero-3-phosphocholine from NIST14	M+H	468.308	0.905015	457.379	468.308
CCMSLIB00003135997	Spectral Match to 3,5-Dimethyladamantan-1-amine from NIST14	M+H-NH3	163.148	0.892895	348.682	163.148
CCMSLIB00003140107	Spectral Match to 3-Hydroxyoctadecanoic Acid from NIST14	M+H-H2O	283.26	0.671987	554.292	283.26

CCMSLIB00003134812	Spectral Match to 9(10)-EpOME from NIST14	M+H-H2O	279.231	0.924502	462.116	279.231
CCMSLIB00003139203	Spectral Match to 9(10)-EpOME from NIST14	M+H	297.243	0.792804	404.816	297.243
CCMSLIB00003135516	Spectral Match to 9,10-Dihydroxy-12Z-octadecenoic acid from NIST14	M+H	315.253	0.717771	425.613	315.253
CCMSLIB00003135516	Spectral Match to 9,10-Dihydroxy-12Z-octadecenoic acid from NIST14	M+H	315.253	0.696521	399.926	315.253
CCMSLIB00003135516	Spectral Match to 9,10-Dihydroxy-12Z-octadecenoic acid from NIST14	M+H	315.253	0.66634	360.847	315.253
CCMSLIB00003137650	Spectral Match to 9-Octadecenamide, (Z)- from NIST14	M+H	282.28	0.927294	536.871	282.28
CCMSLIB00003139019	Spectral Match to 9-OxoOTrE from NIST14	M+H-H2O	275.201	0.707286	368.548	275.201
CCMSLIB00003136996	Spectral Match to 9Z,11E,13E-Octadecatrienoic acid methyl ester from NIST14	M+H	293.247	0.939929	502.349	293.247
CCMSLIB00003140066	Spectral Match to Arg-Ile from NIST14	M+H	288.202	0.819403	38.194	288.202
CCMSLIB00003139461	Spectral Match to Arg-Phe from NIST14	M+H	322.187	0.847995	47.379	322.187
CCMSLIB00003135381	Spectral Match to Asn-Phe from NIST14	M+H	280.129	0.712178	73.069	280.129
CCMSLIB00003137753	Spectral Match to Asp-Leu from NIST14	M+H	247.128	0.736195	69.757	247.128
CCMSLIB00003137753	Spectral Match to Asp-Leu from NIST14	M+H	247.128	0.712457	88.315	247.128
CCMSLIB00003137753	Spectral Match to Asp-Leu from NIST14	M+H	247.128	0.64983	59.17	247.128
CCMSLIB00003138617	Spectral Match to Didodecyl 3,3'-thiodipropionate oxide from NIST14	M+H	531.406	0.890097	637.187	531.406
CCMSLIB00003140080	Spectral Match to D-Mannitol from NIST14	M+H	183.086	0.829778	224.743	183.086
CCMSLIB00003136040	Spectral Match to Dodecanedioic acid from NIST14	M+H-H2O	213.147	0.820731	367.738	213.147
CCMSLIB00003136083	Spectral Match to D-Sorbitol from NIST14	M+H	183.086	0.888185	457.164	183.086
CCMSLIB00003136083	Spectral Match to D-Sorbitol from NIST14	M+H	183.086	0.758578	424.147	183.086
CCMSLIB00003136083	Spectral Match to D-Sorbitol from NIST14	M+H	183.086	0.752965	437.321	183.086
CCMSLIB00003139467	Spectral Match to Glu Phe from METLIN	M+H	295.128	0.948773	144.462	295.128

CCMSLIB00003140059	Spectral Match to Glu-Val-Phe from NIST14	M+H	394.197	0.638619	255.926	394.197
CCMSLIB00003137762	Spectral Match to Ile-Arg from NIST14	M+H	288.203	0.611141	53.333	288.203
CCMSLIB00003139641	Spectral Match to Ile-Gly-Ile from NIST14	M+H	302.207	0.9441	268.224	302.207
CCMSLIB00003136608	Spectral Match to Ile-Val-Lys from NIST14	M+H	359.268	0.641842	59.15	359.268
CCMSLIB00003137120	Spectral Match to Linoleoyl ethanolamide from NIST14	M+H	324.289	0.925841	499.773	324.289
CCMSLIB00003136698	Spectral Match to Lys-Leu from NIST14	M+H	260.197	0.913716	38.813	260.197
CCMSLIB00003138418	Spectral Match to Monolinolenin (9c,12c,15c) from NIST14	M+H	353.269	0.80204	442.608	353.269
CCMSLIB00003138418	Spectral Match to Monolinolenin (9c,12c,15c) from NIST14	M+H	353.269	0.765179	468.11	353.269
CCMSLIB00003138418	Spectral Match to Monolinolenin (9c,12c,15c) from NIST14	M+H	353.269	0.631379	398.163	353.269
CCMSLIB00003137681	Spectral Match to N-Oleoylethanolamine from NIST14	M+H	326.305	0.92625	523.745	326.305
CCMSLIB00003137028	Spectral Match to Pantothenic acid from NIST14	M+H	220.118	0.902976	55.107	220.118
CCMSLIB00003137028	Spectral Match to Pantothenic acid from NIST14	M+H	220.118	0.902976	71.046	220.118
CCMSLIB00003137597	Spectral Match to PyroGlu-Ile from NIST14	M+H	243.134	0.690784	243.216	243.134
CCMSLIB00003137597	Spectral Match to PyroGlu-Ile from NIST14	M+H	243.134	0.66628	222.658	243.134
CCMSLIB00003137591	Spectral Match to PyroGlu-Phe from NIST14	M+H	277.119	0.913438	279.973	277.119
CCMSLIB00003135329	Spectral Match to Ser-Ile from NIST14	M+H	219.134	0.846718	51.295	219.134
CCMSLIB00003137578	Spectral Match to Thr-Ile from NIST14	M+H	233.15	0.931988	41.914	233.15
CCMSLIB00003140084	Spectral Match to Thr-Leu from NIST14	M+H	233.149	0.961403	57.848	233.149
CCMSLIB00003140084	Spectral Match to Thr-Leu from NIST14	M+H	233.149	0.931762	109.642	233.149
CCMSLIB00003135017	Spectral Match to Thr-Phe from NIST14	M+H	267.134	0.949036	82.483	267.134
CCMSLIB00003136298	Spectral Match to Tropic acid from NIST14	M+H-H2O	149.06	0.961715	52.08	149.06

CCMSLIB00003139901	Spectral Match to Tyr-Pro from NIST14	M+H	279.133	0.926564	56.628	279.133
CCMSLIB00003136764	Spectral Match to Tyr-Pro from NIST14	M+H-H2O	261.123	0.667202	156.103	261.123
CCMSLIB00003135481	Spectral Match to Val-Arg from NIST14	M+H	274.187	0.644522	33.629	274.187
CCMSLIB00003134519	Spectral Match to Val-Gly-Val from NIST14	M+H	274.176	0.823784	71.901	274.176
CCMSLIB00003139580	Spectral Match to Val-Leu from NIST14	M+H	231.17	0.902491	64.129	231.17
CCMSLIB00003138480	Spectral Match to Val-Met from NIST14	M+H	249.126	0.92198	52.93	249.126
CCMSLIB00003136667	Spectral Match to Val-Val from NIST14	M+H	217.155	0.894688	42.938	217.155
CCMSLIB00010114542	stearic acid CollisionEnergy:102040	M+H-H2O	267.268	0.775069	502.049	267.268
CCMSLIB00005464529	TREHALOSE	M-H	341.109	0.926405	28.403	341.109
CCMSLIB00004719766	Trehalose	[M-H]-	341.109	0.864239	48.725	341.109

Supplementary figures

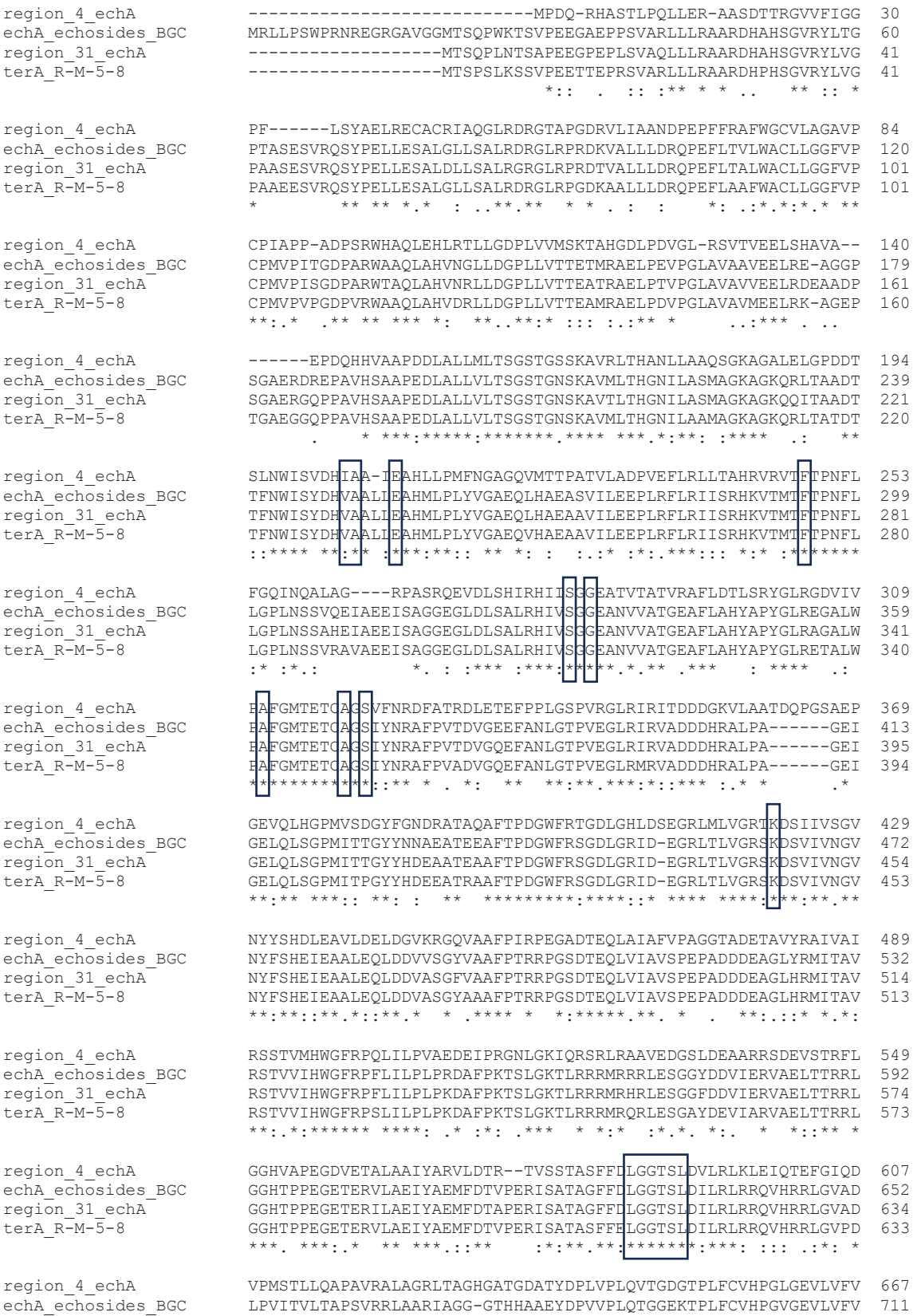

```
region_31_echA          LPVITVLTAPSVRQLAARLGDG-GTPDAAVYDPVVPLQTGGEKTPLFCVHPGVGEVLVFV  693
terA_R-M-5-8            LPVITVLTAPSVRQLAARLADG-GAPAAAAYDPVVPLQTGGRKTPLFCVHPGVGEVLVFV  692
                        :*: *:* **:** **.*:  * *:   * ***:****. *  *********:*******

region_4_echA           NLAKYFTGERPFYALRARGFGAGETHFESFADMVSTYVEAIRRAQPSGPYAVAGYSYGGA  727
echA_echosides_BGC      NLAKYFVGDRPFYALRARGFNEGEKPFTSFEEMVECYVEAIRARQPHGPYAIAGYSYGGA  771
region_31_echA          NLAKYFVGDRPFYALRARGFNEHEKPFTSFEEMVECYVEAIRARQPHGPYAVAGYSYGGA  753
terA_R-M-5-8            NLAKYFVGDRPFYALRARGFDEGEKPYTSFEEMVDCYVAAIRARQPHGPYAVAGYSYGGA  752
                        ******.*:***********.  *. : ** :**. ** ***  ** ****:*******

region_4_echA           VAFEIAKRLEADGDQVGFVGVFNLPPRISDRMNEITFTDGAINLALFLELIDASDIERLT  787
echA_echosides_BGC      VAFEIAKALEAQGERVDFAGSFNLPPHIKYRMDELDFIETATNLAFFLDLINKKQSLDLP  831
region_31_echA          VAFEIAKALEAQGERVDFVGSFNLPPHIKYRMEELDFVETATNLAFFLDLINKKQSLDLP  813
terA_R-M-5-8            VAFEIAKALEAQGERVDFVGSFNLPPHIKYRMEELDFVETATNLAFFLDLINKKQSLDLP  812
                        ******* ***:*::*.*.* *****:*. **:*: * : * ***:**:**: .:   *

region_4_echA           ATLRPLPEADQLAYLIDHAPKRRLTELDLSVERFTAWVHLAQSMVHLGRTYEPSGSVGQV  847
echA_echosides_BGC      AELRPLPREEQLAHLLRIAPRGRLDELDLDLGKFTAWAELAHGLTTLGRDYHPSGTTRSM  891
region_31_echA          AELRPLPQAEQLAHLLRIAPRGRLDELDLDLDTFSAWAELAHGLTTLGRDYHPSGTTRSM  873
terA_R-M-5-8            AELRPLPKEEQLARLLRIAPRGRLRELDLDLEKFTAWAELAHGLTALGRDYRPSGTTRSM  872
                        * *****. :*** *:  **: ** ****.:  *:**..**:.:. *** *.***:. .:

region_4_echA           KVFYCTPLRGTKEEWLEGQLSHWDEFTRDPNTYIEVDGEHYTLMSPQHVQTFQATLRQEL  907
echA_echosides_BGC      TVFYAIPLRGTKEDWLANELRRWDEFTTEPNRYLDVPGEHYTLMGPRHVAAFQAVLRREL  951
region_31_echA          TVFYAIPLRGTKEDWLANELRRWDEHTTEPNRYLDVPGEHYTLMGPRHVAAFQAVLRREL  933
terA_R-M-5-8            TVFYAIPLRGTKEDWLEHELRRWDEHTTEPNRYVDVPGEHYTLMGPRHVAAFQAILRREL  932
                        .***. *******:**  :* :***.* :** *::* *******.*:** :*** **:**

region_4_echA           ARALG-----------        912
echA_echosides_BGC      DRALGDADRARATGRA        967
region_31_echA          DHALGDADRARTAGQG        949
terA_R-M-5-8            DRALGDADRARTTGQA        948
                         :***
```

Figure S4.1. Clustal Omega alignment of the amino acid sequences of EchA homologues. The EchA amino acid sequence from regions 4 and 31 of 11-1-2 and from the terfestatin/echosides BGCs from *Streptomyces* sp. LZ35 and *Streptomyces* sp. R-M-5-8 were used for the alignment. The boxes represent signature domains of the proteins.

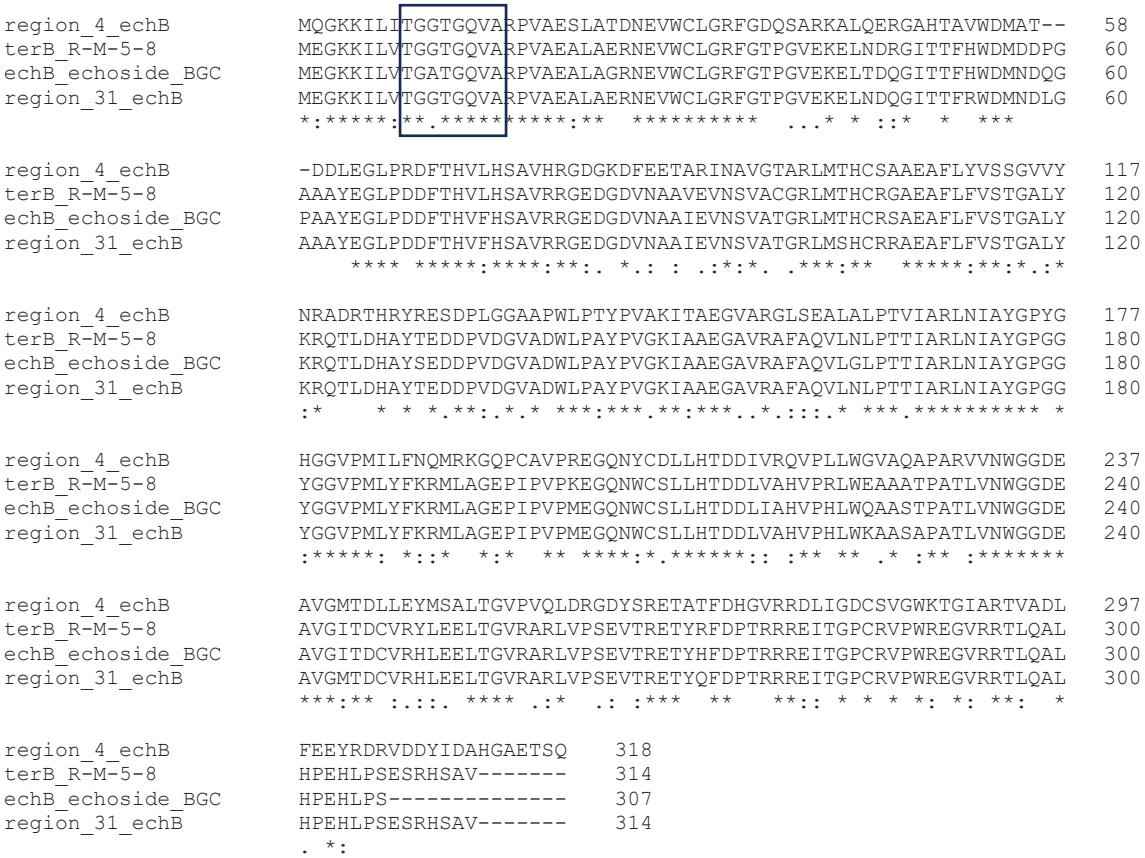

Figure S4.2. Clustal Omega alignment of the amino acid sequences of EchB homologues. The EchB amino acid sequence from regions 4 and 31 of 11-1-2 and from the terfestatin/echosides BGCs from *Streptomyces* sp. LZ35 and *Streptomyces* sp. R-M-5-8 were used for the alignment. The boxes represent signature domains of the proteins.

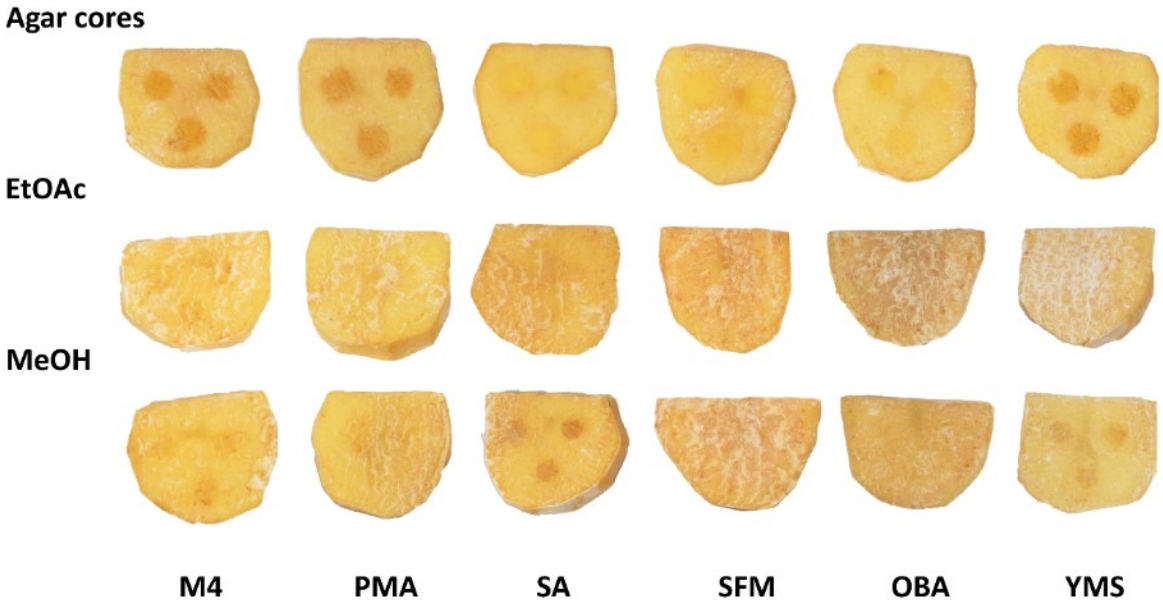

Figure S4.3. Control slices for the potato tuber slice assays using agar cores and organic culture extracts.

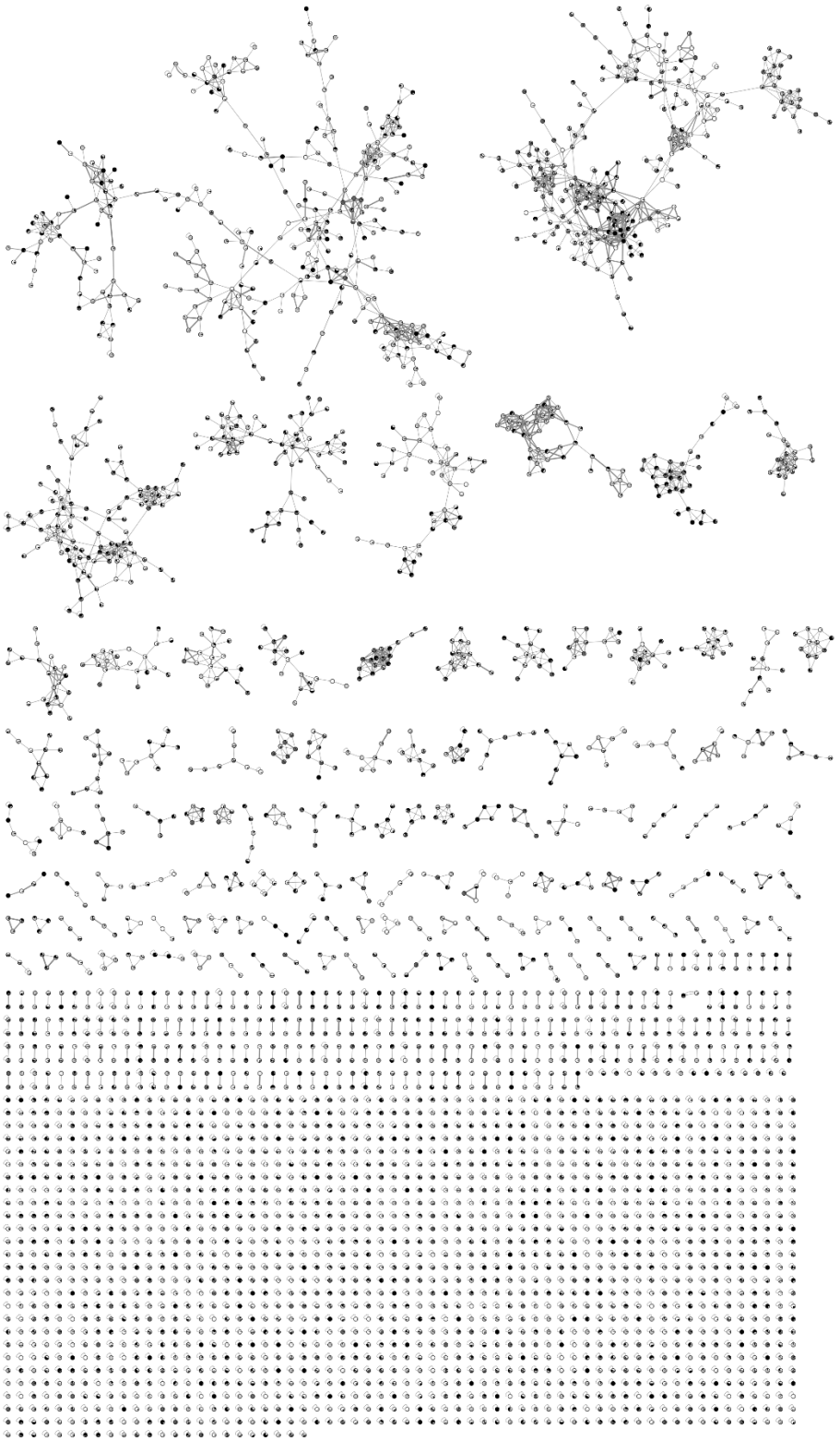

Figure S4.4. Molecular networks for the ethyl acetate extracts in the first dataset (IIMN_6.2). The pie chart represents a relative distribution of the peak area for different media: white = mMYM-, black = mMYM+, light grey = YMS-, dark grey = YMS+.

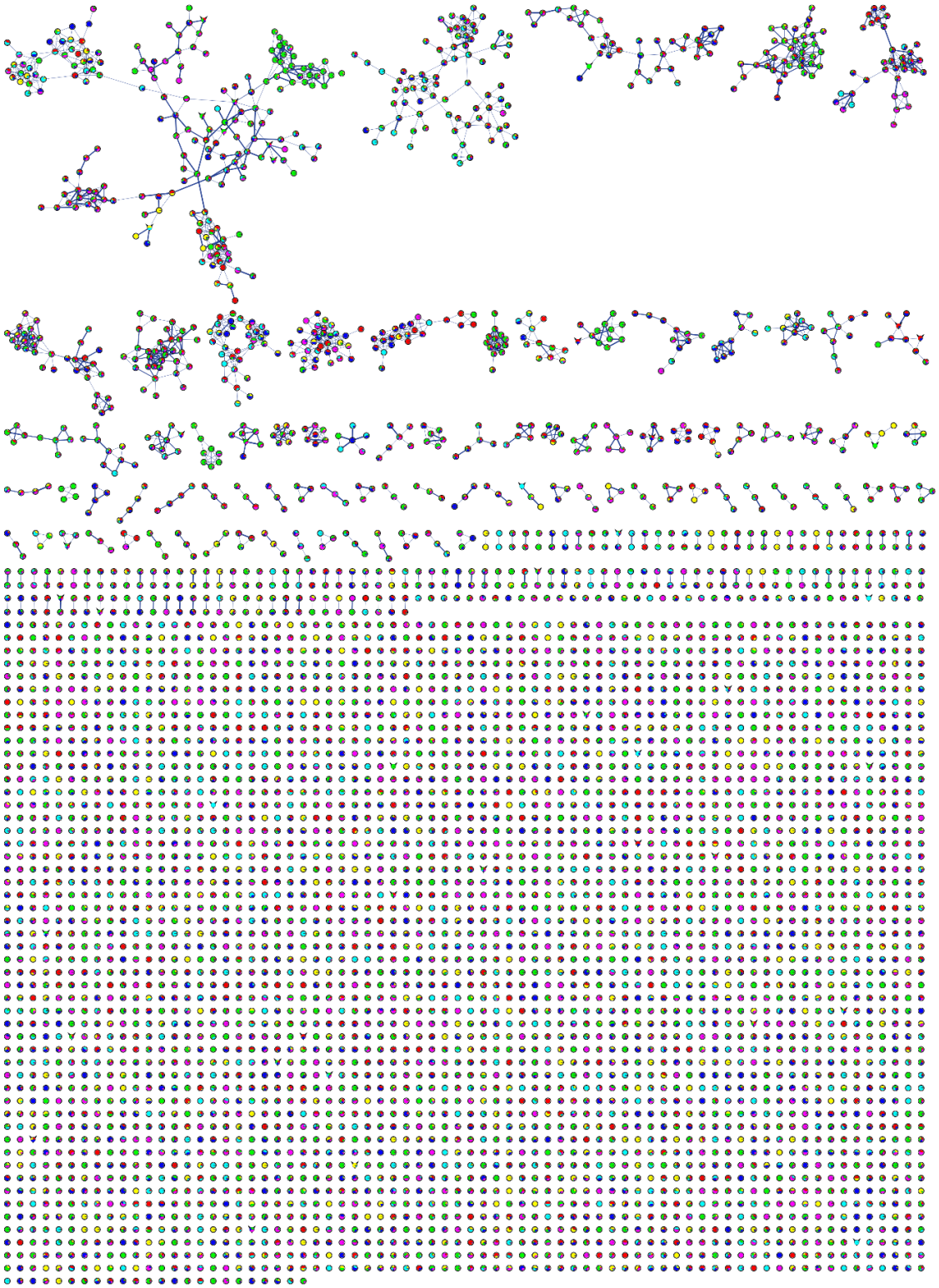

Figure S4.5. Molecular networks for the ethyl acetate extracts in the second dataset (IIMN_EtOAc). The pie chart represents a relative distribution of the peak area for different media: Red = M4, Yellow = OBA, Light green = PMA, Teal = SA, Blue = SFM, Violet = YMS.

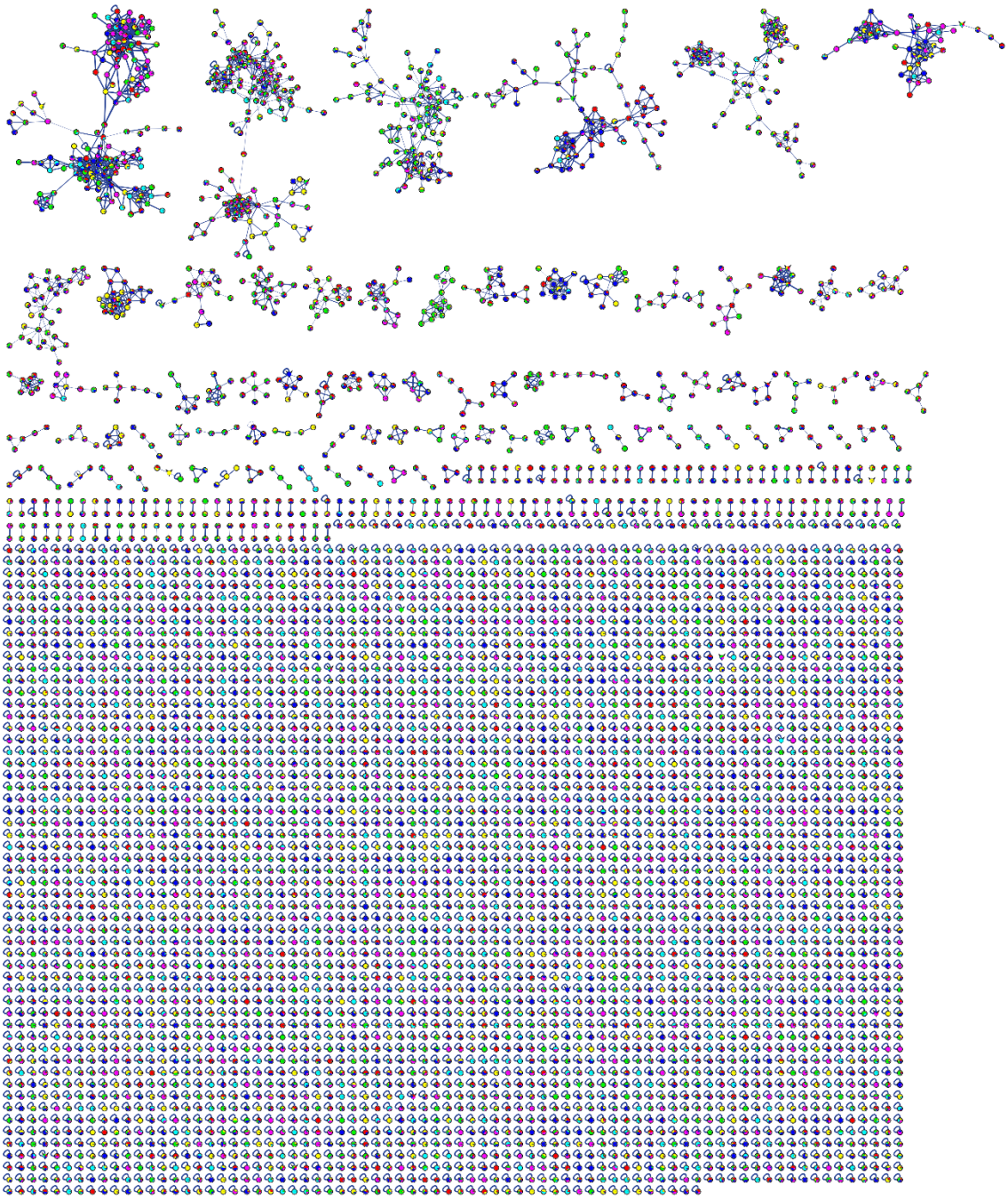

Figure S4.6. Molecular networks for the methanol extracts in the second dataset (IIMN_MeOH). The pie chart represents a relative distribution of the peak area for different media: Red = M4, Yellow = OBA, Light green = PMA, Teal = SA, Blue = SFM, Violet = YMS.

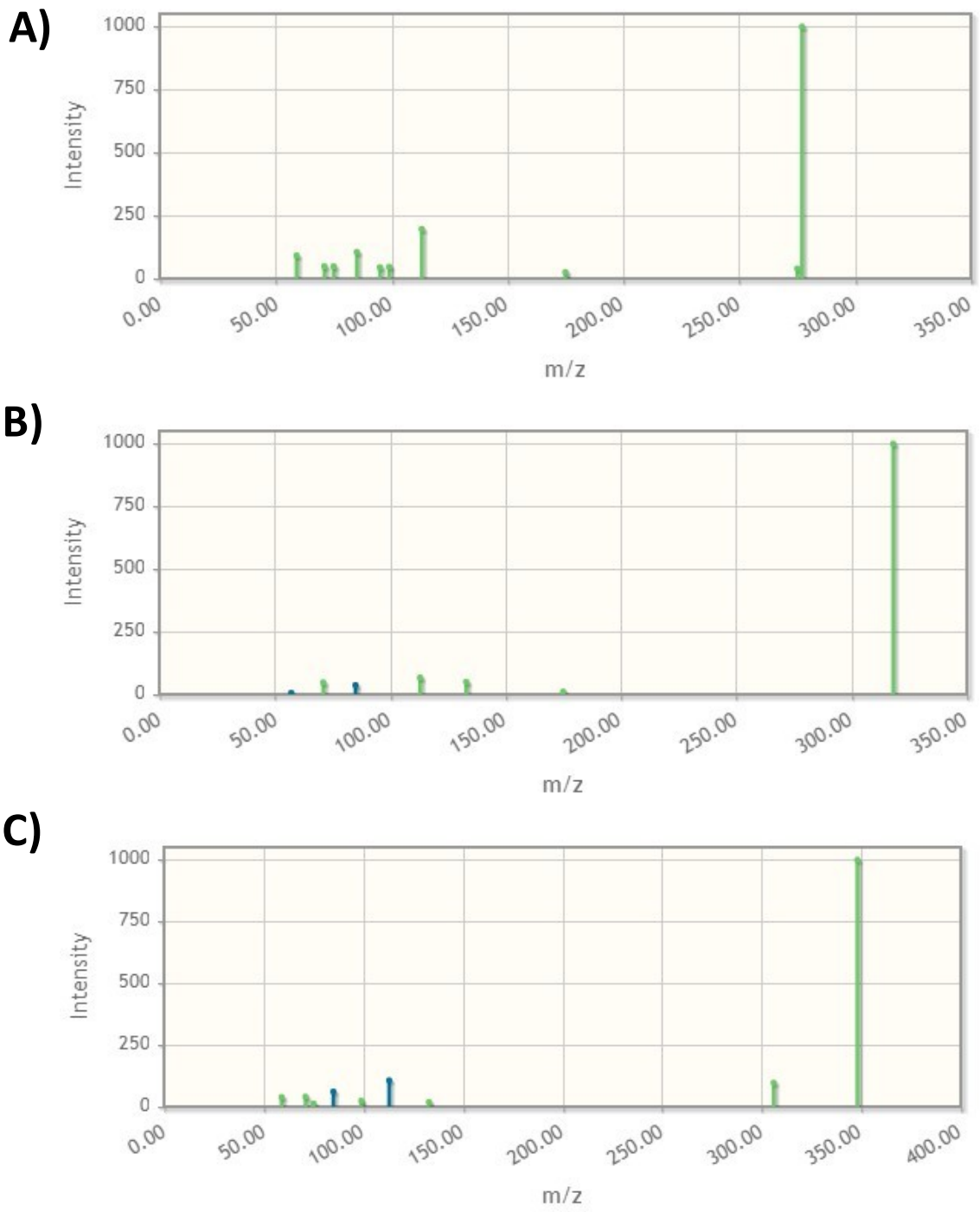

Figure S4.7. Fragmentation pattern comparison plot for echosides. The plots for echoside C (A), echoside D (B) and echoside E (C) are shown. Peaks in green represent matches between predicted and experimental spectra, while peaks in blue did not match. Peaks in grey were excluded from the comparison by MetFrag.

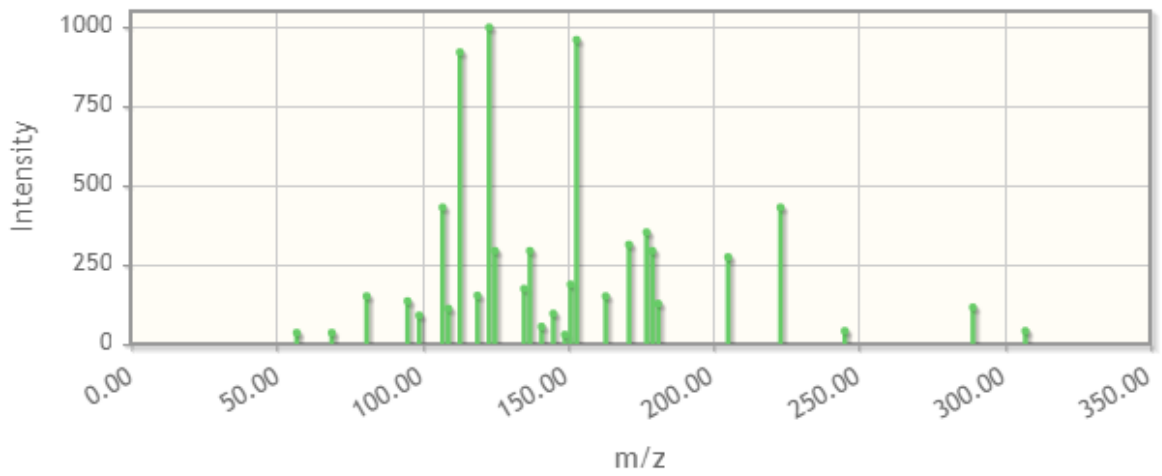

Figure S4.8. Fragmentation pattern comparison plot for galbobolide B. Peaks in green represent matches between predicted and experimental spectra, while peaks in blue did not match. Peaks in grey were excluded from the comparison by MetFrag.

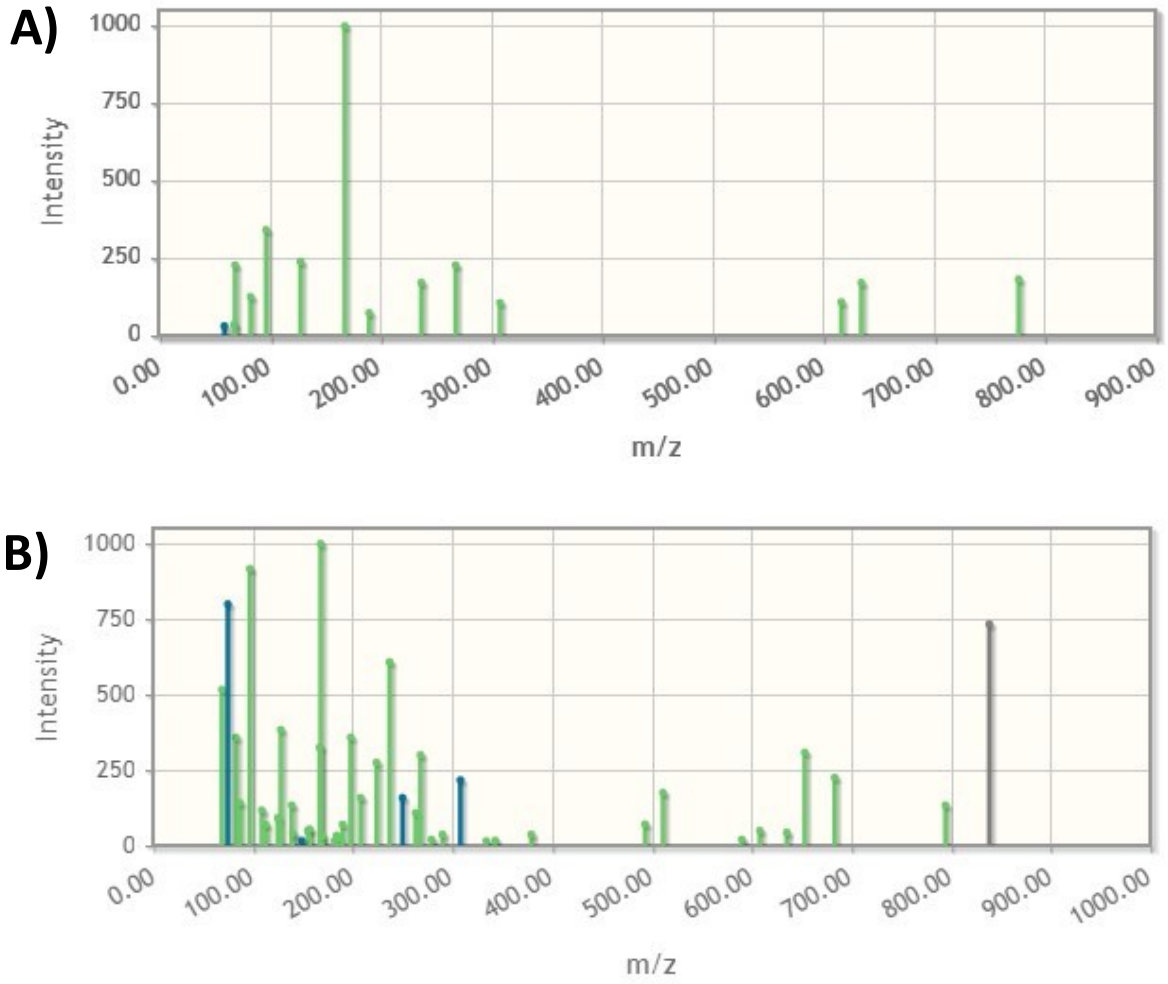

Figure S4.9. Fragmentation pattern comparison plot for meridamycins. The plots for meridamycin (A) and meridamycin A (B) are shown. Peaks in green represent matches between predicted and experimental spectra, while peaks in blue did not match. Peaks in grey were excluded from the comparison by MetFrag.

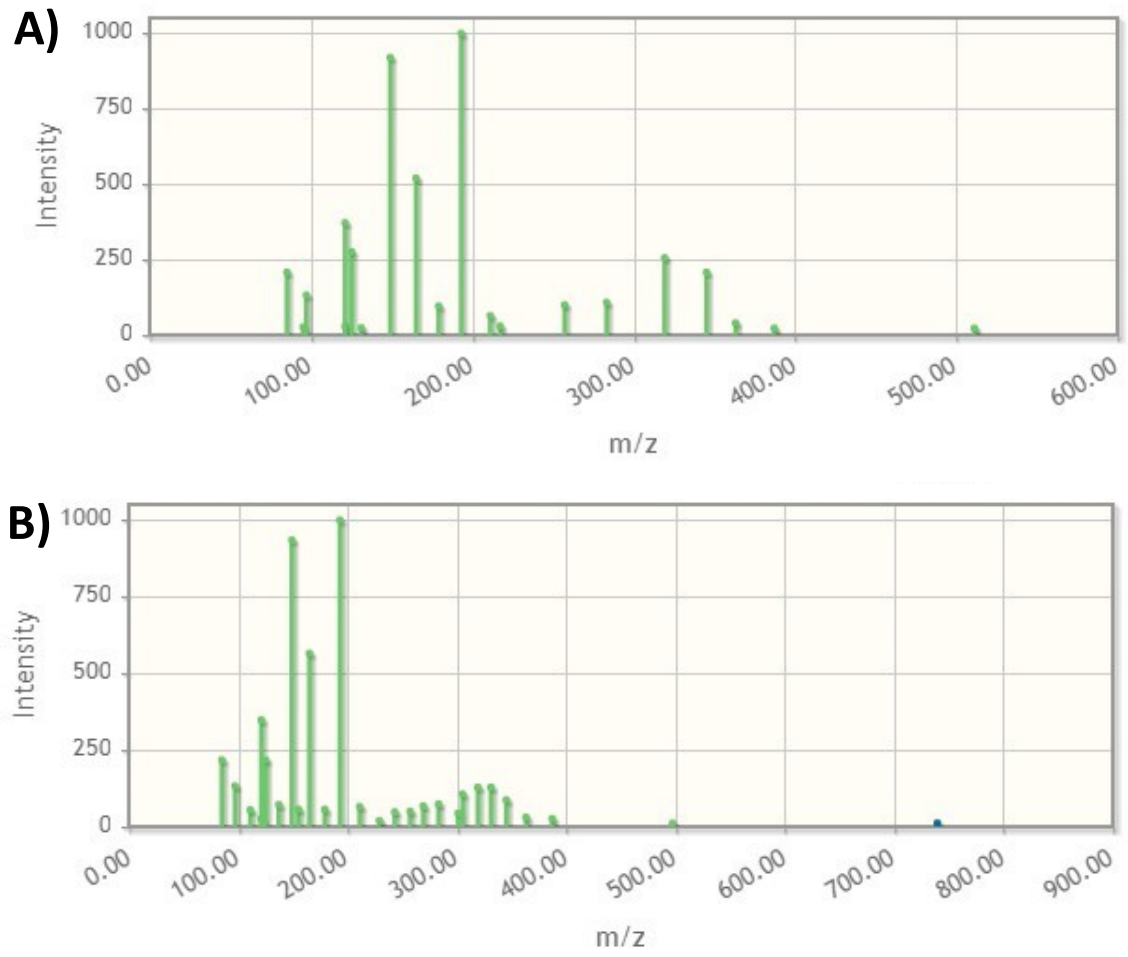

Figure S4.10. Fragmentation pattern comparison plot for elaiophylins. The plots for elaiophylin (A) and efomycin G (B) are shown. Peaks in green represent matches between predicted and experimental spectra, while peaks in blue did not match. Peaks in grey were excluded from the comparison by MetFrag.

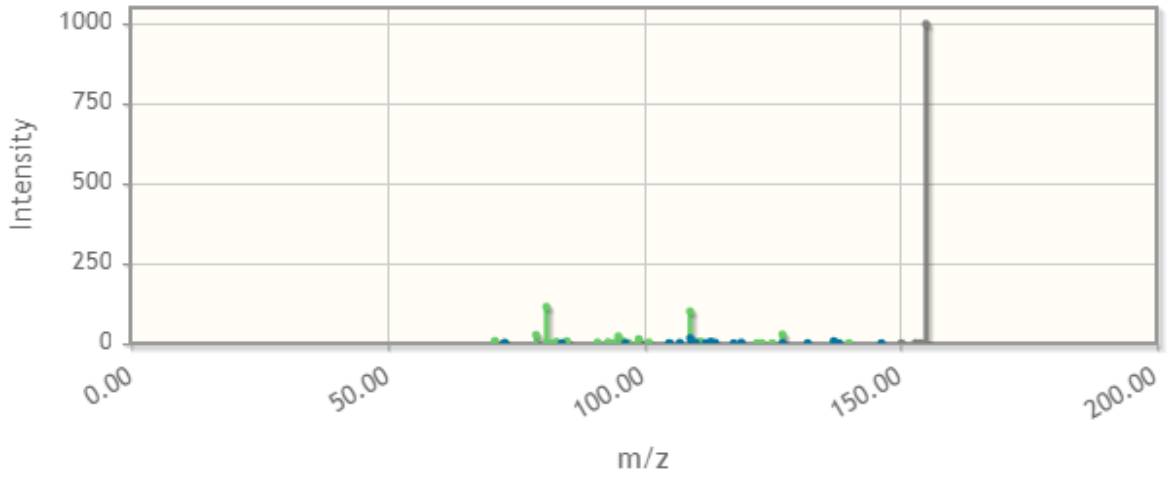

Figure S4.11. Fragmentation pattern comparison plot for musacin D. Peaks in green represent matches between predicted and experimental spectra, while peaks in blue did not match. Peaks in grey were excluded from the comparison by MetFrag.

A)

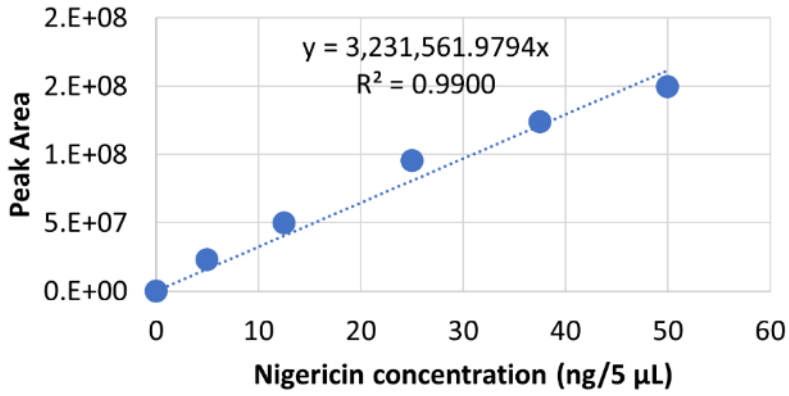

B)

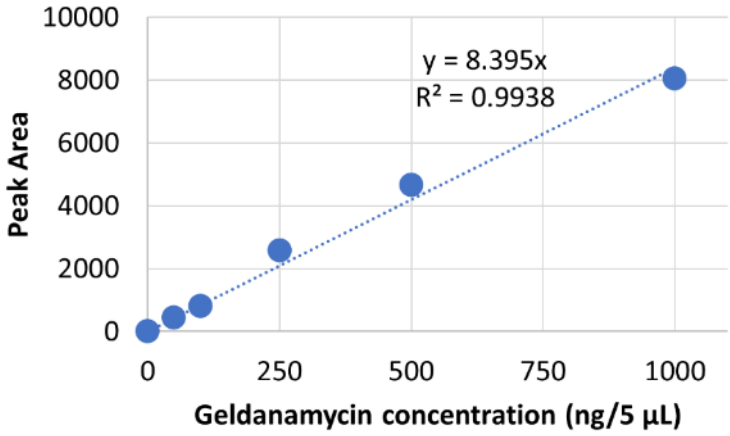

C)

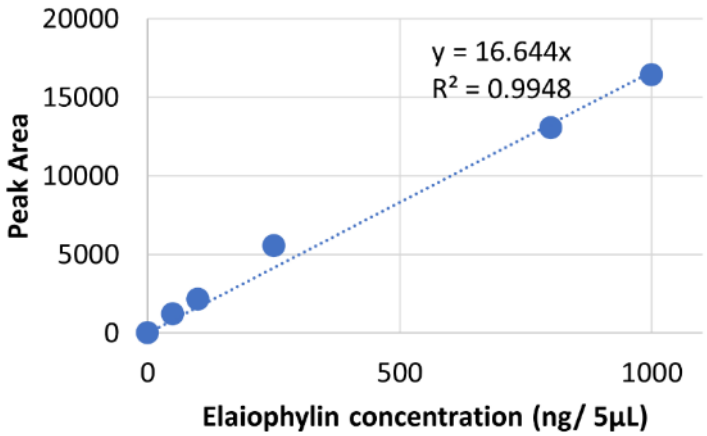

Figure S4.12. Standard curves for quantification of different molecules. A) Nigericin standard curve for LC-MS quantification. B) Geldanamycin standard curve for RP-HPLC quantification. C) Elaiophylin quantification using RP-HPLC for RP-HPLC quantification.

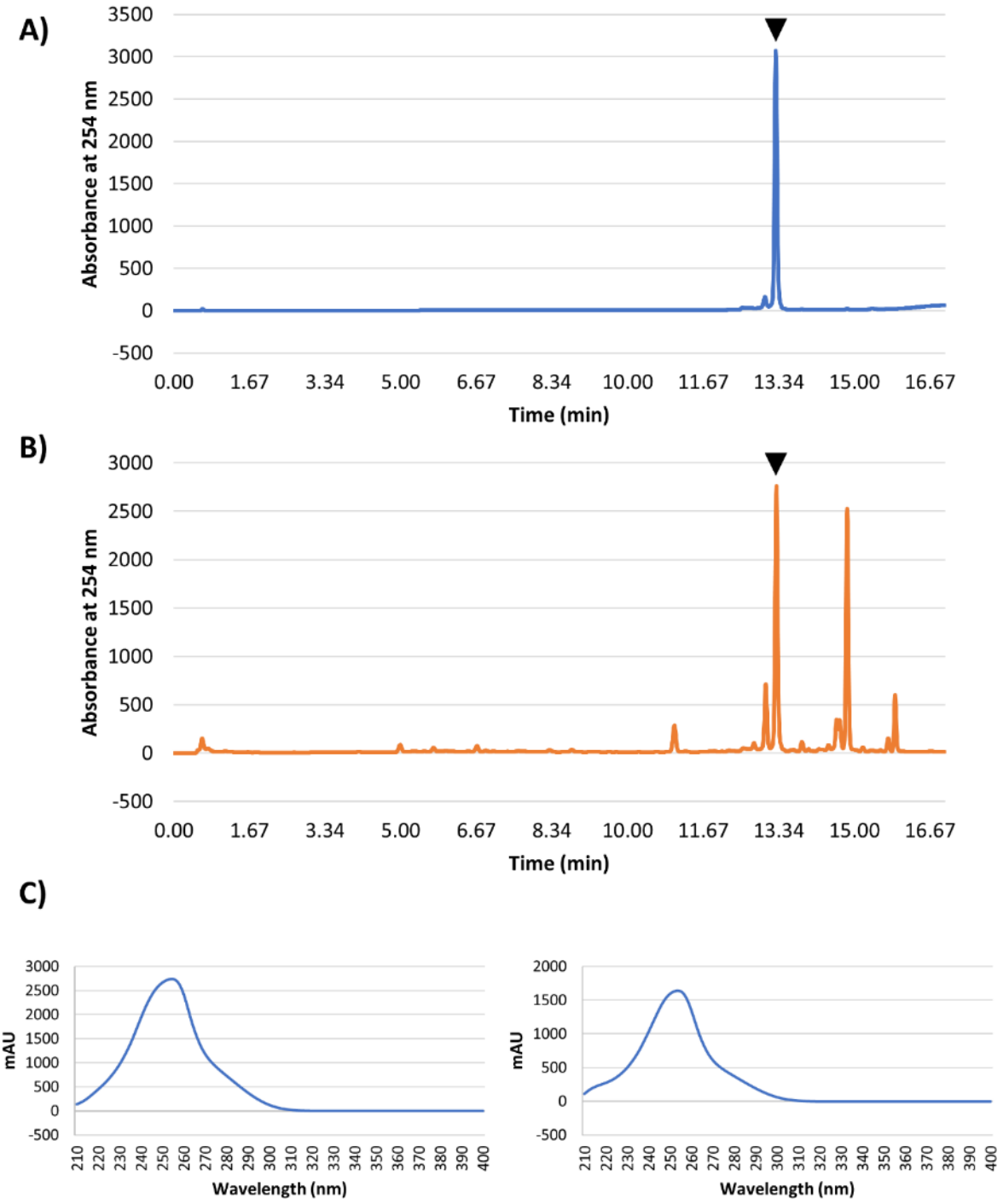

Figure S4.13. Elaiophylin detection using RP-HPLC. Shown are the chromatograms of A) the elaiophylin standard and B) a representative PMA organic extract. The inverted triangle indicates the peak corresponding to elaiophylin. C) Absorbance spectrum of the elaiophylin standard (left) and the elaiophylin peak from the PMA extract (right).

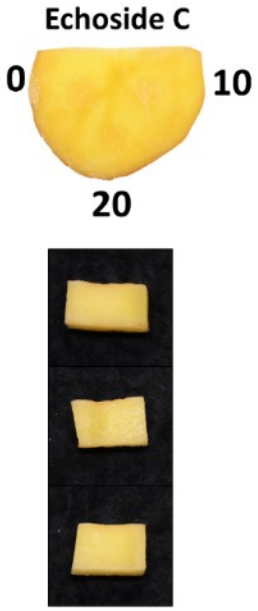

Figure S4.14. Top and side view of potato tuber slice treated with pure echoside C. The tuber slice contained disks inoculated with 0 (control), 10, and 20 nmol of the respective compound in a fixed volume of 20 µL. Three biological replicates per treatment were, with similar results obtained each time.

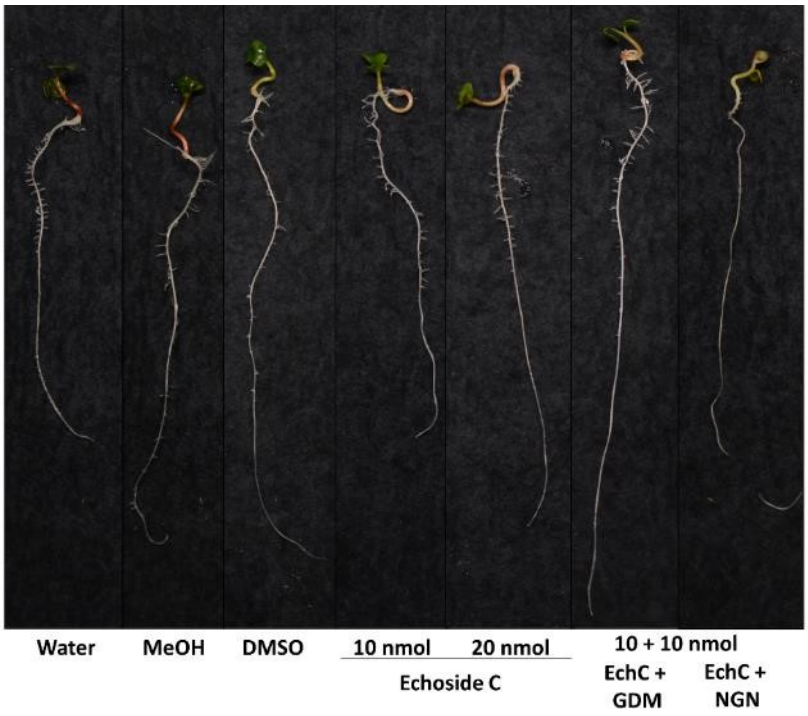

Figure S4.15. Representative radish seedlings treated with different pure compounds. The photos were taken after five days of incubation.

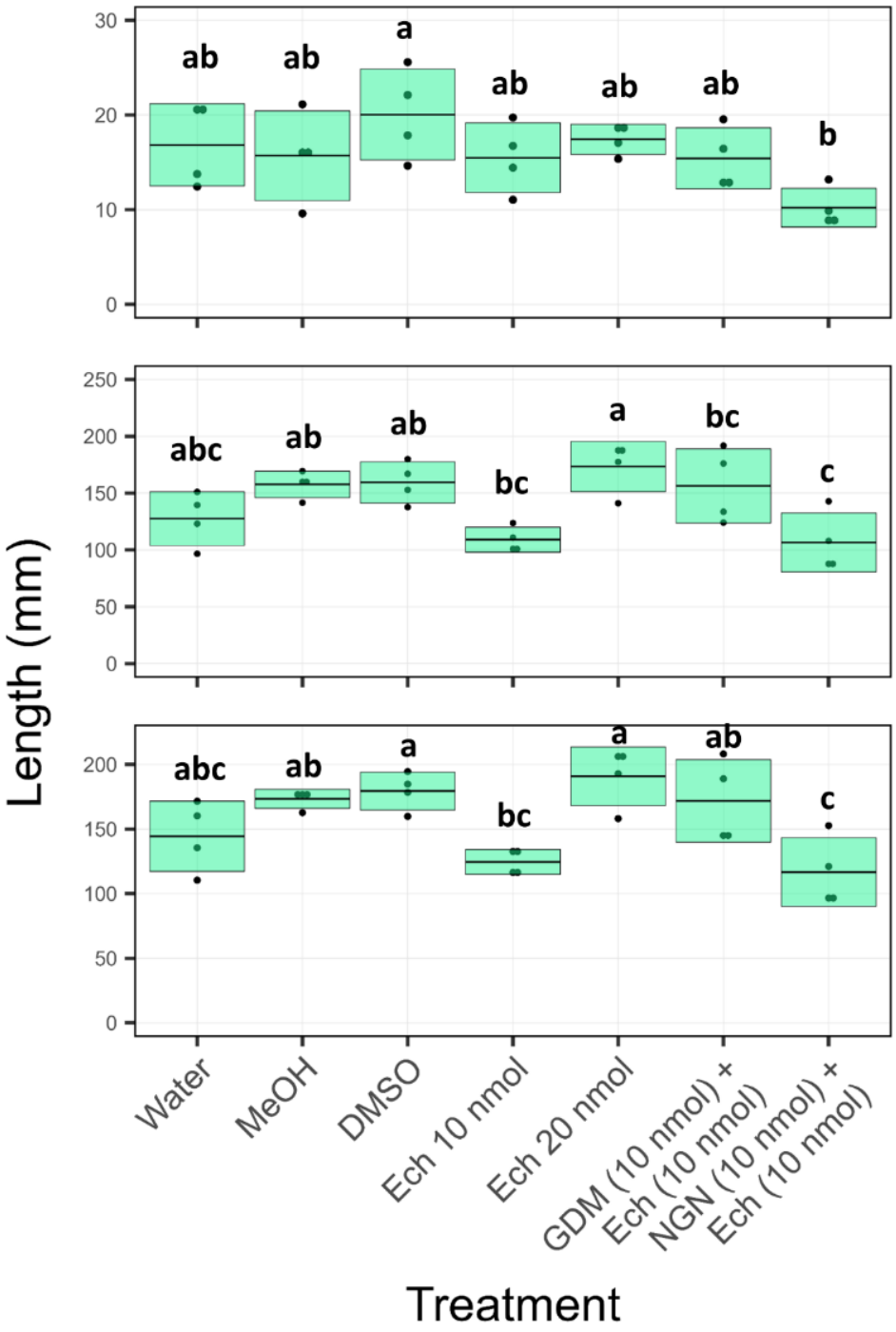

Figure S4.16. Effect of echoside C (Ech) on radish seedlings. Geldanamycin (GDM) and nigericin (NGN) were added for comparison to measure the effects on shoot (top), root (middle) and total length (bottom) of radish seedlings. Each box represents the average of the measurement ± standard deviation. Seedlings were treated with 10 or 20 nmol of each compound, or a combination of 10 nmol of each compound. The data was analyzed using an ANOVA with Tukey's test. Values with different letter are statistically different ($P < 0.05$).

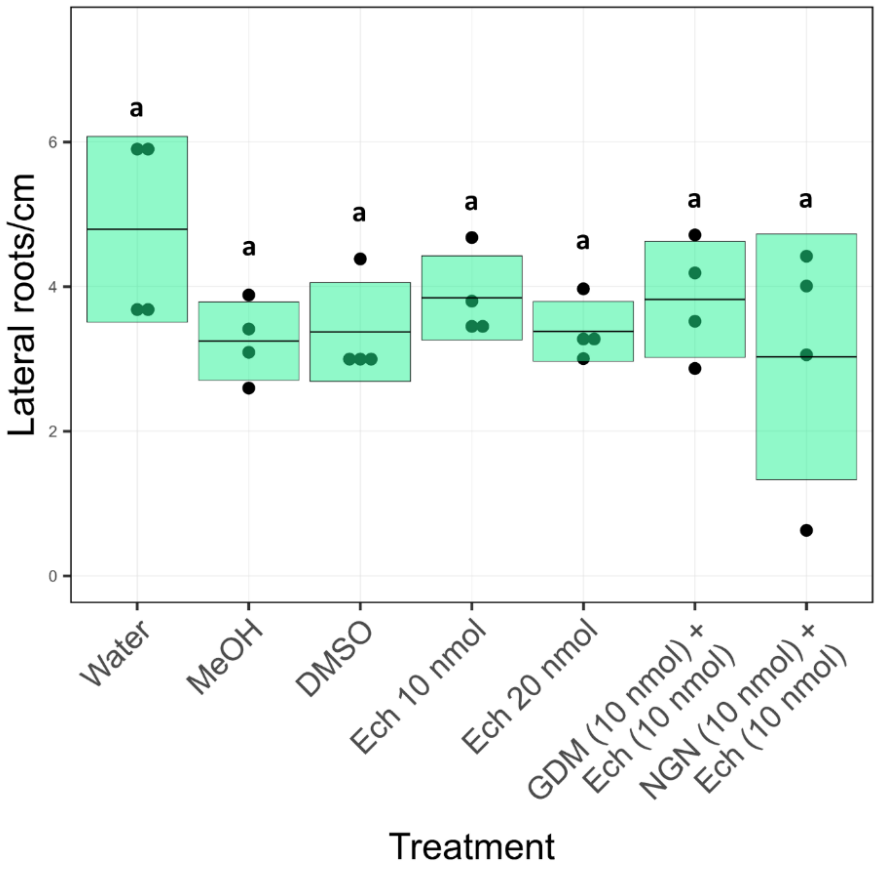

Figure S4.17. Effect of echoside C on the number of lateral roots/cm of root length in radish seedlings. Geldanamycin (GDM) and nigericin (NGN) were added to test their combined effects with echoside C. Each box represents the average of the measurement ± standard deviation. The data was analyzed using an ANOVA with Tukey's test. Values with different letter are statistically different ($P < 0.05$).

CHAPTER 5

CONSTRUCTION OF *STREPTOMYCES* SP. 11-1-2 ENGINEERED STRAINS

5.1 Abstract

Plant pathogenic *Streptomyces* require pathogenicity and virulence factors to establish infection and cause disease. These factors are often specialized metabolites produced by biosynthetic gene clusters within the genome of the pathogen. Previously, the plant pathogenic strain *Streptomyces* sp. 11-1-2 was shown to produce geldanamycin and nigericin, two phytotoxic compounds that are putatively involved in causing common scab disease. To establish the role of these molecules as pathogenicity or virulence factors, it is necessary to generate strains of 11-1-2 that are unable to produce either metabolite. Targeted gene replacement with an antibiotic-resistance marker is a common strategy used to generate engineered strains for studying the function of a target gene or gene product. Here, the creation of mutant strains of *Streptomyces* sp. 11-1-2 was attempted to investigate the role of geldanamycin and nigericin in the plant-pathogenic phenotype of the organism, and to gain insights into the regulation of nigericin biosynthesis. Plasmids were constructed to disrupt two PKS genes, one located within the geldanamycin BGC and one within the nigericin BGC, and two putative regulators located within the nigericin BGC. To determine the most efficient method for introducing DNA into 11-1-2, intergeneric conjugation, mycelial electroporation, and protoplast transformation were conducted using the *Streptomyces* integrative plasmid pSET152. Of the methods tested, intergeneric conjugation using *Escherichia coli* as the donor enabled the introduction of pSET152 into the 11-1-2 strain. However, conjugations

using the geldanamycin PKS-targeting plasmid failed to generate the desired mutant strain despite multiple attempts using different protocols. The presence of a unique restriction-methylation system in 11-1-2 might be partially responsible for the difficulty in obtaining exconjugants with the desired mutation.

5.2 Introduction

The biosynthesis of specialized metabolites (SM) in *Streptomyces* bacteria is typically performed by the joint activity of multiple genes that are arranged in biosynthetic gene clusters (BGC) (Osbourn 2010; Donald et al. 2022). Currently, the prediction of BGCs in bacterial genomes is greatly facilitated by the availability of online resources such as antiSMASH and the MiBIG database (Blin et al. 2021; Terlouw et al. 2022). However, the biological activity of each gene must be experimentally determined by *in vitro* and/or *in vivo* approaches. One of the most effective methods to elucidate the role of a gene is to remove it from the chromosome using insertional inactivation (Kieser et al. 2000). Genes can be disrupted or replaced using a non-replicating plasmid or cosmid containing flanking regions of the target gene (≥ 1 kb each) and an antibiotic resistance gene cloned between those regions. To introduce the plasmid or cosmid into *Streptomyces*, procedures such as polyethylene glycol (PEG)-assisted protoplast transformation (Kieser et al. 2000), mycelial electroporation (Kieser et al. 2000; Hamano et al. 2006), and *E. coli*-*Streptomyces* intergeneric conjugation (Kieser et al. 2000; Du et al. 2012; Zhang et al. 2019) can be performed. Once inside the cells, the flanking sequences on the plasmid/cosmid will enable replacement of the target gene on the chromosome with the antibiotic resistance gene via homologous recombination, and mutant strains can then be selected based on growth in the presence of the corresponding antibiotic (Kieser et al. 2000; Liu et al. 2018; Kormanec et al.

2019; Zhao et al. 2020b). A common strategy for creating gene deletion plasmids or cosmids involves the Redirect PCR targeting method, which relies on the λ Red proteins to mediate replacement of the target gene in a plasmid or cosmid using short flanking sequences at the ends of an antibiotic resistance cassette (Gust et al. 2003b, 2003a, 2004). More recently, efforts have been made to develop clustered regularly interspaced short palindromic repeats-Cas9 (CRISPR/Cas9) systems for the genetic manipulation of *Streptomyces*. However, there are challenges regarding the edition stability, specificity of the methods, efficiency of manipulations, and the toxicity of the Cas proteins for the host (Kormanec et al. 2019; Zhao et al. 2020b).

The selection of the method to introduce DNA into *Streptomyces* has been based on factors such as the efficiency of introducing DNA and the number of successful colonies, and different variables have been adjusted to improve the methods in particular strains (Enríquez et al. 2006; Luzhetskyy et al. 2006; Klimishin et al. 2007; Galm et al. 2008; Huiqun et al. 2010; Phornphisutthimas et al. 2010; Du et al. 2012; Wang and Jin 2014; Sun et al. 2014; Zhang et al. 2019; Song et al. 2019; Makitrynskyy et al. 2022). A factor limiting the incorporation of foreign DNA into *Streptomyces* is the presence of restriction-methylase (RM) systems. The RMs can be divided into four types (I-IV) based on their architecture, though their activity is generally similar. The endogenous DNA is methylated in a host-specific way, which prevents its digestion by the restriction enzymes. On the other hand, foreign DNA that is methylated in a different pattern is digested to prevent it from being expressed in the cell (Bruijn et al. 1998; Suzuki 2012; Moreno 2018). To bypass the RM systems of *Streptomyces*, the DNA can be passed through *E. coli* strains lacking

methyltransferase genes, thus preventing digestion of the newly introduced DNA by the host RMs (Suzuki 2012).

Once deletion mutants of the target gene are isolated, it is possible to assess phenotypical, physiological, and metabolic changes that can be correlated with the gene's activity. Similarly, the overexpression of specific genes can provide useful information on the function of those genes within the organism (Kieser et al. 2000). In plant-pathogenic *Streptomyces*, the ability to generate genetically engineered strains has been essential in understanding the role of different specialized metabolites in the pathosystem. For example, the deletion of *txtA* in *S. acidiscabies* resulted in the loss of thaxtomin A production and virulence on potato tubers (Healy et al. 2000), indicating that thaxtomin A is a critical pathogenicity factor in *S. acidiscabies*. On the other hand, higher production levels of the CFA-Ile phytotoxin were obtained by creating an *S. scabiei* strain overexpressing the *cfaR* regulator, and the resulting strain caused an increase in severity of disease symptoms on potato tuber tissue, supporting the notion that CFA-Ile is a virulence factor in *S. scabiei* (Cheng et al. 2019).

The strain *Streptomyces* sp. 11-1-2 was originally isolated from CS-infected potato tubers on the island of Newfoundland, and it was shown to be highly pathogenic in bioassays using different plant hosts (potato, radish, *Nicotiana benthamiana*) (Fyans et al. 2016). However, this strain is not phylogenetically related to the known plant pathogenic *Streptomyces* species (Chapter 3), and initial screening for specialized metabolite BGCs confirmed that the strain does not harbour the genes for biosynthesizing thaxtomin A, CFA-Ile, concanamycin A or borrelidin (Bown and Bignell 2017). Instead, the genomic analysis of 11-1-2 predicted the presence of BGCs for the production of nigericin and geldanamycin,

and LC-MS^2 analysis of 11-1-2 organic culture extracts confirmed that the strain produces these metabolites (Chapters 3 and 4). Furthermore, it was demonstrated that both geldanamycin and nigericin are phytotoxic against radish seedlings and potato tuber slices (Chapters 3 and 4). Based on these results, it was hypothesized that the production of these compounds contributes to the plant pathogenic phenotype of the 11-1-2 strain. The objective of this study, therefore, was to investigate the potential role of geldanamycin and nigericin as virulence factors by creating mutants of 11-1-2 that are impaired in the biosynthesis of one or both compounds.

5.3 Results and Discussion

5.3.1 Plasmid construction for deletion of geldanamycin and nigericin biosynthetic genes in *Streptomyces* sp. 11-1-2

The geldanamycin BGC is classified as a type I polyketide synthase, and its original description was proposed to contain 23 genes, although the antiSMASH prediction for 11-1-2 shows 38 genes (Fig. 5.1). The cluster contains three modular PKSs, namely, *gdmAI*, *gdmAII,* and *gdmAIII*, and at least three genes involved in the regulation of metabolite production (He et al. 2008; Kim et al. 2010; Jiang et al. 2017). Previous studies using *Streptomyces* sp. LZ35 (Zhao et al. 2013) and *S. autolyticus* CGMCC0516 (Yin et al. 2011) showed that deletion of the *gdmAI* gene, which ecodes the PKS involved in the first step of geldanamycin biosynthesis, abolished the production of geldanamycin in these strains. Thus, *gdmAI* was selected for construction of a geldanamycin-deficient mutant of 11-1-2 in the current study.

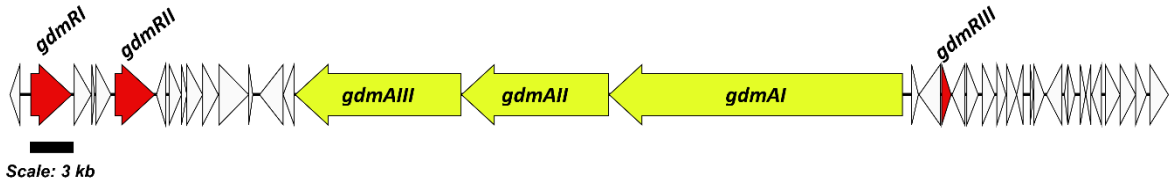

Figure 5.1. The biosynthetic gene cluster for geldanamycin as predicted using antiSMASH 7.0. The yellow arrows represent the PKS genes, while the red arrows indicate the regulatory genes. White arrows indicate other genes. The direction of each arrow indicates the direction of transcription of the corresponding gene.

To delete *gdmAI*, the plasmid pGDC1 was constructed as described in Chapter 2 (Section 2.2.7). The regions flanking the gene (~1 kb) in the chromosome were PCR-amplified, and then they were ligated together following digestion with Ssp1, which cut each fragment at one end. Following ligation, the ~2 kb DNA fragment was cloned into the pCR™-Blunt II-TOPO® vector, and the cloned DNA was sequenced to confirm the absence of mutations. Then, an apramycin resistance cassette was cloned into the Ssp1 site between the two *gdmAI* flanking sequences, resulting in the plasmid pGDC1 (Fig. 5.2A). Digestion of pGDC1 with Ssp1 confirmed the presence of the apramycin resistance cassette (Fig. 5.2B), and the plasmid was sequenced to determine the orientation of the cassette relative to the flanking sequences.

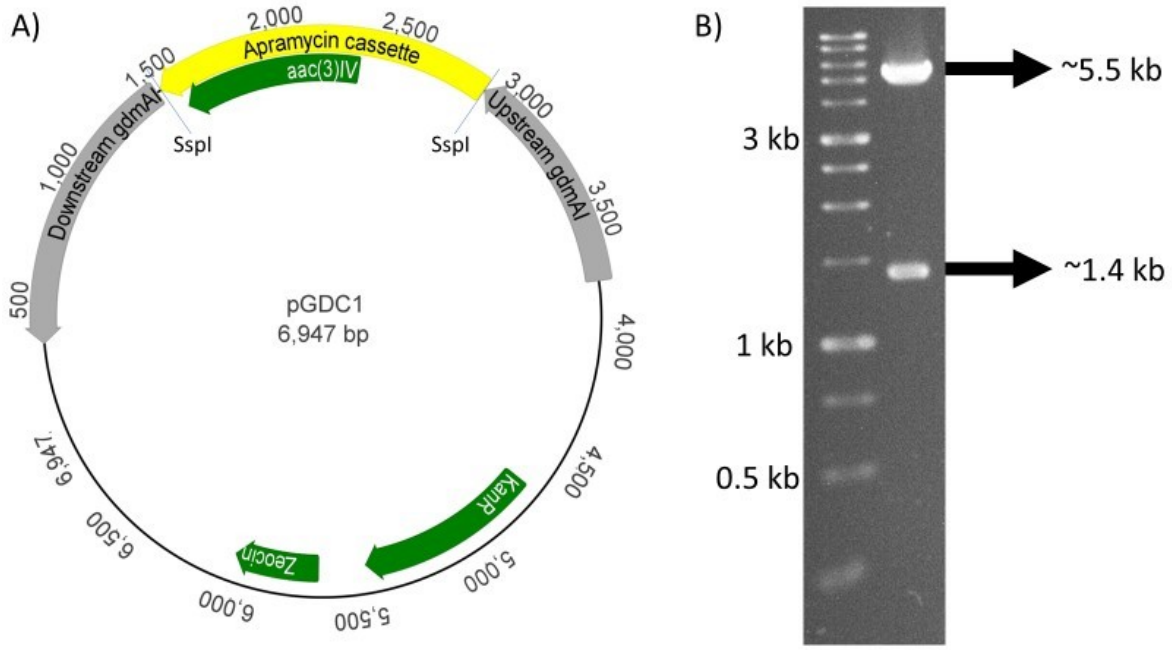

Figure 5.2. Map of plasmid pGDC1. A) The plasmid contains the flanking regions to *gdmAI* and the apramycin cassette with the apramycin resistance gene *aac(3)IV*. B) Digestion of pGDC1 with the restriction enzyme SspI. Left lane: 1 kb DNA ladder. Right lane: digested pGDC1. The ~1.4 kb fragment represents the apramycin resistance cassette.

The nigericin BGC is classified as a type I polyketide synthase, and its original description proposed the presence of 18 genes (Harvey et al. 2007), although the antiSMASH prediction using the 11-1-2 genome extended the BGC to 47 genes (Fig. 5.3). The cluster contains nine modular PKSs (*nigAI-IX*), of which *nigAI* encodes the loading domain and the first module involved in polyketide chain extension, while the remaining genes encode the extension modules (Harvey et al. 2007). Thus, deletion of the *nigAI* gene is desirable, as it would remove the loading module and prevent the initiation of molecule biosynthesis. This was previously demonstrated in *Streptomyces* sp. LZ35, where deletion of *nigAI* was shown to impair nigericin production (Zhao et al. 2013).

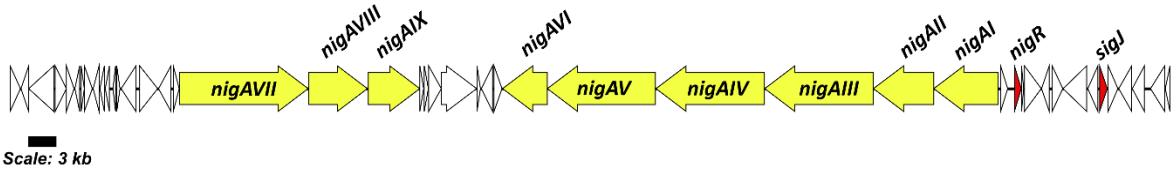

Figure 5.3. The biosynthetic gene cluster for nigericin production in *Streptomyces* sp. 11-1-2 as predicted by antiSMASH 7.0. The yellow arrows represent the PKS genes, while the red genes represent the regulatory genes. The white arrows indicate other genes. The direction of each arrow indicates the direction of transcription of the corresponding gene.

To generate a *nigAI* deletion mutant of the 11-1-2 strain, the plasmid pGDC2 (Fig. 5.4) was constructed as described in Chapter 2 (Section 2.2.7). The flanking regions of the gene (~1 and 1.6 kb) were PCR-amplified, and the resulting products were digested with SspI, which cut each fragment at one end. The regions were ligated to generate a 2.6 kb fragment, which was then cloned into pCR™-Blunt II-TOPO. After sequencing the cloned insert, a hygromycin resistance cassette was cloned into the Ssp1 site between the *nigA1* flanking sequences (Fig. 5.4A). Digestion of the pGDC2 plasmid confirmed the presence of the hygromycin resistance cassette (Fig. 5.4B), and the plasmid was sequenced to determine the orientation of the cassette relative to the flanking sequences.

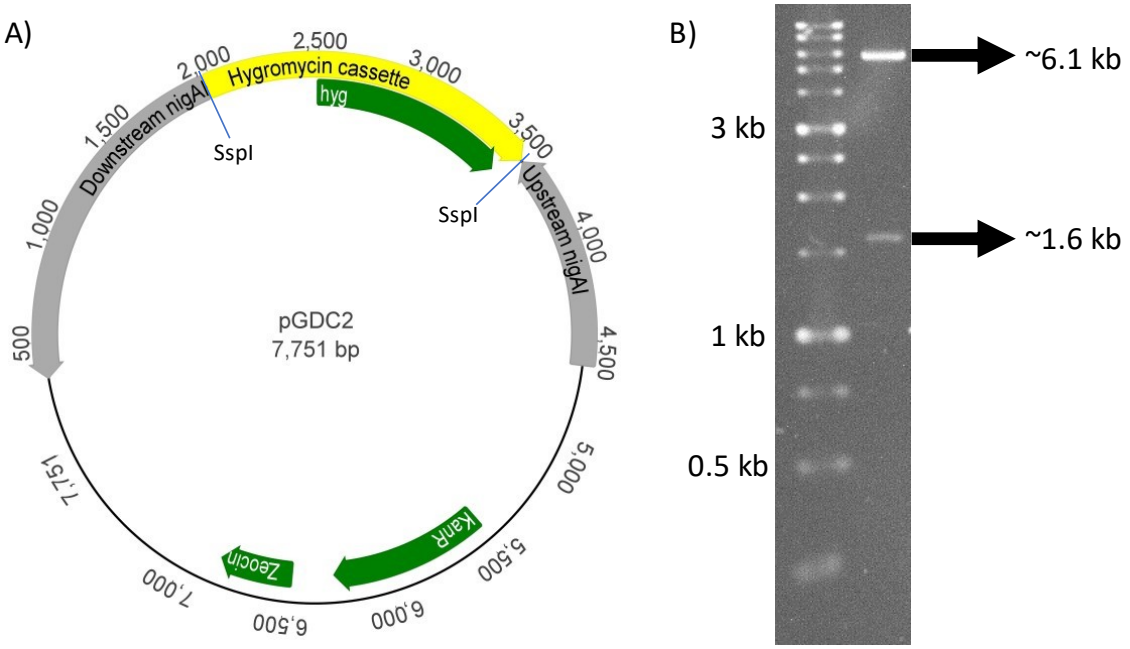

Figure 5.4. Map of plasmid pGDC2. A) The plasmid contains the flanking regions to *nigAI* and the hygromycin cassette with the hygromycin resistance gene *hyg*. B) Digestion of pGDC2 using the restriction enzyme SspI. Left lane: 1 kb DNA ladder. Right lane: digested pGDC2. The ~1.6 kb fragment represents the hygromycin resistance cassette.

Due to the interest in creating a Δ*gdmAI*/Δ*nigAI* double mutant strain, the use of two different selection markers (apramycin and hygromycin resistance) was planned. However, preliminary conjugation attempts showed that the 11-1-2 strain is resistant to hygromycin B. Therefore, the plasmid pGDC2 was redesigned. First, the kanamycin resistance gene on the pCR™-Blunt II-TOPO® vector backbone was replaced with an apramycin resistance cassette using the Redirect PCR targeting method (see Section 2.2.7). Then, a kanamycin resistance gene was cloned into the SspI site in between the flanking regions, resulting in pGDC4 (Fig. 5.5A). To confirm the orientation of the kanamycin resistance gene, the plasmid was digested with the restriction enzymes HindIII and EcoRV. Clones with the expected fragmentation pattern (Fig. 5.5B) were kept for further work.

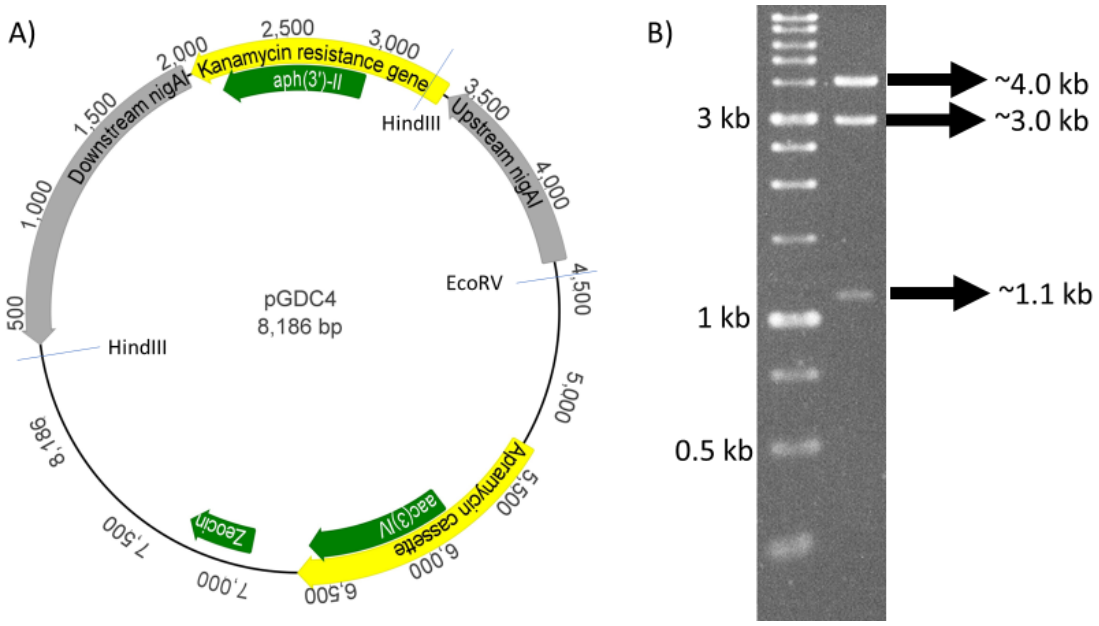

Figure 5.5. Map of plasmid pGDC4. A) The plasmid contains the flanking regions to *nigAI* and the kanamycin/neomycin resistance gene *aph(3')-II.* B) Digestion of pGDC4 using the restriction enzymes HindIII and EcoRV. Left lane: 1 kb DNA ladder. Right lane: digested pGDC4 showing the expected digestion pattern.

5.3.2 Plasmid construction for deletion of putative regulatory genes in the nigericin BGC of *Streptomyces* sp. 11-1-2.

Previous studies examined the role of putative regulatory genes in the geldanamycin BGC. The proteins encoded by *gdmRI* and *gdmRII* are similar to LuxR transcriptional regulators, and the deletion of either gene resulted in the loss of geldanamycin biosynthesis, as well as in no expression of the majority of genes involved in the biosynthesis of the compound in *S. hygroscopicus* strains 17997 (He et al. 2008) and JCM4427 (Kim et al. 2010). Another putative regulatory gene, *gdmRIII*, encodes a TetR family regulator. Deleting this gene resulted in significantly lower geldanamycin production and decreased biosynthetic gene expression in *S. hygroscopicus* JCM4427 (Kim et al. 2010) and *S. autolyticus* CGMCC0516 (Jiang et al. 2017). Given that all three genes are conserved in the 11-1-2

geldanamycin BGC (Fig. 5.1), they likely play a similar role in controlling geldanamycin production in this strain.

There is little known about the regulation of nigericin production in *Streptomyces* spp. The first description of the nigericin BGC from *Streptomyces* sp. DSM 4137 analyzed the similarity between the *nigR* protein product and the known regulators MonR1 and NanR2, which are encoded within the monensin and nanchagmycin BGCs, respectively (Harvey et al. 2007). *nigR* is predicted to encode a *Streptomyces* antibiotic regulatory protein (SARP) family regulator based on the antiSMASH prediction of the nigericin BGC. In *Streptomyces*, the SARP regulators are characterized by the presence of a motif similar to the DNA-binding domain of the OmpR protein (present in *E. coli* and other bacteria) and a winged HTH configuration (Wietzorrek and Bibb 1997). On the other hand, the BTAD domain was first described as part of the AfsR protein in *S. coelicolor*, and its disruption resulted in decreased actinorhodin production (Horinouchi et al. 1990). Both domains are sufficient to exhibit DNA-binding activity by AfsR, even when the other domains have been truncated (Tanaka et al. 2007). An analysis of the nigR amino acid sequence using InterProScan revealed the presence of two domains: an N-terminal OmpR/PhoB-type DNA-binding domain (IPR001867) and a C-terminal Bacterial transcriptional activator domain (BTAD; IPR005158). Moreover, the nigR amino acid sequence shows high similarity to other SARP regulators available in the MIBiG database (Fig. 5.6). The antiSMASH prediction also showed the presence of a TTA codon within the beginning region of the *nigR* gene, suggesting that the regulator's expression is affected by the activity of the global regulator bldA, a feature that has been reported in several antibiotic biosynthesis regulators (Leskiw et al. 1991; Chandra and Chater 2008; Hackl and Bechthold 2015).

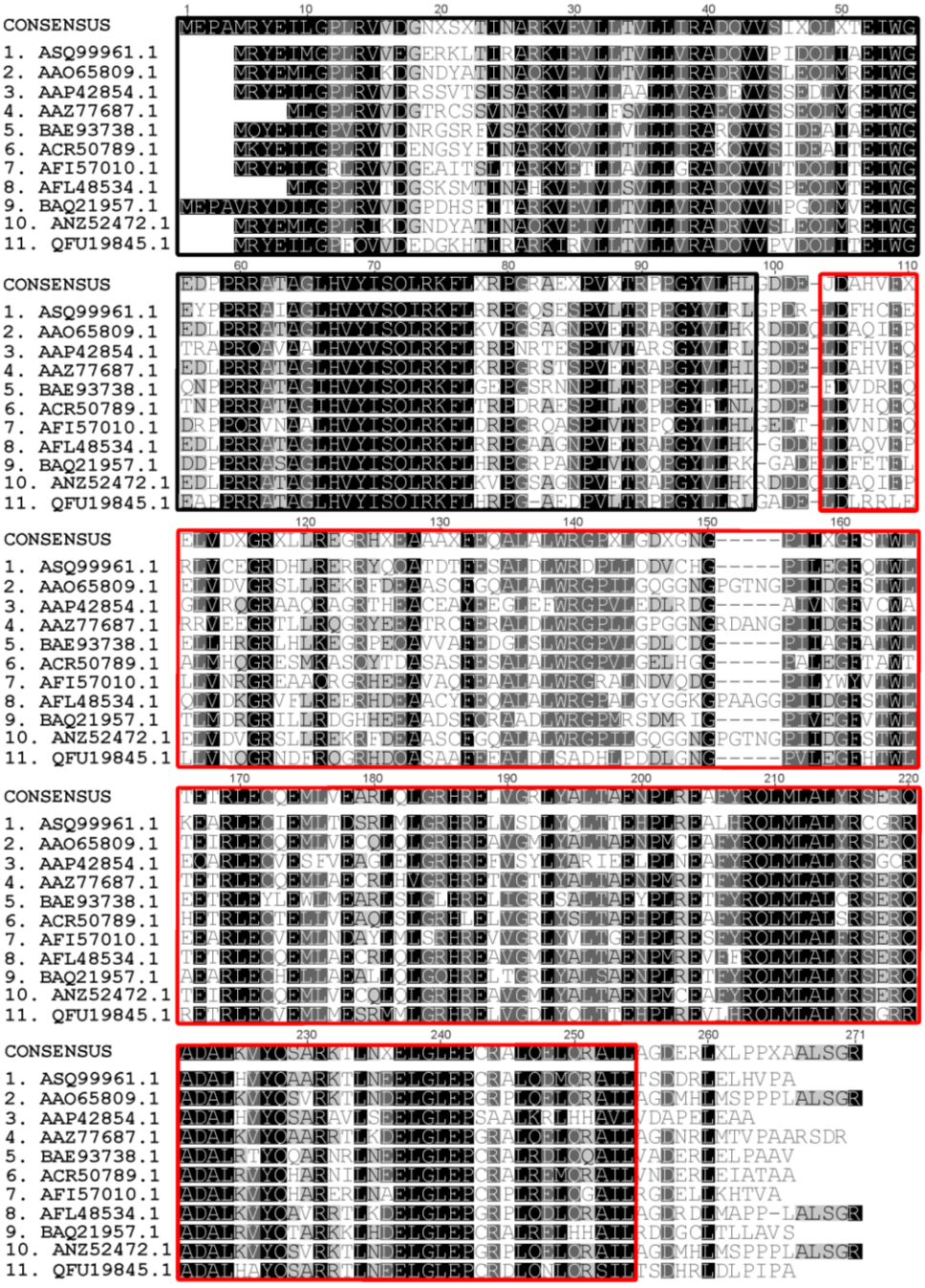

Figure 5.6 Amino acid alignment of NigR from *Streptomyces* sp. 11-1-2 with the top 10 most similar SARP sequences in the MIBiG database. Highly conserved amino acids are highlighted as follows: black, 100% identity; dark grey, 80–99% identity; gray, 60–79% identity; light gray, <60% identity. The NCBI accession numbers are in the left column. The OmpR/PhoB DNA binding domain (black) and the BTAD domain (red) are highlighted. 1: *Streptomyces* sp. 11-1-2. 2: *Streptomyces virginiae*. 3: *Streptomyces nanchangensis*. 4: *Streptomyces antibioticus*. 5: *Streptomyces* sp. NRRL 11266. 6: *Streptomyces longisporoflavus*. 7: *Amycolatopsis orientalis*. 8: *Streptomyces* sp. CS684. 9: *Streptomyces versipellis*. 10: *Streptomyces virginiae*. 11: *Actinomadura* sp.

Given the location of *nigR* within the nigericin BGC (Fig. 5.3) and the similarity of the protein product with known SARP regulators, it was hypothesized that *nigR* functions as a positive activator of nigericin biosynthesis in the 11-1-2 strain. To investigate this further, the plasmid pGDC6 (Fig. 5.7) was constructed as described in Chapter 2 (Section 2.2.7). in order to create a Δ*nigR* deletion mutant of the 11-1-2 strain. In the process of creating this plasmid, a publication was released showing that the deletion of *nigR* in *S. malaysiensis* inactivates the expression of the nigericin BGC and, consequently, the biosynthesis of the compound (Wei et al. 2022). However, it is unknown what effects this deletion would have on nigericin biosynthesis and pathogenicity in 11-1-2, as there might be differences in the regulation of the BGC in this strain.

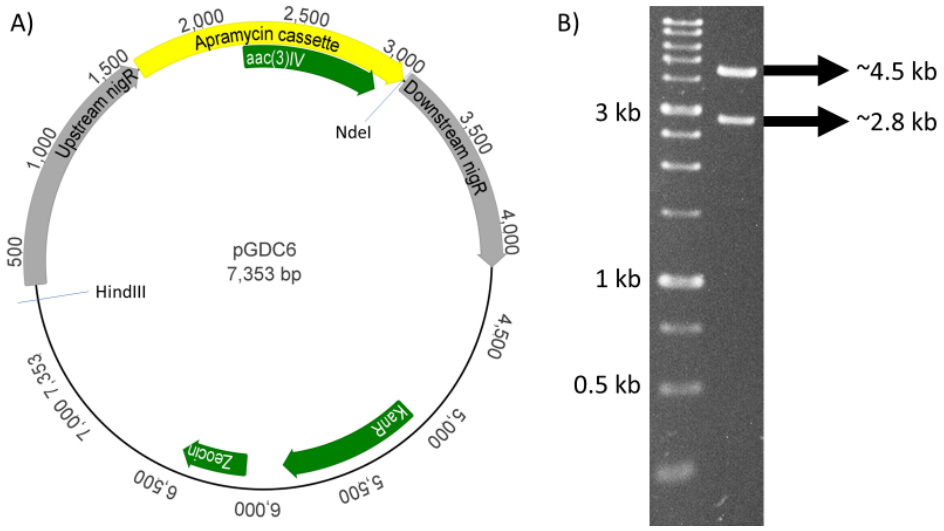

Figure 5.7. Map of plasmid pGDC6. A) The plasmid contains the flanking regions to *nigR* and the apramycin cassette with the apramycin resistance gene *aac(3)IV*. B) Digestion of pGDC6 using the restriction enzymes HindIII and NdeI. Left lane: 1 kb DNA ladder. Right lane: digested pGDC6 showing the expected digestion pattern.

The antiSMASH prediction also expanded the number of genes that could be involved in the nigericin BGC beyond the original description. One of the genes included in the prediction is *sigJ*, which putatively encodes the RNA polymerase sigma factor SigJ. A limited number of hits were obtained from the MIBiG database, which shows high similarity to the SigJ amino acid sequence (Fig. 5.8).

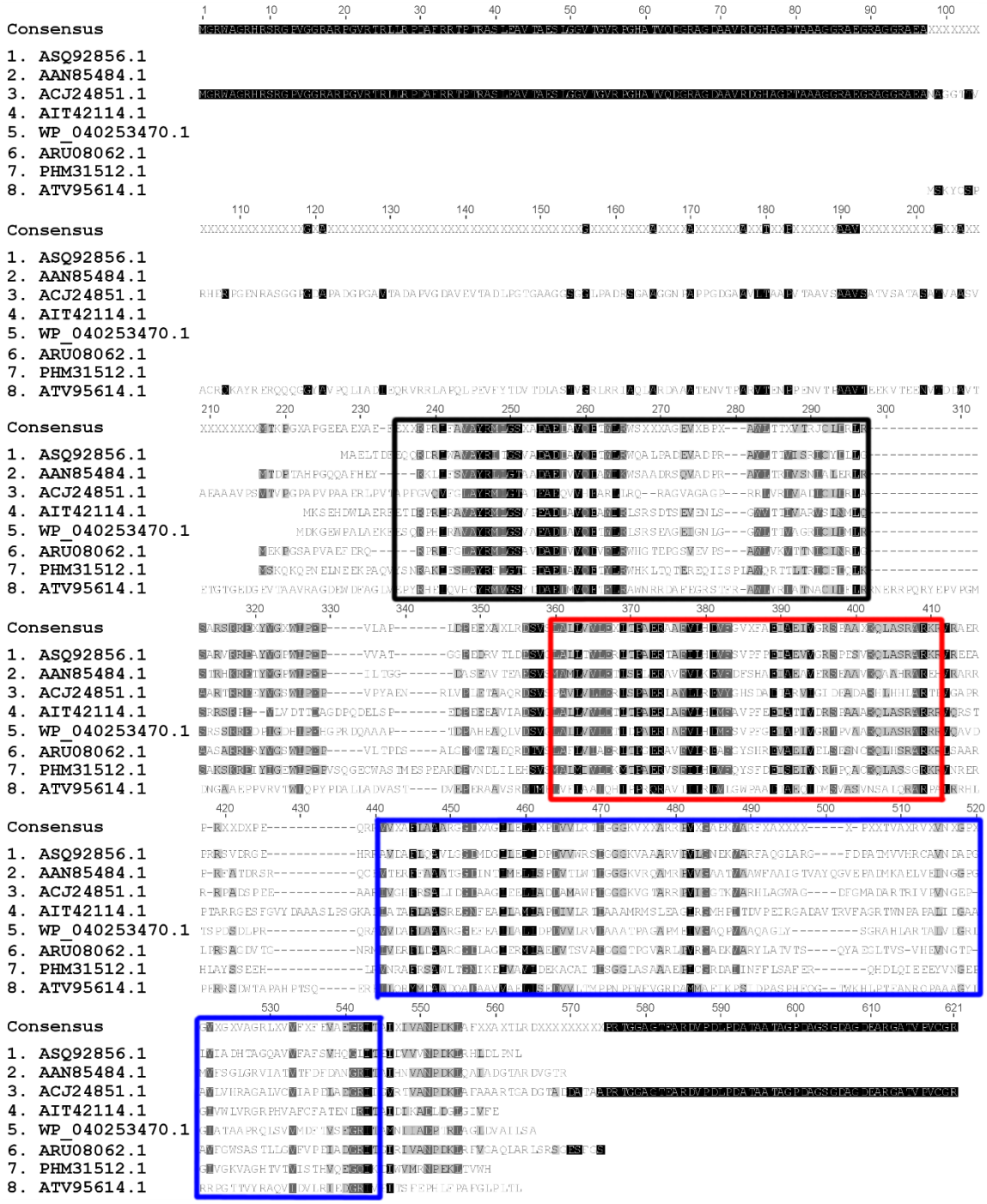

Figure 5.8. Amino acid alignment of SigJ from *Streptomyces* sp. 11-1-2 with similar proteins in the MIBiG database. Highly conserved amino acids are highlighted as follows: black, 100% identity; dark grey, 80–99% identity; grey, 60–79% identity; light grey, <60% identity. The RNA polymerase sigma-70 region 2 (black), region 4 type 2 (red) and Snoal-like domain (blue) are highlighted. The NCBI accession numbers are in the left column. 1: *Streptomyces* sp. 11-1-2. 2: *Streptomyces atroolivaceus*. 3: *Streptomyces pactum*. 4: *Streptomyces* sp. CNQ-509. 5: *Streptomyces* spp. 6: Uncultured bacterium. 7: *Xenorhabdus szentirmaii* DSM 16338. 8: *Amycolatopsis* sp.

SigJ is part of the extracytoplasmic function (ECF) family of sigma factors, and an InterProScan analysis revealed the presence of two conserved regions for ECFs: an RNA polymerase sigma-70 region 2 (IPR007627) and an RNA polymerase sigma factor 70, region 4 type 2 (IPR013249), located in the N-terminus of the sequence. The region 2 domain binds to DNA in the -10 promoter element of the non-template strand, while the region 4 domain binds to DNA in the -35 region of the promoter (Heimann 2002; Sineva et al. 2017). The InterProScan analysis also predicted the presence of a Snoal-like domain (IPR037401) within the C-terminal region of SigJ. This domain is also found in σ^J proteins from *Bacillus licheniformes*, *Rhodobacter sphaeroides,* and *Mycobacterium tuberculosis*, where it facilitates the proper conformation of the DNA-binding domain for attachment and initiation of transcription (Wecke et al. 2012; Goutam et al. 2017; Wu et al. 2019).

The presence of an additional domain in the C-terminal region is a characteristic of the ECF41 family, thus making SigJ part of this family. Furthermore, antiSMASH has predicted a gene encoding a pyridine nucleotide-disulfide oxidoreductase immediately downstream from *sigJ*. The ECF41 family is also characterized by the presence of genes encoding carboxymuconolactone decarboxylases, oxidoreductases, or epimerases adjacent to the ECF-encoding gene (Wecke et al. 2012). This contrasts with other types of ECF sigma factors, which are usually encoded next to an anti-sigma factor-encoding gene (Mascher 2013).

The role of an ECF as a CSR for specialized metabolite production in *Streptomyces* has only been reported once before. The gene *antA* encodes the ECF sigma factor σ^{AntA}, which regulates the expression of *antG* and *antH,* two genes that are located in separate operons within the antimycin BGC in *Streptomyces albus* (Seipke et al. 2014). The factor

σ^{AntA} does not have an anti-sigma associated with it, but it is controlled by the ClpXP protease, which also represents a novel mechanism of ECF regulation (Bilyk et al. 2020). Thus, *sigJ* became a gene of interest for the present work. To investigate the role of *sigJ* as a regulator of nigericin production in 11-1-2, the plasmid pGDC3 was constructed as described in Chapter 2 (Section 2.2.7). The flanking regions of the gene (~1.2 and 1 kb) were PCR-amplified and digested with NheI, which cut the fragments at one end. The regions were then ligated together to produce a single DNA fragment (~2.3 kb), which was cloned into the pCR™-Blunt II-TOPO®. Next, a hygromycin resistance cassette was inserted into the NheI site located in between the *nigR* flanking sequences (Fig. 5.9). Due to the resistance of 11-1-2 to hygromycin B, an additional plasmid was constructed (pGDC5, Fig. 5.10) in which the hygromycin resistance cassette was substituted for an apramycin resistance cassette. The orientation of the apramycin resistance cassette was confirmed by digestion with the restriction enzymes BamHI and NdeI.

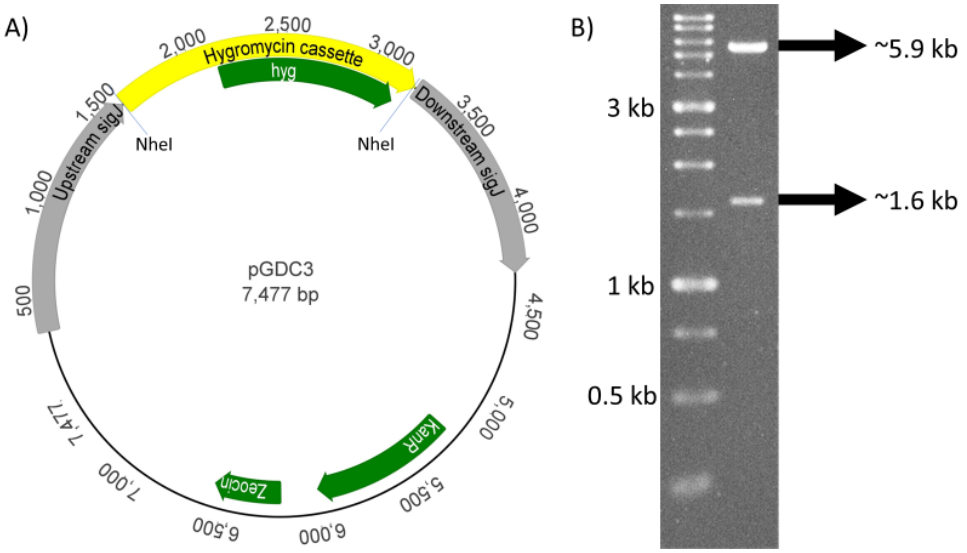

Figure 5.9. Map of plasmid pGDC3. A) The plasmid contains the flanking regions to *sigJ* and the hygromycin cassette with the hygromycin resistance gene *hyg*. B) Digestion of pGDC3 using the restriction enzyme NheI. Left lane: 1 kb DNA ladder. Right lane: digested pGDC3. The ~1.6 kb fragment corresponds to the hygromycin cassette.

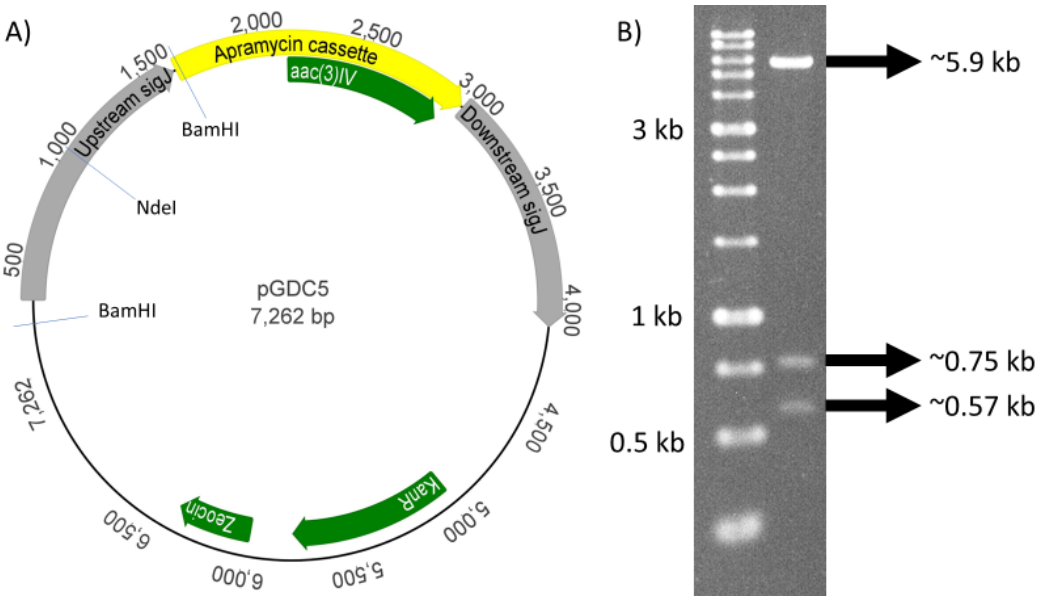

Figure 5.10. Map of plasmid pGDC5. A) The plasmid is identical to pGDC3 but containing the apramycin cassette instead of the hygromycin cassette. B) Digestion of pGDC5 using the restriction enzymes BamHI and NdeI. Left lane: 1 kb DNA ladder. Right lane: digested pGDC5 showing the expected digestion pattern.

5.3.3 Introduction of DNA in *Streptomyces* sp. 11-1-2

To perform genetic manipulations of *Streptomyces* sp. 11-1-2, it was necessary to develop a protocol because there were no previous attempts to introduce DNA into this strain. For this purpose, the plasmid pSET152, which integrates into the *Streptomyces* chromosome at the ϕC31 *attB* site and provides apramycin resistance, was used. pSET152 is widely employed in the genetic engineering of *Streptomyces* as it is very stable and results in good exconjugant efficiency (Bierman et al. 1992). The integration occurs due to the interaction between the ϕC31 bacteriophage *attB* site in the *Streptomyces* chromosome and the corresponding *attP* site on the plasmid (Bierman et al. 1992).

The ϕC31 *attB* sequence from *S. coelicolor* was used as a query in a BLASTn analysis against the *Streptomyces* sp. 11-1-2 genome, and this showed some minor differences between the *attB* sequences from the two species (Fig. 5.11). Natural variation in the ϕC31 *attB* site has been previously shown for different *Streptomyces* strains (Combes et al. 2002), and some mutations in the sequence have been associated with decreasing integrase activity (Gupta et al. 2007). However, the differences seen in the 11-1-2 genome do not correspond to the mutations reported. Further investigation is required to determine the impact of the mutations in the 11-1-2 strain on the integration efficiency of the pSET152 plasmid.

Figure 5.11. Nucleotide alignment of the ϕC31 attB site. The site from *S. coelicolor* (top; NCBI accession number AL939117.1) was used as reference against the predicted ϕC31 *attB* site from *Streptomyces* sp. 11-1-2 (bottom).

Intergeneric conjugation between *E. coli* and *Streptomyces* has been widely used to genetically manipulate *Streptomyces* strains due to its effiency in comparison to other methods such as protoplast transformation (Kieser et al. 2000). Thus, intergeneric conjugation was first selected to create the mutant strains of 11-1-2. The plasmids pSET152 and pGDC1-pGDC6 were transformed into *E. coli* ET12567/pUZ8002 to perform intergeneric conjugation (Section 2.1.11.1). Initially, plasmids pSET152 and pGDC1 were utilized, but no successful exconjugants were obtained when tested with 11-1-2. The plasmid pSET152 was used for conjugations with *S. scabiei* 87-22 as a positive control, which resulted in colonies that were successfully transferred to fresh media with the selective

antibiotic, suggesting that the lack of exconjugants with the 11-1-2 strain was not due to errors with the conjugation protocol.

One modification that can facilitate intergeneric conjugation is subjecting spores to a pregermination step with different liquid culture media and/or heat shock that would induce germination (Kieser et al. 2000). To induce faster germination, 11-1-2 spores were added to 2×YT medium and then heat shocked at 50°C for ten minutes, followed by a cool down step. Another method used was the use of pregermination medium inoculated with spores and incubated at 30°C with shaking for 4 hours. Additionally, the use of culture media other than SFM + 10 mM of $MgCl_2$ to incubate the *E.coli-Streptomyces* mixture has been reported for other *Streptomyces*. Media AS-1 (Baltz 1999; Park and Choi 2014), GSY (Wang and Jin 2014), and YMS were tested. The latter was included since it has shown excellent development of mycelia and spores of 11-1-2. However, none of these modifications provided exconjugants when plasmids pSET152 and pGDC1 were tested.

Another modification for intergeneric conjugation is the use of mycelia instead of spores. Different *Streptomyces* species have successfully incorporated DNA using this method (Phornphisutthimas et al. 2010; Du et al. 2012; Zhang et al. 2019). Thus, a protocol was adapted to the conditions of this study and evaluated for the incorporation of pSET152 into 11-1-2 (see Section 2.1.11.2). In order to identify the culture conditions that promote suitable growth of 11-1-2 for mycelial conjugations, a modified methylene blue adsorption assay was first used to generate growth curves of the strain in different liquid media (Section 2.1.10). Using SLB and SM resulted in more growth than the other media, while adding 1% w/v soluble starch to TSB improved the growth 11-1-2 as compared to TSB without added starch (Figure 5.12). Based on the growth curves, SLB and SM media were good choices for

mycelia conjugation, as they provide more biomass in less time than the other media. Multiple attempts at mycelial conjugation were performed; however, no apramycin-resistant exconjugants were obtained.

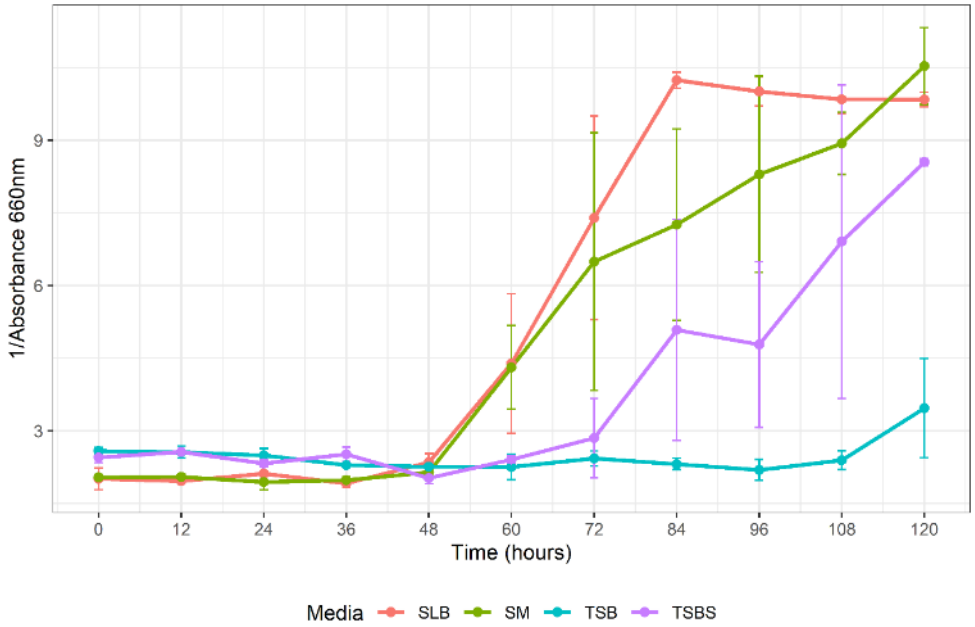

Figure 5.12. Growth curves of *Streptomyces* sp. 11-1-2 using different liquid culture media. Each point is the average of three independent replicates ± standard deviation.

The use of mycelial electroporation to introduce pSET152 into the 11-1-2 strain was also evaluated. The protocol was adapted from a previously published study with *Streptomyces albulus* that achieved the replacement of the gene *sttH* for an apramycin resistance cassette (Hamano et al. 2006). To generate mycelia for the electroporation, SLB liquid medium was used, since it supports good growth of 11-1-2 (Fig. 5.12). However, this method also did not yield any apramycin-resistant exconjugants.

Then, a transformation of 11-1-2 with pSET152 was attempted using a protoplast transformation protocol (Kieser et al. 2000) with some modifications (see Section 2.1.13).

Frozen and fresh protoplasts were used, and denatured and non-denatured DNA were also evaluated. The transformations did not result in apramycin-resistant exconjugants.

Lastly, a fourth modification of the intergeneric conjugation protocol was attempted, in which the 11-1-2 plate cultures were incubated for at least 14 days to obtain more spores, and these spores were mixed with an increased concentration of *E. coli* cells. This protocol resulted in some visible *Streptomyces* colonies after four days of incubation following the antibiotic selection overlay. From the original plates, 20 colonies were transferred and grew successfully on ISP-4 containing nalidixic acid and apramycin, suggesting the successful incorporation of pSET152 into the chromosome. To confirm this, four of the exconjugants were transferred to an SLB agar plate containing apramycin, and following incubation, the resulting vegetative cells from each were used for colony PCR (Section 2.2.3) with primers targeting the apramycin resistance gene (Table 2.3). As shown in Figure 5.13, the expected product was amplified from all four exconjugants, indicating that the conjugal transfer of the pSET152 plasmid had been successful.

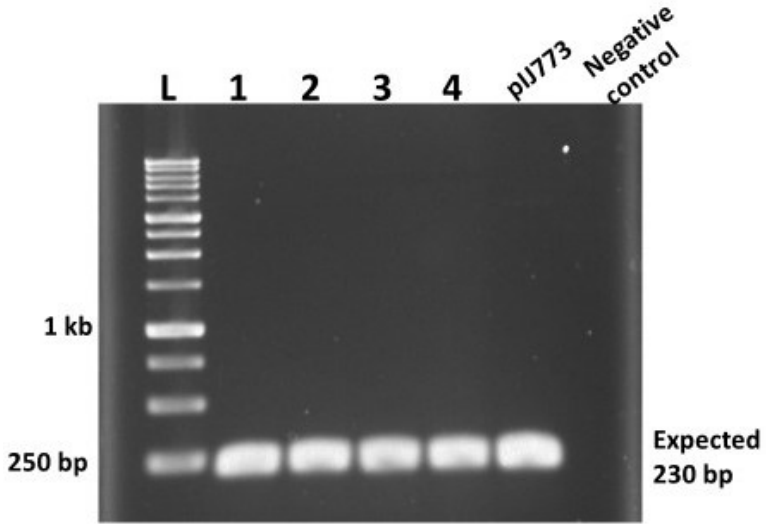

Figure 5.13. PCR verification of transfer of the apramycin resistance gene in *Streptomyces* sp. 11-1-2. L: 1kb ladder. 1-4: 11-1-2 colonies. pIJ773: positive control for the apramycin resistance gene. Negative control: water.

Given the success in introducing pSET152 into the 11-1-2 strain, the same protocol was then attempted using plasmid pGDC1 in order to obtain a geldanamycin-deficient mutant. However, despite multiple attempts, no successful exconjugants were obtained.

The failed attempts to create mutant strains motivated an investigation into the restriction-methylation (RM) systems of 11-1-2. Different organisms have evolved to use RM systems that can distinguish foreign from endogenous DNA and degrade it using restriction enzymes (Suzuki 2012).

An analysis of the 11-1-2 genome in the REBASE website showed that some genes encoding different RM systems are present in the chromosome (Table 5.1). To avoid the activity of these systems, the most common strategy is to first pass the DNA through a methylation-deficient *E. coli* strain such as ET12567, and this was done using this particular strain in the current study. Interestingly, *S. hygroscopicus* XM201 (closely related to 11-1-2) and *S. scabiei* 87-22 (model plant-pathogenic *Streptomyces*) have been successfully modified using the intergeneric conjugation protocol (Wang et al. 2017; Li et al. 2019b). An analysis and comparison of their REBASE profile show that *S. hygroscopicus* XM201 has fewer RM systems than 11-1-2, but *S. scabiei* has more RM systems than the other two strains (Table 5.2). Whether these differences could account for the failure to obtain mutant strains is unknown. However, the strain *Streptomyces xianamensis* 318 contains eleven genes predicted to encode for RM systems of the four types, and this was not a limitation for performing intergeneric conjugation (Xu et al. 2016).

Table 5.1. Restriction-methylation systems of *Streptomyces* sp. 11-1-2 annotated in the REBASE database.

RM Type	Gene*	Name	Predicted Recognition Sequence	Coordinates
I	R	Ssp1112IIP	GACCNNNNNGCTG	7387550-7389901
	M	M.Ssp1112II	GACCNNNNNGCTG	7390140-7391555
	S	S.Ssp1112II	GACCNNNNNGCTG	7391654-7392691
I	M	M.Ssp1112I	TCGANNNNNNNVTCGC	8658621-8660639
	S	S.Ssp1112I	TCGANNNNNNNVTCGC	8660636-8661952
	R	Ssp1112IP	TCGANNNNNNNVTCGC	8661949-8665245
II	M	M.Ssp1112ORF16350P	ND**	3908771-3910261 c
II	M	M.Ssp1112ORF36785P	ND**	8656312-8658522
IV	R	Ssp1112ORF25950P	ND**	6175719-6178859 c

*The gene encodes for the R, M, or S subunit of the system

**Not determined

Table 5.2. Number of restriction-methylation systems annotated in the REBASE database for three different *Streptomyces* strains.

Type	***Streptomyces* sp. 11-1-2**	***S. hygroscopicus* XM201**	***S. scabiei* 87-22**
I	2	0	1
II	2	2	14
III	0	0	0
IV	1	0	3

Using other *E. coli* strains that facilitate the DNA intake by the target bacteria is a potential solution. For *Streptomyces avermitilis*, intergeneric conjugation is also performed with *E. coli* F^- *dcm* Δ(*srl-recA*)306::Tn*10* carrying pUB307-aph::Tn*7* while unmethylated DNA is obtained from *E. coli* GM2929 *(dam13::*Tn*9 dcm-6) hsdS::*Tn*10*) (Kitani et al. 2009;

Ulanova et al. 2013). The use of pUB307-aph::Tn*7* seems to prevent the occurrence of Dam^+ or Dcm^+ phenotypes that would make the DNA susceptible to restriction by *S. avermitilis* (Liot 2016). Another method previously evaluated involves transferring plasmids into a different, non-methylating *Streptomyces* species prior to transformation, such as *S. lividans* (MacNeil 1988).

5.4 Conclusions

Creating mutant strains of organisms of interest has been a method of understanding the biological relevance of genes or gene clusters in producing specialized metabolites. To investigate the role of two specialized metabolites, geldanamycin, and nigericin, in the phytopathogenic phenotype of *Streptomyces* sp. 11-1-2, the creation of mutants was attempted using different known genetic engineering methods suitable for *Streptomyces* species. The gene replacement plasmids were designed and constructed using molecular cloning and Redirect PCR targeting methods. However, the attempts of intergeneric conjugation, electroporation, and protoplast transformation remained unsuccessful. The modification of various factors regarding the donor and recipient strain preparation and culture media was attempted, as these have been reported as critical in other *Streptomyces* species. One modified protocol rendered successful exconjugants with pSET152, thus conferring apramycin resistance to 11-1-2. This protocol was replicated with pGDC1 to target the deletion of the gene *gdmAI*, which encodes for the first PKS in the geldanamycin biosynthesis, but no colonies were obtained despite multiple attempts. Future work should be focused on further modification of conjugation conditions and using alternative *E. coli* and plasmids for conjugation to obtain 11-1-2 mutant strains.

CHAPTER 6

CONCLUSIONS AND FUTURE DIRECTIONS

6.1 Conclusions

Overall, this study provides new knowledge of the phytotoxic specialized metabolites produced by the novel plant pathogen *Streptomyces* sp. 11-1-2, which was isolated in 2011 from a CS-infected potato tuber in Newfoundland, Canada. By using multiple bioassays paired with genomic and metabolomic approaches, it was determined that at least two specialized metabolites, geldanamycin and nigericin, can cause damage to potato tuber tissue and affect radish seedling development. Importantly, this is the first description of these molecules being associated with CS disease of potato. Geldanamycin is of particular interest as it is known to be a potent inhibitor of the eukaryotic HSP90 chaperone, which in plants is an essential component of the innate immune system (Sangster and Queitsch 2005; Kadota and Shirasu 2012). The Gram-negative plant pathogen *P. syringae* produces the effector HopBF1 that catalytically inactivates HSP90, and this is sufficient to induce severe disease symptoms in plants infected with this pathogen (Lopez et al. 2019). Thus, geldanamycin could possibly play a similar role during plant host infection by 11-1-2. Both geldanamycin and nigericin are predicted to be co-produced with a number of closely related molecules that could also potentially exhibit phytotoxic activity and contribute to the phytopathogenic phenotype of 11-1-2. Moreover, this study showed that the production of geldanamycin and nigericin is supressed by NAG, indicating that these molecules are subject to at least one global regulatory mechanism in 11-1-2. It has been hypothesized that NAG supresses specialized metabolite biosynthesis in *Streptomyces* due to the ability of the organism to distinguish between NAG from external sources (i.e. chitin) from the internal sources (cell

wall lysis). Under nutrient-rich conditions, NAG signals the organism to allocate resources for the vegetative growth, but under nutrient-poor conditions, NAG induces specialized metabolite production to outcompete other organisms for nutritional resources (Rigali et al. 2008).

The use of untargeted metabolomics and molecular networking predicted the production of several other specialized metabolites and related molecules by 11-1-2, including elaiophylin, echosides, niphimycins and galbonolides, which is consistent with the predicted BGCs that are present in the 11-1-2 genome. Among these compounds, elaiophylin and echoside C were evaluated for their bioactivity against plants, as they have structural resemblance to plant bioactive molecules, something that had not been investigated before. Elaiophylin was found to exhibit limited effects against potato tissue by itself, but when combined with geldanamycin and nigericin, it increased the severity of the tissue damage induced by these compounds. Importantly, the production of all three compounds was highest when the strain was cultured on the potato-based PMA solid medium, which may indicate that the production of these metabolites is upregulated during tuber colonization. Although the untargeted LC-MS^2 analysis suggested that echoside C production is also highest on the PMA medium, the presence of this compound in the organic culture extracts could not be confirmed, and pure echoside C did not show any phytotoxicity in the plant bioassays conducted in this study. Whether echosides have any role in mediating plant-pathogen interactions will require further investigation.

The use of untargeted metabolomics also showed that many predicted compounds were affected by the addition of NAG to the culture media, suggesting that this elicitor can have a significant impact on the metabolic profile of 11-1-2, likely due to its role as a

hypothetical signal of nutrient availability and as a global regulator. Furthermore, most extracts displayed antimicrobial activity against Gram-positive bacteria and antifungal activity against *S. cerevisiae*. Compounds such as guanidylfungin A, galbonolides, elaiophylin, and efomycin G have some level of antimicrobial and antifungal activity; thus, it is likely they are at least partially responsible for the activity recorded in this study. Considering that *Streptomyces* generally encode for around thirty specialized metabolites (Nett et al. 2009; Lee et al. 2020a), the presence of multiple antimicrobial compounds is expected among *Streptomyces*, and it might represent a mechanism that helps with the colonization of the environment (e.g. soil), and the diverse mode of action of these molecules could expand the number and type of organisms that could compete with *Streptomyces*.

Different plasmids were designed and constructed for the creation of 11-1-2 mutant strains impaired for geldanamycin and nigericin production. Additionally, two plasmids were constructed to investigate the role of two different putative regulators in the nigericin BGC. The creation of mutant strains of 11-1-2 was attempted in this study, but unfortunately all efforts to create such strains were unsucessful and no mutants were obtained. However, a protocol was developed that enabled the successful introdution of the integrative plasmid pSET152 into the 11-1-2 strain. This protocol should serve as the basis for further attempts at the creation of 11-1-2 mutants.

6.2 Future directions

The isolation and characterization of a non-thaxtomin producing strain unrelated to *S. scabiei* is intriguing, as it indicates that different pathogenicity mechanisms have evolved to establish infections. The identification of geldanamycin and nigericin as phytotoxins produced by 11-1-2 leads to many questions. The nigericin mode of action in other organisms

has been described, but its target in plant tissues is unknown. Also, it is unclear whether the molecules predicted to be produced by 11-1-2 and which are closely related to nigericin also contribute to the tissue damage observed. For example, monensin, an ionophore with structural similarity to nigericin, has shown inhibition of gene expression associated with salicylic acid and jasmonate in mutant *Arabidopsis* lines (Joglekar et al. 2018). Thus, how nigericin affects the expression of genes associated with plant defence and how this correlates with the effects recorded in this study should be explored.

The effect of NAG was tested in this study, which showed that geldanamycin and nigericin production is diminished in a dose-dependant manner. Interestingly, the addition of NAG to the YMS medium also resulted in a significant increase of 15-hydroxygeldanamycin while the geldanamycin concentration was reduced. The use of transcriptomics would be beneficial to understand how the expression of the geldanamycin BGC is affected and explain the shift in the biosynthesis of the two compounds. Also, the phytotoxicity of 15-hydroxygeldanamycin remains unknown and should be the focus of future work.

The effect of plant-based compounds like suberin, cellotriose and cellobiose on geldanamycin and nigericin production by the 11-1-2 strain remains unexplored. Thaxtomin A production in *S. scabiei* and *S. turgidiscabies* is induced by cellobiose and cellotriose, which are detected in root exudates during plant growth, suggesting that these organism can sense live tissue as opposed to decaying matter (Johnson et al. 2007; Jourdan et al. 2017). Furthermore, the addition of suberin to minimal medium induces the production of selected specialized metabolites in different *Streptomyces*, most notably, thaxtomin A in *S. scabiei* and geldanamycin in *S. melanosporofaciens* (Lerat et al. 2012). Thus, the role of these plant-

based compounds should be investigated to determine if they modify the gene expression and phytotoxic specialized metabolite biosynthesis in 11-1-2.

Likewise, the carbohydrate-degrading enzymes encoded by 11-1-2 should be experimentally explored, as plant pathogens are expected to benefit from more effective enzymes to colonize host tissues. It has been predicted that plant-associated *Streptomyces*, including 11-1-2, contain an enhanced enzymatic machinery to interact with their hosts (Gayrard et al. 2023), but their role in the pathogenic phenotype must be determined.

New surveys should be conducted to assess the presence of plant pathogenic strains belonging to the *S. violaceusniger* clade in potato growing farms across the island of Newfoundland and beyond. A new survey will provide information regarding how common pathogenic strains related to 11-1-2 are, differences in severity and phytotoxin production, and potential co-infection events.

The production of many different specialized metabolites by 11-1-2 was predicted in this study, but their identity and production levels should be confirmed with targeted metabolomics and chemical characterization. For example, guanidylfungin A is likely to be involved in the antimicrobial and antifungal activity seen in the organic extracts. Similarly, the presence of galbonolides should be confirmed in the extracts, as they can also exert antifungal activity. In both cases, the plant bioactivity must also be determined. Furthermore, the prediction of some molecules like 12-hydroxyjasmonic acid and musacin D is intriguing and must be further explored to determine their contribution in the pathogenic phenotype of the strain. These two compounds and those for which a structure could not be assigned with chemoinformatics tools are a desirable target for further research. The addition of a transcriptomics approach could also provide more evidence regarding the production of these

uncharacterized specialized metabolites by revealing the gene expression profile of the predicted BGCs in 11-1-2 under conditions that promote higher phytotoxicity (e.g. growing on PMA medium).

The further optimization of a protocol for the construction of 11-1-2 mutant strains would be a great development in furthering our understanding of this pathogen. It would allow for the construction of mutant strains that are deficient in the production of putative pathogenicity or virulence factors such as geldanamycin and nigericin in order to better understand the molecular mechanisms of pathogenicity in the 11-1-2 strain. Likewise, the creation of strains that overexpress regulatory genes in the nigericin and geldanamycin BGCs, thus increasing their biosynthesis, would enable studies that could confirm their role as virulence or pathogenicity factors. The investigation of *sigJ* and its potential role in the regulation of nigericin production is of particular interest given that there is only one other instance of an ECF sigma factor serving as a specialized metabolite CSR. Finally, the ability to genetically engineer the 11-1-2 strain could facilitate future studies on the uncharacterized specialized metabolites that were detected in this study along with those that are produced by BGCs that are silent under lab conditions.

The characterization of non-thaxtomin producing plant pathogenic *Streptomyces* such as 11-1-2 indicates that using potato varieties with tolerance or resistance to thaxtomin A might be insufficient to avoid the development of CS, as the targets of geldanamycin and nigericin are different from that of thaxtomin A. Similarly, the identification of plant pathogenic *Streptomyces* by PCR amplification of the *txtAB* genes only provides genomic evidence of thaxtomin A production, but it excludes potential phytopathogenic species that use other phytotoxins to colonize and inflict damage to plant tissues. Thus, research programs

in potato breeding, plant pathogenic *Streptomyces* identification, and CS disease management should consider the outcomes of this study to better understand the pathosystem.

BIBLIOGRAPHY

van der Aart, L.T., Spijksma, G.K., Harms, A., Vollmer, W., Hankemeier, T., and van Wezel, G.P. 2018. High-Resolution Analysis of the Peptidoglycan Composition in *Streptomyces coelicolor*. J. Bacteriol. **200**(20). doi:10.1128/JB.00290-18.

Ahlmann-Eltze, C. 2019. ggsignif: Significance Brackets for "ggplot2."

Alanjary, M., Steinke, K., and Ziemert, N. 2019. AutoMLST: An automated web server for generating multi-locus species trees highlighting natural product potential. Nucleic Acids Res. **47**(W1): W276–W282. Oxford University Press. doi:10.1093/nar/gkz282.

Allen, I.W., and Ritchie, D.A. 1994. Cloning and analysis of DNA sequences from *Streptomyces hygroscopicus* encoding geldanamycin biosynthesis. MGG Mol. Gen. Genet. **243**(5): 593–599. doi:10.1007/BF00284208.

Andam, C.P., Doroghazi, J.R., Campbell, A.N., Kelly, P.J., Choudoir, M.J., and Buckley, D.H. 2016. A latitudinal diversity gradient in terrestrial bacteria of the genus *Streptomyces*. MBio **7**(2). doi:10.1128/mBio.02200-15.

Aravind, L., Anantharaman, V., Balaji, S., Babu, M.M., and Iyer, L.M. 2005. The many faces of the helix-turn-helix domain: Transcription regulation and beyond. FEMS Microbiol. Rev. **29**(2): 231–262. doi:10.1016/j.femsre.2004.12.008.

Arias, P., Fernández-Moreno, M.A., and Malpartida, F. 1999. Characterization of the pathway-specific positive transcriptional regulator for actinorhodin biosynthesis in *Streptomyces coelicolor* A3(2) as a DNA-binding protein. J. Bacteriol. **181**(22): 6958–6968. doi:10.1128/jb.181.22.6958-6968.1999.

Bakker, M.G., Glover, J.D., Mai, J.G., and Kinkel, L.L. 2010. Plant community effects on the diversity and pathogen suppressive activity of soil streptomycetes. Appl. Soil Ecol. **46**(1): 35–42. Elsevier B.V. doi:10.1016/j.apsoil.2010.06.003.

Baltz, R.H. 1999. Genetic recombination by protoplast fusion in *Streptomyces*. J. Ind. Microbiol. Biotechnol. **22**(4–5): 460–471. doi:10.1038/sj.jim.2900659.

Barry, S.M., Kers, J.A., Johnson, E.G., Song, L., Aston, P.R., Patel, B., Krasnoff, S.B., Crane, B.R., Gibson, D.M., Loria, R., and Challis, G.L. 2012. Cytochrome P450-catalyzed L-tryptophan nitration in thaxtomin phytotoxin biosynthesis. Nat. Chem. Biol. **8**(10): 814–816. doi:10.1038/nchembio.1048.

Bayona, L.M., de Voogd, N.J., and Choi, Y.H. 2022. Metabolomics on the study of marine organisms. Metabolomics **18**(3): 1–24. Springer US. doi:10.1007/s11306-022-01874-y.

Becher, P.G., Verschut, V., Bibb, M.J., Bush, M.J., Molnár, B.P., Barane, E., Al-Bassam, M.M., Chandra, G., Song, L., Challis, G.L., Buttner, M.J., and Flärdh, K. 2020. Developmentally regulated volatiles geosmin and 2-methylisoborneol attract a soil arthropod to *Streptomyces* bacteria promoting spore dispersal. Nat. Microbiol. **5**(6): 821–829. doi:10.1038/s41564-020-0697-x.

van den Belt, M., Gilchrist, C., Booth, T.J., Chooi, Y.-H., Medema, M.H., and Alanjary, M. 2023. CAGECAT: The CompArative GEne Cluster Analysis Toolbox for rapid search and visualisation of homologous gene clusters. BMC Bioinformatics **24**(1): 181. BioMed Central. doi:10.1186/s12859-023-05311-2.

Bentley, S.D., Chater, K.F., Cerdeño-Tárraga, A.M., Challis, G.L., Thomson, N.R., James,

K.D., Harris, D.E., Quail, M.A., Kieser, H., Harper, D., Bateman, A., Brown, S., Chandra, G., Chen, C.W., Collins, M., Cronin, A., Fraser, A., Goble, A., Hidalgo, J., Hornsby, T., Howarth, S., Huang, C.H., Kieser, T., Larke, L., Murphy, L., Oliver, K., O'Neil, S., Rabbinowitsch, E., Rajandream, M.A., Rutherford, K., Rutter, S., Seeger, K., Saunders, D., Sharp, S., Squares, R., Squares, S., Taylor, K., Warren, T., Wietzorrek, A., Woodward, J., Barrell, B.G., Parkhill, J., and Hopwood, D.A. 2002. Complete genome sequence of the model actinomycete *Streptomyces coelicolor* A3(2). Nature **417**(6885): 141–147. doi:10.1038/417141a.

van Bergeijk, D.A., Terlouw, B.R., Medema, M.H., and van Wezel, G.P. 2020. Ecology and genomics of Actinobacteria: new concepts for natural product discovery. Nat. Rev. Microbiol. **18**(10): 546–558. Springer US. doi:10.1038/s41579-020-0379-y.

Besaury, L., Martinet, L., Mühle, E., Clermont, D., and Rémond, C. 2021. *Streptomyces silvae* sp. Nov., isolated from forest soil. Int. J. Syst. Evol. Microbiol. **71**(12). doi:10.1099/ijsem.0.005147.

Bibb, M.J. 2005. Regulation of secondary metabolism in streptomycetes. Curr. Opin. Microbiol. **8**(2): 208–215. doi:10.1016/j.mib.2005.02.016.

Bierman, M., Logan, R., O'Brien, K., Seno, E.T., Nagaraja Rao, R., and Schoner, B.E. 1992. Plasmid cloning vectors for the conjugal transfer of DNA from *Escherichia coli* to *Streptomyces* spp. Gene **116**(1): 43–49. doi:10.1016/0378-1119(92)90627-2.

Bignell, D.R.D., Cheng, Z., and Bown, L. 2018. The coronafacoyl phytotoxins: structure, biosynthesis, regulation and biological activities. Antonie Van Leeuwenhoek **111**(5): 649–666. Springer International Publishing. doi:10.1007/s10482-017-1009-1.

Bignell, D.R.D., Francis, I.M., Fyans, J.K., and Loria, R. 2014. Thaxtomin A Production and Virulence Are Controlled by Several bld Gene Global Regulators in *Streptomyces scabies*. Mol. Plant-Microbe Interact. **27**(8): 875–885. doi:10.1094/MPMI-02-14-0037-R.

Bignell, D.R.D., Huguet-Tapia, J.C., Joshi, M. V., Pettis, G.S., and Loria, R. 2010. What does it take to be a plant pathogen: Genomic insights from *Streptomyces* species. Antonie Van Leeuwenhoek **98**(2): 179–194. doi:10.1007/s10482-010-9429-1.

Bilyk, B., Kim, S., Fazal, A., Baker, T.A., and Seipke, R.F. 2020. Regulation of Antimycin Biosynthesis Is Controlled by the ClpXP Protease. mSphere **5**(2). doi:10.1128/msphere.00144-20.

Bisson-Filho, A.W., Hsu, Y.P., Squyres, G.R., Kuru, E., Wu, F., Jukes, C., Sun, Y., Dekker, C., Holden, S., VanNieuwenhze, M.S., Brun, Y. V., and Garner, E.C. 2020. Treadmilling by FtsZ filaments drives peptidoglycan synthesis and bacterial cell division. Science (80-.). **367**(6475): 6–10. doi:10.1126/science.aba6311.

Blin, K., Shaw, S., Augustijn, H.E., Reitz, Z.L., Biermann, F., Alanjary, M., Fetter, A., Terlouw, B.R., Metcalf, W.W., Helfrich, E.J.N., van Wezel, G.P., Medema, M.H., and Weber, T. 2023. antiSMASH 7.0: new and improved predictions for detection, regulation, chemical structures and visualisation. Nucleic Acids Res.: 1–5. Oxford University Press. doi:10.1093/nar/gkad344.

Blin, K., Shaw, S., Kloosterman, A.M., Charlop-Powers, Z., Van Wezel, G.P., Medema, M.H., and Weber, T. 2021. AntiSMASH 6.0: Improving cluster detection and comparison capabilities. Nucleic Acids Res. **49**(W1): W29–W35. Oxford University

Press. doi:10.1093/nar/gkab335.

Bobek, J., Šmídová, K., and Čihák, M. 2017. A waking review: Old and novel insights into the spore germination in *Streptomyces*. Front. Microbiol. **8**(NOV): 1–12. doi:10.3389/fmicb.2017.02205.

Bode, H.B., Bethe, B., Höfs, R., and Zeeck, A. 2002. Big effects from small changes: Possible ways to explore nature's chemical diversity. ChemBioChem **3**(7): 619–627. doi:10.1002/1439-7633(20020703)3:7<619::AID-CBIC619>3.0.CO;2-9.

Book, A.J., Lewin, G.R., McDonald, B.R., Takasuka, T.E., Doering, D.T., Adams, A.S., Blodgett, J.A.V., Clardy, J., Raffa, K.F., Fox, B.G., and Currie, C.R. 2014. Cellulolytic *Streptomyces* strains associated with herbivorous insects share a phylogenetically linked capacity to degrade lignocellulose. Appl. Environ. Microbiol. **80**(15): 4692–4701. doi:10.1128/AEM.01133-14.

Bouchek-Mechiche, K., Pasco, C., Andrivon, D., and Jouan, B. 2000. Differences in host range, pathogenicity to potato cultivars and response to soil temperature among *Streptomyces* species causing common and netted scab in France. Plant Pathol. **49**(1): 3–10. doi:10.1046/j.1365-3059.2000.00419.x.

Bown, L., and Bignell, D.R.D. 2017. Draft Genome Sequence of the Plant Pathogen *Streptomyces* sp. Strain 11-1-2. Genome Announc. **5**(37): 14–16. doi:10.1128/genomeA.00968-17.

Braun, S., Gevens, A., Charkowski, A., Allen, C., and Jansky, S. 2017. Potato Common Scab: a Review of the Causal Pathogens, Management Practices, Varietal Resistance Screening Methods, and Host Resistance. Am. J. Potato Res. **94**(4): 283–296.

American Journal of Potato Research. doi:10.1007/s12230-017-9575-3.

Bruijn, F.J. de, Lupski, J.R., and Weinstock, G.M. 1998. Bacterial Genomes. *Edited By*F.J. de Bruijn, J.R. Lupski, and G.M. Weinstock. Springer US, Boston, MA. doi:10.1007/978-1-4615-6369-3.

Buell, C.R., Joardar, V., Lindeberg, M., Selengut, J., Paulsen, I.T., Gwinn, M.L., Dodson, R.J., Deboy, R.T., Durkin, A.S., Kolonay, J.F., Madupu, R., Daugherty, S., Brinkac, L., Beanan, M.J., Haft, D.H., Nelson, W.C., Davidsen, T., Zafar, N., Zhou, L., Liu, J., Yuan, Q., Khouri, H., Fedorova, N., Tran, B., Russell, D., Berry, K., Utterback, T., Van Aken, S.E., Feldblyum, T. V., D'Ascenzo, M., Deng, W.-L., Ramos, A.R., Alfano, J.R., Cartinhour, S., Chatterjee, A.K., Delaney, T.P., Lazarowitz, S.G., Martin, G.B., Schneider, D.J., Tang, X., Bender, C.L., White, O., Fraser, C.M., and Collmer, A. 2003. The complete genome sequence of the Arabidopsis and tomato pathogen *Pseudomonas syringae* pv. *tomato* DC3000. Proc. Natl. Acad. Sci. **100**(18): 10181–10186. doi:10.1073/pnas.1731982100.

Burkhardt, K., Fiedler, H.-P., Grabley, S., Thiericke, R., and Zeeck, A. 1996. New Cineromycins and Musacins Obtained by Metabolite Pattern Analysis of *Streptomyces griseoviridis* (FH-S 1832). I. Taxonomy, Fermentation, Isolation and Biological Activity. J. Antibiot. (Tokyo). **49**(5): 432–437. doi:10.7164/antibiotics.49.432.

Bush, M.J., Gallagher, K.A., Chandra, G., Findlay, K.C., and Schlimpert, S. 2022. Hyphal compartmentalization and sporulation in *Streptomyces* require the conserved cell division protein SepX. Nat. Commun. **13**(1). Springer US. doi:10.1038/s41467-021-27638-1.

Cai, P., Kong, F., Fink, P., Ruppen, M.E., Williamson, R.T., and Keiko, T. 2007. Polyene antibiotics from *Streptomyces mediocidicus*. J. Nat. Prod. **70**(2): 215–219. doi:10.1021/np060542f.

Caicedo-Montoya, C., Manzo-Ruiz, M., and Ríos-Estepa, R. 2021. Pan-Genome of the Genus *Streptomyces* and Prioritization of Biosynthetic Gene Clusters With Potential to Produce Antibiotic Compounds. Front. Microbiol. **12**(September). doi:10.3389/fmicb.2021.677558.

Cao, Z., Khodakaramian, G., Arakawa, K., and Kinashi, H. 2012. Isolation of Borrelidin as a phytotoxic compound from a potato pathogenic *Streptomyces* strain. Biosci. Biotechnol. Biochem. **76**(2): 353–357. doi:10.1271/bbb.110799.

Casadevall, A., and Pirofski, L.A. 1999. Host-pathogen interactions: Redefining the basic concepts of virulence and pathogenicity. Infect. Immun. **67**(8): 3703–3713. doi:10.1128/iai.67.8.3703-3713.1999.

Celenza, J.L., Grisafi, P.L., and Fink, G.R. 1995. A pathway for lateral root formation in *Arabidopsis thaliana*. Genes Dev. **9**(17): 2131–2142. doi:10.1101/gad.9.17.2131.

Chakraborty, S., Khopade, A., Kokare, C., Mahadik, K., and Chopade, B. 2009. Isolation and characterization of novel α-amylase from marine *Streptomyces* sp. D1. J. Mol. Catal. B Enzym. **58**(1–4): 17–23. doi:10.1016/j.molcatb.2008.10.011.

Chaleckis, R., Meister, I., Zhang, P., and Wheelock, C.E. 2019. Challenges, progress and promises of metabolite annotation for LC–MS-based metabolomics. Curr. Opin. Biotechnol. **55**: 44–50. Elsevier Ltd. doi:10.1016/j.copbio.2018.07.010.

Chalupowicz, L., Tsror, L., Hazanovsky, M., Erlich, O., Reuven, M., Dror, O., Lebiush, S.,

and Manulis-Sasson, S. 2022. Isolation and characterization of *Streptomyces* spp. from potato and peanut in Israel. Plant Pathol. **71**(9): 1870–1879. doi:10.1111/ppa.13619.

Chambers, M.C., Maclean, B., Burke, R., Amodei, D., Ruderman, D.L., Neumann, S., Gatto, L., Fischer, B., Pratt, B., Egertson, J., Hoff, K., Kessner, D., Tasman, N., Shulman, N., Frewen, B., Baker, T.A., Brusniak, M.-Y., Paulse, C., Creasy, D., Flashner, L., Kani, K., Moulding, C., Seymour, S.L., Nuwaysir, L.M., Lefebvre, B., Kuhlmann, F., Roark, J., Rainer, P., Detlev, S., Hemenway, T., Huhmer, A., Langridge, J., Connolly, B., Chadick, T., Holly, K., Eckels, J., Deutsch, E.W., Moritz, R.L., Katz, J.E., Agus, D.B., MacCoss, M., Tabb, D.L., and Mallick, P. 2012. A cross-platform toolkit for mass spectrometry and proteomics. Nat. Biotechnol. **30**(10): 918–920. doi:10.1038/nbt.2377.

Chandra, G., and Chater, K.F. 2008. Evolutionary flux of potentially bldA-dependent *Streptomyces* genes containing the rare leucine codon TTA. Antonie van Leeuwenhoek, Int. J. Gen. Mol. Microbiol. **94**(1): 111–126. doi:10.1007/s10482-008-9231-5.

Charkowski, A., Sharma, K., Parker, M.L., Secor, G.A., and Elphinstone, J. 2020. Bacterial Diseases of Potato. *In* The Potato Crop: Its Agricultural, Nutritional and Social Contribution to Humankind. *Edited by* H. Campos and O. Ortiz. Springer International Publishing, Cham. pp. 351–388. doi:10.1007/978-3-030-28683-5_10.

Chater, K.F., Biró, S., Lee, K.J., Palmer, T., and Schrempf, H. 2010. The complex extracellular biology of *Streptomyces*. FEMS Microbiol. Rev. **34**(2): 171–198. doi:10.1111/j.1574-6976.2009.00206.x.

Chen, H., Cui, J., Wang, P., Wang, X., and Wen, J. 2020. Enhancement of bleomycin production in *Streptomyces verticillus* through global metabolic regulation of N-acetylglucosamine and assisted metabolic profiling analysis. Microb. Cell Fact. **19**(1): 1–17. BioMed Central. doi:10.1186/s12934-020-01301-8.

Chen, Y., Wei, Y., Cai, B., Zhou, D., Qi, D., Zhang, M., Zhao, Y., Li, K., Wedge, D.E., Pan, Z., Xie, J., and Wang, W. 2022. Discovery of Niphimycin C from *Streptomyces yongxingensis* sp. nov. as a Promising Agrochemical Fungicide for Controlling Banana Fusarium Wilt by Destroying the Mitochondrial Structure and Function. J. Agric. Food Chem. **70**(40): 12784–12795. doi:10.1021/acs.jafc.2c02810.

Cheng, Z. 2018. Regulation of coronafacoyl phytotoxin production in the potato common scab pathogen *Streptomyces scabies*. Memorial University of Newfoundland.

Cheng, Z., Bown, L., Piercey, B., and Bignell, D.R.D. 2019. Positive and Negative Regulation of the Virulence-Associated Coronafacoyl Phytotoxin in the Potato Common Scab Pathogen *Streptomyces scabies*. Mol. Plant-Microbe Interact. **32**(10): 1348–1359. doi:10.1094/MPMI-03-19-0070-R.

Cheng, Z., Bown, L., Tahlan, K., and Bignell, D.R.D. 2015. Regulation of coronafacoyl phytotoxin production by the PAS-LuxR family regulator CfaR in the common scab pathogen *Streptomyces scabies*. PLoS One **10**(3): 1–17. doi:10.1371/journal.pone.0122450.

Chevrette, M.G., Carlson, C.M., Ortega, H.E., Thomas, C., Ananiev, G.E., Barns, K.J., Book, A.J., Cagnazzo, J., Carlos, C., Flanigan, W., Grubbs, K.J., Horn, H.A., Hoffmann, F.M., Klassen, J.L., Knack, J.J., Lewin, G.R., McDonald, B.R., Muller, L.,

Melo, W.G.P., Pinto-Tomás, A.A., Schmitz, A., Wendt-Pienkowski, E., Wildman, S., Zhao, M., Zhang, F., Bugni, T.S., Andes, D.R., Pupo, M.T., and Currie, C.R. 2019. The antimicrobial potential of *Streptomyces* from insect microbiomes. Nat. Commun. **10**(1): 1–11. Springer US. doi:10.1038/s41467-019-08438-0.

Čihák, M., Kameník, Z., Šmídová, K., Bergman, N., Benada, O., Kofronová, O., Petrícková, K., and Bobek, J. 2017. Secondary metabolites produced during the germination of *Streptomyces coelicolor*. Front. Microbiol. **8**(DEC): 1–13. doi:10.3389/fmicb.2017.02495.

Claessen, D., Stokroos, L., Deelstra, H.J., Penninga, N.A., Bormann, C., Salas, J.A., Dijkhuizen, L., and Wösten, H.A.B. 2004. The formation of the rodlet layer of streptomycetes is the result of the interplay between rodlins and chaplins. Mol. Microbiol. **53**(2): 433–443. doi:10.1111/j.1365-2958.2004.04143.x.

Clarke, C.R., Kramer, C.G., Kotha, R.R., and Luthria, D.L. 2022. The Phytotoxin Thaxtomin A Is the Primary Virulence Determinant for Scab Disease of Beet, Carrot, and Radish Caused by *Streptomyces scabiei*. Phytopathology® **112**(11): 2288–2295. doi:10.1094/PHYTO-03-22-0072-R.

Cline, K., Werner-Washburne, M., Lubben, T.H., and Keegstra, K. 1985. Precursors to two nuclear-encoded chloroplast proteins bind to the outer envelope membrane before being imported into chloroplasts. J. Biol. Chem. **260**(6): 3691–3696. Â© 1985 ASBMB. Currently published by Elsevier Inc; originally published by American Society for Biochemistry and Molecular Biology. doi:10.1016/s0021-9258(19)83678-5.

Clinger, J.A., Zhang, Y., Liu, Y., Miller, M.D., Hall, R.E., Van Lanen, S.G., Phillips, G.N., Thorson, J.S., and Elshahawi, S.I. 2021. Structure and Function of a Dual Reductase–Dehydratase Enzyme System Involved in p-Terphenyl Biosynthesis. ACS Chem. Biol. **16**(12): 2816–2824. doi:10.1021/acschembio.1c00701.

Cohen, G.N. 2011. Microbial Biochemistry. *In* Microbial Biochemistry. Springer Netherlands, Dordrecht. doi:10.1007/978-90-481-9437-7.

Colson, S., Stephan, J., Hertrich, T., Saito, A., Van Wezel, G.P., Titgemeyer, F., and Rigali, S. 2006. Conserved cis-acting elements upstream of genes composing the chitinolytic system of *Streptomycetes* are DasR-responsive elements. J. Mol. Microbiol. Biotechnol. **12**(1–2): 60–66. doi:10.1159/000096460.

Combes, P., Till, R., Bee, S., and Smith, M.C.M. 2002. The *Streptomyces* genome contains multiple pseudo-attB sites for the φC31-encoded site-specific recombination system. J. Bacteriol. **184**(20): 5746–5752. doi:10.1128/JB.184.20.5746-5752.2002.

Cornforth, D.M., and Foster, K.R. 2013. Competition sensing: The social side of bacterial stress responses. Nat. Rev. Microbiol. **11**(4): 285–293. Nature Publishing Group. doi:10.1038/nrmicro2977.

Craig, M., Lambert, S., Jourdan, S., Tenconi, E., Colson, S., Maciejewska, M., Ongena, M., Martin, J.F., van Wezel, G., and Rigali, S. 2012. Unsuspected control of siderophore production by N-acetylglucosamine in streptomycetes. Environ. Microbiol. Rep. **4**(5): 512–521. doi:10.1111/j.1758-2229.2012.00354.x.

Craig, S., and Goodchild, D.J. 1984. Golgi-mediated vicilin accumulation in pea cotyledon cells is re-directed by monensin and nigericin. Protoplasma **122**(1–2): 91–97.

doi:10.1007/BF01279441.

Croce, V., López-Radcenco, A., Lapaz, M.I., Pianzzola, M.J., Moyna, G., and Siri, M.I. 2021. An Integrative Approach for the Characterization of Plant-Pathogenic *Streptomyces* spp. Strains Based on Metabolomic, Bioactivity, and Phylogenetic Analysis. Front. Microbiol. **12**(March): 1–11. doi:10.3389/fmicb.2021.643792.

Cruywagen, E.M., Pierneef, R.E., Chauke, K.A., Nkosi, B.Z., Labeda, D.P., and Cloete, M. 2021. Major Streptomyces species associated with fissure scab of potato in South Africa including description of *Streptomyces solaniscabiei* sp. nov. Antonie van Leeuwenhoek, Int. J. Gen. Mol. Microbiol. **114**(12): 2033–2046. Springer International Publishing. doi:10.1007/s10482-021-01659-8.

Davies, J. 2013. Specialized microbial metabolites: Functions and origins. J. Antibiot. (Tokyo). **66**(7): 361–364. Nature Publishing Group. doi:10.1038/ja.2013.61.

DeBoer, C., and Dietz, A. 1976. The description and antibiotic production of *Streptomyces hygroscopicus* var. *geldanus*. J. Antibiot. (Tokyo). **29**(11): 1182–1188.

Dedrick, R.M., Wildschutte, H., and McCormick, J.R. 2009. Genetic interactions of smc, ftsK, and parB genes in *Streptomyces coelicolor* and their developmental genome segregation phenotypes. J. Bacteriol. **91**(1): 320–332. doi:10.1128/JB.00858-08.

Dees, M.W., and Wanner, L.A. 2012. In Search of Better Management of Potato Common Scab. Potato Res. **55**(3–4): 249–268. doi:10.1007/s11540-012-9206-9.

Deng, J., Lu, C., Li, S., Hao, H., Li, Z., Zhu, J., Li, Y., and Shen, Y. 2014. P-Terphenyl O-β-glucuronides, DNA topoisomerase inhibitors from *Streptomyces* sp. LZ35ΔgdmAI. Bioorganic Med. Chem. Lett. **24**(5): 1362–1365. Elsevier Ltd.

doi:10.1016/j.bmcl.2014.01.037.

Donald, L., Pipite, A., Subramani, R., Owen, J., Keyzers, R.A., and Taufa, T. 2022. *Streptomyces*: Still the Biggest Producer of New Natural Secondary Metabolites, a Current Perspective. Microbiol. Res. (Pavia). **13**(3): 418–465. doi:10.3390/microbiolres13030031.

Du, L., Liu, R.H., Ying, L., and Zhao, G.R. 2012. An efficient intergeneric conjugation of DNA from *Escherichia coli* to mycelia of the lincomycin-producer *Streptomyces lincolnensis*. Int. J. Mol. Sci. **13**(4): 4797–4806. doi:10.3390/ijms13044797.

Du, Y., and Scheres, B. 2018. Lateral root formation and the multiple roles of auxin. J. Exp. Bot. **69**(2): 155–167. doi:10.1093/jxb/erx223.

Duangupama, T., Intaraudom, C., Pittayakhajonwut, P., Suriyachadkun, C., Tadtong, S., Sirirote, P., Tanasupawat, S., and Thawai, C. 2021. *Streptomyces musisoli* sp. nov., an actinomycete isolated from soil. Int. J. Syst. Evol. Microbiol. **71**(7). doi:10.1099/ijsem.0.004857.

Duban, M., Cociancich, S., and Leclère, V. 2022. Nonribosomal Peptide Synthesis Definitely Working Out of the Rules. Microorganisms **10**(3). doi:10.3390/microorganisms10030577.

Dührkop, K., Fleischauer, M., Ludwig, M., Aksenov, A.A., Melnik, A. V., Meusel, M., Dorrestein, P.C., Rousu, J., and Böcker, S. 2019a. SIRIUS 4: a rapid tool for turning tandem mass spectra into metabolite structure information. *In* Nature Methods. doi:10.1038/s41592-019-0344-8.

Dührkop, K., Fleischauer, M., Ludwig, M., Aksenov, A.A., Melnik, A. V., Meusel, M.,

Dorrestein, P.C., Rousu, J., and Böcker, S. 2019b. SIRIUS 4: a rapid tool for turning tandem mass spectra into metabolite structure information. Nat. Methods **16**(4): 299–302. Springer US. doi:10.1038/s41592-019-0344-8.

Dührkop, K., Shen, H., Meusel, M., Rousu, J., and Böcker, S. 2015. Searching molecular structure databases with tandem mass spectra using CSI:FingerID. Proc. Natl. Acad. Sci. U. S. A. **112**(41): 12580–12585. doi:10.1073/pnas.1509788112.

Duval, I., Brochu, V., Simard, M., Beaulieu, C., and Beaudoin, N. 2005. Thaxtomin A induces programmed cell death in *Arabidopsis thaliana* suspension-cultured cells. Planta **222**(5): 820–831. doi:10.1007/s00425-005-0016-z.

Elliot, M.A., Bibb, M.J., Buttner, M.J., and Leskiw, B.K. 2001. BldD is a direct regulator of key developmental genes in *Streptomyces coelicolor* A3(2). Mol. Microbiol. **40**(1): 257–269. doi:10.1046/j.1365-2958.2001.02387.x.

Enríquez, L.L., Mendes, M. V., Antón, N., Tunca, S., Guerra, S.M., Martín, J.F., and Aparicio, J.F. 2006. An efficient gene transfer system for the pimaricin producer *Streptomyces natalensis*. FEMS Microbiol. Lett. **257**(2): 312–318. doi:10.1111/j.1574-6968.2006.00189.x.

Ernst, M., Kang, K. Bin, Caraballo-Rodríguez, A.M., Nothias, L.-F., Wandy, J., Chen, C., Wang, M., Rogers, S., Medema, M.H., Dorrestein, P.C., and van der Hooft, J.J.J. 2019a. MolNetEnhancer: Enhanced Molecular Networks by Integrating Metabolome Mining and Annotation Tools. Metabolites **9**(7): 144. doi:10.3390/metabo9070144.

Ernst, M., Kang, K. Bin, Caraballo-Rodríguez, A.M., Nothias, L.F., Wandy, J., Chen, C., Wang, M., Rogers, S., Medema, M.H., Dorrestein, P.C., and van der Hooft, J.J.J.

2019b. Molnetenhancer: Enhanced molecular networks by integrating metabolome mining and annotation tools. Metabolites **9**(7). doi:10.3390/metabo9070144.

Evidente, A., Cimmino, A., and Andolfi, A. 2013. The Effect of Stereochemistry on the Biological Activity of Natural Phytotoxins, Fungicides, Insecticides and Herbicides. Chirality **25**(2): 59–78. doi:10.1002/chir.22124.

Fang, A., Wong, G.K., and Demain, A.L. 2000. Enhancement of the Antifungal Activity of Rapamycin by the coproduced elaiophylin and nigericin. J. Antibiot. (Tokyo). **53**(2).

Fehr, T., King, H.D., and Kuhn, M. 1977. Mutalomycin, a new polyether antibiotic: Taxonomy, fermentation, isolation and characterization. J. Antibiot. (Tokyo). **30**(11): 903–907. doi:10.7164/antibiotics.30.903.

Ferguson, N.L., Peña-Castillo, L., Moore, M.A., Bignell, D.R.D., and Tahlan, K. 2016. Proteomics analysis of global regulatory cascades involved in clavulanic acid production and morphological development in *Streptomyces clavuligerus*. J. Ind. Microbiol. Biotechnol. **43**(4): 537–555. Springer Berlin Heidelberg. doi:10.1007/s10295-016-1733-y.

Fernández-Martínez, L.T., and Hoskisson, P.A. 2019. Expanding, integrating, sensing and responding: the role of primary metabolism in specialised metabolite production. Curr. Opin. Microbiol. **51**: 16–21. doi:10.1016/j.mib.2019.03.006.

Fischer, M., and Sawers, R.G. 2013. A universally applicable and rapid method for measuring the growth of *Streptomyces* and other filamentous microorganisms by methylene blue adsorption-desorption. Appl. Environ. Microbiol. **79**(14): 4499–4502. doi:10.1128/AEM.00778-13.

Flärdh, K. 2003. Essential role of DivlVA in polar growth and morphogenesis in *Streptomyces coelicolor* A3(2). Mol. Microbiol. **49**(6): 1523–1536. doi:10.1046/j.1365-2958.2003.03660.x.

Flärdh, K., and Buttner, M.J. 2009. *Streptomyces* morphogenetics: Dissecting differentiation in a filamentous bacterium. Nat. Rev. Microbiol. **7**(1): 36–49. doi:10.1038/nrmicro1968.

Flärdh, K., Richards, D.M., Hempel, A.M., Howard, M., and Buttner, M.J. 2012. Regulation of apical growth and hyphal branching in *Streptomyces*. Curr. Opin. Microbiol. **15**(6): 737–743. doi:10.1016/j.mib.2012.10.012.

Francis, I.M., Jourdan, S., Fanara, S., Loria, R., and Rigali, S. 2015. The Cellobiose Sensor CebR Is the Gatekeeper of *Streptomyces scabies* Pathogenicity. MBio **6**(2): 31–39. doi:10.1128/mBio.02018-14.

Fry, B.A., and Loria, R. 2002. Thaxtomin A: Evidence for a plant cell wall target. Physiol. Mol. Plant Pathol. **60**(1): 1–8. doi:10.1006/pmpp.2001.0371.

Fukushima, T., Tanaka, M., Gohbara, M., and Fujimori, T. 1998. Phytotoxicity of three lactones from *Nigrospora sacchari*. Phytochemistry **48**(4): 625–630. doi:10.1016/S0031-9422(97)01023-6.

Fyans, J.K., Altowairish, M.S., Li, Y., and Bignell, D.R.D. 2015. Characterization of the Coronatine-Like Phytotoxins Produced by the Common Scab Pathogen *Streptomyces scabies*. Mol. Plant. Microbe. Interact. **28**(4): 443–54. doi:10.1094/MPMI-09-14-0255-R.

Fyans, J.K., Bown, L., and Bignell, D.R.D. 2016. Isolation and characterization of plant

pathogenic *Streptomyces* species associated with common scab - infected potato tubers in Newfoundland. Phytopathology **106**(334): 1–46. doi:10.1094/PHYTO-05-15-0125-R.

Galm, U., Wang, L., Wendt-Pienkowski, E., Yang, R., Liu, W., Tao, M., Coughlin, J.M., and Shen, B. 2008. *In vivo* manipulation of the bleomycin biosynthetic gene cluster in *Streptomyces verticillus* ATCC15003 revealing new insights into its biosynthetic pathway. J. Biol. Chem. **283**(42): 28236–28245. © 2008 ASBMB. Currently published by Elsevier Inc; originally published by American Society for Biochemistry and Molecular Biology. doi:10.1074/jbc.M804971200.

Gao, Y., Ning, Q., Yang, Y., Liu, Y., Niu, S., Hu, X., Pan, H., Bu, Z., Chen, N., Guo, J., Yu, J., Cao, L., Qin, P., Xing, J., Liu, B., Liu, X., and Zhu, Y. 2021. Endophytic *Streptomyces hygroscopicus* OsiSh-2-Mediated Balancing between Growth and Disease Resistance in Host Rice. MBio **12**(4). doi:10.1128/mBio.01566-21.

Gayrard, D., Nicolle, C., Veyssiere, M., Adam, K., Martinez, Y., Vandecasteele, C., Vidal, M., Dumas, B., and Rey, T. 2023. Genome sequence of a *Streptomyces* strain revealed expansion and acquisition of gene repertoires potentially involved in adaptation to the root rhizosphere. PhytoFrontiers^{TM}: 1–35. doi:10.1094/phytofr-11-22-0131-r.

Geng, X., Cheng, J., Gangadharan, A., and Mackey, D. 2012. The Coronatine Toxin of *Pseudomonas syringae* Is a Multifunctional Suppressor of *Arabidopsis* Defense. Plant Cell **24**(11): 4763–4774. doi:10.1105/tpc.112.105312.

Gilchrist, C.L.M., and Chooi, Y.-H. 2021. Clinker & Clustermap.Js: Automatic Generation of Gene Cluster Comparison Figures. Bioinformatics **37**(16): 2473–2475.

doi:10.1093/bioinformatics/btab007.

Gong, C., Yang, M.P., Yu, D.C., Du, W.F., Song, S.W., Wang, R.X., Zhang, H.J., and Jiang, S.Y. 2017. First report of *Streptomyces caviscabies* causing common scab on potato in China. Plant Dis. **101**(7): 1316. doi:10.1094/PDIS-11-16-1608-PDN.

Goutam, K., Gupta, A.K., and Gopal, B. 2017. The fused SnoaL-2 domain in the *Mycobacterium tuberculosis* sigma factor σj modulates promoter recognition. Nucleic Acids Res. **45**(16): 9760–9772. Oxford University Press. doi:10.1093/nar/gkx609.

Goyer, C., Vachon, J., and Beaulieu, C. 1998. Pathogenicity of *Streptomyces scabies* Mutants Altered in Thaxtomin A Production. Phytopathology **88**(5): 442–445. doi:10.1094/phyto.1998.88.5.442.

Grabley, S., Hammann, P., Raether, W., Wink, J., and Zeeck, A. 1990. Secondary metabolites by chemical screening: II. Amycins a and b, two novel niphimycin analogs isolated from a high producer strain of elaiophylin and nigericin. J. Antibiot. (Tokyo). **43**(6): 639–647. doi:10.7164/antibiotics.43.639.

Grotewold, E. 2006. The genetics and biochemistry of floral pigments. Annu. Rev. Plant Biol. **57**: 761–780. doi:10.1146/annurev.arplant.57.032905.105248.

Gui, M., Zhang, M. xue, Wu, W. hui, and Sun, P. 2019. Natural occurrence, bioactivity and biosynthesis of elaiophylin analogues. Molecules **24**(21): 1–13. doi:10.3390/molecules24213840.

Gupta, M., Till, R., and Smith, M.C.M. 2007. Sequences in attB that affect the ability of ϕC31 integrase to synapse and to activate DNA cleavage. Nucleic Acids Res. **35**(10): 3407–3419. doi:10.1093/nar/gkm206.

Gust, B., Challis, G.L., Fowler, K., Kieser, T., and Chater, K.F. 2003a. PCR-targeted *Streptomyces* gene replacement identifies a protein domain needed for biosynthesis of the sesquiterpene soil odor geosmin. Proc. Natl. Acad. Sci. **100**(4): 1541–1546. doi:10.1073/pnas.0337542100.

Gust, B., Chandra, G., Jakimowicz, D., Yuqing, T., Bruton, C.J., and Chater, K.F. 2004. λ Red-Mediated Genetic Manipulation of Antibiotic-Producing *Streptomyces*. *In* Advances in Applied Microbiology. pp. 107–128. doi:10.1016/S0065-2164(04)54004-2.

Gust, B., Kieser, T., and Chater, K. 2003b. Recombineering in *Streptomyces coelicolor*. John Innes Centre, Norwich.

Gutierrez, J., Bakke, A., Vatta, M., and Merrill, A.R. 2022. Plant Natural Products as Antimicrobials for Control of *Streptomyces scabies*: A Causative Agent of the Common Scab Disease. Front. Microbiol. **12**(January). doi:10.3389/fmicb.2021.833233.

Hackl, S., and Bechthold, A. 2015. The Gene bldA, a Regulator of Morphological Differentiation and Antibiotic Production in *Streptomyces*. Arch. Pharm. (Weinheim). **348**(7): 455–462. doi:10.1002/ardp.201500073.

Hamano, Y., Maruyama, C., and Kimoto, H. 2006. Construction of a Knockout Mutant of the Streptothricin-Resistance Gene in *Streptomyces albulus* by Electroporation. Actinomycetologica **20**(2): 35–41. doi:10.3209/saj.20.35.

Hamid, M.E., Reitz, T., Joseph, M.R.P., Hommel, K., Mahgoub, A., Elhassan, M.M., Buscot, F., and Tarkka, M. 2020. Diversity and geographic distribution of soil

streptomycetes with antagonistic potential against actinomycetoma-causing *Streptomyces sudanensis* in Sudan and South Sudan. BMC Microbiol. **20**(1). BMC Microbiology. doi:10.1186/s12866-020-1717-y.

Han, Y., Tian, E., Xu, D., Ma, M., Deng, Z., and Hong, K. 2016. Halichoblelide D, a new elaiophylin derivative with potent cytotoxic activity from mangrove-derived *Streptomyces* sp. 219807. Molecules **21**(8). doi:10.3390/molecules21080970.

Harrison, K.J., Crécy-Lagard, V. De, and Zallot, R. 2018. Gene Graphics: A genomic neighborhood data visualization web application. Bioinformatics **34**(8): 1406–1408. doi:10.1093/bioinformatics/btx793.

Harvey, B.M., Mironenko, T., Sun, Y., Hong, H., Deng, Z., Leadlay, P.F., Weissman, K.J., and Haydock, S.F. 2007. Insights into Polyether Biosynthesis from Analysis of the Nigericin Biosynthetic Gene Cluster in *Streptomyces* sp. DSM4137. Chem. Biol. **14**(6): 703–714. doi:10.1016/j.chembiol.2007.05.011.

Hayashi, K.-I., Ogino, K., Oono, Y., Uchimiya, H., and Nozaki, H. 2001. Yokonolide A, a New Inhibitor of Auxin Signal Transduction, from *Streptomyces diastatochromogenes* B59. J. Antibiot. (Tokyo). **54**(7): 573–581. doi:10.7164/antibiotics.54.573.

Hayashi, K. ichiro, Jones, A.M., Ogino, K., Yamazoe, A., Oono, Y., Inoguchi, M., Kondo, H., and Nozaki, H. 2003. Yokonolide B, a novel inhibitor of auxin action, blocks degradation of AUX/IAA factors. J. Biol. Chem. **278**(26): 23797–23806. Â© 2003 ASBMB. Currently published by Elsevier Inc; originally published by American Society for Biochemistry and Molecular Biology. doi:10.1074/jbc.M300299200.

Hayashi, K. ichiro, Yamazoe, A., Ishibashi, Y., Kusaka, N., Oono, Y., and Nozaki, H.

2008. Active core structure of terfestatin A, a new specific inhibitor of auxin signaling. Bioorganic Med. Chem. **16**(9): 5331–5344. doi:10.1016/j.bmc.2008.02.085.

Hayashi, K.I. 2021. Chemical Biology in Auxin Research. Cold Spring Harb. Perspect. Biol. **13**(5). doi:10.1101/CSHPERSPECT.A040105.

Haydock, S.F., Appleyard, A.N., Mironenko, T., Lester, J., Scott, N., and Leadlay, P.F. 2005. Organization of the biosynthetic gene cluster for the macrolide concanamycin A in *Streptomyces neyagawaensis* ATCC 27449. Microbiology **151**(10): 3161–3169. doi:10.1099/mic.0.28194-0.

He, M., Haltli, B., Summers, M., Feng, X., and Hucul, J. 2006. Isolation and characterization of meridamycin biosynthetic gene cluster from *Streptomyces* sp. NRRL 30748. Gene **377**(1–2): 109–118. doi:10.1016/j.gene.2006.03.021.

He, W., Lei, J., Liu, Y., and Wang, Y. 2008. The LuxR family members GdmRI and GdmRII are positive regulators of geldanamycin biosynthesis in *Streptomyces hygroscopicus* 17997. Arch. Microbiol. **189**(5): 501–510. doi:10.1007/s00203-007-0346-2.

Healy, F.G., Krasnoff, S.B., Wach, M., Gibson, D.M., and Loria, R. 2002. Involvement of a cytochrome P450 monooxygenase in thaxtomin A biosynthesis by *Streptomyces acidiscabies*. J. Bacteriol. **184**(7): 2019–2029. doi:10.1128/JB.184.7.2019-2029.2002.

Healy, F.G., Wach, M., Krasnoff, S.B., Gibson, D.M., and Loria, R. 2000. The *txtAB* genes of the plant pathogen *Streptomyces acidiscabies* encode a peptide synthetase required for phytotoxin thaxtomin A production and pathogenicity. Mol. Microbiol. **38**(4): 794–804. doi:10.1046/j.1365-2958.2000.02170.x.

Heimann, J.D. 2002. The extracytoplasmic function (ECF) sigma factors. *In* Advances in Microbial Physiology. doi:10.1016/S0065-2911(02)46002-X.

Heisey, R.M., and Putnam, A.R. 1986. Herbicidal Effects of Geldanamycin and Nigericin, Antibiotics from *Streptomyces hygroscopicus*. J. Nat. Prod. **49**(5): 859–865. doi:10.1021/np50047a016.

Heisey, R.M., and Putnam, A.R. 1990. Herbicidal activity of the antibiotics geldanamycin and nigericin. J. Plant Growth Regul. **9**(1–3): 19–25. doi:10.1007/BF02041937.

Hempel, A.M., Cantlay, S., Molle, V., Wang, S.B., Naldrett, M.J., Parker, J.L., Richards, D.M., Jung, Y.G., Buttner, M.J., and Flärdh, K. 2012. The Ser/Thr protein kinase AfsK regulates polar growth and hyphal branching in the filamentous bacteria *Streptomyces*. Proc. Natl. Acad. Sci. U. S. A. **109**(35). doi:10.1073/pnas.1207409109.

Hempel, A.M., Wang, S.B., Letek, M., Gil, J.A., and Flärdh, K. 2008. Assemblies of DivIVA mark sites for hyphal branching and can establish new zones of cell wall growth in *Streptomyces coelicolor*. J. Bacteriol. **190**(22): 7579–7583. doi:10.1128/JB.00839-08.

Higgens, C.E., and Kastner, R.E. 1971. *Streptomyces clavuligerus* sp. nov., a beta-Lactam Antibiotic Producer. Int. J. Syst. Bacteriol. **21**(4): 326–331. doi:10.1099/00207713-21-4-326.

Hill, J., and Lazarovits, G. 2005. A mail survey of growers to estimate potato common scab prevalence and economic loss in Canada. Can. J. Plant Pathol. **27**(1): 46–52. doi:10.1080/07060660509507192.

Hodgson, D.A. 1982. Glucose repression of carbon source uptake and metabolism in

Streptomyces coelicolor A3(2) and its perturbation in mutants resistant to 2-deoxyglucose. J. Gen. Microbiol. **128**(10): 2417–2430. doi:10.1099/00221287-128-10-2417.

Hodgson, D.A. 2000. Primary metabolism and its control in streptomycetes: A most unusual group of bacteria. *In* Advances in Microbial Physiology. Academic Press. pp. 47–238. doi:10.1016/S0065-2911(00)42003-5.

Höltzel, A., Kempter, C., Metzger, J.W., Jung, G., Groth, I., Fritz, T., and Fiedler, H.P. 1998. Spirofungin, a new antifungal antibiotic from *Streptomyces violaceusniger* Tu 4113. J. Antibiot. (Tokyo). **51**(8): 699–707. doi:10.7164/antibiotics.51.699.

Horbal, L., Rebets, Y., Rabyk, M., Makitrynskyy, R., Luzhetskyy, A., Fedorenko, V., and Bechthold, A. 2012. SimReg1 is a master switch for biosynthesis and export of simocyclinone D8 and its precursors. AMB Express **2**(1): 1–12. doi:10.1186/2191-0855-2-1.

Horinouchi, S., Kito, M., Nishiyama, M., Furuya, K., Hong, S.K., Miyake, K., and Beppu, T. 1990. Primary structure of AfsR, a global regulatory protein for secondary metabolite formation in *Streptomyces coelicolor* A3(2). Gene **95**(1): 49–56. doi:10.1016/0378-1119(90)90412-K.

Hoskisson, P.A., and Fernández-Martínez, L.T. 2018. Regulation of specialised metabolites in Actinobacteria – expanding the paradigms. Environ. Microbiol. Rep. **10**(3): 231–238. doi:10.1111/1758-2229.12629.

Hou, B., Tao, L., Zhu, X., Wu, W., Guo, M., Ye, J., Wu, H., and Zhang, H. 2018. Global regulator BldA regulates morphological differentiation and lincomycin production in

Streptomyces lincolnensis. Appl. Microbiol. Biotechnol. **102**(9): 4101–4115. Applied Microbiology and Biotechnology. doi:10.1007/s00253-018-8900-1.

Houfani, A.A., Anders, N., Spiess, A.C., Baldrian, P., and Benallaoua, S. 2020. Insights from enzymatic degradation of cellulose and hemicellulose to fermentable sugars– a review. Biomass and Bioenergy **134**(January 2019): 105481. Elsevier Ltd. doi:10.1016/j.biombioe.2020.105481.

Hsu, S.-Y. 2010. IAA Production by *Streptomyces scabies* and its role in plant-microbe interaction. Cornell University, Ithaca, NY.

Hu, Y., Wang, M., Wu, C., Tan, Y., Li, J., Hao, X., Duan, Y., Guan, Y., Shang, X., Wang, Y., Xiao, C., and Gan, M. 2018. Identification and Proposed Relative and Absolute Configurations of Niphimycins C-E from the Marine-Derived *Streptomyces* sp. IMB7-145 by Genomic Analysis. J. Nat. Prod. **81**(1): 178–187. doi:10.1021/acs.jnatprod.7b00859.

Hu, Z., Liu, Y., Tian, Z.Q., Ma, W., Starks, C.M., Regentin, R., Licari, P., Myles, D.C., and Hutchinson, C.R. 2004. Isolation and characterization of novel geldanamycin analogues. J. Antibiot. (Tokyo). **57**(7): 421–428. doi:10.7164/antibiotics.57.421.

Huguet-Tapia, J.C., Badger, J.H., Loria, R., and Pettis, G.S. 2011. *Streptomyces turgidiscabies* Car8 contains a modular pathogenicity island that shares virulence genes with other actinobacterial plant pathogens. Plasmid **65**(2): 118–124. doi:10.1016/j.plasmid.2010.11.002.

Huguet-Tapia, J.C., Lefebure, T., Badger, J.H., Guan, D., Pettis, G.S., Stanhope, M.J., and Loria, R. 2016. Genome content and phylogenomics reveal both ancestral and lateral

evolutionary pathways in plant-pathogenic *Streptomyces* species. Appl. Environ. Microbiol. **82**(7): 2146–2155. doi:10.1128/AEM.03504-15.

Huiqun, D., Xiaofeng, C., Jianxin, P., Huazhu, H., Koji, I., and Aiying, L. 2010. Practical procedures for genetic manipulation systems for medermycin-producing *Streptomyces* sp. AM-7161. J. Basic Microbiol. **50**(3): 299–301. doi:10.1002/jobm.200900240.

Hwang, K.S., Kim, H.U., Charusanti, P., Palsson, B.T., and Lee, S.Y. 2014. Systems biology and biotechnology of *Streptomyces* species for the production of secondary metabolites. Biotechnol. Adv. **32**(2): 255–268. Elsevier Inc. doi:10.1016/j.biotechadv.2013.10.008.

Hwang, S., Lee, N., Cho, S., Palsson, B., and Cho, B.K. 2020. Repurposing Modular Polyketide Synthases and Non-ribosomal Peptide Synthetases for Novel Chemical Biosynthesis. Front. Mol. Biosci. **7**(May): 1–27. doi:10.3389/fmolb.2020.00087.

Hwang, S.Y., Nakashima, K., Okai, N., Okazaki, F., Miyake, M., Harazono, K., Ogino, C., and Kondo, A. 2013. Thermal stability and starch degradation profile of α-amylase from *Streptomyces avermitilis*. Biosci. Biotechnol. Biochem. **77**(12): 2449–2453. doi:10.1271/bbb.130556.

Ichinose, Y., Taguchi, F., and Mukaihara, T. 2013. Pathogenicity and virulence factors of *Pseudomonas syringae*. J. Gen. Plant Pathol. **79**(5): 285–296. doi:10.1007/s10327-013-0452-8.

Igarashi, Y., Iida, T., Yoshida, R., and Furumai, T. 2002. Pteridic Acids A and B, Novel Plant Growth Promoters with Auxin-like Activity from *Streptomyces hygroscopicus* TP-A0451. J. Antibiot. (Tokyo). **55**(8): 764–767. doi:10.7164/antibiotics.55.764.

Ikeda, H., Kotaki, H., Tanaka, H., and Omura, S. 1988. Involvement of glucose catabolism in avermectin production by *Streptomyces avermitilis*. Antimicrob. Agents Chemother. **32**(2): 282–284. doi:10.1128/AAC.32.2.282.

Inoue, H., Nojima, H., and Okayama, H. 1990. High efficiency transformation of *Escherichia coli* with plasmids. Gene **96**(1): 23–28. doi:10.1016/0378-1119(90)90336-P.

Ivanova, V., Schlegel, R., and Dornberger, K. 1998. N′-Methylniphimycin, a novel minor congener of niphimycin from *Streptomyces*spec. 57-13. J. Basic Microbiol. **38**(5–6): 415–419. doi:10.1002/(SICI)1521-4028(199811)38:5/6<415::AID-JOBM415>3.0.CO;2-Z.

Jakimowicz, D., and Van Wezel, G.P. 2012. Cell division and DNA segregation in *Streptomyces*: How to build a septum in the middle of nowhere? Mol. Microbiol. **85**(3): 393–404. doi:10.1111/j.1365-2958.2012.08107.x.

Jiang, H.H., Meng, Q.X., Hanson, L.E., and Hao, J.J. 2012. First Report of *Streptomyces stelliscabiei* Causing Potato Common Scab in Michigan. Plant Dis. **96**(6): 904–904. doi:10.1094/PDIS-02-12-0132-PDN.

Jiang, M.X., Yin, M., Wu, S.H., Han, X.L., Ji, K.Y., Wen, M.L., and Lu, T. 2017. GdmRIII, a TetR Family Transcriptional Regulator, Controls Geldanamycin and Elaiophylin Biosynthesis in *Streptomyces autolyticus* CGMCC0516. Sci. Rep. **7**(1): 1–11. Springer US. doi:10.1038/s41598-017-05073-x.

Joglekar, S., Suliman, M., Bartsch, M., Halder, V., Maintz, J., Bautor, J., Zeier, J., Parker, J.E., and Kombrink, E. 2018. Chemical Activation of EDS1/PAD4 Signaling Leading

to Pathogen Resistance in Arabidopsis. Plant Cell Physiol. **59**(8): 1592–1607. doi:10.1093/pcp/pcy106.

Johnson, E.G., Joshi, M. V., Gibson, D.M., and Loria, R. 2007. Cello-oligosaccharides released from host plants induce pathogenicity in scab-causing *Streptomyces* species. Physiol. Mol. Plant Pathol. **71**(1–3): 18–25. doi:10.1016/j.pmpp.2007.09.003.

Johnson, E.G., Krasnoff, S.B., Bignell, D.R.D., Chung, W.-C., Tao, T., Parry, R.J., Loria, R., and Gibson, D.M. 2009. 4-Nitrotryptophan is a substrate for the non-ribosomal peptide synthetase TxtB in the thaxtomin A biosynthetic pathway. Mol. Microbiol. **73**(3): 409–418. doi:10.1111/j.1365-2958.2009.06780.x.

Jones, S.E., Ho, L., Rees, C.A., Hill, J.E., Nodwell, J.R., and Elliot, M.A. 2017. *Streptomyces* exploration is triggered by fungal interactions and volatile signals. Elife **6**: 1–21. doi:10.7554/eLife.21738.

Jonsbu, E., McIntyre, M., and Nielsen, J. 2002. The influence of carbon sources and morphology on nystatin production by *Streptomyces noursei*. J. Biotechnol. **95**(2): 133–144. doi:10.1016/S0168-1656(02)00003-2.

Joshi, M. V., Bignell, D.R.D., Johnson, E.G., Sparks, J.P., Gibson, D.M., and Loria, R. 2007. The AraC/XylS regulator TxtR modulates thaxtomin biosynthesis and virulence in *Streptomyces scabies*. Mol. Microbiol. **66**(3): 633–642. doi:10.1111/j.1365-2958.2007.05942.x.

Joshi, M. V., and Loria, R. 2007. *Streptomyces turgidiscabies* possesses a functional cytokinin biosynthetic pathway and produces leafy galls. Mol. Plant-Microbe Interact. **20**(7): 751–758. doi:10.1094/MPMI-20-7-0751.

Jourdan, S., Francis, I.M., Deflandre, B., Loria, R., and Rigali, S. 2017. Tracking the Subtle Mutations Driving Host Sensing by the Plant Pathogen *Streptomyces scabies*. mSphere **2**(2): 1–7. doi:10.1128/msphere.00367-16.

Kadota, Y., and Shirasu, K. 2012. The HSP90 complex of plants. Biochim. Biophys. Acta - Mol. Cell Res. **1823**(3): 689–697. Elsevier B.V. doi:10.1016/j.bbamcr.2011.09.016.

Karki, S., Kwon, S.Y., Yoo, H.G., Suh, J.W., Park, S.H., and Kwon, H.J. 2010. The methoxymalonyl-acyl carrier protein biosynthesis locus and the nearby gene with the β-ketoacyl synthase domain are involved in the biosynthesis of galbonolides in *Streptomyces galbus*, but these loci are separate from the modular polyketide synt. FEMS Microbiol. Lett. **310**(1): 69–75. doi:10.1111/j.1574-6968.2010.02048.x.

Katsir, L., Schilmiller, A.L., Staswick, P.E., Sheng, Y.H., and Howe, G.A. 2008. COI1 is a critical component of a receptor for jasmonate and the bacterial virulence factor coronatine. Proc. Natl. Acad. Sci. U. S. A. **105**(19): 7100–7105. doi:10.1073/pnas.0802332105.

Katsuyama, Y., and Ohnishi, Y. 2012. Type III polyketide synthases in microorganisms. *In* Methods in Enzymology, 1st edition. Elsevier Inc. doi:10.1016/B978-0-12-394290-6.00017-3.

Kers, J.A., Wach, M.J., Cameron, K.D., Gibson, D.M., Loria, R., Morello, J.E., Joshi, M. V., and Bukhalid, R.A. 2005. A large, mobile pathogenicity island confers plant pathogenicity on *Streptomyces* species. Mol. Microbiol. **55**(4): 1025–1033. doi:10.1111/j.1365-2958.2004.04461.x.

Kevin II, D.A., Meujo, D.A., and Hamann, M.T. 2009. Polyether ionophores: broad-

spectrum and promising biologically active molecules for the control of drug-resistant bacteria and parasites. Expert Opin. Drug Discov. **4**(2): 109–146. doi:10.1517/17460440802661443.

Khatri, B.B., Tegg, R.S., Brown, P.H., and Wilson, C.R. 2011. Temporal association of potato tuber development with susceptibility to common scab and *Streptomyces scabiei*-induced responses in the potato periderm. Plant Pathol. **60**(4): 776–786. doi:10.1111/j.1365-3059.2011.02435.x.

Kieser, T., Bibb, M.J., Buttner, M.J., Chater, K.F., and Hopwood, D.A. 2000. Practical *Streptomyces* Genetics. The John Innes Foundation, Norwich, U.K.

Kim, D.R., Cho, G., Jeon, C.W., Weller, D.M., Thomashow, L.S., Paulitz, T.C., and Kwak, Y.S. 2019. A mutualistic interaction between *Streptomyces* bacteria, strawberry plants and pollinating bees. Nat. Commun. **10**(1). Springer US. doi:10.1038/s41467-019-12785-3.

Kim, E.S., Hong, H.J., Choi, C.Y., and Cohen, S.N. 2001. Modulation of actinorhodin biosynthesis in *Streptomyces lividans* by glucose repression of *afsR2* gene transcription. J. Bacteriol. **183**(7): 2198–2203. doi:10.1128/JB.183.7.2198-2203.2001.

Kim, W., Lee, J.J., Paik, S.G., and Hong, Y.S. 2010. Identification of three positive regulators in the geldanamycin PKS gene cluster of *Streptomyces hygroscopicus* JCM4427. J. Microbiol. Biotechnol. **20**(11): 1484–1490. doi:10.4014/jmb.1005.05040.

Kim, Y.H., Yoo, J.S., Lee, C.H., Goo, Y.M., and Kim, M.S. 1996. Application of fast atom bombardment combined with tandem mass spectrometry to the structural elucidation of O-demethylabierixin and related polyether antibiotics. J. Mass Spectrom. **31**(8):

855–60. doi:10.1002/(SICI)1096-9888(199608)31:8<855::AID-JMS363>3.0.CO;2-U.

Kinashi, H., Someno, K., and Sakaguchi, K. 1984. Isolation and characterization of concanamycins A, B and C. J. Antibiot. (Tokyo). **37**(11): 1333–1343. doi:10.7164/antibiotics.37.1333.

Kind, T., Tsugawa, H., Cajka, T., Ma, Y., Lai, Z., Mehta, S.S., Wohlgemuth, G., Barupal, D.K., Showalter, M.R., Arita, M., and Fiehn, O. 2018. Identification of small molecules using accurate mass MS/MS search. Mass Spectrom. Rev. **37**(4): 513–532. doi:10.1002/mas.21535.

King, R.R., Harold Lawrence, C., and Gray, J.A. 2001. Herbicidal properties of the thaxtomin group of phytotoxins. J. Agric. Food Chem. **49**(5): 2298–2301. doi:10.1021/jf0012998.

Kinkel, L.L., Schlatter, D.C., Bakker, M.G., and Arenz, B.E. 2012. *Streptomyces* competition and co-evolution in relation to plant disease suppression. Res. Microbiol. **163**(8): 490–499. Elsevier Masson SAS. doi:10.1016/j.resmic.2012.07.005.

Kitani, S., Ikeda, H., Sakamoto, T., Noguchi, S., and Nihira, T. 2009. Characterization of a regulatory gene, aveR, for the biosynthesis of avermectin in *Streptomyces avermitilis*. Appl. Microbiol. Biotechnol. **82**(6): 1089–1096. doi:10.1007/s00253-008-1850-2.

Kitson, R.R.A., Chang, C.-H., Xiong, R., Williams, H.E.L., Davis, A.L., Lewis, W., Dehn, D.L., Siegel, D., Roe, S.M., Prodromou, C., Ross, D., and Moody, C.J. 2013. Synthesis of 19-substituted geldanamycins with altered conformations and their binding to heat shock protein Hsp90. Nat. Chem. **5**(4): 307–314. doi:10.1038/nchem.1596.

Klassen, J.L., Lee, S.R., Poulsen, M., Beemelmanns, C., and Kim, K.H. 2019. Efomycins K and L from a termite-associated *Streptomyces* sp. M56 and their putative biosynthetic origin. Front. Microbiol. **10**(JULY): 1–8. doi:10.3389/fmicb.2019.01739.

Klimishin, D.O., Gromyko, O.M., and Fedorenko, V.O. 2007. The use of intergeneric conjugation *Escherichia coli* - *Streptomyces* for transfer of recombinant DNA into *S. nogalater* IMET 43360 strain. Cytol. Genet. **41**(5): 3–8. doi:10.3103/S0095452707050015.

Kormanec, J., Rezuchova, B., Homerova, D., Csolleiova, D., Sevcikova, B., Novakova, R., and Feckova, L. 2019. Recent achievements in the generation of stable genome alterations/mutations in species of the genus *Streptomyces*. Appl. Microbiol. Biotechnol. **103**(14): 5463–5482. Applied Microbiology and Biotechnology. doi:10.1007/s00253-019-09901-0.

Koshla, O., Lopatniuk, M., Rokytskyy, I., Yushchuk, O., Dacyuk, Y., Fedorenko, V., Luzhetskyy, A., and Ostash, B. 2017. Properties of *Streptomyces albus* J1074 mutant deficient in tRNALeuUAA gene bldA. Arch. Microbiol. **199**(8): 1175–1183. Springer Berlin Heidelberg. doi:10.1007/s00203-017-1389-7.

Kovinich, N., Kayanja, G., Chanoca, A., Riedl, K., Otegui, M.S., and Grotewold, E. 2014. Not all anthocyanins are born equal: distinct patterns induced by stress in Arabidopsis. Planta **240**(5): 931–940. doi:10.1007/s00425-014-2079-1.

Kukurba, K.R., and Montgomery, S.B. 2015. RNA sequencing and analysis. Cold Spring Harb. Protoc. **2015**(11): 951–969. doi:10.1101/pdb.top084970.

Kunkel, B.N., and Harper, C.P. 2018. The roles of auxin during interactions between

bacterial plant pathogens and their hosts. J. Exp. Bot. **69**(2): 245–254. doi:10.1093/jxb/erx447.

Kutas, P., Feckova, L., Rehakova, A., Novakova, R., Homerova, D., Mingyar, E., Rezuchova, B., Sevcikova, B., and Kormanec, J. 2013. Strict control of auricin production in *Streptomyces aureofaciens* CCM 3239 involves a feedback mechanism. Appl. Microbiol. Biotechnol. **97**(6): 2413–2421. doi:10.1007/s00253-012-4505-2.

Labeda, D.P. 2011. Multilocus sequence analysis of phytopathogenic species of the genus *Streptomyces*. Int. J. Syst. Evol. Microbiol. **61**(10): 2525–2531. doi:10.1099/ijs.0.028514-0.

Labeda, D.P. 2016. Taxonomic evaluation of putative *Streptomyces scabiei* strains held in the ARS Culture Collection (NRRL) using multi-locus sequence analysis. Antonie van Leeuwenhoek, Int. J. Gen. Mol. Microbiol. **109**(3): 349–356. Springer International Publishing. doi:10.1007/s10482-015-0637-6.

Labeda, D.P., Goodfellow, M., Brown, R., Ward, A.C., Lanoot, B., Vanncanneyt, M., Swings, J., Kim, S.-B., Liu, Z., Chun, J., Tamura, T., Oguchi, A., Kikuchi, T., Kikuchi, H., Nishii, T., Tsuji, K., Yamaguchi, Y., Tase, A., Takahashi, M., Sakane, T., Suzuki, K.I., and Hatano, K. 2012. Phylogenetic study of the species within the family *Streptomycetaceae*. Antonie Van Leeuwenhoek **101**(1): 73–104. doi:10.1007/s10482-011-9656-0.

Lacombe-Harvey, M.È., Brzezinski, R., and Beaulieu, C. 2018. Chitinolytic functions in actinobacteria: ecology, enzymes, and evolution. Appl. Microbiol. Biotechnol. **102**(17): 7219–7230. Applied Microbiology and Biotechnology. doi:10.1007/s00253-

018-9149-4.

Lakshmi, S.A., Shafreen, R.M.B., Priyanga, A., Shiburaj, S., and Pandian, S.K. 2020. A highly divergent α-amylase from *Streptomyces* spp.: An evolutionary perspective. Int. J. Biol. Macromol. **163**: 2415–2428. Elsevier B.V. doi:10.1016/j.ijbiomac.2020.09.103.

Lambert, D.H., and Loria, R. 1989. *Streptomyces acidiscabies* sp. nov. Int. J. Syst. Bacteriol. **39**(4): 393–396. doi:10.1099/00207713-39-4-393.

Lapaz, M.I., Huguet-Tapia, J.C., Siri, M.I., Verdier, E., Loria, R., and Pianzzola, M.J. 2017. Genotypic and Phenotypic Characterization of *Streptomyces* Species Causing Potato Common Scab in Uruguay. Plant Dis. **101**(8): 1362–1372. doi:10.1094/PDIS-09-16-1348-RE.

Lapaz, M.I., López, A., Huguet-Tapia, J.C., Pérez-Baldassari, M.F., Iglesias, C., Loria, R., Moyna, G., and Pianzzola, M.J. 2018. Isolation and structural characterization of a non-diketopiperazine phytotoxin from a potato pathogenic *Streptomyces* strain. Nat. Prod. Res. **0**(0): 1–7. Taylor & Francis. doi:10.1080/14786419.2018.1511554.

Lawlor, E.J., Baylis, H.A., and Chater, K.F. 1987. Pleiotropic morphological and antibiotic deficiencies result from mutations in a gene encoding a tRNA-like product in *Streptomyces coelicolor* A3(2). Genes Dev. **1**(10): 1305–1310. doi:10.1101/gad.1.10.1305.

Lawrence, C.H., Clark, M.C., and King, R.R. 1990. Induction of Common Scab Symptoms in Aseptically Cultured Potato Tubers by the Vivotoxin, Thaxtomin. Phytopathology **80**(7): 606. doi:10.1094/Phyto-80-606.

Lee, J.K., Jang, J.H., Park, D.J., Kim, C.J., Ahn, J.S., Hwang, B.Y., and Hong, Y.S. 2017. Identification of new geldanamycin derivatives from unexplored microbial culture extracts using a MS/MS library. J. Antibiot. (Tokyo). **70**(3): 323–327. Nature Publishing Group. doi:10.1038/ja.2016.143.

Lee, N., Hwang, S., Kim, J., Cho, S., Palsson, B., and Cho, B.K. 2020a. Mini review: Genome mining approaches for the identification of secondary metabolite biosynthetic gene clusters in *Streptomyces*. Comput. Struct. Biotechnol. J. **18**: 1548–1556. The Author(s). doi:10.1016/j.csbj.2020.06.024.

Lee, S.Y., Kim, M.S., Kim, H.S., Kim, Y.H., Hong, S.D., and Lee, J.J. 1996. Structure determination and biological activities of elaiophylin produced by *Streptomyces* sp. MCY-846.

Lee, Y., Lee, N., Hwang, S., Kim, K., Kim, W., Kim, J., Cho, S., Palsson, B.O., and Cho, B.K. 2020b. System-level understanding of gene expression and regulation for engineering secondary metabolite production in *Streptomyces*. J. Ind. Microbiol. Biotechnol. **47**(9–10): 739–752. Springer International Publishing. doi:10.1007/s10295-020-02298-0.

Legault, G.S., Lerat, S., Nicolas, P., and Beaulieu, C. 2011. Tryptophan Regulates Thaxtomin A and Indole-3-Acetic Acid Production in *Streptomyces scabiei* and Modifies Its Interactions with Radish Seedlings. Phytopathology **101**(9): 1045–1051. doi:10.1094/phyto-03-11-0064.

Leiner, R.H., Fry, B.A., Carling, D.E., and Loria, R. 1996. Probable involvement of thaxtomin A in pathogenicity of *Streptomyces scabies* on seedlings. Phytopathology

86(7): 709–713. doi:10.1094/Phyto-86-709.

Lerat, S., Forest, M., Lauzier, A., Grondin, G., Lacelle, S., and Beaulieu, C. 2012. Potato Suberin Induces Differentiation and Secondary Metabolism in the Genus *Streptomyces*. Microbes Environ. **27**(1): 36–42. doi:10.1264/jsme2.ME11282.

Lerat, S., Simao-Beaunoir, A.M., and Beaulieu, C. 2009. Genetic and physiological determinants of *Streptomyces scabies* pathogenicity. Mol. Plant Pathol. **10**(5): 579–585. doi:10.1111/j.1364-3703.2009.00561.x.

Leskiw, B.K., Lawlor, E.J., Fernandez-Abalos, J.M., and Chater, K.F. 1991. TTA codons in some genes prevent their expression in a class of developmental, antibiotic-negative, *Streptomyces* mutants. Proc. Natl. Acad. Sci. U. S. A. **88**(6): 2461–2465. doi:10.1073/pnas.88.6.2461.

Li, J., Wang, N., Tang, Y., Cai, X., Xu, Y., Liu, R., Wu, H., and Zhang, B. 2019a. Developmental regulator BldD directly regulates lincomycin biosynthesis in *Streptomyces lincolnensis*. Biochem. Biophys. Res. Commun. **518**(3): 548–553. Elsevier Ltd. doi:10.1016/j.bbrc.2019.08.079.

Li, Q., Wang, L., Xie, Y., Wang, S., Chen, R., and Hong, B. 2013. SsaA, a member of a novel class of transcriptional regulators, controls sansanmycin production in *Streptomyces* sp. strain SS through a feedback mechanism. J. Bacteriol. **195**(10): 2232–2243. doi:10.1128/JB.00054-13.

Li, X., Ren, W., Li, Y., Shi, Y., Sun, H., Wang, L., Wu, L., Xie, Y., Du, Y., Jiang, Z., and Hong, B. 2022. Production of chain-extended cinnamoyl compounds by overexpressing two adjacent cluster-situated LuxR regulators in *Streptomyces*

globisporus C-1027. Front. Microbiol. **13**(August): 1–13. doi:10.3389/fmicb.2022.931180.

Li, Y., Liu, J., Adekunle, D., Bown, L., Tahlan, K., and Bignell, D.R.D. 2019b. TxtH is a key component of the thaxtomin biosynthetic machinery in the potato common scab pathogen *Streptomyces scabies*. Mol. Plant Pathol. **20**(10): 1379–1393. doi:10.1111/mpp.12843.

Li, Y., Liu, J., Díaz-Cruz, G., Cheng, Z., and Bignell, D.R.D. 2019c. Virulence mechanisms of plant-pathogenic *Streptomyces* species: An updated review. Microbiol. (United Kingdom) **165**(10): 1025–1040. doi:10.1099/mic.0.000818.

Lin, C.Y., Ni, H.F., and Huang, C.W. 2018. First report of common scab on potato caused by *Streptomyces europaeiscabiei* in Taiwan. Plant Dis. **102**(4): 818. doi:10.1094/PDIS-05-17-0667-PDN.

Liot, Q. 2016. Investigation du rôle physiologique de l'hydrogénase [NiFe] à haute affinité du groupe 5 chez *Streptomyces avermitilis*. Université du Québec.

Liu, C., Zhang, J., Lu, C., and Shen, Y. 2015. Heterologous expression of galbonolide biosynthetic genes in *Streptomyces coelicolor*. Antonie van Leeuwenhoek, Int. J. Gen. Mol. Microbiol. **107**(5): 1359–1366. doi:10.1007/s10482-015-0415-5.

Liu, J., Nothias, L.-F., Dorrestein, P.C., Tahlan, K., and Bignell, D.R.D. 2021a. Genomic and Metabolomic Analysis of the Potato Common Scab Pathogen *Streptomyces scabiei*. ACS Omega: acsomega.1c00526. doi:10.1021/acsomega.1c00526.

Liu, J., Nothias, L.F., Dorrestein, P.C., Tahlan, K., and Bignell, D.R.D. 2021b. Genomic and Metabolomic Analysis of the Potato Common Scab Pathogen *Streptomyces*

scabiei. ACS Omega **6**(17): 11474–11487. doi:10.1021/acsomega.1c00526.

Liu, M., Lu, C., and Shen, Y. 2016. Four new meridamycin congeners from: *Streptomyces* sp. SR107. RSC Adv. **6**(55): 49792–49796. Royal Society of Chemistry. doi:10.1039/c6ra09772c.

Liu, R., Deng, Z., and Liu, T. 2018. *Streptomyces* species: Ideal chassis for natural product discovery and overproduction. Metab. Eng. **50**(May): 74–84. Elsevier Inc. doi:10.1016/j.ymben.2018.05.015.

Liu, X., Li, J., Ni, S., Wu, L., Wang, H., Lin, L., He, W., and Wang, Y. 2011. A pair of sulfur-containing geldanamycin analogs, 19-S-methylgeldanamycin and 4,5-dihydro-19-S-methylgeldanamycin, from *Streptomyces hygroscopicus* 17997. J. Antibiot. (Tokyo). **64**(7): 519–522. Nature Publishing Group. doi:10.1038/ja.2011.39.

van Loon, L.C., Geraats, B.P.J., and Linthorst, H.J.M. 2006. Ethylene as a modulator of disease resistance in plants. doi:10.1016/j.tplants.2006.02.005.

López-García, M.T., Yagüe, P., González-Quiñónez, N., Rioseras, B., and Manteca, A. 2018. The SCO4117 ECF sigma factor pleiotropically controls secondary metabolism and morphogenesis in *Streptomyces coelicolor*. Front. Microbiol. **9**(FEB): 1–12. doi:10.3389/fmicb.2018.00312.

Lopez, V.A., Park, B.C., Nowak, D., Sreelatha, A., Zembek, P., Fernandez, J., Servage, K.A., Gradowski, M., Hennig, J., Tomchick, D.R., Pawłowski, K., Krzymowska, M., and Tagliabracci, V.S. 2019. A Bacterial Effector Mimics a Host HSP90 Client to Undermine Immunity. Cell **179**(1): 205-218.e21. doi:10.1016/j.cell.2019.08.020.

Loria, R., Bukhalid, R.A., Creath, R.A., Leiner, R.H., Olivier, M., and Steffens, J.C. 1995.

Differential production of thaxtomins by pathogenic *Streptomyces* species in vitro. Phytopathology **85**(5): 537–541. doi:10.1094/Phyto-85-537.

Loria, R., Bukhalid, R.A., Fry, B.A., and King, R.R.R. 1997. Plant pathogenicity in the genus *Streptomyces*. Plant Dis. **81**(8): 836–846. doi:10.1094/PDIS.1997.81.8.836.

Loria, R., Kers, J., and Joshi, M. 2006. Evolution of Plant Pathogenicity in *Streptomyces*. Annu. Rev. Phytopathol. **44**(1): 469–487. doi:10.1146/annurev.phyto.44.032905.091147.

Luzhetskyy, A., Fedoryshyn, M., Gromyko, O., Ostash, B., Rebets, Y., Bechthold, A., and Fedorenko, V. 2006. IncP plasmids are most effective in mediating conjugation between *Escherichia coli* and streptomycetes. Russ. J. Genet. **42**(5): 476–481. doi:10.1134/S1022795406050036.

MacNeil, D.J. 1988. Characterization of a unique methyl-specific restriction system in *Streptomyces avermitilis*. J. Bacteriol. **170**(12): 5607–5612. doi:10.1128/jb.170.12.5607-5612.1988.

MacNeil, D.J., Gewain, K.M., Ruby, C.L., Dezeny, G., Gibbons, P.H., and MacNeil, T. 1992. Analysis of *Streptomyces avermitilis* genes required for avermectin biosynthesis utilizing a novel integration vector. Gene **111**(1): 61–68. doi:10.1016/0378-1119(92)90603-M.

Maglangit, F., Yu, Y., and Deng, H. 2021. Bacterial pathogens: Threat or treat (a review on bioactive natural products from bacterial pathogens). Nat. Prod. Rep. **38**(4): 782–821. doi:10.1039/d0np00061b.

Makitrynskyy, R., Tsypik, O., and Bechthold, A. 2022. Genetic engineering of

Streptomyces ghanaensis ATCC14672 for improved production of moenomycins. Microorganisms **10**(1). doi:10.3390/microorganisms10010030.

Manteca, A., Mäder, U., Connolly, B.A., and Sanchez, J. 2006. A proteomic analysis of *Streptomyces coelicolor* programmed cell death. Proteomics **6**(22): 6008–6022. doi:10.1002/pmic.200600147.

Manteca, A., and Sanchez, J. 2009. *Streptomyces* development in colonies and soils. Appl. Environ. Microbiol. **75**(9): 2920–2924. doi:10.1128/AEM.02288-08.

Mascher, T. 2013. Signaling diversity and evolution of extracytoplasmic function (ECF) σ factors. Curr. Opin. Microbiol. **16**(2): 148–155. Elsevier Ltd. doi:10.1016/j.mib.2013.02.001.

Mazza, P., Noens, E.E., Schirner, K., Grantcharova, N., Mommaas, A.M., Koerten, H.K., Muth, G., Flärdh, K., Van Wezel, G.P., and Wohlleben, W. 2006. MreB of *Streptomyces coelicolor* is not essential for vegetative growth but is required for the integrity of aerial hyphae and spores. Mol. Microbiol. **60**(4): 838–852. doi:10.1111/j.1365-2958.2006.05134.x.

McGettigan, P.A. 2013. Transcriptomics in the RNA-seq era. Curr. Opin. Chem. Biol. **17**(1): 4–11. doi:10.1016/j.cbpa.2012.12.008.

de Melo, R.R., Tomazetto, G., Persinoti, G.F., Sato, H.H., Ruller, R., and Squina, F.M. 2018. Unraveling the cellulolytic and hemicellulolytic potential of two novel *Streptomyces* strains. Ann. Microbiol. **68**(10): 677–688. Annals of Microbiology. doi:10.1007/s13213-018-1374-7.

de Mendiburu, F. 2020. agricolae: Statistical Procedures for Agricultural Research.

Meng, S., Wu, H., Wang, L., Zhang, B., and Bai, L. 2017. Enhancement of antibiotic productions by engineered nitrate utilization in actinomycetes. Appl. Microbiol. Biotechnol. **101**(13): 5341–5352. Applied Microbiology and Biotechnology. doi:10.1007/s00253-017-8292-7.

Mitrović, I., Grahovac, J., Hrustić, J., Jokić, A., Dodić, J., Mihajlović, M., and Grahovac, M. 2021. Utilization of waste glycerol for the production of biocontrol agents nigericin and niphimycin by *Streptomyces hygroscopicus*: bioprocess development. Environ. Technol. (United Kingdom) **0**(0): 1–14. Taylor & Francis. doi:10.1080/09593330.2021.1913241.

Miyajima, K., Tanaka, F., Takeuchi, T., and Kuninaga, S. 1998. *Streptomyces turgidiscabies* sp. nov. Int. J. Syst. Bacteriol. **48**(2): 495–502. doi:10.1099/00207713-48-2-495.

Miyawaki, K., Inoue, S., Kitaoka, N., and Matsuura, H. 2021. Potato tuber-inducing activities of jasmonic acid and related-compounds (II). Biosci. Biotechnol. Biochem. **85**(12): 2378–2382. doi:10.1093/bbb/zbab161.

Mohimani, H., Gurevich, A., Shlemov, A., Mikheenko, A., Korobeynikov, A., Cao, L., Shcherbin, E., Nothias, L.-F., Dorrestein, P.C., and Pevzner, P.A. 2018. Dereplication of microbial metabolites through database search of mass spectra. Nat. Commun. **9**(1): 4035. doi:10.1038/s41467-018-06082-8.

Moreno, L.B. 2018. Cellular Ecophysiology of Microbe: Hydrocarbon and Lipid Interactions. *In* Cellular Ecophysiology of Microbe: Hydrocarbon and Lipid Interactions. *Edited By*T. Krell. Springer International Publishing, Cham.

doi:10.1007/978-3-319-50542-8.

Mouslim, J., and David, L. 1995. Biosynthetic Study on the Polyether Carboxylic Antibiotic, Nigericin Production and Biohydroxylation of Grisorixin by Nigericin-producing *Streptomyces hygroscopicus* NRRL B-1865. J. Antibiot. (Tokyo). **48**(9): 1011–1014. doi:10.7164/antibiotics.48.1011.

Muok, A.R., Claessen, D., and Briegel, A. 2021. Microbial hitchhiking: how *Streptomyces* spores are transported by motile soil bacteria. ISME J. **15**(9): 2591–2600. Springer US. doi:10.1038/s41396-021-00952-8.

Myers, O.D., Sumner, S.J., Li, S., Barnes, S., and Du, X. 2017. One Step Forward for Reducing False Positive and False Negative Compound Identifications from Mass Spectrometry Metabolomics Data: New Algorithms for Constructing Extracted Ion Chromatograms and Detecting Chromatographic Peaks. Anal. Chem. **89**(17): 8696–8703. doi:10.1021/acs.analchem.7b00947.

Natsume, M., Komiya, M., Koyanagi, F., Tashiro, N., Kawaide, H., and Abe, H. 2005. Phytotoxin produced by *Streptomyces* sp. causing potato russet scab in Japan. J. Gen. Plant Pathol. **71**(5): 364–369. doi:10.1007/s10327-005-0211-6.

Natsume, M., Ryu, R., and Abe, H. 1996. Production of phytotoxins, concanamycins A and B by *Streptomyces* spp. causing potato scab. Japanese J. Phytopathol. **62**(4): 411–413. doi:10.3186/jjphytopath.62.411.

Natsume, M., Tashiro, N., Doi, A., Nishi, Y., and Kawaide, H. 2017. Effects of concanamycins produced by *Streptomyces scabies* on lesion type of common scab of potato. J. Gen. Plant Pathol. **83**(2): 78–82. Springer Japan. doi:10.1007/s10327-017-

0696-9.

Navarro-Muñoz, J.C., Selem-Mojica, N., Mullowney, M.W., Kautsar, S.A., Tryon, J.H., Parkinson, E.I., De Los Santos, E.L.C., Yeong, M., Cruz-Morales, P., Abubucker, S., Roeters, A., Lokhorst, W., Fernandez-Guerra, A., Cappelini, L.T.D., Goering, A.W., Thomson, R.J., Metcalf, W.W., Kelleher, N.L., Barona-Gomez, F., and Medema, M.H. 2020. A computational framework to explore large-scale biosynthetic diversity. Nat. Chem. Biol. **16**(1): 60–68. Springer US. doi:10.1038/s41589-019-0400-9.

Nett, M., Ikeda, H., and Moore, B.S. 2009. Genomic basis for natural product biosynthetic diversity in the actinomycetes. Nat. Prod. Rep. **26**(11): 1362–1384. doi:10.1039/b817069j.

Ni, S., Jiang, B., Wu, L., Wang, Y., Zhou, H., He, W., Wang, H., Zhu, J., Li, S., Li, T., and Zhang, K. 2014. Identification of 6-demethoxy-6-methylgeldanamycin and its implication of geldanamycin biosynthesis. J. Antibiot. (Tokyo). **67**(2): 183–185. Nature Publishing Group. doi:10.1038/ja.2013.94.

Nikolaidis, M., Hesketh, A., Frangou, N., Mossialos, D., Van de Peer, Y., Oliver, S.G., and Amoutzias, G.D. 2023. A panoramic view of the genomic landscape of the genus *Streptomyces*. Microb. Genomics **9**(6): 1–15. doi:10.1099/mgen.0.001028.

Niu, G., Chater, K.F., Tian, Y., Zhang, J., and Tan, H. 2016. Specialised metabolites regulating antibiotic biosynthesis in *Streptomyces* spp. FEMS Microbiol. Rev. **40**(4): 554–573. doi:10.1093/femsre/fuw012.

Nivina, A., Yuet, K.P., Hsu, J., and Khosla, C. 2019. Evolution and Diversity of Assembly-Line Polyketide Synthases. Chem. Rev. **119**(24): 12524–12547.

doi:10.1021/acs.chemrev.9b00525.

Nothias, L.F., Petras, D., Schmid, R., Dührkop, K., Rainer, J., Sarvepalli, A., Protsyuk, I., Ernst, M., Tsugawa, H., Fleischauer, M., Aicheler, F., Aksenov, A.A., Alka, O., Allard, P.M., Barsch, A., Cachet, X., Caraballo-Rodriguez, A.M., Da Silva, R.R., Dang, T., Garg, N., Gauglitz, J.M., Gurevich, A., Isaac, G., Jarmusch, A.K., Kameník, Z., Kang, K. Bin, Kessler, N., Koester, I., Korf, A., Le Gouellec, A., Ludwig, M., Martin H, C., McCall, L.I., McSayles, J., Meyer, S.W., Mohimani, H., Morsy, M., Moyne, O., Neumann, S., Neuweger, H., Nguyen, N.H., Nothias-Esposito, M., Paolini, J., Phelan, V. V., Pluskal, T., Quinn, R.A., Rogers, S., Shrestha, B., Tripathi, A., van der Hooft, J.J.J., Vargas, F., Weldon, K.C., Witting, M., Yang, H., Zhang, Z., Zubeil, F., Kohlbacher, O., Böcker, S., Alexandrov, T., Bandeira, N., Wang, M., and Dorrestein, P.C. 2020. Feature-based molecular networking in the GNPS analysis environment. Nat. Methods **17**(9): 905–908. Springer US. doi:10.1038/s41592-020-0933-6.

O'Brien, J., and Wright, G.D. 2011. An ecological perspective of microbial secondary metabolism. Curr. Opin. Biotechnol. **22**(4): 552–558. Elsevier Ltd. doi:10.1016/j.copbio.2011.03.010.

O'Connor, S.E. 2015. Engineering of Secondary Metabolism. Annu. Rev. Genet. **49**(September): 71–94. doi:10.1146/annurev-genet-120213-092053.

Oh, D.C., Scott, J.J., Currie, C.R., and Clardy, J. 2009. Mycangimycin, a polyene peroxide from a mutualist *Streptomyces* sp. Org. Lett. **11**(3): 633–636. doi:10.1021/ol802709x.

Oikawa, H., Aihara, Y., Ichihara, A., and Sakamura, S. 1992. Accumulation of Grisorixin

Caused by Treating a Nigericin-producing Strain with a P-450 Inhibitor. Biosci. Biotechnol. Biochem. **56**(4): 684. doi:10.1271/bbb.56.684.

Onodera, H., Kaneko, M., Takahashi, Y., Uochi, Y., Funahashi, J., Nakashima, T., Soga, S., Suzuki, M., Ikeda, S., Yamashita, Y., Rahayu, E.S., Kanda, Y., and Ichimura, M. 2008. Conformational significance of EH21A1-A4, phenolic derivatives of geldanamycin, for Hsp90 inhibitory activity. Bioorganic Med. Chem. Lett. **18**(5): 1588–1591. doi:10.1016/j.bmcl.2008.01.072.

Osbourn, A. 2010. Secondary metabolic gene clusters: Evolutionary toolkits for chemical innovation. Trends Genet. **26**(10): 449–457. Elsevier Ltd. doi:10.1016/j.tig.2010.07.001.

Padilla-Reynaud, R., Simao-Beaunoir, A.-M., Lerat, S., Bernards, M.A., and Beaulieu, C. 2015. Suberin Regulates the Production of Cellulolytic Enzymes in *Streptomyces scabiei*, the Causal Agent of Potato Common Scab. Microbes Environ. **30**(3): 245–253. doi:10.1264/jsme2.ME15034.

Paget, M.S.B., Chamberlin, L., Atrih, A., Foster, S.J., and Buttner, M.J. 1999. Evidence that the Extracytoplasmic Function Sigma Factor ς E Is Required for Normal Cell Wall Structure in *Streptomyces coelicolor* A3(2). J. Bacteriol. **181**(1): 204–211. doi:10.1128/JB.181.1.204-211.1999.

Palazzotto, E., and Weber, T. 2018. Omics and multi-omics approaches to study the biosynthesis of secondary metabolites in microorganisms. Curr. Opin. Microbiol. **45**: 109–116. Elsevier Ltd. doi:10.1016/j.mib.2018.03.004.

Palmer, C.M., and Alper, H.S. 2019. Expanding the Chemical Palette of Industrial

Microbes: Metabolic Engineering for Type III PKS-Derived Polyketides. Biotechnol. J. **14**(1): 1–15. doi:10.1002/biot.201700463.

Pánková, I., Sedláková, V., Sedlák, P., and Krejzar, V. 2012. The occurrence of plant pathogenic *Streptomyces* spp. in potato-growing regions in Central Europe. Am. J. Potato Res. **89**(3): 207–215. doi:10.1007/s12230-012-9245-4.

Paradkar, A.S., and Jensen, S.E. 1995. Functional analysis of the gene encoding the clavaminate synthase 2 isoenzyme involved in clavulanic acid biosynthesis in *Streptomyces clavuligerus*. J. Bacteriol. **177**(5): 1307–1314. doi:10.1128/jb.177.5.1307-1314.1995.

Park, J.Y., and Choi, S.U. 2014. Optimization of transconjugation and characterization of attB integration site for *Streptomyces cinnamoneus* producing transglutaminase. Biol. **69**(8): 953–958. doi:10.2478/s11756-014-0408-2.

Parte, A.C., Carbasse, J.S., Meier-Kolthoff, J.P., Reimer, L.C., and Göker, M. 2020. List of prokaryotic names with standing in nomenclature (LPSN) moves to the DSMZ. Int. J. Syst. Evol. Microbiol. **70**(11): 5607–5612. doi:10.1099/ijsem.0.004332.

Pasco, C., Jouan, B., and Andrivon, D. 2005. Resistance of potato genotypes to common and netted scab-causing species of *Streptomyces*. Plant Pathol. **54**(3): 383–392. doi:10.1111/j.1365-3059.2005.01178.x.

Passot, F.M., Cantlay, S., and Flärdh, K. 2022. Protein phosphatase SppA regulates apical growth and dephosphorylates cell polarity determinant DivIVA in *Streptomyces coelicolor*. Mol. Microbiol. **117**(2): 411–428. doi:10.1111/mmi.14856.

Patkar, R.N., Benke, P.I., Qu, Z., Chen, Y.Y.C., Yang, F., Swarup, S., and Naqvi, N.I.

2015. A fungal monooxygenase-derived jasmonate attenuates host innate immunity. Nat. Chem. Biol. **11**(9): 733–740. Nature Publishing Group. doi:10.1038/nchembio.1885.

Pedersen, T.L. 2020. patchwork: The Composer of Plots.

Phornphisutthimas, S., Sudtachat, N., Bunyoo, C., Chotewutmontri, P., Panijpan, B., and Thamchaipenet, A. 2010. Development of an intergeneric conjugal transfer system for rimocidin-producing *Streptomyces rimosus*. Lett. Appl. Microbiol. **50**(5): 530–536. doi:10.1111/j.1472-765X.2010.02835.x.

Planckaert, S., Jourdan, S., Francis, I.M., Deflandre, B., Rigali, S., and Devreese, B. 2018. Proteomic response to the thaxtomin phytotoxin elicitor cellobiose and to the deletion of the cellulose utilization regulator CebR in *Streptomyces scabies*. J. Proteome Res. doi:10.1021/acs.jproteome.8b00528.

Plitzko, B., Kaweesa, E.N., and Loesgen, X.S. 2017. The natural product mensacarcin induces mitochondrial toxicity and apoptosis in melanoma cells. J. Biol. Chem. **292**(51): 21102–21116. doi:10.1074/jbc.M116.774836.

Pluskal, T., Castillo, S., Villar-Briones, A., and Orešič, M. 2010. MZmine 2: Modular framework for processing, visualizing, and analyzing mass spectrometry-based molecular profile data. BMC Bioinformatics **11**(1): 395. doi:10.1186/1471-2105-11-395.

Qu, X., Wanner, L.A., and Christ, B.J. 2008. Using the TxtAB Operon to Quantify Pathogenic *Streptomyces* in Potato Tubers and Soil. Phytopathology **98**(4): 405–412. doi:10.1094/phyto-98-4-0405.

Quick, P., Scheibe, R., and Stitt, M. 1989. Use of tentoxin and nigericin to investigate the possible contribution of ΔpH to energy dissipation and the control of electron transport in spinach leaves. Biochim. Biophys. Acta - Bioenerg. **974**(3): 282–288. doi:10.1016/S0005-2728(89)80245-2.

Rascher, A., Hu, Z., Buchanan, G.O., Reid, R., and Hutchinson, C.R. 2005. Insights into the biosynthesis of the benzoquinone ansamycins geldanamycin and herbimycin, obtained by gene sequencing and disruption. Appl. Environ. Microbiol. **71**(8): 4862–4871. doi:10.1128/AEM.71.8.4862-4871.2005.

Rey, T., and Dumas, B. 2017. Plenty Is No Plague: *Streptomyces* Symbiosis with Crops. Trends Plant Sci. **22**(1): 30–37. Elsevier Ltd. doi:10.1016/j.tplants.2016.10.008.

Rigali, S., Nothaft, H., Noens, E.E.E., Schlicht, M., Colson, S., Müller, M., Joris, B., Koerten, H.K., Hopwood, D.A., Titgemeyer, F., and Van Wezel, G.P. 2006. The sugar phosphotransferase system of *Streptomyces coelicolor* is regulated by the GntR-family regulator DasR and links *N*-acetylglucosamine metabolism to the control of development. Mol. Microbiol. **61**(5): 1237–1251. doi:10.1111/j.1365-2958.2006.05319.x.

Rigali, S., Titgemeyer, F., Barends, S., Mulder, S., Thomae, A.W., Hopwood, D.A., and van Wezel, G.P. 2008. Feast or famine: The global regulator DasR links nutrient stress to antibiotic production by *Streptomyces*. EMBO Rep. **9**(7): 670–675. doi:10.1038/embor.2008.83.

Risdian, C., Mozef, T., and Wink, J. 2019. Biosynthesis of polyketides in *Streptomyces*. Microorganisms **7**(5): 1–18. doi:10.3390/microorganisms7050124.

Roberts, R.J., Vincze, T., Posfai, J., and Macelis, D. 2023. REBASE: a database for DNA restriction and modification: enzymes, genes and genomes. Nucleic Acids Res. **51**(D1): D629–D630. doi:10.1093/nar/gkac975.

Rodríguez, H., Rico, S., Díaz, M., and Santamaría, R.I. 2013. Two-component systems in *Streptomyces*: Key regulators of antibiotic complex pathways. Microb. Cell Fact. **12**(1): 1–10. doi:10.1186/1475-2859-12-127.

Romano, S., Jackson, S.A., Patry, S., and Dobson, A.D.W. 2018. Extending the "one strain many compounds" (OSMAC) principle to marine microorganisms. Mar. Drugs **16**(7): 1–29. doi:10.3390/md16070244.

Romero-Rodríguez, A., Maldonado-Carmona, N., Ruiz-Villafán, B., Koirala, N., Rocha, D., and Sánchez, S. 2018. Interplay between carbon, nitrogen and phosphate utilization in the control of secondary metabolite production in *Streptomyces*. Antonie van Leeuwenhoek, Int. J. Gen. Mol. Microbiol. **111**(5): 761–781. doi:10.1007/s10482-018-1073-1.

Romero-Rodríguez, A., Robledo-Casados, I., and Sánchez, S. 2015. An overview on transcriptional regulators in *Streptomyces*. Biochim. Biophys. Acta - Gene Regul. Mech. **1849**(8): 1017–1039. Elsevier B.V. doi:10.1016/j.bbagrm.2015.06.007.

Romero-Rodríguez, A., Rocha, D., Ruiz-Villafán, B., Guzmán-Trampe, S., Maldonado-Carmona, N., Vázquez-Hernández, M., Zelarayán, A., Rodríguez-Sanoja, R., and Sánchez, S. 2017. Carbon catabolite regulation in *Streptomyces*: new insights and lessons learned. World J. Microbiol. Biotechnol. **33**(9): 1–11. Springer Netherlands. doi:10.1007/s11274-017-2328-0.

Rong, X., and Huang, Y. 2012. Taxonomic evaluation of the *Streptomyces hygroscopicus* clade using multilocus sequence analysis and DNA-DNA hybridization, validating the MLSA scheme for systematics of the whole genus. Syst. Appl. Microbiol. **35**(1): 7–18. Elsevier GmbH. doi:10.1016/j.syapm.2011.10.004.

Rong, X., and Huang, Y. 2014. Multi-locus sequence analysis. Taking prokaryotic systematics to the next level. *In* Methods in Microbiology, 1st edition. Elsevier Ltd. pp. 221–251. doi:10.1016/bs.mim.2014.10.001.

Russell, D.W., and Sambrook, J. 2001. Molecular cloning: a laboratory manual. *In* 1st edition. Cold Spring Harbor Laboratory, NY.

Ruttkies, C., Schymanski, E.L., Wolf, S., Hollender, J., and Neumann, S. 2016. MetFrag relaunched: Incorporating strategies beyond in silico fragmentation. J. Cheminform. **8**(1): 1–16. Springer International Publishing. doi:10.1186/s13321-016-0115-9.

Salituro, G.M., Zink, D.L., Dahl, A., Nielsen, J., Wu, E., Huang, L., Kastner, C., and Dumont, F.J. 1995. Meridamycin: A novel nonimmunosuppressive FKBP12 ligand from *Streptomyces hygroscopicus*. Tetrahedron Lett. **36**(7): 997–1000. doi:10.1016/0040-4039(94)02425-B.

Sangster, T.A., and Queitsch, C. 2005. The HSP90 chaperone complex, an emerging force in plant development and phenotypic plasticity. Curr. Opin. Plant Biol. **8**(1): 86–92. doi:10.1016/j.pbi.2004.11.012.

Sarwar, A., Latif, Z., and Cabaleiro, C. 2017. First report of *Streptomyces turgidiscabies* causing potato common scab in Spain. Plant Dis. **101**(9): 1671. doi:10.1094/PDIS-03-17-0385-PDN.

Sarwar, A., Latif, Z., and Cabaleiro, C. 2018. First report of *Streptomyces bottropensis* causing potato common scab in Galicia, Spain. Plant Dis. **102**(7): 1445. doi:10.1094/PDIS-11-17-1803-PDN.

Sarwar, A., Latif, Z., Cabaleiro, C., Amin, A., and Saleem, M.A. 2019a. First Report of *Streptomyces europaeiscabiei*Causing Potato Common Scab in Galicia, Spain. Plant Dis. **103**(6): 1407–1407. doi:10.1094/PDIS-08-18-1397-PDN.

Sarwar, A., Latif, Z., Zhang, S., Bechthold, A., and Hao, J. 2019b. A Potential Biocontrol Agent *Streptomyces violaceusniger* AC12AB for Managing Potato Common Scab. Front. Microbiol. **10**(February): 1–10. doi:10.3389/fmicb.2019.00202.

Scheible, W., Fry, B., Kochevenko, A., Schindelasch, D., Zimmerli, L., Somerville, S., Loria, R., and Somerville, C.R. 2003. An *Arabidopsis* mutant resistant to thaxtomin A, a cellulose synthesis inhibitor from *Streptomyces* species. Plant Cell **15**(8): 1781–1794. doi:10.1105/tpc.013342.

Schlatter, D., Fubuh, A., Xiao, K., Hernandez, D., Hobbie, S., and Kinkel, L. 2009. Resource amendments influence density and competitive phenotypes of *Streptomyces* in soil. Microb. Ecol. **57**(3): 413–420. doi:10.1007/s00248-008-9433-4.

Schmid, R., Petras, D., Nothias, L.F., Wang, M., Aron, A.T., Jagels, A., Tsugawa, H., Rainer, J., Garcia-Aloy, M., Dührkop, K., Korf, A., Pluskal, T., Kameník, Z., Jarmusch, A.K., Caraballo-Rodríguez, A.M., Weldon, K.C., Nothias-Esposito, M., Aksenov, A.A., Bauermeister, A., Albarracin Orio, A., Grundmann, C.O., Vargas, F., Koester, I., Gauglitz, J.M., Gentry, E.C., Hövelmann, Y., Kalinina, S.A., Pendergraft, M.A., Panitchpakdi, M., Tehan, R., Le Gouellec, A., Aleti, G., Mannochio Russo, H.,

Arndt, B., Hübner, F., Hayen, H., Zhi, H., Raffatellu, M., Prather, K.A., Aluwihare, L.I., Böcker, S., McPhail, K.L., Humpf, H.U., Karst, U., and Dorrestein, P.C. 2021. Ion identity molecular networking for mass spectrometry-based metabolomics in the GNPS environment. Nat. Commun. **12**(1). doi:10.1038/s41467-021-23953-9.

Schneider, A., Späth, J., Breiding-Mack, S., Zeeck, A., Grabley, S., and Thiericke, R. 1996. New Cineromycins and Musacins Obtained by Metabolite Pattern Analysis of *Streptomyces griseoviridis* FH-S 1832). II. Structure Elucidation. J. Antibiot. (Tokyo). **49**(5): 438–446. doi:10.7164/antibiotics.49.438.

Schumacher, M.A., Zeng, W., Findlay, K.C., Buttner, M.J., Brennan, R.G., and Tschowri, N. 2017. The *Streptomyces* master regulator BldD binds c-di-GMP sequentially to create a functional BldD2-(c-di-GMP)4 complex. Nucleic Acids Res. **45**(11): 6923–6933. doi:10.1093/nar/gkx287.

Scott, J.J., Oh, D., Yuceer, M.C., Klepzig, K.D., Clardy, J., and Currie, C.R. 2008. Bacterial Protection of Beetle-Fungus Mutualism. Science (80-.). **322**(5898): 63–63. doi:10.1126/science.1160423.

Seipke, R.F., Kaltenpoth, M., and Hutchings, M.I. 2012. *Streptomyces* as symbionts: An emerging and widespread theme? FEMS Microbiol. Rev. **36**(4): 862–876. doi:10.1111/j.1574-6976.2011.00313.x.

Seipke, R.F., Patrick, E., and Hutchings, M.I. 2014. Regulation of antimycin biosynthesis by the orphan ECF RNA polymerase sigma factor σAntA. PeerJ **2014**(1). doi:10.7717/peerj.253.

Shannon, P., Markiel, A., Ozier, O., Baliga, N.S., Wang, J.T., Ramage, D., Amin, N.,

Schwikowski, B., and Ideker, T. 2003. Cytoscape: A Software Environment for Integrated Models of Biomolecular Interaction Networks. Genome Res. **13**(11): 2498–2504. doi:10.1101/gr.1239303.

Shavit, N., Dilley, R.A., and Pietro, A.S. 1968. Ion Translocation in Isolated Chloroplasts. Uncoupling of Photophosphorylation and Translocation of K+ and H+ Ions Induced by Nigericin. Biochemistry **7**(6): 2356–2363. doi:10.1021/bi00846a043.

Shavit, N., and San Pietro, A. 1967. K+ - Dependent uncoupling of Photophosphorylation by nigericin. Biochem. Biophys. Res. Commun. **28**(8): 277–283.

Sheng, Y., Lam, P.W., Shahab, S., Santosa, D.A., Proteau, P.J., Zabriskie, T.M., and Mahmud, T. 2015. Identification of Elaiophylin Skeletal Variants from the Indonesian *Streptomyces* sp. ICBB 9297. J. Nat. Prod. **78**(11): 2768–2775. doi:10.1021/acs.jnatprod.5b00752.

Shepherdson, E.M.F., and Elliot, M.A. 2022. Cryptic specialized metabolites drive *Streptomyces* exploration and provide a competitive advantage during growth with other microbes. Proc. Natl. Acad. Sci. U. S. A. **119**(40). doi:10.1073/pnas.2211052119.

Shi, J., Liu, C.L., Zhang, B., Guo, W.J., Zhu, J., Chang, C.-Y., Zhao, E.J., Jiao, R.H., Tan, R.X., and Ge, H.M. 2019. Genome mining and biosynthesis of kitacinnamycins as a STING activator. Chem. Sci. **10**(18): 4839–4846. Royal Society of Chemistry. doi:10.1039/C9SC00815B.

Shi, L., Wu, Z., Zhang, Y., Zhang, Z., Fang, W., Wang, Y., Wan, Z., Wang, K., and Ke, S. 2020. Herbicidal Secondary Metabolites from Actinomycetes: Structure Diversity,

Modes of Action, and Their Roles in the Development of Herbicides. J. Agric. Food Chem. **68**(1): 17–32. doi:10.1021/acs.jafc.9b06126.

da Silva, R.R., Wang, M., Nothias, L.-F.F., van der Hooft, J.J.J.J., Caraballo-Rodríguez, A.M., Fox, E., Balunas, M.J., Klassen, J.L., Lopes, N.P., and Dorrestein, P.C. 2018. Propagating annotations of molecular networks using in silico fragmentation. PLOS Comput. Biol. **14**(4): e1006089. doi:10.1371/journal.pcbi.1006089.

Sineva, E., Savkina, M., and Ades, S.E. 2017. Themes and variations in gene regulation by extracytoplasmic function (ECF) sigma factors. Curr. Opin. Microbiol. **36**: 128–137. Elsevier Ltd. doi:10.1016/j.mib.2017.05.004.

Som, N.F., Heine, D., Holmes, N., Knowles, F., Chandra, G., Seipke, R.F., Hoskisson, P.A., Wilkinson, B., and Hutchings, M.I. 2017. The MtrAB two-component system controls antibiotic production in *Streptomyces coelicolor* A3(2). Microbiology **163**(10): 1415–1419. doi:10.1099/mic.0.000524.

Song, Z. qing, Liao, Z. jun, Hu, Y. feng, Ma, Z., Bechthold, A., and Yu, X. ping. 2019. Development and optimization of an intergeneric conjugation system and analysis of promoter activity in *Streptomyces rimosus* M527. J. Zhejiang Univ. Sci. B **20**(11): 891–900. doi:10.1631/jzus.B1900270.

Spear, L., Gallagher, J., McHale, L., and McHale, A.P. 1993. Production of cellulase and β-glucosidase activities following growth of *Streptomyces hygroscopicus* on cellulose containing media. Biotechnol. Lett. **15**(12): 1265–1268. doi:10.1007/BF00130309.

St-Onge, R., Goyer, C., Coffin, R., and Filion, M. 2008. Genetic diversity of *Streptomyces* spp. causing common scab of potato in eastern Canada. Syst. Appl. Microbiol. **31**(6–

8): 474–484. doi:10.1016/j.syapm.2008.09.002.

Staswick, P.E. 2009. The tryptophan conjugates of jasmonic and indole-3-acetic acids are endogenous auxin inhibitors. Plant Physiol. **150**(3): 1310–1321. doi:10.1104/pp.109.138529.

Stebbins, C.E., Russo, A.A., Schneider, C., Rosen, N., Hartl, F.U., and Pavletich, N.P. 1997. Crystal structure of an Hsp90-geldanamycin complex: Targeting of a protein chaperone by an antitumor agent. Cell **89**(2): 239–250. doi:10.1016/S0092-8674(00)80203-2.

Stoeckle, D., Thellmann, M., and Vermeer, J.E. 2018. Breakout — lateral root emergence in *Arabidopsis thaliana*. Curr. Opin. Plant Biol. **41**: 67–72. Elsevier Ltd. doi:10.1016/j.pbi.2017.09.005.

Strakova, E., Bobek, J., Zikova, A., Rehulka, P., Benada, O., Rehulkova, H., Kofronova, O., and Vohradsky, J. 2013. Systems insight into the spore germination of *Streptomyces coelicolor*. J. Proteome Res. **12**(1): 525–536. doi:10.1021/pr300980v.

Sun, D., Liu, C., Zhu, J., and Liu, W. 2017. Connecting metabolic pathways: Sigma factors in *Streptomyces* spp. Front. Microbiol. **8**(DEC): 1–7. doi:10.3389/fmicb.2017.02546.

Sun, F.H., Luo, D., Shu, D., Zhong, J., and Tan, H. 2014. Development of an intergeneric conjugal transfer system for xinaomycins-producing *Streptomyces noursei* Xinao-4. Int. J. Mol. Sci. **15**(7): 12217–12230. doi:10.3390/ijms150712217.

Sun, Y., Hong, H., Samboskyy, M., Mironenko, T., Leadlay, P.F., and Haydock, S.F. 2006. Organization of the biosynthetic gene cluster in *Streptomyces* sp. DSM 4137 for the novel neuroprotectant polyketide meridamycin. Microbiology **152**(12): 3507–3515.

doi:10.1099/mic.0.29176-0.

Supong, K., Thawai, C., Choowong, W., Kittiwongwattana, C., Thanaboripat, D., Laosinwattana, C., Koohakan, P., Parinthawong, N., and Pittayakhajonwut, P. 2016. Antimicrobial compounds from endophytic *Streptomyces* sp. BCC72023 isolated from rice (*Oryza sativa* L.). Res. Microbiol. **167**(4): 290–298. Elsevier Masson SAS. doi:10.1016/j.resmic.2016.01.004.

Süssmuth, R.D., and Mainz, A. 2017. Nonribosomal Peptide Synthesis—Principles and Prospects. Angew. Chemie - Int. Ed. **56**(14): 3770–3821. doi:10.1002/anie.201609079.

Suzuki, H. 2012. Host-Mimicking Strategies in DNA Methylation for Improved Bacterial Transformation. *In* Methylation - From DNA, RNA and Histones to Diseases and Treatment. InTech. p. 13. doi:10.5772/51691.

Syed, D.G., Agasar, D., and Pandey, A. 2009. Production and partial purification of α-amylase from a novel isolate *Streptomyces gulbargensis*. J. Ind. Microbiol. Biotechnol. **36**(2): 189–194. doi:10.1007/s10295-008-0484-9.

Tachibana, K., and Kaneko, K. 1986. Development of a New Herbicide, Bialaphos. J. Pestic. Sci. **11**(2): 297–304. doi:10.1584/jpestics.11.297.

Takano, E. 2006. γ-Butyrolactones: *Streptomyces* signalling molecules regulating antibiotic production and differentiation. Curr. Opin. Microbiol. **9**(3): 287–294. doi:10.1016/j.mib.2006.04.003.

Takesako, K., and Beppu, T. 1984. Studies on new antifungal antibiotics, guanidylfungins A and B. I. Taxonomy, fermentation, isolation and characterization. J. Antibiot.

(Tokyo). **37**(10): 1161–1169. doi:10.7164/antibiotics.37.1161.

Tanaka, A., Takano, Y., Ohnishi, Y., and Horinouchi, S. 2007. AfsR Recruits RNA Polymerase to the afsS Promoter: A Model for Transcriptional Activation by SARPs. J. Mol. Biol. **369**(2): 322–333. doi:10.1016/j.jmb.2007.02.096.

Tanida, S., Muroi, M., and Hasegawa, T. 1983. Antibiotic TAN-420, its production and producer.

Tashiro, N., Manabe, K., Saito, A., and Miyashita, K. 2012. Identification of potato scab-causing *Streptomyces* sp. occurring in strongly acidic soils in Saga Prefecture in Japan. J. Gen. Plant Pathol. **78**(5): 353–359. doi:10.1007/s10327-012-0393-7.

Terlouw, B.R., Blin, K., Navarro-Muñoz, J.C., Avalon, N.E., Chevrette, M.G., Egbert, S., Lee, S., Meijer, D., Recchia, M.J.J., Reitz, Z.L., van Santen, J.A., Selem-Mojica, N., Tørring, T., Zaroubi, L., Alanjary, M., Aleti, G., Aguilar, C., Al-Salihi, S.A.A., Augustijn, H.E., Avelar-Rivas, J.A., Avitia-Domínguez, L.A., Barona-Gómez, F., Bernaldo-Agüero, J., Bielinski, V.A., Biermann, F., Booth, T.J., Carrion Bravo, V.J., Castelo-Branco, R., Chagas, F.O., Cruz-Morales, P., Du, C., Duncan, K.R., Gavriilidou, A., Gayrard, D., Gutiérrez-García, K., Haslinger, K., Helfrich, E.J.N., van der Hooft, J.J.J., Jati, A.P., Kalkreuter, E., Kalyvas, N., Kang, K. Bin, Kautsar, S., Kim, W., Kunjapur, A.M., Li, Y., Lin, G., Loureiro, C., Louwen, J.J.R., Louwen, N.L.L., Lund, G., Parra, J., Philmus, B., Pourmohsenin, B., Pronk, L.J.U., Rego, A., Rex, D.A.B., Robinson, S., Rosas-Becerra, L.R., Roxborough, E.T., Schorn, M.A., Scobie, D.J., Singh, K.S., Sokolova, N., Tang, X., Udwary, D., Vigneshwari, A., Vind, K., Vromans, S.P.J.M., Waschulin, V., Williams, S.E., Winter, J.M., Witte, T.E., Xie,

H., Yang, D., Yu, J., Zdouc, M., Zhong, Z., Collemare, J., Linington, R.G., Weber, T., and Medema, M.H. 2022. MIBiG 3.0: a community-driven effort to annotate experimentally validated biosynthetic gene clusters. Nucleic Acids Res. **51**(November 2022): epub ahead of print. doi:10.1093/nar/gkac1049.

Thangavel, T., Tegg, R.S., and Wilson, C.R. 2016. Toughing It Out—Disease-Resistant Potato Mutants Have Enhanced Tuber Skin Defenses. Phytopathology **106**(5): 474–483. doi:10.1094/phyto-08-15-0191-r.

Tian, X., Zhang, Z., Yang, T., Chen, M., Li, J., Chen, F., Yang, J., Li, W., Zhang, B., Zhang, Z., Wu, J., Zhang, C., Long, L., and Xiao, J. 2016. Comparative genomics analysis of *Streptomyces* species reveals their adaptation to the marine environment and their diversity at the genomic level. Front. Microbiol. **7**(JUN): 1–16. doi:10.3389/fmicb.2016.00998.

Tillotson, R.D., Wösten, H.A.B., Richter, M., and Willey, J.M. 1998. A surface active protein involved in aerial hyphae formation in the filamentous fungus *Schizophillum commune* restores the capacity of a bald mutant of the filamentous bacterium *Streptomyces coelicolor* to erect aerial structures. Mol. Microbiol. **30**(3): 595–602. doi:10.1046/j.1365-2958.1998.01093.x.

Traxler, M.F., and Kolter, R. 2015. Natural products in soil microbe interactions and evolution. Nat. Prod. Rep. **32**(7): 956–970. Royal Society of Chemistry. doi:10.1039/c5np00013k.

Trejo-Estrada, S.R., Paszczynski, A., and Crawford, D.L. 1998. Antibiotics and enzymes produced by the biocontrol agent *Streptomyces violaceusniger* YCED-9. J. Ind.

Microbiol. Biotechnol. **21**(1–2): 81–90. doi:10.1038/sj.jim.2900549.

Tyc, O., Song, C., Dickschat, J.S., Vos, M., and Garbeva, P. 2017. The Ecological Role of Volatile and Soluble Secondary Metabolites Produced by Soil Bacteria. Trends Microbiol. **25**(4): 280–292. Elsevier Ltd. doi:10.1016/j.tim.2016.12.002.

Ulanova, D., Kitani, S., Fukusaki, E., and Nihira, T. 2013. SdrA, a new DeoR family regulator involved in *Streptomyces avermitilis* morphological development and antibiotic production. Appl. Environ. Microbiol. **79**(24): 7916–7921. doi:10.1128/AEM.02843-13.

Umurzokov, M., Lee, Y.M., Kim, H.J., Cho, K.M., Kim, Y.S., Choi, J.S., and Park, K.W. 2022. Herbicidal characteristics and structural identification of a potential active compound produced by *Streptomyces* sp. KRA18–249. Pestic. Biochem. Physiol. **187**(August): 105213. Elsevier Inc. doi:10.1016/j.pestbp.2022.105213.

Uppalapati, S.R., Ayoubi, P., Weng, H., Palmer, D.A., Mitchell, R.E., Jones, W., and Bender, C.L. 2005. The phytotoxin coronatine and methyl jasmonate impact multiple phytohormone pathways in tomato. Plant J. **42**(2): 201–217. doi:10.1111/j.1365-313X.2005.02366.x.

Usuki, Y., Matsumoto, K., Inoue, T., Yoshioka, K., Iio, H., and Tanaka, T. 2006. Structure-activity relationship studies on niphimycin, a guanidylpolyol macrolide antibiotic. Part 1: The role of the N-methyl-N″-alkylguanidinium moiety. Bioorganic Med. Chem. Lett. **16**(6): 1553–1556. Elsevier Ltd. doi:10.1016/j.bmcl.2005.12.024.

Vaz Jauri, P., and Kinkel, L.L. 2014. Nutrient overlap, genetic relatedness and spatial origin influence interaction-mediated shifts in inhibitory phenotype among

Streptomyces spp. FEMS Microbiol. Ecol. **90**(1): 264–275. doi:10.1111/1574-6941.12389.

Viaene, T., Langendries, S., Beirinckx, S., Maes, M., and Goormachtig, S. 2016. *Streptomyces* as a plant's best friend? FEMS Microbiol. Ecol. **92**(8): 1–10. doi:10.1093/femsec/fiw119.

Visvanathan, R., Qader, M., Jayathilake, C., Jayawardana, B.C., Liyanage, R., and Sivakanesan, R. 2020. Critical review on conventional spectroscopic α-amylase activity detection methods: merits, demerits, and future prospects. J. Sci. Food Agric. **100**(7): 2836–2847. doi:10.1002/jsfa.10315.

Wang, A., and Lazarovits, G. 2004. Enumeration of plant pathogenic *Streptomyces* on postharvest potato tubers under storage conditions. Can. J. Plant Pathol. **26**(4): 563–572. doi:10.1080/07060660409507177.

Wang, J., Zhang, R., Chen, X., Sun, X., Yan, Y., Shen, X., and Yuan, Q. 2020. Biosynthesis of aromatic polyketides in microorganisms using type II polyketide synthases. Microb. Cell Fact. **19**(1): 1–11. BioMed Central. doi:10.1186/s12934-020-01367-4.

Wang, L., Tian, X., Wang, J., Yang, H., Fan, K., Xu, G., Yang, K., and Tan, H. 2009. Autoregulation of antibiotic biosynthesis by binding of the end product to an atypical response regulator. Proc. Natl. Acad. Sci. U. S. A. **106**(21): 8617–8622. doi:10.1073/pnas.0900592106.

Wang, L., Yu, Y., He, X., Zhou, X., Deng, Z., Chater, K.F., and Tao, M. 2007. Role of an FtsK-like protein in genetic stability in *Streptomyces coelicolor* A3(2). J. Bacteriol.

189(6): 2310–2318. doi:10.1128/JB.01660-06.

Wang, M., Carver, J.J., Phelan, V. V., Sanchez, L.M., Garg, N., Peng, Y., Nguyen, D.D., Watrous, J., Kapono, C.A., Luzzatto-Knaan, T., Porto, C., Bouslimani, A., Melnik, A. V., Meehan, M.J., Liu, W.T., Crüsemann, M., Boudreau, P.D., Esquenazi, E., Sandoval-Calderón, M., Kersten, R.D., Pace, L.A., Quinn, R.A., Duncan, K.R., Hsu, C.C., Floros, D.J., Gavilan, R.G., Kleigrewe, K., Northen, T., Dutton, R.J., Parrot, D., Carlson, E.E., Aigle, B., Michelsen, C.F., Jelsbak, L., Sohlenkamp, C., Pevzner, P., Edlund, A., McLean, J., Piel, J., Murphy, B.T., Gerwick, L., Liaw, C.C., Yang, Y.L., Humpf, H.U., Maansson, M., Keyzers, R.A., Sims, A.C., Johnson, A.R., Sidebottom, A.M., Sedio, B.E., Klitgaard, A., Larson, C.B., Boya, C.A.P., Torres-Mendoza, D., Gonzalez, D.J., Silva, D.B., Marques, L.M., Demarque, D.P., Pociute, E., O'Neill, E.C., Briand, E., Helfrich, E.J.N., Granatosky, E.A., Glukhov, E., Ryffel, F., Houson, H., Mohimani, H., Kharbush, J.J., Zeng, Y., Vorholt, J.A., Kurita, K.L., Charusanti, P., McPhail, K.L., Nielsen, K.F., Vuong, L., Elfeki, M., Traxler, M.F., Engene, N., Koyama, N., Vining, O.B., Baric, R., Silva, R.R., Mascuch, S.J., Tomasi, S., Jenkins, S., Macherla, V., Hoffman, T., Agarwal, V., Williams, P.G., Dai, J., Neupane, R., Gurr, J., Rodríguez, A.M.C., Lamsa, A., Zhang, C., Dorrestein, K., Duggan, B.M., Almaliti, J., Allard, P.M., Phapale, P., Nothias, L.F., Alexandrov, T., Litaudon, M., Wolfender, J.L., Kyle, J.E., Metz, T.O., Peryea, T., Nguyen, D.T., VanLeer, D., Shinn, P., Jadhav, A., Müller, R., Waters, K.M., Shi, W., Liu, X., Zhang, L., Knight, R., Jensen, P.R., Palsson, B., Pogliano, K., Linington, R.G., Gutiérrez, M., Lopes, N.P., Gerwick, W.H., Moore, B.S., Dorrestein, P.C., and Bandeira, N. 2016. Sharing and community curation of mass spectrometry data with Global Natural Products Social

Molecular Networking. Nat. Biotechnol. **34**(8): 828–837. doi:10.1038/nbt.3597.

Wang, X., Ning, X., Zhao, Q., Kang, Q., and Bai, L. 2017. Improved PKS Gene Expression With Strong Endogenous Promoter Resulted in Geldanamycin Yield Increase. Biotechnol. J. **12**(11): 1700321. doi:10.1002/biot.201700321.

Wang, X., Reynolds, A.R., Elshahawi, S.I., Shaaban, K.A., Ponomareva, L. V., Saunders, M.A., Elgumati, I.S., Zhang, Y., Copley, G.C., Hower, J.C., Sunkara, M., Morris, A.J., Kharel, M.K., Van Lanen, S.G., Prendergast, M.A., and Thorson, J.S. 2015. Terfestatins B and C, new p -terphenyl glycosides produced by *Streptomyces* sp. RM-5-8. Org. Lett. **17**(11): 2796–2799. doi:10.1021/acs.orglett.5b01203.

Wang, X.K., and Jin, J.L. 2014. Crucial factor for increasing the conjugation frequency in *Streptomyces netropsis* SD-07 and other strains. FEMS Microbiol. Lett. **357**(1): 99–103. doi:10.1111/1574-6968.12507.

Wanner, L.A. 2004. Field Isolates of *Streptomyces* Differ in Pathogenicity and Virulence on Radish. Plant Dis. **88**(8): 785–796. doi:10.1094/PDIS.2004.88.8.785.

Wanner, L.A. 2006. A Survey of Genetic Variation in *Streptomyces* Isolates Causing Potato Common Scab in the United States. Phytopathology **96**(12): 1363–1371. doi:10.1094/phyto-96-1363.

Wanner, L.A. 2007. High proportions of nonpathogenic *Streptomyces* are associated with common scab-resistant potato lines and less severe disease. Can. J. Microbiol. **53**(9): 1062–1075. doi:10.1139/W07-061.

Wanner, L.A. 2009. A patchwork of *Streptomyces* species isolated from potato common scab lesions in North America. Am. J. Potato Res. **86**(4): 247–264.

doi:10.1007/s12230-009-9078-y.

Wanner, L.A., and Kirk, W.W. 2015. *Streptomyces* – from Basic Microbiology to Role as a Plant Pathogen. Am. J. Potato Res. **92**(2): 236–242. doi:10.1007/s12230-015-9449-5.

Wecke, T., Halang, P., Staroń, A., Dufour, Y.S., Donohue, T.J., and Mascher, T. 2012. Extracytoplasmic function σ factors of the widely distributed group ECF41 contain a fused regulatory domain. Microbiologyopen **1**(2): 194–213. doi:10.1002/mbo3.22.

Wei, J., Ma, M., Guo, S., Xu, Y., Xie, J., Pan, G., and Zhou, Z. 2022. Characterization of Pathway-Specific Regulator NigR for High Yield Production of Nigericin in *Streptomyces malaysiensis* F913. Antibiotics **11**(7). doi:10.3390/antibiotics11070938.

Westhoff, S., Kloosterman, A.M., van Hoesel, S.F.A., van Wezel, G.P., and Rozen, D.E. 2021. Competition sensing changes antibiotic production in *Streptomyces*. MBio **12**(1): 1–13. doi:10.1128/mBio.02729-20.

Westhoff, S., Otto, S.B., Swinkels, A., Bode, B., van Wezel, G.P., and Rozen, D.E. 2020. Spatial structure increases the benefits of antibiotic production in *Streptomyces**. Evolution (N. Y). **74**(1): 179–187. doi:10.1111/evo.13817.

Van Wezel, G.P., and McDowall, K.J. 2011. The regulation of the secondary metabolism of *Streptomyces*: New links and experimental advances. Nat. Prod. Rep. **28**(7): 1311–1333. doi:10.1039/c1np00003a.

Wickham, H. 2016. ggplot2: Elegant Graphics for Data Analysis. Springer-Verlag, New York.

Wietzorrek, A., and Bibb, M. 1997. A novel family of proteins that regulates antibiotic

production in streptomycetes appears to contain an OmpR-like DNA-binding fold. Mol. Microbiol. **25**(6): 1181–1184. doi:10.1046/j.1365-2958.1997.5421903.x.

Wilhelm, B.T., and Landry, J.R. 2009. RNA-Seq-quantitative measurement of expression through massively parallel RNA-sequencing. Methods **48**(3): 249–257. Elsevier Inc. doi:10.1016/j.ymeth.2009.03.016.

Willemse, J., Mommaas, A.M., and Van Wezel, G.P. 2012. Constitutive expression of ftsZ overrides the whi developmental genes to initiate sporulation of *Streptomyces coelicolor*. Antonie van Leeuwenhoek, Int. J. Gen. Mol. Microbiol. **101**(3): 619–632. doi:10.1007/s10482-011-9678-7.

Willey, J.M., Willems, A., Kodani, S., and Nodwell, J.R. 2006. Morphogenetic surfactants and their role in the formation of aerial hyphae in *Streptomyces coelicolor*. Mol. Microbiol. **59**(3): 731–742. doi:10.1111/j.1365-2958.2005.05018.x.

Wu, C., Kim, H.K., Van Wezel, G.P., and Choi, Y.H. 2015. Metabolomics in the natural products field - A gateway to novel antibiotics. Drug Discov. Today Technol. **13**: 11–17. Elsevier Ltd. doi:10.1016/j.ddtec.2015.01.004.

Wu, C., Tan, Y., Gan, M., Wang, Y., Guan, Y., Hu, X., Zhou, H., Shang, X., You, X., Yang, Z., and Xiao, C. 2013. Identification of elaiophylin derivatives from the marine-derived actinomycete *Streptomyces* sp. 7-145 using PCR-based screening. J. Nat. Prod. **76**(11): 2153–2157. doi:10.1021/np4006794.

Wu, H., Liu, Q., Casas-Pastor, D., Dürr, F., Mascher, T., and Fritz, G. 2019. The role of C-terminal extensions in controlling ECF σ factor activity in the widely conserved groups ECF41 and ECF42. Mol. Microbiol. **112**(2): 498–514.

doi:10.1111/mmi.14261.

Wu, Z., Bai, L., Wang, M., Shen, Y., Science, B.L., Soedinenii, P., and June, M. 2009. STRUCTURE – ANTIBACTERIAL RELATIONSHIP OF NIGERICIN DERIVATIVES. Chem. Nat. Compd. **45**(3): 285–288. doi:0009-3130/09/4503-0333.

Xing, S., Shen, S., Xu, B., Li, X., and Huan, T. 2023. BUDDY: molecular formula discovery via bottom-up MS/MS interrogation. Nat. Methods: 2022.08.03.502704. Springer US. doi:10.1038/s41592-023-01850-x.

Xu, M.J., Wang, J.H., Bu, X.L., Yu, H.L., Li, P., Ou, H.Y., He, Y., Xu, F. Di, Hu, X.Y., Zhu, X.M., Ao, P., and Xu, J. 2016. Deciphering the streamlined genome of *Streptomyces xiamenensis* 318 as the producer of the anti-fibrotic drug candidate xiamenmycin. Sci. Rep. **6**(December 2015): 1–11. Nature Publishing Group. doi:10.1038/srep18977.

Xu, T., Cao, L., Zeng, J., Franco, C.M.M., Yang, Y., Hu, X., Liu, Y., Wang, X., Gao, Y., Bu, Z., Shi, L., Zhou, G., Zhou, Q., Liu, X., and Zhu, Y. 2019. The antifungal action mode of the rice endophyte *Streptomyces hygroscopicus* OsiSh-2 as a potential biocontrol agent against the rice blast pathogen. Pestic. Biochem. Physiol. **160**(April): 58–69. Elsevier. doi:10.1016/j.pestbp.2019.06.015.

Yamazoe, A., Hayashi, K.I., Kepinski, S., Leyser, O., and Nozaki, H. 2005. Characterization of terfestatin A, a new specific inhibitor for auxin signaling. Plant Physiol. **139**(2): 779–789. doi:10.1104/pp.105.068924.

Yamazoe, A., Hayashi, K.I., Kuboki, A., Ohira, S., and Nozaki, H. 2004. The isolation, structural determination, and total synthesis of terfestatin A, a novel auxin signaling

inhibitor from *Streptomyces* sp. Tetrahedron Lett. **45**(45): 8359–8362. doi:10.1016/j.tetlet.2004.09.055.

Yan, H., Lu, X., Sun, D., Zhuang, S., Chen, Q., Chen, Z., Li, J., and Wen, Y. 2020. BldD, a master developmental repressor, activates antibiotic production in two *Streptomyces* species. Mol. Microbiol. **113**(1): 123–142. doi:10.1111/mmi.14405.

Yang, X., Lyu, Z., Miguel, A., McQuillen, R., Huang, K.C., and Xiao, J. 2017. GTPase activity-coupled treadmilling of the bacterial tubulin FtsZ organizes septal cell wall synthesis. Science (80-.). **355**(6326): 744–747. doi:10.1126/science.aak9995.

Yang, Z., Strøbech, E., Qiao, Y., Konakall, N.C., Harris, P., Peschel, G., Agler-Rosenbaum, M., Weber, T., Andreasson, E., and Ding, L. 2022. *Streptomyces* alleviate abiotic stress in plant by producing pteridic acids. bioRxiv: 2022.11.18.517137.

Yin, M., Lu, T., Zhao, L.X., Chen, Y., Huang, S.X., Lohman, J.R., Xu, L.H., Jiang, C.L., and Shen, B. 2011. The missing C-17 O-methyltransferase in geldanamycin biosynthesis. Org. Lett. **13**(14): 3726–3729. doi:10.1021/ol201383w.

Yu, G., Smith, D.K., Zhu, H., Guan, Y., and Lam, T.T. 2017. ggtree: an R package for visualization and annotation of phylogenetic trees with their covariates and other associated data. Methods Ecol. Evol. **8**(1): 28–36. doi:10.1111/2041-210X.12628.

Zhang, J., Chang, X., Li, Y., and Lu, C. 2016a. Galbonolides from *Streptomyces* sp. SR107. Nat. Prod. Commun. **11**(12): 1869–1870. doi:10.1177/1934578x1601101224.

Zhang, J., Yuzawa, S., Thong, W.L., Shinada, T., Nishiyama, M., and Kuzuyama, T. 2021. Reconstitution of a highly reducing type II PKS system reveals 6π-electrocyclization is required for O-dialkylbenzene biosynthesis. J. Am. Chem. Soc. **143**(7): 2962–2969.

doi:10.1021/jacs.0c13378.

Zhang, P., Wu, L., Zhu, Y., Liu, M., Wang, Y., Cao, G., Chen, X.L., Tao, M., and Pang, X. 2017. Deletion of mtrA inhibits cellular development of *Streptomyces coelicolor* and alters expression of developmental regulatory genes. Front. Microbiol. **8**(OCT): 1–18. doi:10.3389/fmicb.2017.02013.

Zhang, S., Chen, T., Jia, J., Guo, L., Zhang, H., Li, C., and Qiao, R. 2019. Establishment of a highly efficient conjugation protocol for *Streptomyces kanamyceticus* ATCC12853. Microbiologyopen **8**(6): 1–8. doi:10.1002/mbo3.747.

Zhang, Y., Bignell, D.R.D., Zuo, R., Fan, Q., Huguet-Tapia, J.C., Ding, Y., and Loria, R. 2016b. Promiscuous Pathogenicity Islands and Phylogeny of Pathogenic *Streptomyces* spp. Mol. Plant-Microbe Interact. **29**(8): 640–650. doi:10.1094/MPMI-04-16-0068-R.

Zhang, Y., Lin, C.Y., Li, X.M., Tang, Z.K., Qiao, J., and Zhao, G.R. 2016c. DasR positively controls monensin production at two-level regulation in *Streptomyces cinnamonensis*. J. Ind. Microbiol. Biotechnol. **43**(12): 1681–1692. Springer Berlin Heidelberg. doi:10.1007/s10295-016-1845-4.

Zhao, G., Li, S., Wang, Y., Hao, H., Shen, Y., and Lu, C. 2013. 16,17-dihydroxycyclooctatin, a new diterpene from *Streptomyces* sp. LZ35. Drug Discov. Ther. **7**(5): 185–188. doi:10.5582/ddt.2013.v7.5.185.

Zhao, J., Tang, X., Li, K., Guo, Y., Feng, M., and Gao, J. 2020a. *Streptomyces paludis* sp. Nov., isolated from an alpine wetland soil. Int. J. Syst. Evol. Microbiol. **70**(2): 773–778. doi:10.1099/ijsem.0.003821.

Zhao, Y., Li, G., Chen, Y., and Lu, Y. 2020b. Challenges and advances in genome editing

technologies in *Streptomyces*. Biomolecules **10**(5): 1–14. doi:10.3390/biom10050734.

Zhou, Z., Gu, J., Li, Y.Q., and Wang, Y. 2012. Genome plasticity and systems evolution in *Streptomyces*. BMC Bioinformatics **13 Suppl 1**(Suppl 10). doi:10.1186/1471-2105-13-S10-S8.

Zhu, J., Chen, W., Li, Y.Y., Deng, J.J., Zhu, D.Y., Duan, J., Liu, Y., Shi, G.Y., Xie, C., Wang, H.X., and Shen, Y.M. 2014. Identification and catalytic characterization of a nonribosomal peptide synthetase-like (NRPS-like) enzyme involved in the biosynthesis of echosides from *Streptomyces* sp. LZ35. Gene **546**(2): 352–358. Elsevier B.V. doi:10.1016/j.gene.2014.05.053.

Zhu, J., Liu, M., Deng, J., Chen, W., Zhu, D., Duan, J., Li, Y., Wang, H., and Shen, Y. 2021. The coupled reaction catalyzed by EchB and EchC lead to the formation of the common 2′,3′,5′-trihydroxy-benzene core in echosides biosynthesis. Biochem. Biophys. Res. Commun. **559**: 62–69. Elsevier Ltd. doi:10.1016/j.bbrc.2021.04.087.